DYNAMIC HYDROGELS FOR STUDYING TUMOR-STROMA INTERACTIONS IN PANCREATIC CANCER

by

Hung-Yi Liu

A Dissertation

Submitted to the Faculty of Purdue University

In Partial Fulfillment of the Requirements for the degree of

Doctor of Philosophy

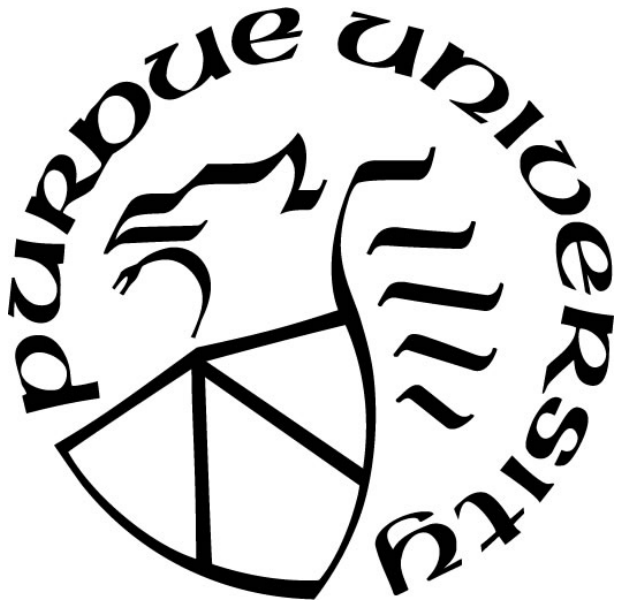

Weldon School of Biomedical Engineering

West Lafayette, Indiana, IN

August 2019

THE PURDUE UNIVERSITY GRADUATE SCHOOL
STATEMENT OF COMMITTEE APPROVAL

Dr. Chien-Chi Lin, Chair

Department of Biomedical Engineering, Indiana University-Purdue University Indianapolis, Indianapolis, Indiana

Dr. Sherry L. Voytik-Harbin, Co-Chair

Weldon School of Biomedical Engineering, Purdue University, West Lafayette, Indiana

Dr. Hiroki Yokota

Department of Biomedical Engineering, Indiana University-Purdue University Indianapolis, Indianapolis, Indiana

Dr. Luis Solorio

Weldon School of Biomedical Engineering, Purdue University, West Lafayette, Indiana

Approved by:

Dr. George R. Wodicka

Head of the Graduate Program

To my family.

ACKNOWLEDGMENTS

I would like to acknowledge people who make this journey unforgettable and meaningful. First, I would like to give considerable gratitude to my advisor, Dr. Chien-Chi Lin for providing the opportunity to advance my professional knowledge. Throughout the Ph.D. training, he spent much time on improving my writing skill, critical thinking, gave much freedom to develop my creativity, and shaped me into an independent scientist/engineer. I would also like to thank my co-advisor, Dr. Harbin, thesis committee, Dr. Yokota, and Dr. Solorio for their invaluable feedback and input.

Second, I would like to thank the colleagues in Lin lab: Dr. Han Shih, Tanja Green, Camron Daws, John Bragg, Britney Hudson, Matt Arkenberg, Dustin Moore, Kevin Peuler, Han Nguyen, and Hunter Johnson for the patience, advice and technical support. Additionally, they have made days in lab interesting and meaningful. Special thanks to a group of people who have been pursuing Ph.D. degree or stayed in Indy with me these years, Hui-Chen Wang, Wei-Neng Hsu, Fang-Yi Lin, Tzu-Ling Chen, Wen-Hao Chiang, Arnold Huang, and Robin Yeh for all the encourage and accompany in U.S.

Finally, I express the deepest gratitude to my parents: Shui-En Liu, Li-Hsien Tsai, brother: Hung-Chi Liu, and my best friend: Eddie Guo, Jim Lin for their support and understanding throughout the time in graduate school.

TABLE OF CONTENTS

LIST OF FIGURES

LIST OF TABLES

LIST OF ABBREVIATIONS

2D	Two-dimensional
3D	Three-dimensional
4-HPA	4-Hydroxyphenylacetic acid
4D	Four-dimensional
5-FU	5-Fluorouracil
ACN	Acetonitrile
AKT1	Serine-threonine protein kinase
AKT2	AKT Serine/Threonine Kinase 2
ANOVA	Analysis of variance
BCL2L1	Bcl-2-Like Protein 1
CAFs	Cancer-associated fibroblasts
CAMPTOSAR	Irinotecan hydrochloride
CAT	Catalase
CAT	Catalase
CDKN2A	Cyclin Dependent Kinase Inhibitor 2A
cDNA	Complementary DNA
CM	culture media
CSCs	Cancer stem cells
ddH2O	Double distilled water
DMEM	Dulbecco's modified eagle medium
DOPA	Dihydroxyphenylalanine
DMSO	Dimethyl sulfoxide
DTT	dithiothreitol
Tyr_{ase}^{Deoxy}	Deoxy-tyrosinase
Tyr_{ase}^{Oxy}	Oxy-tyrosinase
EC	Enzyme Commission
ECM	Extracellular matrix
EDC	1-Ethyl-3-(3-dimethylaminopropyl) carbodiimide
EGF	Epidermal growth factor
ELK1	ETS Transcription Factor

EMMPRIN	Extracellular-matrix metalloproteinase inducer
EMT	Epithelial-mesenchymal-transition
ERBB2	Encodes Receptor Tyrosine Kinase 2
ERK	Extracellular-signal-regulated kinase
FAD	Flavin
FBS	Fetal bovine serum
FGF	Fibroblast growth factors
FMN	Flavin mononucleotide
FOLFIRINOX	Oxaliplatin
GAGs	Glycosaminoglycans
Gel_{NB}	Norbornene functionalized gelatin
Gel_{NBHPA}	Norbornene and 4-hydroxy functionalized gelatin
GEMM	Genetically engineered mouse model
GEMZAR	Gemcitabine hydrochloride
GOX	Glucose oxidase
HA	Hyaluronic acid
HGF	Hepatocyte growth factor
HTS	High-throughput screening
HIF-1α	hypoxia-inducible factor-1α
HRP	Horseradish peroxidase
HSCs	Hepatic stellate cells
IL	Interleukin
IPMNs	intraductal papillary mucinous neoplasms
JAK	Janus kinase
JAK3	Janus Kinase 3
JNK	c-Jun N-terminal kinase
L-DOPA	L-Dopamine
L-tyr	L-tyrosine
LAP	lithium phenyl-2,4,6-trimethylbenzoylphosphinate
MAO B	Monoamine oxidase B
MAP2K2	Mitogen-Activated Protein Kinase 2
MAPK	Mitogen-activated protein kinase

MBTH	3-Methyl-2-benzothiazolinone hydrazone
MCNs	Mucinous cystic neoplasms
MeHA	Methacrylated hyaluronan
MMPs	Matrix metalloproteinases
NHS	N-Hydroxysuccinimide
NF-κB	Nuclear factor kappa-light-chain-enhancer of activated B cells
PanIN	Pancreatic preneoplastic lesion
PCCs	Pancreatic cancer cells
PDAC	Pancreatic ductal adenocarcinoma
PDGF	Platelet-derived growth factor
PEG	Poly(ethylene glycol)
PEG8NB	Poly(ethylene glycol)-8 arm-norbornene
PEGDA	PEG-diacrylate
PLA	Poly(lactic acid)
POSTN	Periostin
PPO	Polyphenol oxidases
PSCs	Pancreatic stellate cells
PVA	Poly(vinyl alcohol)
RAC1	Small GTP Binding Protein Rac1
RAC2	Small GTP Binding Protein Rac2
RF	Riboflavin
RHAMM	Receptor for hyaluronic-acid-mediated motility
RHOA	Ras Homolog Family Member A
ROCK	Rho/Rho-associated kinase
ROS	Reactive oxygen species
SHH	Sonic hedgehog
SOS1	SOS Ras/Rac Guanine Nucleotide Exchange Factor 1
STAT	Signal transducer and activator of transcription protein
STAT5B	Signal Transducer and Activator of Transcription 5B
STAT6	Signal Transducer and Activator of Transcription 6
TARCEVA	Erlotinib hydrochloride
TAZ	TEA-domain DNA-binding transcription factors

TFA	Trifluoroacetic acid
TGF-β	Transforming growth factor-β
TGFβR1	TGF-β receptor 1
THA	Thiolated hyaluronic acid
TIMPs	Tissue inhibitors of matrix metalloproteinases
TIS	Triisopropylsilane
TME	Tumor microenvironment
TP53	Tumor protein 53
Tyr_{ase}	Tyrosinase
UV	Ultraviolet
VEGF	Vascular endothelial growth factor
VICs	Valvular interstitial cells
Wnt	Wingless-related integration site
YAP	Yes-associated protein
α-SMA	α-Smooth muscle actin

NOMENCLATURE

Symbol	Unit	Description
G’	Pa	Storage or elastic modulus
G”	Pa	Loss or viscous modulus
M_c	Da	Average molecular weight between crosslinks
MW_A	g/mole	Molecular weight of macromer
MW_B	g/mole	Molecular weight of crosslinker
ρ_{H2O}	g/cm^3	Density of water
ρ_{PEG}	g/cm^3	Density of PEG
ξ	nm	Mesh size
q	-	Mass swelling ratio
Q	-	Volume swelling ratio
f_A	-	Number of reactive functionalities for macromers
f_B	-	Number of reactive functionalities for crosslinkers
V_c	-	Density of elastically active chains
χ_{12}	-	Flory-Huggins interaction parameter for a PEG-H2O system
K_i	mM	Substrate inhibition constant
K_m	mM	Enzyme-substrate affinity
k_{cat}	1/s	Turnover rate
W_{Dried}	mg	Dried polymer weight
$W_{Swollen}$	mg	Swollen weight
r_E	nm	Hydrodynamic radius of the solute molecule
$D_E^{solution}$	m^2/s	Enzyme diffusivity in solution
D_E^{gel}	m^2/s	Enzyme diffusivity in hydrogel
V_P	μM/min	Enzymatic reaction rate
Y	-	Critical volume for the water molecule

ABSTRACT

Author: Liu, Hung-Yi. Ph.D.
Institution: Purdue University
Degree Received: August 2019
Title: Dynamic hydrogels for studying tumor-stroma interactions in pancreatic cancer
Major Professor: Lin, Chien-Chi. Ph.D.

Pancreatic cancer is the present third leading cause of all cancer-associated deaths with a under 9% 5-year survival rate. Aggressive tumor progression and lack of early detection technique lead to the fact that most patients are diagnosed at terminal stage - pancreatic ductal adenocarcinoma (PDAC). Despite that numerous therapeutic approaches have been introduced, most options cannot advance to or fail at the clinical trials. It has been suggested that previous failure is due to insufficient understanding of PDAC tumor microenvironment (TME). Human PDAC is composed of severely fibrotic tissue (i.e., desmoplasia) that harbors a variety of malignant cells (e.g., pancreatic stellate cells, cancer-associated fibroblasts, macrophages, etc.), excessive extracellular matrices (ECM), as well as abnormal expression of growth factors, cytokines, and chemokines. Multiple cell-cell and cell-ECM interactions jointly result in a stiffened, hypoxic, and fluid pressure-elevated PDAC tissue. The resulting pancreatic TME not only physically hinders penetration of therapeutics, but also dynamically interacts with the residing cells, regulating their behaviors.

Increasing tumor tissue stiffness in PDAC is not only a passive outcome from desmoplasia, but an active environmental factor that promotes tumor survival, growth, and invasion. However, traditional in vitro cell culture systems such as two-dimensional (2D) culture plate and animal models are not ideal for mechanistic understanding of specific cell-matrix interactions. Therefore, dynamic hydrogels have been introduced as a category of advanced biomaterials that exhibit biomimetic, adaptable, and modularly tunable physiochemical property. Dynamic hydrogels can be precisely engineered to recapitulate a variety of aspects in TME, from which to investigate the role of dynamic tumor-stroma interaction in PDAC progression. The goal of this dissertation was to exploit synthetic polymers (i.e., poly(ethylene glycol) (PEG)) or natural ECM (i.e., gelatin and hyaluronic acid (HA)) as precursors to prepare the dynamic cancer-cell laden gels. The design utilized the orthogonal thiol-norbornene photopolymerization to prepare the primary homogenous

gel network. Next, through further functionalizing gel precursors with phenolic derivatives, enzymatic reaction (i.e., tyrosinase) or flavin mononucleotide (FMN)-mediated photochemistry could be harnessed to manipulate the dynamic changes of substrate mechanics. Experimentally, a computational model and the associated validation were presented to investigate the process of gel stiffening. Finally, these techniques were integrated to prepare cell-laden gels with spatial-temporally tunable properties that were instrumental in exploring the synergistic effects of dynamical matrix stiffening and presence of HA in promoting epithelial-mesenchymal transition (EMT) in PDAC cancer and stromal cells.

CHAPTER 1. INTRODUCTION

1.1 Pancreatic cancer overview

Cancer is a class of disease which initiates from a subset of cells with genetic aberration in human tissue [1, 2]. These mutated cells exhibit rapid proliferation and develop capability of resistance to apoptosis [3]. The multiple abnormal cellular events collectively result in formation of a begin tumor [4]. At the initial stage, tumor is still localized at its onset, which can be simply removed through surgical intervention. Few cancer types lack noticeable symptoms or early diagnosis techniques, which results in the consequently poor prognosis. It leads to the fact that patients are commonly diagnosed cancer at the advanced stage, where cancer cells develop capability of distant metastasis and weak response to anti-cancer drugs [5]. With the lowest 5-year survival rate (i.e., ~9 %) (Figure 1.1A) and the minimal improvement (Figure 1.1B), pancreatic cancer shares all the above lethal characteristics [6]. Moreover, pancreatic cancer is the present third leading cause of all cancer-related deaths and projected to be the second by 2030 in United States [6, 7].

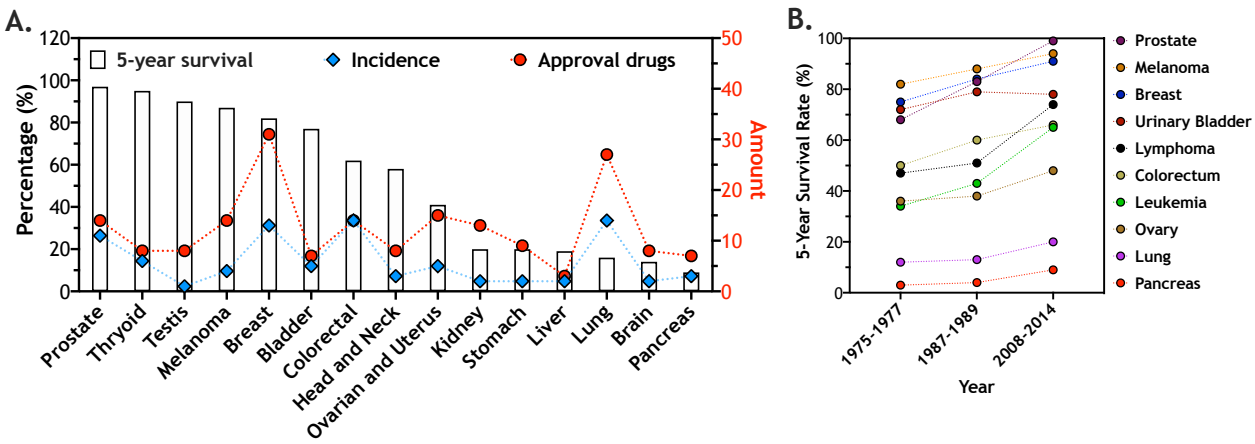

Figure 1.1. Statistical report among all cancer types, including (A) 5-year survival rate, number of available drugs, and disease incidence. (B) Change of 5-year survival rate among all the cancer types from year 1975 to 2014 [8].

Development of pancreatic cancer is a multi-stage but rapid process, from few stages of pancreatic preneoplastic lesions (PanINs) that consists of intraductal papillary mucinous neoplasms (IPMNs) and mucinous cystic neoplasms (MCNs) to the last stage - pancreatic ductal

adenocarcinoma (PDAC) [9-15]. In the clinical practice, more than 50 % patients are diagnosed at PDAC stage when malignant cells have already metastasized to lung or liver, forming the secondary tumor tissue. Few available anti-cancer drugs have been presented to treat patients with pancreatic cancer since 1997, such as gemcitabine (GEMZAR), 5-fluorouacil (5-FU), and FOLFIRINOX (i.e., combination of leucovorin (folinic acid), 5-FU, irinotecan (campto), and oxaliplatin) [16, 17]. Unfortunately, these options are mostly categorized in the purely cytotoxic therapeutics without the targeting capability, which can eliminate both healthy and cancer cells. Thus, the high-dose will cause strong side effect (e.g., fatigue, nausea, diarrhea, and loss of appetite), whereas the low-dose may have weak drug response on tumor [16]. Both the consequences are far from optimistic to patients.

Nowadays, numerous innovative therapeutics have been introduced to target the universal generic mutation in human pancreatic cancer, such as a subset of small GTPases (KRAS, ~95 %), cyclin-dependent kinase inhibitor 2A (CDKN2A, ~90 %), and tumor suppressors (i.e., tumor protein 53 (TP53), ~75 % and SMAD4, ~50 %). Additional to these oncogenes, it has been indicated the irregular signaling transductions such as mitogen-activated protein kinase/extracellular-signal-regulated kinase (MAPK/ERK), Wnt/β-catenin [18, 19], phosphoinositide 3-kinase/protein kinase B (PI3K/AKT) [20, 21], nuclear factor kappa-light-chain-enhancer of activated B cells (NF-κB), janus kinase/signal transducer and activator of transcription protein (JAK/STAT), yes-associated protein/TEA-domain DNA-binding transcription factors (YAP/TAZ) [22-24], transforming growth factor-β/SMAD (TGF-β/SMAD) [25, 26], c-Jun N-terminal kinase (JNK) [27, 28], and sonic hedgehog (SHH) [24] collectively contributing to the aggressiveness and chemoresistance of PDAC [29-32]. The current improvement on high-throughput screening (HTS) technique, such as expansion of drug analogue library (e.g., genome sequencing and development of transgenic mice), higher HTS efficiency, and the advanced approaches for characterizing therapeutic structure, it allows researchers to efficiently recognize the potential targets within pancreatic TME. However, while these advanced therapeutics have shown promising results in the drug discovery phase, almost 95% of them showed high discrepancy on evaluation of tumor response to the treatment that cannot advance to clinical success [33-35].

1.2 Tumor microenvironment (TME) in pancreatic cancer

The previous failure on developing therapeutics against pancreatic cancer has been attributed to lack of considering the PDAC tumor microenvironment (TME) when evaluating drug efficacy in the preclinical trial [9, 36]. Tumor formation not only affects the adjacent cell behavior, but also changes the cell residing microenvironment, as well as local tissue homeostasis [9-12, 14, 15, 29-32]. Human PDAC is notorious for the presence of abundant fibrotic stroma in primary tumor tissue, which occupies almost 90% of overall tumor volume. Accumulation of the cancer stroma has been associated to the desmoplastic reaction (i.e., desmoplasia) [32, 37, 38]. Such unique tumor tissue property has been suggested not just a passive outcome from desmoplasia, but an important environmental factor aggravating tumor progression [21, 39]. Presence of desmoplasia results in the abnormal expression of stromal cells and extracellular matrix (ECM), which dynamically interact with cancer cells, generating multiple homotypic/heterotypic cell-cell and cell-ECM interactions [40-44]. These abnormal biological events collectively contribute to a dense, hypoxic, hypovascular, and fluid-pressure elevated TME [18, 19]. Hence, current strategy has been focused on proposing approaches to inactivate the signature signaling transductions or inhibit the synthesis of some specific soluble factors within pancreatic TME, as shown in Figure 1.2 [24, 45].

In addition to target the non-cellular components mentioned above, pancreatic stromal cells (e.g., pancreatic stellate cells (PSCs), cancer-associated fibroblasts (CAFs)) is a group of cellular component within pancreatic TME that has been drawn attention at early 2000s, owing to their capability on stroma deposition [46-50]. The cell-cell interaction between stromal and pancreatic cancer cells (PCCs) has been found to foster tumor invasion [32, 51-56]. For example, PSCs are normally distinguished by their spherical cell morphology and capability of vitamin-B storage in the healthy pancreas [46-49]. In the PDAC tissue, PSCs surprisingly exhibit the myofibroblast-like morphology and produce high level of α-smooth muscle actin (α-SMA), ECM, matrix metalloproteinases (MMPs), and tissue inhibitors of matrix metalloproteinases (TIMPs) [47, 53, 57]. These factors are commonly presented during tissue fibrosis and remodeling. Nowadays, although the different PSCs behavior have been reasoned to be outcome of the cell-cell interaction or the tissue stiffening during PDAC progression, it is still under exploring [49, 58].

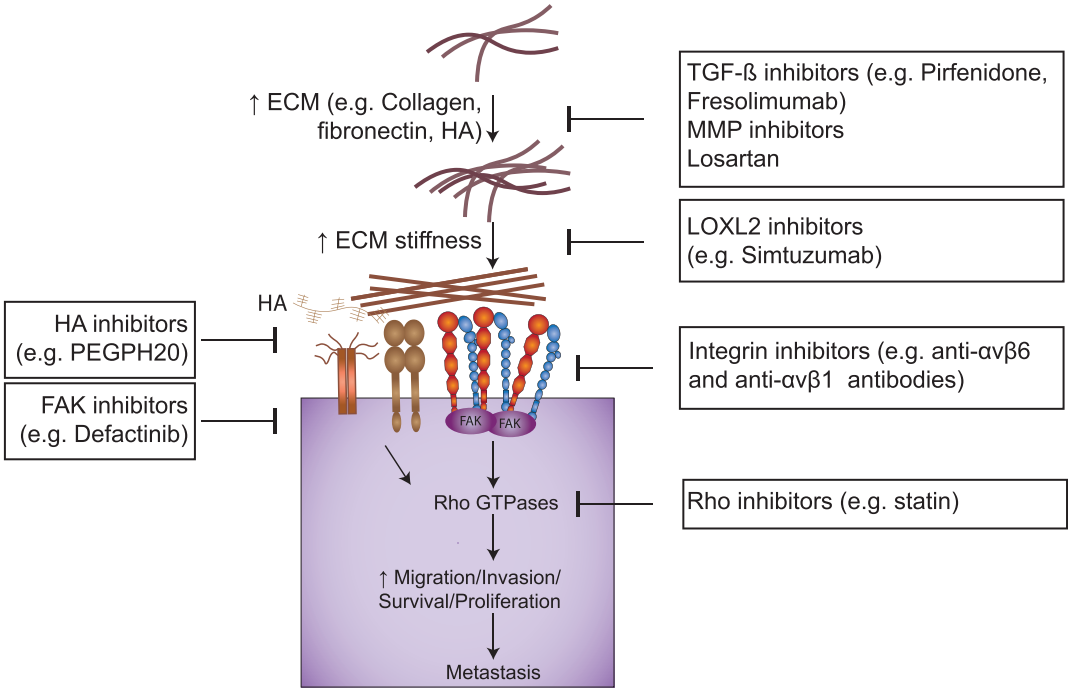

Figure 1.2. Developing therapeutics to target the critical signaling cascades or the important environmental factors in PDAC tumor tissue [17, 45].

Current advances have shed light on influences of tumor ECM in PDAC development [29, 31, 59-61]. Some specific natural ECM has been identified in PDAC stroma, such as collagen, fibronectin, laminin, periostin (POSTN), proteoglycans (i.e., hyaluronic acid (HA)), and glycosaminoglycans (GAGs). While these ECMs can support tissue structure and functionality, they are found to accelerate tumor progression, dictate cancer metastasis and drug resistance. Collagen, as one of the primary PDAC stroma, has been suggested to increase tumor tissue stiffness and enhance tumor invasion [62-65]. Especially, type I collagen has been revealed to reduce cancer cell epithelial characteristics (e.g., E-Cadherin), but to augment its mesenchymal characteristics (e.g., N-Cadherin, Vimentin, SNAIL, TWIST, SLUG, and ZEB-1), which typically presents on cell with epithelial-mesenchymal transition (EMT) [66-71]. When undergoing EMT, cells lose the epithelial junctions, apical-basal polarity, and reorganize the cytoskeleton that modifies local tissue organization [72-76]. Activation of EMT on the malignant cells is an essential and vital cellular activity at onset of cancer metastasis, which initiates from primary tumor formation, tissue fibrosis, remodeling, cell invasion, extravasation, and intravasation to secondary

colonization. All of these steps have been shown influenced by cell-ECM interaction. Another pancreatic tumor ECM, hyaluronic acid (HA) is a type of polysaccharide, commonly overexpressed in both human (hTME) and mouse PDAC (mTME) tissue, as shown in Figure 1.3 [77]. HA has the distinctive physicochemical property, such as high-water retention and viscosity. Depends on the molecular weight or amount of HA, it can alter the physicochemical property of PDAC tissue from different aspects [77-87]. The low molecular weight HA can enhance tissue inflammation and angiogenesis, whereas the high molecular weight HA elevates local tissue interstitial fluid pressure, anti-angiogenic, immune-suppressive, and hinders drug penetration physically [30, 50, 59, 60, 88-90]. Furthermore, HA can bind to some distinct cell membrane receptors (e.g., CD44, extracellular-matrix metalloproteinase inducer (EMMPRIN), and receptor for hyaluronic-acid-mediated motility (RHAMM)), which induces the corresponding downstream signaling (i.e., FAK, PI3K, MAPK, and KRAS) to promote cancer cell growth, chemoresistance, and self-renewal [79, 91-95]. Moreover, HA can also induce MMP-2 and MMP-9 secretion which direct cancer invasion [84].

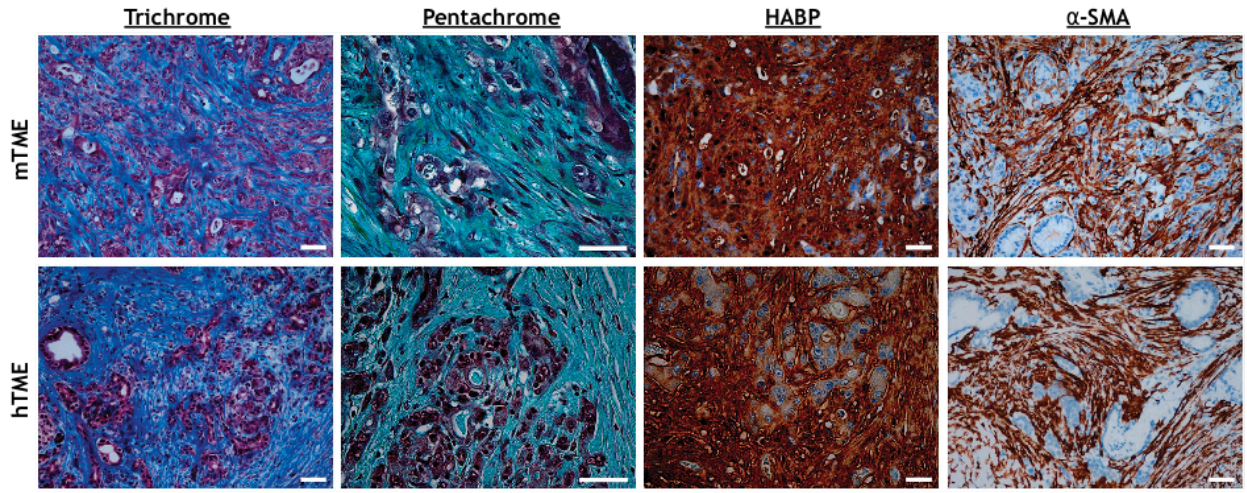

Figure 1.3. Tissue composition of desmoplastic stroma in mouse (mTME) and human (hTME) pancreatic cancer tissue at PDAC stage. Masson's trichrome stains the collagen in TME (blue), while Movat's pentachrome highlights the presence of glycosaminoglycans (GAGs) and mucins (blue) co-localized with collagen (turquoise/green). Histochemistry with hyaluronic acid binding protein (HABP) confirms the abundance of HA in TME and immunohistochemistry for a-SMA identifies activated PSCs, or myofibroblasts (Scale bars: 50 mm) [77].

While previous research has greatly enriched the knowledge about cell-cell and cell-ECM interactions within PDAC tissue, there are few unique cell-ECM interactions still far from well-

understood. For example, the increasing PDAC tissue stiffness has been indicated to impose biophysical signals on residing malignant cells (i.e., mechanotransduction), regulating several biological events, such as cell migration, differentiation, and tissue organization [96, 97]. However, limited *in vitro* cell culture systems can integrate the tunable mechanics (i.e., stiffness, porosity, and viscoelasticity) into the substrate property. Two-dimensional (2D) cell culture is a simple and fundamental technique for researchers to conveniently identify generic target, validate biomarker, and apply drug screening [98, 99]. Since the 2D culture plate and dish are generally produced by the flattened glass or polystyrene, they have the static substrate property and mechanics (G' ~3 GPa) [100-102]. Another frequently-used approach, genetically engineered mouse model (GEMM) with natural matrices (e.g., laminin, fibronectin, elastin, and collagen) but beneficial for assessing PDAC pathobiology or generic mutation during tumor angiogenesis, metastatic processes and evaluating drug uptake during blood circulation [103, 104]. These animal-based models are manipulated through subcutaneous transplanting human cancer cells into living animals. Nonetheless, they have the complex substrate property and the tumor response to drug treatment in animal models are rarely (i.e., ~8 %) corresponded with that to human [105]. Owing to advantages as standardized manufacturing technique, convenience, commercial availability, and ease for accessing biological information, 2D culture platform and animal models are still the major platform to study cancer in pre-clinical trial. However, the static or the confounding substrate physicochemical property is difficult for these systems to perform reductionist study in cell-ECM interactions within pancreatic TME. Moreover, impact of tissue physical property (i.e., stiffness, porosity, and viscoelasticity) on tumor behaviors cannot be explored using these systems [33, 106-108].

1.3 Hydrogel systems for recapitulating the tumor microenvironment

Three-dimensional (3D) cell culture systems, such as tumor spheroids and cell-laden hydrogels are more sophisticated platforms capable of preserving native tumor structure and permitting cell to receive environmental stimuli from 3D [109-113]. With high biocompatibility and controllable substrate physiochemical property, cancer cell-laden hydrogels are highly attractive as tumor models for studying impact of cell-ECM interaction on cell fate [114-121]. For example, matrigel extracted from the decellularized animal tissue, has been frequently employed

as artificial cell microenvironment. Matrigel resembles several natural ECM and growth factors that can easily retain cells outside of the living body with high cell viability and functionality. The matrigel-based gel systems have been used to study tumor angiogenesis and invasion [122-124]. Unfortunately, a critical drawback for using matrigel-based system to study cell-ECM interaction is its confounding substrate compositions. Furthermore, when using matrigel-based systems to study tissue mechanics (i.e., biophysical signal), it is essential to adjust amount of precursors to produce gel with varying mechanics. However, the native ECM and growth factors within matrigels are also changed between conditions at the same time. It convolutes the interpretation from two different cell-ECM interactions (i.e., biochemical and biophysical signaling). Synthetic hydrogels (e.g., poly(ethylene glycol) (PEG), poly(vinyl alcohol) (PVA), and poly(lactic acid) (PLA)) can be endowed with user-defined composition and mechanical property [125-127]. Through incorporating biomimetic peptides or natural matrices, the semi-synthetic gel systems can present the tissue heterogeneity [128-133]. The adaptability and versatility of the synthetic hydrogels are also convenient for researchers to decouple different interactions within tumor tissue. Additionally, these chemically defined hydrogels are advantageous owing to their high reproducibility, cost-efficiency, and amenability for the scale-up production.

A group of innovative approaches, dynamic hydrogel systems have been appealing for studying cell-ECM interaction in a physiological manner. This technique allows for tuning the physicochemical property in the presence of cells [134-137]. The design principle of a dynamic gel system is to perform two-step reaction on the functionalized polymeric materials. The first reaction is for building hydrogel primary network, whereas the second is for manipulating the property changes, such as matrix stiffening, degradation, and presence of bioactive ligand. For example, Young *et al.* have presented a cardiomyocytes-encapsulated gel system with feature of temporal gel stiffening [138]. Cells were encapsulated in gel by crosslinking thiolated HA (THA) and PEG-diacrylate (PEGDA) via the thiol-ene click reaction. The gel stiffening was then achieved by the additional thiol-diacrylate crosslinkings. The degree of gel stiffening was tunable via applying varying molecular weight of macromers (i.e., PEGDA) as gel precursors. Interestingly, the result suggested that the temporal matrix stiffening promoted differentiation of cardiomyocytes, which has not been shown when cells were cultured in a static stiff matrix. Although it noted the importance of dynamic mechanical changes on cellular processes, the process of gel stiffening in this study was spontaneous, not capable of precisely controlling the initiation of stiffening process.

Stimuli-responsive hydrogels with the higher controllability are a group of advanced approaches that have been introduced to dynamic hydrogels fabrication [139-145]. Substrate property of these systems can be user-defined through applying an exogenous stimuli, as list in Table 1.1 [146-153]. All of these approaches not only demonstrated capability of stimuli-responsive hydrogels for mimicking the spatial-temporal nature in TME, but also emphasized impact of the environmental inputs on cellular processes [143, 151, 154].

Table 1.1. Stimuli-responsive gel systems for dynamical cell culturing.

Stimuli		Material	Parameters	References
Physical	**pH**	• Anionic or cationic material (e.g., alginate, collagen, chitosan) • Poly(diethylaminoethyl methacrylate) (PDEAEMA) • Poly(N-vinyl caprolactam) (pNVCL) • Pluronic F-127	• Anion or cation contents • Exposure time	[15, 96, 155] [156] [142]
	Temperature	• Poly(ethyl pyrrolidine methacrylate) (PEP) • Poly(ethyl piperazine acrylate) (PAcrNEP) • Poly(N-isopropylacrylamide) (pNIPAAm) • poly(N'N'-diethyl acrylamide) (PDEAAm)	• Temperature • Exposure time	[157-161]
	Electromagnetic field	• Poly(ethylenimine) (PEI) • Polyelectrolyte • Poly(2-(acrylamide)-2 methylpropanesulfonic acid) (PAMPS) • Poly(2-hydroxyethy methacrylate) (PHEMA)	• Field force • Field flux • Electroconductivity • Exposure time	[15, 162]
Chemical	**Light**	• Polyacrylamide • Methacrylated polymers • Polyethylene glycol diacrylate (PEGDA)	• Wave length • Light intensity • Exposure time • Path length • Quantum efficiency	[101, 163-165]
	Enzyme	• Oxidoreductase • Ligase • Lyase • Isomerase • Hydrolase • Transferase	• Enzyme or substrate concentration • Exposure time • Turnover number • Enzyme-substrate binding affinity	[166-170]

Various external stimuli (Table 1.1.) have been used to initiate property changes in hydrogels. However, some of these techniques lack tunability or flexibility. For example, pH and temperature are the parameters heavily associated with cell culturing condition. Variation of these parameters may lead to reduced cell viability or abnormal cell behavior. On the other hand, photo-responsive systems can be applied in a spatial-temporally controlled manner. Current photochemistry is largely limited to the utilization of ultraviolet light (UV) light and synthetic photoinitiators, which may cause additional cytotoxicity. Therefore, current advances have been dedicated to preparing hydrogels using visible light irradiation and more cytocompatible photoinitiators.

In addition to photochemistry, enzymatic reaction is increasingly used in hydrogel synthesis and modification. Enzymes are advantageous owing to their substrate specificity, mild reaction conditions, and predictable kinetics. As such, enzymatic reactions have been employed for gel fabrication in drug delivery and tissue regeneration [171-173]. According to the Enzyme Commission (EC) database, enzymes are classified into seven categories based on their functionality [174], including oxidoreductase (EC1), transferase (EC2), hydrolase (EC3), lyase (EC4), isomerase (EC5), ligase (EC6), translocases (EC7). Among these enzymes, oxidoreductase-catalytic reactions involve electrons transfer, which can be applied to polymeric crosslinking. The commonly used oxidoreductases include hydrogen peroxide (H_2O_2)-dependent peroxidases and oxygen (O_2)-dependent polyphenol oxidases (PPO), as listed in Table 1.2 [175].

Table 1.2. Oxidoreductases for enzyme-mediated polymerization [175].

Type	Enzyme	Substrate
Oxygen (O_2)-associated polyphenol oxidase (PPO)	• Tyrosinase (tyr_{ase}) • Laccase • Glucose oxidase (GOX)	• Phenol derivatives
Hydrogen peroxide (H_2O_2)-associated peroxidases	• Horseradish peroxidase (HRP) • Catalase (CAT) • Hematin • Cytochrome c peroxidase • Lignin peroxidase • Glutathione peroxidase • Myeloperoxidase • Lactoperoxidase • Haloperoxidases • Glucose oxidase (GOX) • Monoamine oxidase B (MAO B)	• Phenol derivatives • Aniline • Vinyls • Thioanisole • Alkene • N-N-Dimethylaniline • Dihydroxyfumaric acid • Aldehyde

Horseradish peroxidase (HRP) is a typical peroxidase that has been widely used for producing injectable hydrogels or adhesive gel patches in the field of tissue regeneration [176-178]. Macromers with phenolic moieties (e.g., tyramine, dopamine, and catechol) have been crosslinked via HRP-mediated reaction to prepare hydrogels, bioadhesives, and nanoparticles [179-183]. To initiate HRP-catalytic reaction, it is essential to have the addition of hydrogen peroxide (H_2O_2), forming HRP/H_2O_2 complex. In the presence of HRP substrate, with which the resulting HRP/H_2O_2 complex react, generating products via the two-step single electron transferring [175]. The process contains the carbon-carbon (C-C) or carbon-oxygen (C-O) coupling within the HRP substrate [183]. However, such reaction will manipulate reactive oxygen species (ROS), causing potential cytotoxicity to the encapsulated cells. Furthermore, due to the high reactivity of peroxidases, they have multiple types of substrate which minimize the enzyme specificity (Table 1.2). On the other hand, mussel-inspired polyphenol oxidase (PPO)-mediated reactions have also been used for fabricating cell-laden hydrogels [181, 184-186]. For example, tyrosinase (tyr_{ase}) is a PPO-associated enzyme extracted from bacteria or plants [187, 188]. In the presence of oxygen (O_2), copper-containing tyr_{ase} catalyzes the oxidation of tyrosine-contained molecules into 3,4-dihydroxy-phenyl-L-alanine (DOPA), *ortho*-quinone (*o*-quinone), and subsequently DOPA dimers [189-192]. This reaction does not require free radicals, nor does it generate ROS in the process, making it a mild and highly biocompatible reaction for biomedical applications. Finally, this dissertation will focus on using light and enzyme as external stimuli to design dynamic hydrogels as desmoplasia-mimetic systems for studying tumor-stroma interactions.

CHAPTER 2. OBJECTIVES

Dynamical change of tumor tissue physicochemical properties often results in several interactions between cell and its microenvironment. These tumor-stroma interactions have attracted much attention due to their impact on pancreatic cancer malignancy, metastasis, and chemoresistance. These schemes include not only the 3D (i.e., length, width, and height), but also the fourth dimension 4D (i.e., time), such as the spatiotemporally increasing tumor tissue mechanics. While the cell-ECM interactions in pancreatic TME have been shown influential in PDAC progression, minimal *in vitro* culture platforms are capable of representing these unique features. To this end, the main objective of this dissertation was to design cancer cell-laden hydrogels that are adaptable, biomimetic, and with highly tunable mechanics. Next, these systems were used to study the impact of evolving matrix mechanics in TME on pancreatic cancer cell behaviors. The last objective of this dissertation was to integrate the critical matrix components found in PDAC tumor tissue into a biomimetic and dynamic hydrogel platform. The specific objectives of this dissertation were:

Objective 1. Develop dynamic stiffening hydrogels via an enzymatic reaction

Matrix stiffening is a typical but crucial dynamic process in PDAC tissue. To mimic a temporally stiffening TME, a dynamic stiffening gel was designed via first photopolymerizing norbornene-functionalized PEG-based macromer with bi-cysteine bi-tyrosine peptide crosslinker into hydrogels. Next, through incubating in media containing an enzyme (i.e., tyrosinase), the cell-laden hydrogels will be dynamically stiffened owing to the extra crosslinking between peptide-bound tyrosine residues. Chapter 3 of this dissertation describes the hydrogel design principle, crosslinking technique, computational model prediction, as well as corresponding experimental validation. In Chapter 4, additional bifunctionalities (e.g., laminin-derived peptide with RGD sequences and MMP-sensitive crosslinker (i.e., KCYGPQGIWGQYCK) were tailored in this gel system to optimize the condition for cell culture. Finally, pancreatic stellate cells (PSCs) were encapsulated in this gel system to assess system biocompatibility and the effect of matrix stiffening on cell behaviors.

Objective 2. Biomimetic and enzyme-responsive dynamic hydrogels for studying cell-matrix interactions in pancreatic ductal adenocarcinoma

In order to design a pathophysiologically relevant *in vitro* culture system, a biomimetic and dynamic gel system was presented in Objective 2. This PDAC-inspired hydrogel system was fabricated by functionalized hyaluronic acid (HA) and gelatin, a denatured collagen. Specifically, gelatin was dually modified with norbornene (NB) and additional hydroxyphenylacetic acid (4-HPA) moieties. The resulting dual-functionalized gelatin (i.e., Gel_{NBHPA}) enabled both light-initiated thiol-norbornene crosslinking and enzyme-mediated DOPA dimer formation. Physicochemical property of this gel system and experimental validation of the increasing gel mechanics were systematically investigated. To explore the role of HA (i.e., biochemical signaling) or/and matrix stiffening (i.e., biophysical signaling) in PDAC progression, two different human pancreatic cancer cell line (i.e., COLO-357 and PANC-1) were cultured in this gel system with pre-defined compositions, including (1) Gel_{NB} with PEG4SH (Gel_{NB}&PEG), (2) Gel_{NB} with THA (Gel_{NB}&HA), (3) Gel_{NBHPA} with PEG4SH (Gel_{NBHPA}&PEG), and (4) Gel_{NBHPA} with THA (Gel Gel_{NBHPA}&HA) (Chapter 5).

Objective 3. Dynamic PEG-peptide hydrogels via visible light and FMN-induced tyrosine dimerization

Photo-responsive hydrogels are another group of hydrogel system which have shown fundamental in controlling different substrate properties, including stiffness, bioactive motifs. To achieve another important dynamic feature in PDAC tissue, the spatially distributed bioactive motifs, nutrients or the tissue mechanics in gradient. A visible light-mediated dynamic gel system was introduced by using the nature-derived photoinitiator (i.e., flavin mononucleotide (FMN)). Although this system was prepared with the same gel precursors in objective 1, it integrated the FMN and visible light-initiated tyrosine dimerization to achieve the spatial-temporal controllability. To validate the modular tunability in hydrogel stiffening, effect of FMN and visible light treatment on changes of gel mechanics was investigated via adjusting the treating FMN concentration, amount of the built-in tyrosine residues within peptide crosslinkers, dosage, and duration of visible light exposure. To examine spatial tunability of this photo-responsive system, the tyrosine-functionalized fluorescent molecule, photomask, and varying light exposure time

were utilized to exhibit the user-defined gel patterning. For the *in vitro* cell study, pancreatic cancer cells (PCCs) were encapsulated in this gel for evaluation of system biocompatibility and impact of temporal gel stiffening on cancer cell fate. Additionally, to study effect of increasing tissue mechanics on PDAC stromal cells, the pancreatic cancer-associated fibroblasts (CAFs) were seeded on top of the system with regional gel stiffening, achieved by using the soft photolithography technique (Chapter 6).

CHAPTER 3. A DIFFUSION-REACTION MODEL FOR PREDICTING ENZYME-MEDIATED DYNAMIC HYDROGEL STIFFENING

(As published in *Gels*, 2019 (5) 1-17)

3.1 Abstract

Hydrogel systems with the spatiotemporally controllable mechanics have been increasingly employed for studying impact of tissue mechanical property on cell fate processes. These dynamic hydrogels are particularly suitable for recapitulating the temporal stiffening of a tumor microenvironment. To this end, we have reported an enzyme-mediated stiffening hydrogel system where tyrosinase (tyr_{ase}) was used to stiffen the orthogonally crosslinked cell-laden hydrogels. Herein, a mathematical model was proposed to describe enzyme diffusion and reaction within a highly swollen gel network and to elucidate the critical factors affecting the degree of gel stiffening. Briefly, Fick's 2nd Law of Diffusion was used to predict enzyme diffusion in a swollen poly(ethylene glycol) (PEG)-peptide hydrogel, whereas the Michaelis-Menten model was employed for estimating the extent of enzyme-mediated secondary crosslinking. To experimentally validate model predictions, we designed a hydrogel system composed of 8-arm PEG-norbornene (PEG8NB) and bis-cysteine containing peptide crosslinker. Hydrogel was crosslinked in a channel slide that permits one-dimensional diffusion of tyr_{ase} along the micro-channel. Both the model prediction and experimental results suggested that the increasing crosslinking over gel network did not significantly affect enzyme diffusivity during process of the dynamic stiffening. On the other hand, the diffusion path length and the duration of enzyme incubation were more critical for determining distribution of tyr_{ase} and formation of additional crosslinking in the hydrogel network. Finally, we have demonstrated that the enzyme-stiffened hydrogels exhibited elastic properties similar to other chemically crosslinked hydrogels. This study provided a better mechanistic understanding in process of the enzyme-mediated dynamic stiffening gel systems.

3.2 Introduction

Hydrogels are the hydrophilic and crosslinked water-swollen polymers [122, 193, 194], particularly suitable for mimicking extracellular matrix (ECM) in human tissues [195, 196]. The effects of ECM compositions and degradability on cell fate processes have been extensively studied with these systems [197, 198]. In recent years, mechanical properties of cell microenvironment are increasingly considered as a crucial environmental factor, regulating tissue regeneration and disease progression [199, 200]. As such, hydrogels with the spatiotemporally regulated mechanics are increasingly utilized for studying mechanotransduction in healthy and diseased cells. Mechanical properties of a water-swollen hydrogel have been well-established by Anseth and colleges using Flory-Rehner and rubber elasticity theories [201, 202]. In general, hydrogel elasticity, viscosity, and plasticity are characterized via tensile, dynamic mechanical analysis, or shear rheometry [203, 204]. Mechanical properties of a swollen-hydrogel are directly related to gel crosslinking density, which are determined by macromer functionality, precursor compositions, polymerization conditions, and degree of gel swelling [205]. Understanding the impact of these factors on hydrogel crosslinking is instrumental when preparing hydrogels with user-defined and highly tunable mechanical properties [206].

Gels can be prepared through chemical reactions (e.g., chain-growth or step-growth polymerization) or physical interactions (e.g., electrostatic or supramolecular binding) [143, 207]. Regardless of the crosslinking method, however, bulk modulus of a hydrogel generally scales with its crosslinking density [208, 209]. Therefore, hydrogels with a build-in mechanism for post-gelation adjustment of crosslinking density are ideal for mimicking the stiffening process of a diseased tissue. In this regard, various dynamic cell-laden gel systems are being actively introduced for studying the changes of tissue mechanics on cell behaviors [96, 152, 210-212]. In principle, dynamic stiffening hydrogels are fabricated with a two-step crosslinking process. The first crosslinking reaction forms a primary gel network with immobilization of additional polymerizable moieties for the secondary polymerization [118, 164, 212]. The later increases the crosslinking density and hence stiffness of the cell-laden hydrogel. For example, Young *et al.* designed cardiomyocyte-encapsulated hydrogels crosslinked by thiolated hyaluronic acid (THA) and poly(ethylene glycol)-diacrylate (PEGDA) [138]. The cell-laden hydrogels were stiffened gradually via thiol-acrylate Michael-type addition. While the two-step click reactions achieved

dynamic increase in gel crosslinking, the degree of stiffening was pre-determined by the thiol/acrylate contents and could not be modularly and dynamically controlled post-gelation.

In order to control the magnitude of matrix stiffening, our lab has introduced an enzyme-mediated dynamic hydrogel system [166, 213]. The primary cell-laden hydrogel network was formed by thiol-norbornene photochemistry using PEG-8-arm norbornene (PEG8NB) and bis-cysteine, bis-tyrosine-contained peptide crosslinker (i.e., CYGGGYC). Here, we incorporated additional tyrosine residues on the peptide crosslinker sequence to serve as substrates for tyrosinase (tyr_{ase}). Upon diffusing into the gel network, tyr_{ase} oxidizes *tyr* residues on peptide to generate 3,4-dihydroxy-phenylalanine (DOPA) that leads to the formation of additional DOPA-dimer [214, 215]. The later was key to the dynamic gel stiffening scheme. Previously, we have applied the tyr_{ase}-stiffened cell-laden gels to evaluate the impact of dynamic matrix stiffening on activation of pancreatic stellate cells (PSCs) [213] and metastatic potential of pancreatic cancer cells (PCCs) [166]. To provide a better understanding in enzyme diffusion and reaction during the gel stiffening process, we proposed here a mathematical model that accounts for both enzyme diffusion and reaction within the highly swollen hydrogel network. The key parameters associated with Fick's 2^{nd} law and Michaelis-Menten kinetics were investigated, including the catalytic reactions between and tyr-containing peptidyl crosslinkers. Furthermore, we employed a channel slide to experimentally validate model prediction of the one-dimensional diffusion into the PEG-peptide hydrogel [170]. These experimental data were further used to verify and enhance model predictions, which could offer pivotal information when applying enzymatic reaction for dynamic stiffening of cell-laden hydrogels.

3.3 Results and Discussion

3.3.1 Design principle of the dynamic hydrogel network

In this work, we used a bio-inert norbornene-functionalized polymer PEG8NB (Figure 3.1A) and a bifunctional peptidyl crosslinker (CYGGGYC, Figure 3.1B) to prepare gel as an experimental model for verifying computational prediction of the enzyme-induced matrix stiffening. The major advantage of a PEG-based gel prepared from orthogonal step-growth polymerization is its high gelation efficiency that produces a well-defined and nearly ideal network structure (Figure 3.1C). Additionally, thiol–norbornene hydrogel affords much more uniform

distribution of tyrosine residues in the primary gel network, which increases substrate accessibility for tyr_{ase}-mediated reaction (Figure 3.1D). In principle, the infiltrating catalyzes DOPA dimer formation, which leads to the increasing gel crosslinking density, as well as gel stiffness (Figure 3.1E).

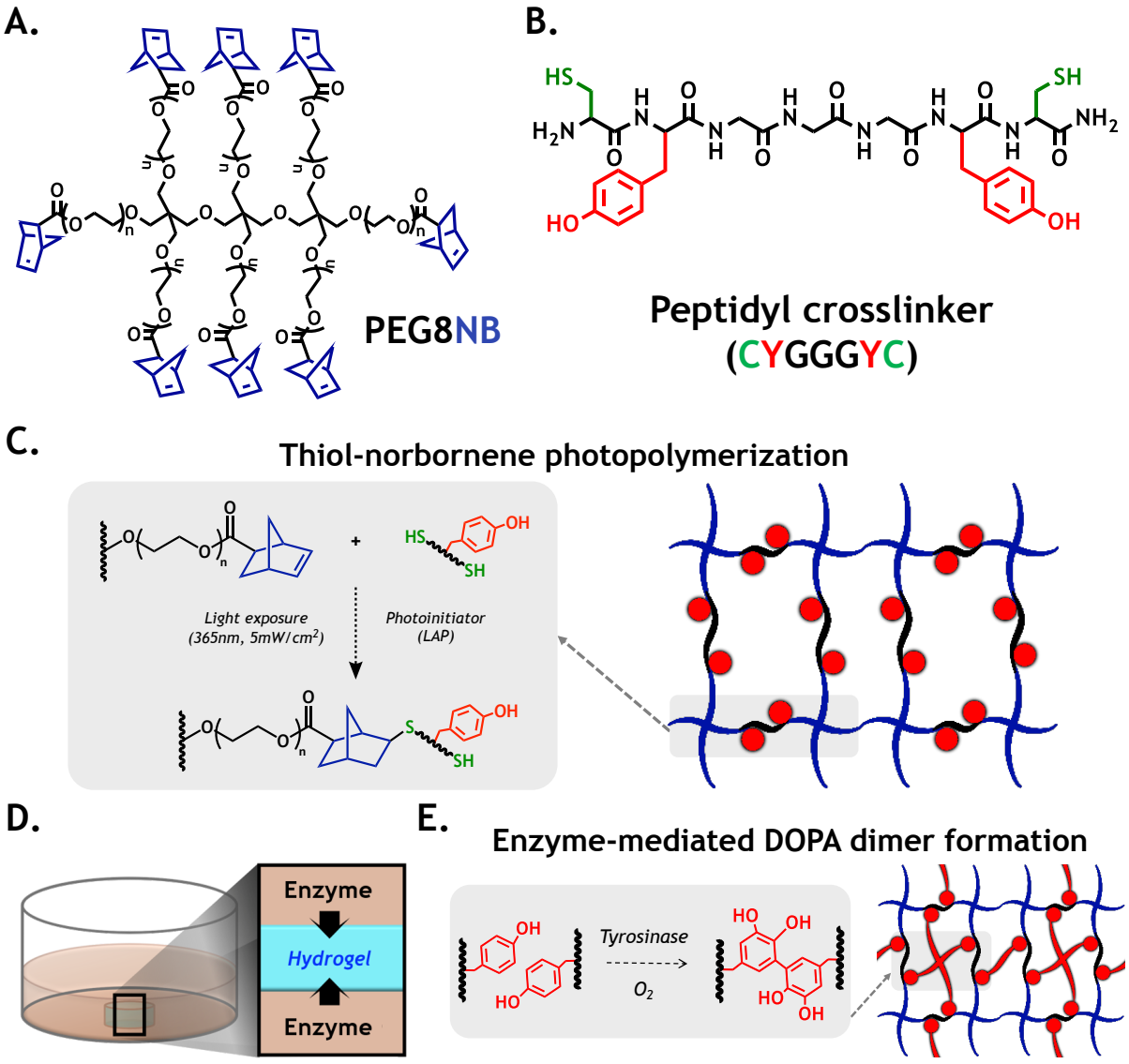

Figure 3.1. Design principle of the enzyme-mediated gel stiffening. (A) Structure of 8-arm PEG-norbornene (PEG8NB, 20 kDa, N ≅ 56); (B) bis-cysteine/bis-tyrosine peptide crosslinker (i.e., CYGGGYC); (C) schematic of thiol–norbornene photopolymerization for forming primary hydrogel network.

3.3.2 Correlation of gel crosslinking density, mesh size, and enzyme diffusivity

Hydrogel crosslinking density has a significant impact on the diffusion of soluble molecules in the network [216]. More specifically, mesh size of a gel network is the primary factor determining diffusivity of any solute into a highly swollen gel. During the process of enzyme-mediated gel stiffening, gel crosslinking density not only increases with time, but also vary spatially. Consequently, the diffusivity may be impacted by the stiffened gel network. The diffusivity of any solute in a highly swollen hydrogel can be estimated by the classical Lustig-Peppas relationship, which describes solute diffusivity (i.e., D_E^{gel}) using a correlation of hydrodynamic radius of the solute (R_E), mesh size of the network (ξ), and the diffusivity of the solute in a solution (see section 3.5.2). These parameters can be obtained from literature or experimentally determined. To gain insight into the impact of gel crosslinking on enzyme diffusion in hydrogels, we prepared hydrogels with different macromer compositions that led to varying shear moduli ranging from ~0.5 kPa to ~10 kPa (Figure 3.2A). At any given formulation (and modulus), the mass (q) and volumetric (Q) swelling ratio, as well as the corresponding mesh size (ξ), of the resulting hydrogels could be readily determined. These results were then used to establish a correlation between gel stiffness and D_E^{gel} (see section 3.5.2).

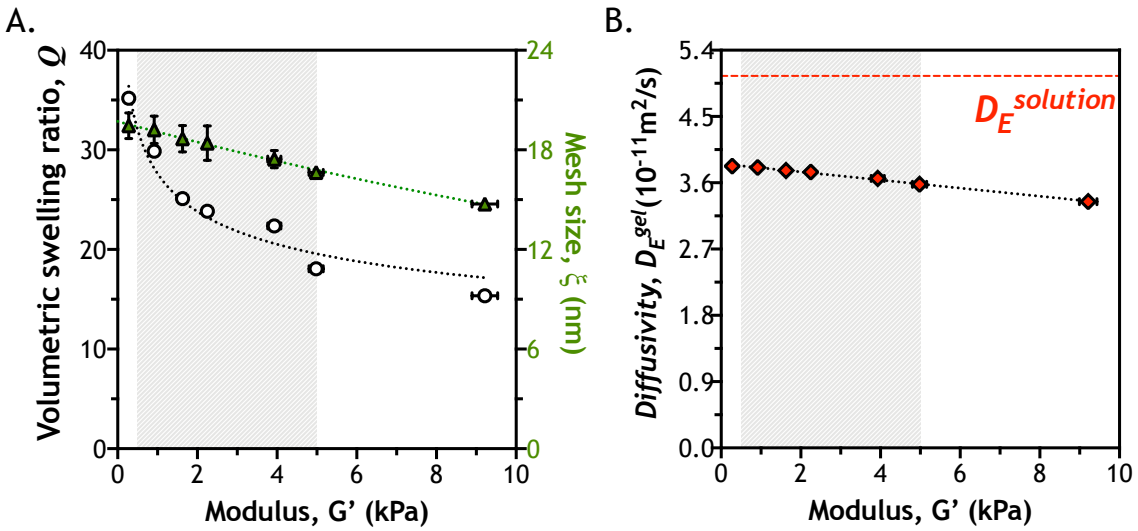

Figure 3.2. Correlation of crosslinking density, mesh size, and enzyme diffusivity. (A) volumetric swelling ratio (Q) and mesh size (ξ) of PEG-peptide (CYGGGYC) hydrogels with different shear moduli (G'); (B) correlation of enzyme diffusivity (D_E^{gel}) with gel modulus. $D_E^{solution}$ is the diffusivity of enzyme (i.e., tyr_{ase}) in solution, independent of the hydrogel modulus.

The shear moduli of gels ranging from ~0.5 kPa to ~5 kPa is relevant to changes of tissue stiffness during tumor progression [217]. In this study, we experimentally determined the Q and ξ of hydrogels within shear moduli from ~0.5 kPa to ~5 kPa. Within this range, Q was decreased from ~30 to ~18, while ξ was correspondingly decreased from ~19 nm to ~15 nm (Figure 3.2A). It is important to note that this range of mesh size is much larger than the hydrodynamic radius of tyr_{ase} (r_E = 4.5 nm) [187]. Next, we used this range of mesh size to estimate D_E^{gel} using the Lustig–Peppas relationship [218]. Clearly, diffusivity of tyr_{ase} in solution ($D_E^{solution}$) was not significantly affected by changes of gel mesh size (i.e., both ξ and Q approach infinity). In a soft gel (G' ~0.5 kPa), D_E^{gel} was 3.80×10^{-11} m^2/s. In a stiff gel (G' ~5 kPa), it was decreased slightly to 3.58×10^{-11} m^2/s (Figure 3.2B). Conceptually, since D_E^{gel} only decreased ~5.8 % in a stiff gel (G' ~5 kPa), the gradually increasing gel crosslinking should not impose a significant hindrance for tyr_{ase} diffusion during the process of gel stiffening.

3.3.3 Prediction of enzyme diffusion in hydrogels with varying gel crosslinking density

Correlations of gel modulus, mesh size, and enzyme diffusivity as shown in , have provided critical information regarding the extent to which D_E^{gel} was affected by increasing gel crosslinking density. To establish the premise that the gradually stiffening hydrogel would not impose significant diffusion hindrance for tyr_{ase}, we first predicted the distribution of diffusing tyr_{ase} within hydrogels using a constant D_E^{gel}**,** which contributed to the following equation (3.1):

$$\frac{\partial C_E(x,t)}{\partial t} = -D_E^{gel} \cdot \frac{\partial^2 C_E(x,t)}{\partial x^2} . \tag{3.1}$$

where 3.80×10^{-11} m^2/s and 3.58×10^{-11} m^2/s were used to represent in a soft and stiff gel (D_E^{gel}), respectively. If distributions of tyr_{ase} in hydrogels with these two diffusivities show negligible differences within a relevant time scale, it can then be safely assumed that the stiffening network can only exhibit a minimal hindrance on enzyme transport. Equation (3.1) was solved numerically using the initial and boundary condition, listed in section 3.5.2 [219]:

$$C_E(x,t) = C_{E0} \cdot \left\{ 1 - \frac{4}{\pi} \sum_{n=0}^{\infty} \left[\frac{1}{2n+1} \cdot e^{-D_E(2n+1)^2\pi^2 \cdot t / h^2} \cdot \sin\left(\frac{x(2n+1)\pi}{h}\right) \right] \right\} \tag{3.2}$$

The computational results from Equation (3.2) represented time- and space-dependent tyr_{ase} diffusion into a soft (Figure 3.3A) or a stiff gel (Figure 3.3B). We plotted the results from 0 hour to 6 hour, a timeline previously used for tyr_{ase}-mediated hydrogel stiffening [166, 213]. From the prediction results, it was clear that, regardless of enzyme diffusivity, the entire hydrogel was

equilibrated (i.e., $C_E/C_{E0} \approx 1$) with the infiltrating enzyme after only 2 hours of diffusion. Furthermore, a symmetrical tyr_{ase} distribution could be clearly seen along the thickness of the gel owing to the bi-directional diffusion condition. While significant variations of tyr_{ase} distribution as a function of time and space were observed in the first 2 hour, there was no discernable differences between enzyme diffusion in softer and stiffer hydrogels, suggesting that the stiffening process would not significantly hinder enzyme diffusion in these hydrogels. Finally, a gradient of enzyme concentration could be expected near the surface of the gel within the first 2 hour. These predictions had justified that, regardless of gel-network crosslinking density, a period of 6-hour tyr_{ase} incubation was sufficient for the gel stiffening.

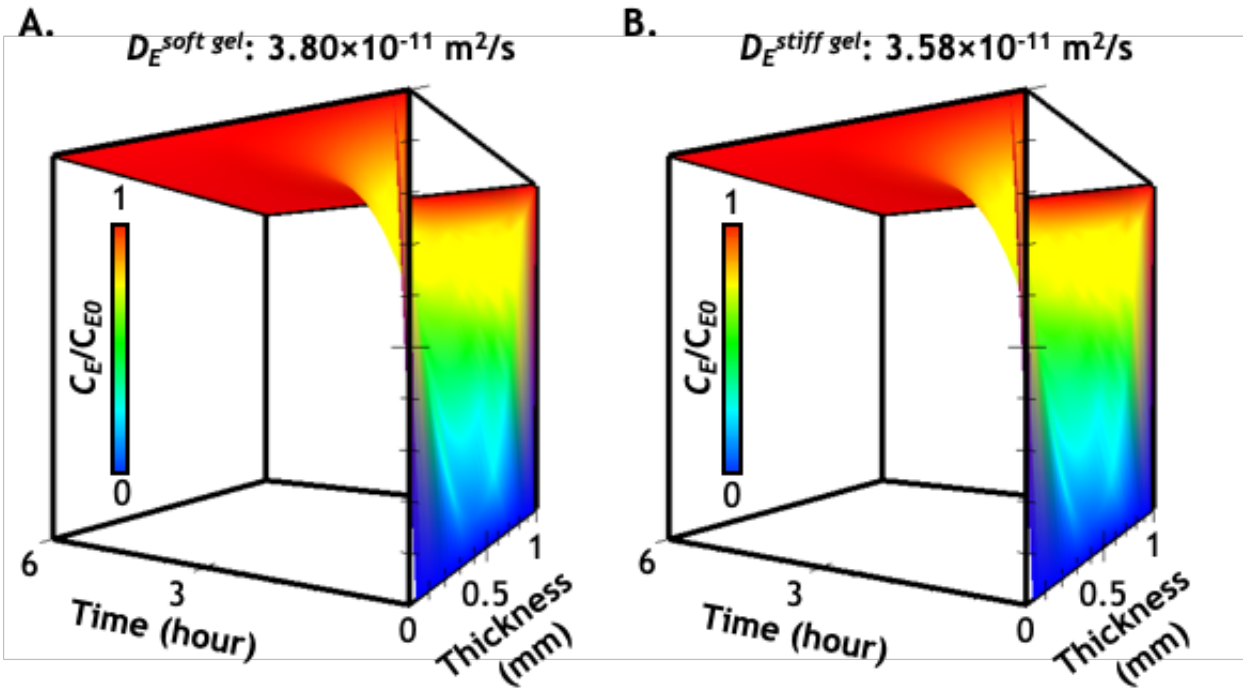

Figure 3.3. Diffusion profile of tyr_{ase} throughout hydrogel systems with varying stiffness: (A) concentration profiles of tyr_{ase} in a soft gel (G' ~0.5 kPa); (B) concentration profiles of tyr_{ase} in a stiff gel (G' ~5 kPa). Note that gel thickness was set at 1 mm with the assumption that tyr_{ase} diffuses symmetrically from the surfaces ($x = 0$ and $x = 1$) to the center of the hydrogel ($x = 0.5$).

3.3.4 Verification of enzyme diffusion in non-stiffening hydrogels

In addition to model predictions, we obtained the experimental tyr_{ase} diffusion results through imaging tyr_{ase} distribution in a hydrogel strip casting in a channel slide, which was connected by two reservoirs with a constant initial enzyme concentration (C_{E0}). We prepared the hydrogel with high shear moduli (G' ~5 kPa), which represented a stiffened hydrogel network that

had the most hindrance in solute transport. Figure 3.4A illustrated the progression of bi-directional tyr_{ase} transport into the thin hydrogel strip (i.e., thickness = 1 mm), where tyr_{ase} concentration in the hydrogel (C_E) increased as more enzyme molecules infiltrate the hydrogel. Figure 3.4B showed the experimental tyr_{ase} diffusion profiles at 1, 3, and 6 hours (i.e., solid symbols), as well as the diffusion model predictions (i.e., dashed lines). After 1 and 3 hours of the bi-directional diffusion, both experimental data and the model prediction exhibited symmetrical tyr_{ase} distribution along the diffusion path. After 6-hour enzyme diffusion, C_E at center of the gel reached equilibrium ($\simeq C_{E0}$) in both experiment and model prediction. Since the gels were formed at a higher crosslinking density (i.e., G' ~5 kPa) in this example, a 6-hour period should be sufficient for hydrogels with lower stiffness (i.e., higher mesh size) to reach equilibrium with C_{E0}. While these assessments have not yet taken enzyme reactions (see section 3.5.4) into account, they complement the diffusion model prediction shown in Figure 3.4B. These results are also supported by experimental stiffening results reported previously, in which gel stiffening was completed within 6 hours tyr_{ase} incubation [213].

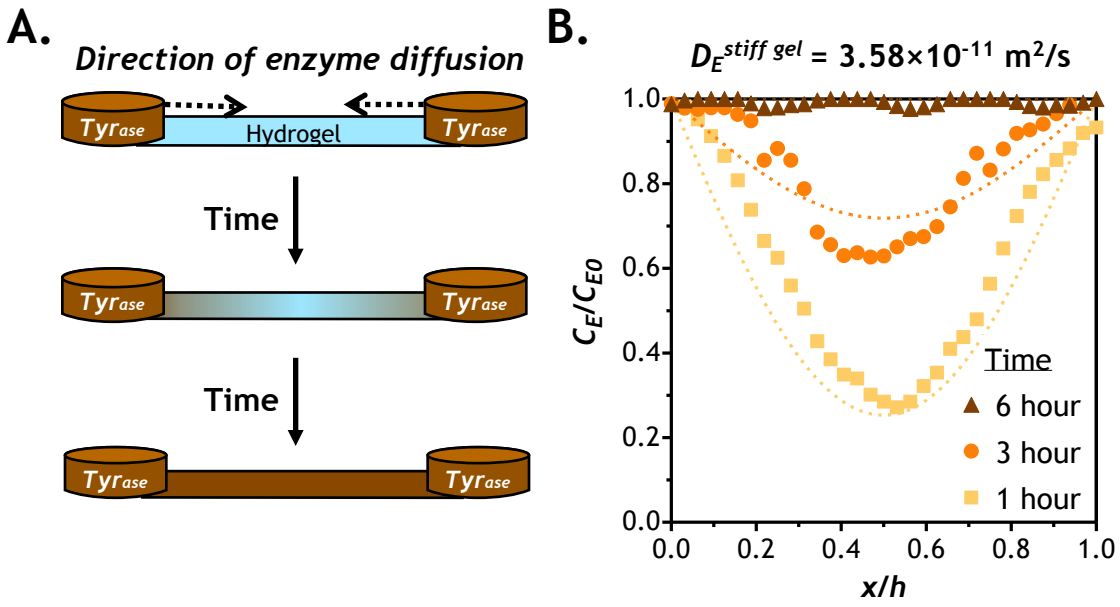

Figure 3.4. Schematic and validation of enzyme diffusion into hydrogel. (A) Experimental set up for validation of tyr_{ase} diffusion into a PEG-peptide (CYGGGYC) hydrogel with 1 mm thickness. (B) Comparison of experimental data (symbols) and computational results (dashed lines). Note that the modeling results were derived from the Fick's second law (See section 3.5.2) using diffusivity of tyr_{ase} in a stiff gel (G' ~5 kPa) at 1, 3, and 6 hour.

3.3.5 Effect of the treating enzyme concentration on reaction velocity

In addition to predicting enzyme diffusion in gels with different crosslinking densities, we investigated catalytic reactions of tyr_{ase} using different phenolic substrates. Tyr_{ase} is known to catalyze oxidization of tyrosine, tyramine, and other phenolic derivatives (e.g., 4-hydroxyphenylacetic acid (4-HPA) into DOPA, DOPAquinone, and finally to DOPA dimers [187]. The catalytic reaction of tyr_{ase} involves several steps, including a monophenol cycle, a diphenol cycle, and substrate inhibition (Figure 3.5A) [188]. First, the non-activated deoxy-tyrosinase (tyr_{ase}^{Deoxy}) binds with the oxygen molecule (O_2) to generate an activated form of tyrosinase (tyr_{ase}^{Oxy}). In the presence of L-*tyr*, tyr_{ase}^{Oxy} initiates the monophenol cycle that produces DOPA. Since DOPA and L-*tyr* are both substrate of the tyr_{ase}^{Oxy}, the excess L-*tyr* can react with both tyr_{ase}^{Oxy} and the DOPA-tyr_{ase}^{Oxy} complexes, and thus reaction may move toward the diphenol cycle or substrate inhibition [214]. To gain more insight into this reaction kinetics, we first monitored the concentration of dissolved O_2, as its disappearance is the first step in the activation of tyr_{ase}. As expected, concentration of dissolved O_2 decreased only after the addition of tyr_{ase} (at the 2-min mark) to the L-*tyr* containing solution (Figure 3.5B). O_2 content dropped rapidly, except for the lowest enzyme concentration used (i.e., 0.3 μM). Furthermore, dissolved O_2 was completely depleted within 5, 3.5, and 2 min when the solution was added to 1.5, 2.25, and 3 μM tyr_{ase}, respectively. At 0.3 μM tyr_{ase}, only ~3% decrease in dissolved O_2 was detected after 6 min of enzyme addition, potentially because the rate of oxygen consumption by the small amount of enzyme was much slower than its replenishment from the air.

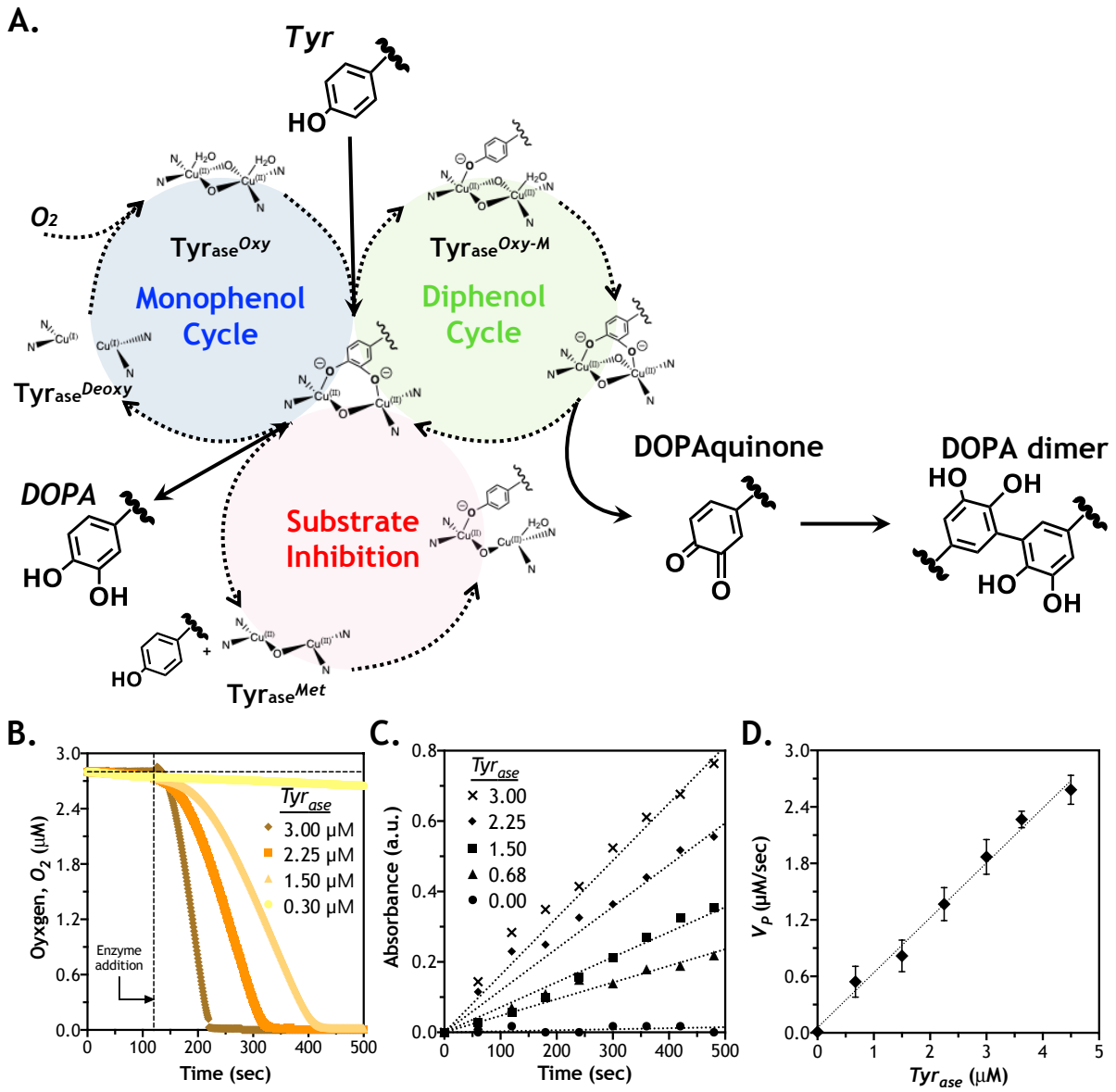

Figure 3.5. Evaluation of enzymatic reaction kinetics using tyr$_{ase}$ and L-*tyr*, (A) steps and kinetics of tyr$_{ase}$-catalyzed DOPA dimer formation; (B) detection of oxygen content (O_2) as a function of time and enzyme concentration (see section 3.5.3); (C) quantification of L-*tyr* oxidation using the MBTH assay (i.e., absorbance at 475 nm); (D) correlation of reaction velocity (V_P) and the treating tyr$_{ase}$ concentration.

Figure 3.5B suggested that a faster tyr$_{ase}$ reaction was owing to the rapid consumption of dissolved oxygen. However, the consumption of dissolved oxygen represented only the first step in the tyr$_{ase}$ reaction cycle (i.e., from tyr$_{ase}^{Deoxy}$ to tyr$_{ase}^{Oxy}$, Figure 3.5A). In order to understand the kinetics of subsequent reaction steps, it was necessary to determine the amount of actual product formation. To this end, we utilized the MBTH assay to monitor the production of DOPA [220,

221]. In principle, MBTH reacts with oxidized substrates through both monophenol and diphenol cycles and produces a visible complex with a pink color [222]. Although higher DOPA contents were detected at higher doses of tyr_{ase} (Table 3.1.), all reactions (except for 0 μM tyr_{ase}) were not completed within 6 min of testing, suggesting that the catalytic step of tyr_{ase}/L-*tyr* reaction was slower than the rate of oxygen binding to tyr_{ase}^{Deoxy}. Additionally, the kinetics of DOPA production appeared to be in a linear relationship with respect to time. After plotting reaction velocity as a function of enzyme concentration, a linear correlation was established (Figure 3.5D). This linear relationship might be due to a relatively high substrate concentration (i.e., 10 mM) when compared with the high binding affinity between L-*tyr* and tyr_{ase}. In the case of a much smaller K_M compared with C_S and K_M can be omitted in either the regular or the modified Michaelis–Menten equation (see section 3.5.4), which yielded the following equations:

$$V_P = \frac{k_{cat} \cdot C_E \cdot C_S}{\cancel{K_M} + C_s(1+\frac{C_S}{K_i})} = k_{cat} \cdot C_E(1+\frac{C_S}{K_i}) \tag{3.3}$$

$$V_P = \frac{k_{cat} \cdot C_E \cdot C_S}{\cancel{K_M} + C_s} = k_{cat} \cdot C_E \tag{3.4}$$

As shown in Equations (3.3) and (3.4), omitting K_M results in a linear correlation between V_p and C_E regardless of the status of substrate inhibition, which can be characterized by a decreasing reaction rate at high substrate concentrations [223]. Using the general or modified Michaelis–Menten equation, we obtained k_{cat} and K_M for tyr_{ase}-mediated reactions (Table 3.1.). Clearly, all three substrates exhibited at least 10-fold lower K_M than the substrate concentration used in the experiments (i.e., 10 mM, Figure 3.6A), thus justifying the omission of K_M in Equation (3.3) and Equation (3.4).

Table 3.1. Kinetic constant in tyr_{ase}-mediated reaction

Parameter	Unit	L-*tyr*	L-DOPA	CYGGGYC
k_{cat}	s^{-1}	0.93	8.63	0.60
K_M	mM	0.85	1.02	0.58
K_i	mM	19.85	-	-
R^2	-	0.956	0.971	0.98

3.3.6 Effect of Substrate Concentration of Enzymatic Reaction

As mentioned earlier, utilization of L-*tyr* for tyr_{ase} may exhibit substrate inhibition that reduces catalytic activity of tyr_{ase}. To evaluate whether such an effect exists when a peptide substrate is used, we treated a model peptide CYGGGYC with tyr_{ase} and used other substrates as controls (e.g., L-*tyr* or L-DOPA). As shown in Figure 3.6A, tyr_{ase} exhibited the highest reactivity for L-DOPA (V_P = 8.6 μM/s) among all substrates. The reaction rates for L-*tyr* and CYGGGYC were 0.88 and 0.70 μM/s, respectively. Tyr_{ase}/L-DOPA reaction appeared to proceed through the diphenol cycle without discernable substrate inhibition, as the reaction velocity reached a plateau value at high substrate concentration. Furthermore, we noticed a slightly lower maximum reaction rate at a higher concentration (2-10 mM) of L-*tyr*, which was indicative of substrate inhibition (Figure 3.5A). Therefore, the modified Michaelis–Menten equation (see section 3.5.4) was utilized to obtain kinetic constants for tyr_{ase}/L-*tyr* reaction. Interestingly, there was no significant substrate inhibition when tyrosine-containing peptide (i.e., CYGGGYC) was used as substrate for tyr_{ase}. It was likely that the peptidyl residues exhibited different affinity (K_M) for tyr_{ase}. Indeed, Marumo *et al*. have investigated the effect of peptide sequencing on tyr_{ase}-catalytic reaction efficiency [189]. Compared to the L-*tyr*, some tyrosine-containing peptide sequences (e.g., *Gly-Tyr-Gly* and *Lys-Glu-Thr-Tyr-Ser-Lys*) have a higher DOPA conversion ratio when reacting with tyr_{ase} due to a higher binding affinity between tyr_{ase} and oxidized L-*tyr*. Upon fitting the reaction velocity data with the general or modified Michaelis–Menten model (see section 3.5.4), we found that peptidyl *tyr* exhibited a higher binding affinity (i.e., lower K_M) with tyr_{ase} than the soluble L-*tyr* (Table 3.1.).

Another key aspect for designing an enzymatic stiffening hydrogel is to understand how fast the enzyme fully converts substrate (e.g., peptidyl tyrosine residues) into product (i.e., additional DOPA dimer crosslinking). At any given enzyme and substrate concentration, the time

needed to convert all substrates into products can be approximated through dividing the initial substrate content (C_{S0}) by reaction velocity (V_P) and catalytic efficiency (k_{cat}). Regardless of substrate concentration, there is a hyperbolic relationship between reaction time and enzyme concentration. Naturally, at a higher enzyme concentration, the time needed to convert all substrates (i.e., 10 mM) into products would be much faster than using a lower enzyme concentration. For example, at 3 µM of tyr_{ase}, it would take about 2 hours to convert all 10 mM of substrate into product. Without considering the enzyme diffusion, Figure 3.6C provides a first pass estimation of the time needed to achieve stiffening at any given enzyme and substrate concentration.

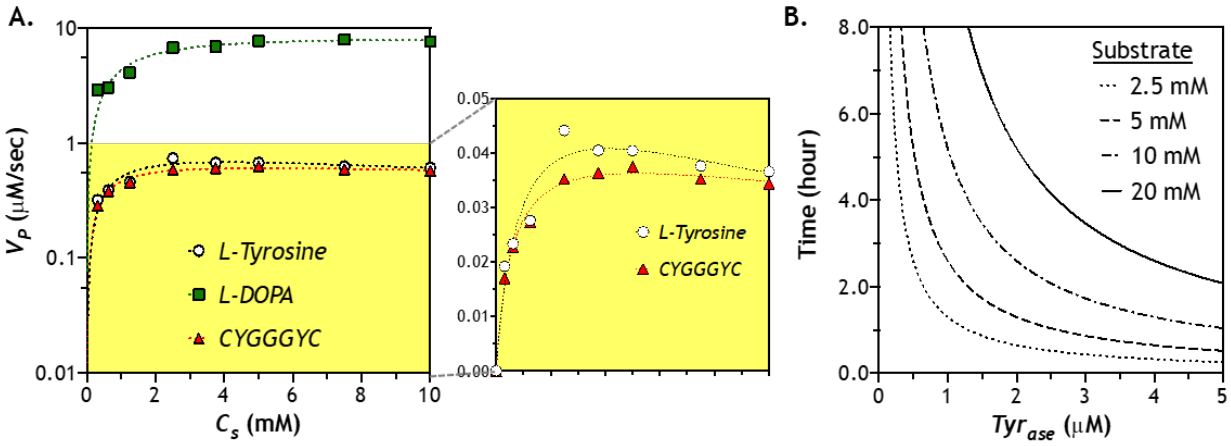

Figure 3.6. Effect of substrate concentration on tyr_{ase}-mediated catalytic reaction: (A) reaction kinetics of tyr_{ase} (0.6 µM) using different substrates (2-10 mM), including L-tyrosine (L-*tyr*), L-Dopamine (L-DOPA), and peptide crosslinker (CYGGGYC) - kinetics of L-*tyr* and CYGGGYC are highlighted in the right panel; (B) estimation of the time for the enzyme to convert all substrates into product.

3.3.7 Analytical simulation of diffusion-reaction in hydrogel

We have separately characterized/analyzed tyr_{ase} diffusion (Figure 3.4B) in hydrogels and studied enzymatic reactions of tyr_{ase} with tyrosine-containing peptide crosslinker (Figure 3.6A). Next, we considered both enzyme diffusion and reaction to obtain profiles of peptide substrate consumption and product formation within the gel network over time and space. First, we generated computational data using tyr_{ase} diffusion profile $C_E(x,t)$, which served as input for the Michaelis–Menten equation. With experimentally obtained k_{cat} and K_M for the peptide linker CYGGGYC (Table 3.1.), we employed the Lambert-W function to numerically solve the

Michaelis–Menten equation (see section 3.5.4) [224, 225]. First, (substrate consumption rate) can be rearranged into the following equation:

$$\frac{dC_S}{dt} = -\frac{V_{Max} \cdot C_S}{K_M + C_S} \qquad \Rightarrow \qquad K_M \cdot \ln(\frac{C_{S0}}{C_S}) + (C_{S0} - C_S) = V_{Max} \cdot t \tag{3.5}$$

where the space- and time-dependent $C_S(x,t)$ could be expressed as equation (3.6):

$$C_S(x,t) = K_M \cdot W\left\{f(x,t)\right\} \tag{3.6}$$

The space- and time-dependent product (i.e., oxidized tyrosine or DOPA) concentration could be expressed using the Equation (3.7), since it was equivalent to the amount of consumed substrate (i.e., L-*tyr*) consumed:

$$C_P(x,t) = C_{S0} - K_M \cdot W\left\{f(x,t)\right\} \tag{3.7}$$

$$\ln\left\{f(x,t)\right\} = W\left\{f(x,t)\right\} + \ln\left\{W\left\{f(x,t)\right\}\right\} \tag{3.8}$$

$$f(x,t) = \frac{C_{S0}}{K_M} \cdot e^{\left(C_{S0} - C_E(x,t) \cdot k_{cat} \cdot t \,/\, K_M\right)} \tag{3.9}$$

We then plotted solution of Equation (3.7), as shown in Figure 3.7A and B, which described the formation of DOPA dimers owing to the tyr_{ase}-mediated reaction within the gel network. The prediction result demonstrated that the majority of network-immobilized tyrosine residues would be converted to product within the first 6 to 8 hour of tyr_{ase} (3 μM) diffusion/reaction. Furthermore, comparing simulation results shown in (i.e., enzyme distribution in hydrogel) with Figure 3.7B (product formation in hydrogel), it was clear that, while enzyme diffusion might not be critically affected during the stiffening process (see Figure 3.3B), the rate of product formation lags behind enzyme diffusion. Hence, it was critically important to take both diffusion and reaction into account when predicting the degree of additional crosslink formation.

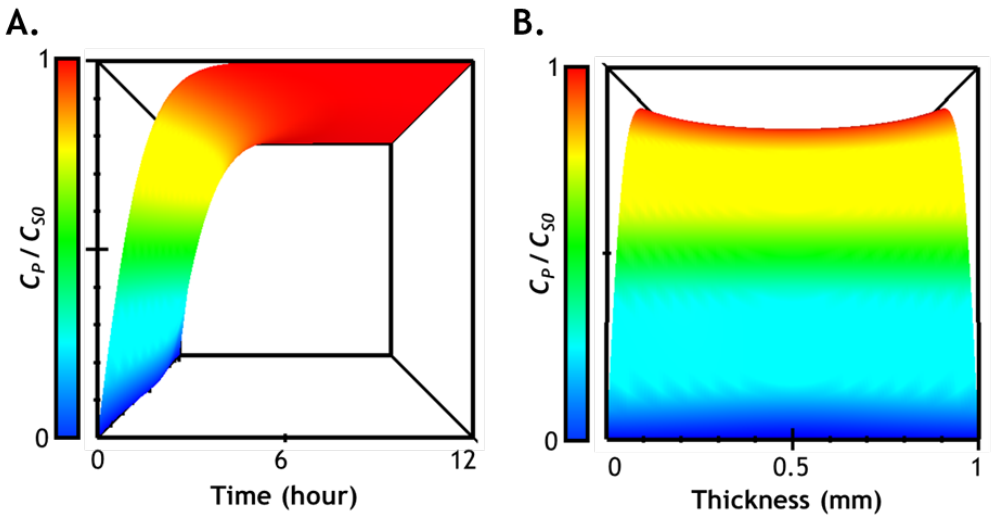

Figure 3.7. Prediction of time- and space-dependent enzyme-catalyzed product formation in a hydrogel. (A) viewing from the *y*-axis (time) in the 3D chart (time, space, and C_P); (B) viewing from *x*-axis (space) in the 3D chart. $D_E^{gel} = 3.58 \times 10^{-11}$ m^2/s, tyr_{ase} = 3 μM.

3.3.8 Correlation of hydrogel mechanical property and its microstructure

In our previous experimental results, we have shown that a period of 6 hour is sufficient to induce enzymatic hydrogel stiffening [166, 213]. Further increasing the enzyme incubation time to 12 h - 48 h only marginally increased gel stiffness. Prior experimental observations were largely in agreement with the diffusion-reaction modeling results shown in Figure 3.7A. To gain a deeper understanding of the crosslinking of enzyme-stiffened hydrogels, we prepared additional PEG8NB–CYGGGYC hydrogels (G_0' ~1 kPa) and performed enzyme-induced stiffening using different concentration of tyr_{ase} (0-3 μM). After 6 hours of stiffening (and overnight washing to remove residue enzyme), the gels were characterized by their moduli and swelling ratio. As shown in Figure 3.8A, tyr_{ase} treatment led to increased gel shear moduli (from ~1 kPa to ~4 kPa) and decreased volumetric swelling ratio (from ~36 to ~12), a correlation commonly observed in chemically crosslinked hydrogels [205, 226]. Next, we examined whether the correlation of G' and the polymer volume fraction ($v_{2,s}$, a reciprocal of Q) of the enzyme-stiffened hydrogels could be described by the classical rubber elasticity theory, which predicts a linear dependency between G' and $v_{2,s}$ [201, 227]. As shown in Figure 3.8B, the correlation of experimentally obtained G' and $v_{2,s}$ followed a power law with an exponent of 1.95. This value was significantly higher than the linear dependence (i.e., exponent = 1) predicted by the theory of rubber elasticity, and suggested the presence of network non-ideality, either due to ineffective initial crosslinking (performed with

low macromer concentration) and/or as a result of enzymatic stiffening [207]. However, it should be noted that this degree of network non-ideality (i.e., the exponent in the power law) is similar to other chemically crosslinked hydrogels [228].

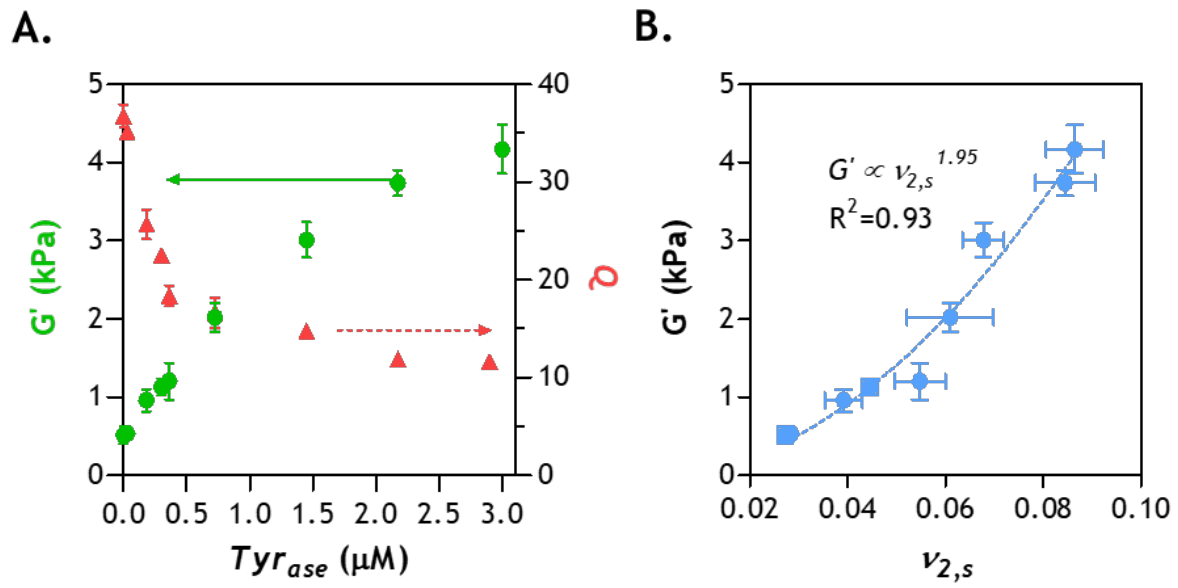

Figure 3.8. Correlation of hydrogel physical properties and enzyme concentration: (A) shear moduli (G') and volumetric swelling ratio (Q) of hydrogel stiffened by different concentrations of tyr_{ase}-all gels were initially crosslinked by thiol-norbornene photopolymerization using 2.5 wt% PEG8NB, 5 mM peptide crosslinker (CYGGGYC), and 1 mM photoinitiator (LAP); (B) correlation of the polymer volume fraction ($\nu_{2,s}$) with G' (N = 3, Mean ± SEM).

3.4 Conclusion

In summary, we have predicted and validated enzyme diffusion in gels with varying stiffness (Figure 3.2-Figure 3.4). We have also monitored tyr_{ase}-mediated reactions and predicted the degree of gel stiffening from the perspective of product formation under varying enzyme and substrate concentrations (Figure 3.5 and Figure 3.6). The modeling and experimental results have demonstrated that while a period of 3 hour is sufficient for the enzyme to equilibrate the entire gel, it would take at least another 3 hour for the reactions to be completed (Figure 3.7A) [213]. Furthermore, the enzyme-stiffened hydrogels exhibited physical properties (e.g., gel swelling ratio and modulus) similar to other chemically crosslinked hydrogels (Figure 3.8A and B). Collectively,

the information acquired from this study should be highly useful in designing enzyme-mediated dynamic hydrogel system for the fundamental material science and tissue engineering applications.

3.5 Materials and Methods

3.5.1 Macromer preparation and peptide synthesis

Hydroxyl-terminated 8-arm PEG (20 kDa) and 5-norbornene-2-carboxylic acid were purchased from JenKem Technology (Plano, TX, USA) and Sigma-Aldrich (St. Louis, MO, USA), respectively. All reagents and Fmoc-capped amino acids for solid-phase peptide synthesis were acquired from Anaspec (Fremont, CA, USA) or ChemPep (Wellington, FL, USA). Other reagents for chemical synthesis were purchased from Sigma-Aldrich or Thermo Fisher (Waltham, MA, USA) unless noted otherwise. PEG8NB and LAP were synthesized as described elsewhere [207, 229]. Bis-cysteine/bis-tyrosine-bearing peptides (CYGGGYC) were synthesized via standard Fmoc coupling chemistry on an automated, microwave-assisted peptide synthesizer (Liberty 1, CEM, Matthews, NC, USA). The crude products (0.25 mmole) were cleaved in a trifluoroacetic acid (TFA) cleavage cocktail composed of 7.6 mL trifluoroacetic acid (TFA), 0.2 mL triisopropylsilane (TIPS), 0.2 mL distilled water, and 400 mg phenol. The cleaved and dried peptides were purified by reverse-phase HPLC (PerkinElmer Flexar system) using 95%/5% (*v*/*v*) water/acetonitrile (ACN) with a trace (0.1% *v*/*v*) of TFA as the starting mobile phase. A linear gradient of ACN was employed to separate the products through a semi-prep peptide C18 column (5 ml/min). The separated products were monitored with a UV/vis detector and the purified peptides were characterized with liquid chromatography coupled with mass spectrometry (Santa Clara, CA, USA, 1200 series LC/MS system, Santa Clara, CA, USA).

3.5.2 Modeling of enzyme diffusion into hydrogels

We harnessed Fick's second law of diffusion (equation (3.10)) to estimate distribution of tyr_{ase} in hydrogel over space and time:

$$\frac{\partial C_E(x,t)}{\partial t} = -\frac{\partial}{\partial x}\left(D_E{}^{gel}(x,t) \times \frac{\partial C_E(x,t)}{\partial x}\right) \tag{3.10}$$

note that the diffusivity of enzyme in hydrogel ($D_E{}^{gel}$) negatively scales with hydrogel crosslinking density and positively correlates to hydrogel mesh size (ξ). As enzyme infiltrates the hydrogel, it catalyzes tyrosine residues into DOPA dimers, resulting in an increase in hydrogel crosslinking

density (i.e., smaller mesh size) that may lead to lower diffusivity. Hence, D_E^{gel} may be dependent on the location of the enzyme in the hydrogel. In this mathematical model, we assume that enzyme diffusion proceeds bi-directionally from the top and bottom (i.e., along the x-axis) of the thin hydrogel with a thickness of h (i.e., neglecting diffusion from the gel edge). Initially, the entire hydrogel (i.e., $0<x<h$) is free of enzyme, which gives the following initial condition (equation (3.11)):

$$C_E(x,0) = 0 \tag{3.11}$$

where we also assume that enzyme concentration in the solution remains unchanged (C_{E0}), which yields the following boundary conditions (equation (3.12)):

$$\begin{aligned} C_E(0,t) &= C_{E0} \\ C_E(h,t) &= C_{E0} \end{aligned} \tag{3.12}$$

Since enzyme diffusion proceeds bi-directionally, at any given time there is no flux at the center of the hydrogel (i.e., $x = h/2$), which yields the second boundary condition (Equation (3.13)):

$$\frac{\partial C_E(\frac{h}{2},t)}{\partial t} = 0 \tag{3.13}$$

As mentioned earlier, diffusivity of any solute in a crosslinked hydrogel is affected by gel mesh size. Hence, it is necessary to determine whether the additional DOPA dimer crosslinks significantly with the affected tyr_{ase} transport in the stiffened gel. In this regard, the Lustig-Peppas estimation of solute diffusivity in a highly swollen gel can be used to establish a correlation between tyr_{ase} diffusivity and hydrogel mesh size (equation (3.14)) [218].

$$D_E^{gel}(x,t) = D_E^{sol} \cdot (1 - \frac{R_E}{\xi}) \cdot e^{-Y/(Q-1)} \tag{3.14}$$

where D_E^{sol} is the diffusivity of enzyme in solution (i.e., 5.05×10^{-10} m^2/s for tyr_{ase}), R_E is the hydrodynamic radius of the enzyme (i.e., 4.5 nm for tyr_{ase}) [230], and Y is the critical volume required for a successful translational movement of the substrate relative to the average free volume of a water molecule (i.e., 1 for PEG-based gels) [218]. Note that this equation is used only when gel mesh size is larger than hydrodynamic radius of the soluble molecule (i.e., $R_E/\xi < 1$) because no diffusion is possible when R_E is larger than ξ. Clearly, when R_E approaches ξ, D_E^{gel} becomes much smaller than D_E^{sol}. Therefore, it is critical to determine the relative sizes of R_E and ξ even for highly swollen PEG-based hydrogels (i.e., $Q >> 10$). To obtain mesh size of a swollen

gel, we first measured the mass swelling ratio (q) by dividing mass (m) of the swollen and dried gels (equation(3.15)):

$$q = \frac{m_{Swollen\ gel}}{m_{Dried\ gel}} \tag{3.15}$$

where the volumetric swelling ratio (Q) of the hydrogel (equation (3.16)) is determined using mass swelling ratio (q) and the density (ρ) of PEG (1.087 g/cm^3 at 37 °C) and water (0.994 g/cm^3 at 37 °C):

$$Q = \frac{\rho_{H_2O}}{(q\text{-}1)\rho_{H_2O} + \rho_{PEG}} \tag{3.16}$$

once Q is obtained, gel mesh size (ξ) can be derived using the equation (3.17):

$$\xi = Q^{\frac{1}{3}} \cdot \ell \cdot \left(\frac{3C_n \overline{M_c}}{\overline{M_n}}\right) \tag{3.17}$$

where ℓ is the average bond length (1.47 Å) in the backbone of an ethylene glycol subunit (i.e., –CH_2–CH_2–O–), 3 is the total number of bonds in a PEG repeat subunit, C_n is the Flory characteristic ratio (4 for PEG-based hydrogel), and $\overline{M_n}$ is the number for average molecular weight of PEG8NB (20 kDa) [122]. To obtain the average molecular weight between crosslinks ($\overline{M_c}$) within a step-growth hydrogel, equation (3.18) can be used:

$$\overline{M_c} = 2\left(\frac{MW_A}{f_A} + \frac{MW_B}{f_B}\right) \tag{3.18}$$

where MW_A and MW_B represent molecular weights of the two macromer crosslinkers PEG8NB and CYGGGYC, and f_A and f_B are the functionality of the macromer and peptide crosslinker (i.e., 8 and 2), respectively. The numerical model predictions were programmed and executed via Grapher (Arizona Software) using a spatial step size (Δx) of 1 μm and a temporal step size (Δt) of 1 second.

3.5.3 Characterization of oxygen consumption

During oxidation of the soluble L-*tyr*, tyr_{ase} exhibits four distinct oxidation states (*deoxy*-, *oxy*-, *met*-, and *deact*-tyr_{ase}), and the oxygen molecule (O_2) is a key component initiating the overall catalytic processes [220]. The association of O_2 and tyr_{ase} forms tyr_{ase}^{oxy} that oxidizes L-*tyr* (or other phenolic precursors) into DOPAquinone. Hence, the consumption of soluble O_2 can be used to gauge the extent of tyr_{ase}-catalyzed DOPA formation. To this end, we measured soluble O_2

contents in a 2 ml microtube which contained L-*tyr* (10 mM) and tyr_{ase} (0.1, 1.5, and 3 μM) by a portable fiber optic oxygen probe and meter (PreSens Microx 4, Regensburg, Germany). The needle-type probe was extended into the center of the solution. Note that the O_2 quantifications were started 2 minutes prior to tyr_{ase} addition.

3.5.4 Tyr_{ase}-Mediated Reaction Kinetics

The kinetics of tyr_{ase}-mediated reactions were modeled using the standard Michaelis–Menten equation (3.19) [231]:

$$-V_S = V_P = \frac{V_{max} \cdot C_S}{K_M + C_S} = \frac{C_E \cdot k_{cat} \cdot C_S}{K_M + C_S} \tag{3.19}$$

where C_S and C_P are the concentration of substrate and product, respectively; V_S and V_P are the velocity of substrate consumption and product formation; and V_{max} is the maximum reaction velocity, which is equivalent to enzyme concentration (C_E) multiplied by the turnover number (k_{cat}). In the event of substrate inhibition, a modified Michaelis-Menten equation was employed (3.20) [232]:

$$V_P = \frac{C_E \cdot k_{cat} \cdot C_S}{K_M + C_S(1 + \frac{C_S}{K_i})} \tag{3.20}$$

here, K_i is the kinetic constant for substrate inhibition [214].

To obtain kinetic constants for tyr_{ase}-mediated reactions with different substrates, we utilized 3-Methyl-2-benzothiazolinone hydrazone (MBTH) as an indicator. MBTH is a hydrazone-based compound capable of reacting with DOPAquinone to produce a pink pigment [221, 222]. In brief, 2 mM MBTH was prepared in pH 6.5 PBS, mixed with 0.6 μM tyr_{ase} and different amounts of substrates (0-10 mM) such as L-tyrosine (L-*tyr*), L-dopamine (L-DOPA), or the peptidyl crosslinker (CYGGGYC). We measured absorbance of the mixture at 475 nm to quantify the production of DOPAquinone-MBTH complex. Note that since cysteine residue within a peptidyl sequence also reacts with MBTH, peptides were first conjugated with the linear norbornene-functionalized PEG (PEGdNB) through photoinitiator (lithium phenyl-2,4,6-trimethylbenzoylphosphinate, LAP) and a light (i.e., 365 nm, 5 mW/cm^2)-initiated thiol–norbornene reaction for 2 minute prior to the MBTH assay. The process of enzymatic reaction was monitored for 20 minutes with a microplate reader (Biotek, Synergy HTX, Winooski, VT, USA). A linearly increased absorbance at 475 nm is indicative of MBTH-resulting pink product formation.

At any given Cs, V_P can be obtained by calculating the slope of absorbance vs. the time curve. Next, V_{Max} and Cs values were fitted to the general or modified Michaelis-Menten model (i.e., equation (3.19) or (3.20)) to acquire the k_{cat} and Michaelis constant (K_M). Additionally, to understand the correlation between C_E and V_P, we also treated the substrate (L-*tyr*, 10 mM) with varying tyr_{ase} concentrations (0-3 μM). The reactions were monitored via the MBTH assay as described above.

3.5.5 Fabrication and Characterization of the Step-Growth PEG-Peptide Hydrogels

PEG-peptide hydrogels were prepared by coupling norbornene moieties of PEG8NB and the terminal cysteine moieties of peptide crosslinker (CYGGGYC) via thiol–norbornene photopolymerization. Hydrogels were prepared with different macromer contents but with the stoichiometric ratio of thiol to norbornene maintained at 1 to minimize network defects. In brief, aliquots of precursor solutions (45 μl) were deposited between two glass slides separated by silicon spacers (1 mm). Hydrogel crosslinking was initiated by 365 nm light (5 mW/cm^2) exposure for 2 minutes. Following the initial photopolymerization, gels were maintained in PBS at 37 °C for 24 hours prior to characterization or tyr_{ase}-mediated stiffening. Shear moduli (strain-sweep mode) of the pre- and post-stiffened hydrogels were characterized using a digital rheometer (Bohlin CVO 100, Malvern Instruments, Malvern, Worcestershire, UK) equipped with an 8-mm diameter parallel plate geometry. Measurements of gel shear moduli (G') were acquired from the average of the linear region on the modulus-strain curve (0.1-5% strain) with oscillation frequency set at 1 Hz.

3.5.6 Statistical Analysis

All experiments were repeated three times independently with four samples per condition. Experimental results were reported as Mean ± SEM with a sample size of at least three (N = 3). The data were analyzed by one-way or two-way ANOVA with GraphPad Prism 8 software. Single, double, and triple asterisks represent $p < 0.05, 0.001$, and 0.0001, respectively, and only $p < 0.05$ is considered statistically significant.

CHAPTER 4. ENZYME-MEDIATED STIFFENING HYDROGELS FOR PROBING ACTIVATION OF PANCREATIC STELLATE CELLS

(As published in *Acta Biomaterialia*, 2017 (48) 258-269)

4.1 Abstract

The complex network of biochemical and biophysical cues in the pancreatic desmoplasia not only presents challenges to the fundamental understanding of tumor progression, but also hinders the development of therapeutic strategies against pancreatic cancer. Residing in the desmoplasia, pancreatic stellate cells (PSCs) are the major stromal cells affecting the growth and metastasis of pancreatic cancer cells by means of paracrine effects and extracellular matrix protein deposition. PSCs remain in a quiescent/dormant state until they are 'activated' by various environmental cues. While the mechanisms of PSCs activation are increasingly being described in literature, the influence of matrix stiffness on PSCs activation is largely unexplored. To test the hypothesis that matrix stiffness affects myofibroblastic activation of PSCs, we have prepared cell-laden hydrogels capable of being dynamically stiffened through an enzymatic reaction. The stiffening of the microenvironment was created by using a peptide linker with additional tyrosine residues, which were susceptible to tyrosinase-mediated crosslinking. Tyrosinase catalyzes the oxidation of tyrosine into dihydroxyphenylalanine (DOPA), DOPAquinone, and finally into DOPA dimer. The formation of DOPA dimer led to additional crosslinks and thus stiffening the cell-laden hydrogel. In addition to systematically studying the various parameters relevant to the enzymatic reaction and hydrogel stiffening, we also designed experiments to probe the influence of dynamic matrix stiffening on cell fate. Protease-sensitive peptides were used to crosslink hydrogels, whereas integrin-binding ligands (e.g., RGD motif) were immobilized in the network to afford cell-matrix interaction. PSC-laden hydrogels were placed in media containing tyrosinase for 6 hours to achieve in situ gel stiffening. We found that PSCs encapsulated and cultured in a stiffened matrix expressed higher levels of α-SMA and hypoxia-inducible factor-1α (HIF-1α), suggestive of a myofibroblastic phenotype. This hydrogel platform offers a facile means of in situ stiffening of cell-laden matrices and should be valuable for probing cell fate process dictated by dynamic matrix stiffness.

4.2 Introduction

The stiffness of extracellular matrices (ECM) increase during the progression of many diseases, including cancers [233, 234]. The implications of a stiffened tissue include abnormal intracellular mechano-sensing and signal transduction, increased expression of ECM proteins, and durotaxis of cells (i.e., cell migration guided by gradients of matrix rigidity). Seminal works concerning the influence of matrix mechanics on cell fate processes relied largely on two-dimensional (2D) polyacrylamide hydrogels with surface-adsorbed or conjugated ECM proteins [235]. Culturing cells on a 2D surface, however, does not truly recapitulate the complex architecture of three-dimensional (3D) ECM [236]. In this regard, cell-laden hydrogels are increasingly being explored for modeling disease progression *in vitro* or *ex vivo*, as well as for regenerating tissues *in vivo*. The high water content and good permeability of a highly swollen hydrogel permits facile nutrient-waste exchange, whereas the crosslinked polymeric network gives rise to tunable elasticity and easy tethering of bioactive motifs for supporting cell survival and function in 3D [237]. Hydrogels prepared from synthetic polymers, such as poly(ethylene glycol) (PEG), are particularly suitable for investigating the influence of extracellular matrix mechanics on cell fate because the crosslinking density, and hence the stiffness, of a biomimetic hydrogel can be precisely engineered [238].

In recent years, hydrogels with dynamically tunable crosslinking kinetics are increasingly being explored for studying mechanobiology in 3D [239-241]. The general principle of designing a dynamic hydrogel is to perform cell encapsulation within a primary hydrogel network that allows for post-gelation modification in gel crosslinking density. Employing a two-stage crosslinking strategy, Burdick and colleagues showed that cell-laden hydrogels could be stiffened in a spatial-temporally controlled manner [241]. The hydrogels were first prepared by thiol-based Michael-type addition between methacrylated hyaluronan (MeHA) and dithiothreitol (DTT) with an off-stoichiometric ratio. The excess methacrylate moieties in the primary hydrogel network permit subsequent light-and-radical-mediated chain-growth polymerization to produce a stiffened gel matrix. Anseth *et al.* showed that a stiffened hydrogel matrix could be achieved simply by performing a secondary step-growth photopolymerization in the presence of a pre-gelled cell-laden hydrogel network [101]. *In situ* hydrogel stiffening could also be achieved through light irradiation. For example, PEG-based hydrogels with azobenzene were prepared to undergo reversible swelling

upon azobenzene *cis-trans* isomerization, which is induced by UV or visible light exposure, respectively [242]. Although the azobenzene-linker chain length, and hence hydrogel swelling, could be modulated by light exposure, the magnitude of gel modulus change was minimal and not physiologically relevant. Alternatively, infrared (IR)-induced heating was used to tune the stiffness of alginate hydrogels across a physiologically relevant range [96]. In this example, temperature-sensitive liposomes were loaded with gold nanorods as well as calcium and were subsequently encapsulated in the alginate gels. Upon IR irradiation, the heated gold nanorods disrupt the liposomes, causing the release of calcium ions to induce gelation of alginate chains. Although IR light is considered safer than UV light, the generation of heat upon IR irradiation might not be ideal for certain applications. Our group has utilized host-guest (cyclodextrin-adamantane) interactions to reversibly tune the stiffness of cell-laden hydrogels across several hundreds to thousands of Pascals [243]. Collectively, these approaches provide a wide variety of options for irreversibly or reversibly tuning the stiffness of cell-laden hydrogels.

Owing to their substrate specificity and predictable enzymatic reaction kinetics, various enzymes (e.g., plasmin, transglutaminase, horseradish peroxidase, glucose oxidase, and tyrosinase) have been successfully used to induce gel crosslinking and, in some cases, cell encapsulation [244-248]. For example, tyrosinase (also named polyphenol oxidase) catalyzes the oxidation of phenol into dihydroxyphenylalanine (DOPA), DOPA quinone, and subsequently into DOPA dimer [249]. Tyrosinase-mediated reactions also consume molecular oxygen and produce water as the only by-product. Tyrosine or DOPA conjugated polymers (e.g., PVA, gelatin, dextran, *etc*.) are susceptible to tyrosinase-mediated crosslinking [250]. Due to its mild reaction conditions, tyrosinase is increasingly being explored for hydrogel crosslinking and *in situ* cell encapsulation [245]. To the best of our knowledge, however, tyrosinase-mediated DOPA crosslinking mechanism has not been exploited for *in situ* stiffening of cell-laden hydrogels. While tyrosinase-mediated DOPA formation was not found in the pancreatic tissue, this strategy provides facile, effective, and cytocompatible means of tuning matrix stiffness for *in vitro* or *ex vivo* tissue engineering applications.

In this contribution, we describe the design of orthogonally crosslinked PEG-peptide thiol-norbornene hydrogels susceptible to tyrosinase-mediated *in situ* gel stiffening. The primary hydrogel network was prepared by a light-mediated thiol-norbornene photopolymerization [251, 252] utilizing bis-cysteine-bis-tyrosine-bearing peptide crosslinkers. The pendant tyrosine

residues in the primary step-growth hydrogel network permit additional crosslinking and gel stiffening triggered by the infiltration of tyrosinase. In addition to verifying the formation of DOPA crosslinks within a PEG-peptide hydrogel network, we also optimized the conditions for achieving a biologically relevant range of stiffening. Finally, we utilized this *in situ* stiffening PEG-peptide hydrogel system to probe the effect of a stiffened matrix on the activation of pancreatic stellate cells.

4.3 Result and Discussion

4.3.1 Design principles of enzyme-mediated in situ stiffening of PEG-peptide gels

Compared with the relatively heterogeneous chain-polymerized gels, step-polymerized hydrogels possess increased network homogeneity and mechanical integrity [253]. Here, we prepared the primary PEG-peptide hydrogel with orthogonal crosslinks and homogeneous network structure using PEG8NB (Figure 4.1A) and a model peptide CYGGGYC (Figure 4.1B). The basic peptide design rationale was to incorporate two terminal cysteines to permit light-mediated orthogonal thiol-norbornene step-polymerization (Figure 4.1C), as well as two pendant tyrosines to allow tyrosinase-mediated DOPA dimer formation (Figure 4.1D). The DOPA dimers formed within a covalently crosslinked hydrogel network would lead to an increased hydrogel crosslinking density, and hence a stiffened matrix. In principle, the step-polymerized PEG-peptide hydrogel can be stiffened at any point in time post-gelation by placing the hydrogels in a solution containing tyrosinase (Figure 4.1E). The degree of gel stiffening is dictated by the diffusion of tyrosinase into the hydrogel network, as well as the enzymatic reaction between infiltrated tyrosinase and pendant tyrosine residues. For most gel formulations used in this study, the concentration of pendant tyrosine is fixed (i.e., 10 mM tyrosine for 2.5 wt% $PEG8NB_{20kDa}$, $R_{[thiol]/[ene]} = 1$). Therefore, the formation of DOPA dimer and therefore the degree of hydrogel stiffening, depends largely on availability of tyrosinase.

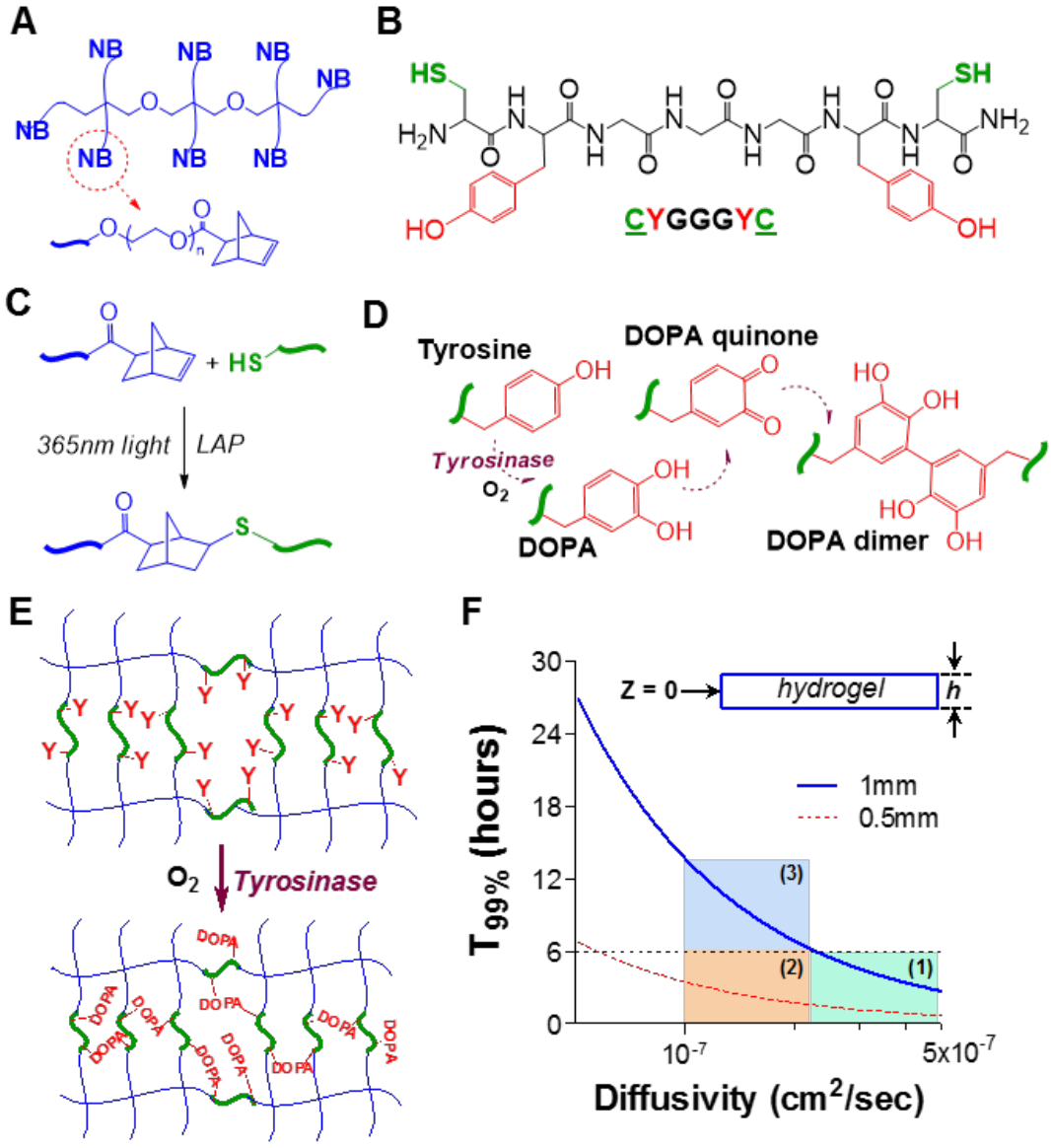

Figure 4.1. Schematics of thiol-norbornene hydrogels susceptible to tyrosinase-mediated in situ gel stiffening. (A) Structure of 8-arm poly(ethylene glycol)-norbornene (PEG8NB). (B) Model bis-cysteine-bis-tyrosine peptide crosslinker CYGGGYC. (C) Light mediated thiol-norbornene photo-click reaction to form PEG8NB-peptide hydrogel. 1 mM LAP was used as the photoinitiator. (D) Tyr_{ase}-mediated oxidation of tyrosine into DOPA, DOPA quinone, and DOPA dimer. (E) PEG8NB-peptide hydrogel bearing pendant tyrosine for tyrosinase-mediated DOPA dimer formation that leads to increased gel crosslinking density. (F) Prediction of $T_{99\%}$ (i.e., $C_{z=0} \geq 0.99 \times C_{z=h}$) in a disc-shape hydrogel with a thickness of h. Regions 1-3 represent scenarios for which a period of 6 hour tyr_{ase} incubation are sufficient (regions 1 & 2) or insufficient (region 3) to fulfill the criterion of $C_{z=0} \geq 0.99 \times C_{z=h}$.

Fick's 2nd Law of Diffusion was used to estimate the time scale of tyrosinase diffusion in the hydrogel (see section 4.5.2). Two parameters are of utmost importance: the thickness of the hydrogel (h) and the diffusivity of tyrosinase (D_E). Gel thickness is easily controlled during hydrogel fabrication (typically between 0.5-1 mm), whereas D_E in hydrogel is affected by hydrogel crosslinking density and can be estimated using a free-volume approach described by Lustig and Peppas (equation (3.21)) [218]. The purpose of this modeling was to understand the minimal time needed for the hydrogel to be equilibrated with the enzyme. Therefore, the enzymatic reaction is not considered in this modeling and future work will focus on developing a comprehensive diffusion-reaction model to predict the degree of gel stiffening.

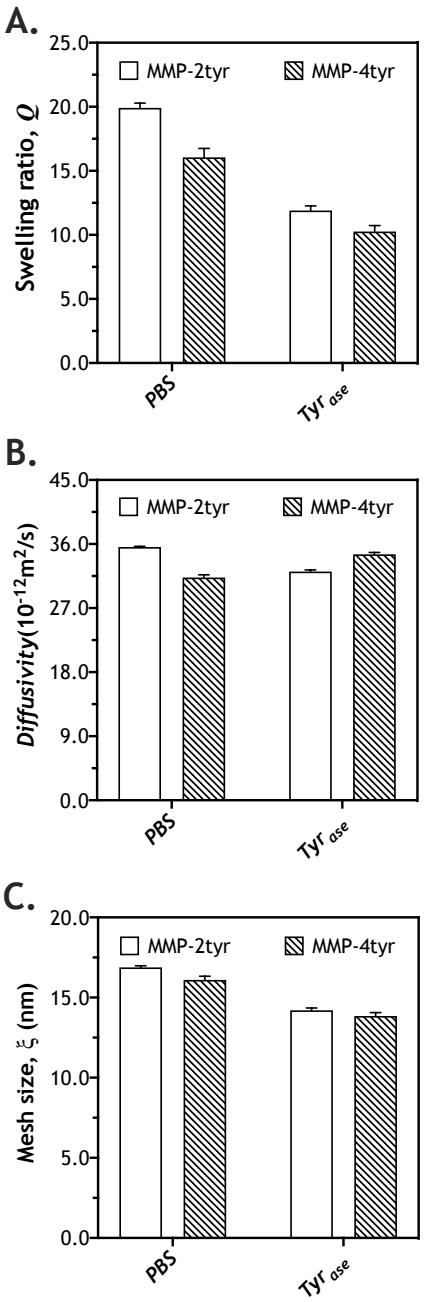

Figure 4.2. Characterization of gel property. (A) Swelling ratio, (B) Mesh size, and (C) Diffusion coefficient of PEG-2Y or PEG-4Y hydrogels before and after tyrosinase-mediated stiffening. PEG8NB 2.5 wt%, 2Y or 4Y peptide 5 mM. Data represent Mean ± SEM (N = 3). ****p<0.0001.*

Depending on its size, the diffusivity of a protein in a highly swollen hydrogel is estimated to be about 20-80% of its value in aqueous solution [254, 255]. Since the diffusivity of tyrosinase (MW: 128 kDa) in water has been determined to be ~5×10^{-7} cm^2/sec [230], the possible range of

tyrosinase diffusivity in the highly swollen PEG-peptide hydrogels should be 1×10^{-7} to 4×10^{-7} cm^2/sec. This assumption was also supported by our determination of tyrosinase diffusivity in either non-stiffened or stiffened hydrogels (i.e., 3×10^{-7} to 4×10^{-7} cm^2/sec, see Figure 4.2C). Fick's 2nd Law of Diffusion in planar geometry (Equations 1-4) was used to estimate the time scale of tyrosinase diffusion in the highly swollen PEG-peptide hydrogel. As shown in Figure 4.2F, the minimal time required to achieve 99% ($T_{99\%}$) of equilibrium tyrosinase concentration at the center of the hydrogel (i.e., $C_{T,z=0}/C_{T,z=h}$ = 99%) is governed by the diffusivity of tyrosinase and the thickness of the hydrogel. From the numerical solutions, we randomly selected $T_{99\%}$ = 6 hour to gauge the relative influence of h and D_T on tyrosinase diffusion in hydrogels. Intuition suggests that h is positively correlated to $T_{99\%}$, while D_T is negatively correlated to $T_{99\%}$. Indeed, we found that when the gel is thin (e.g., h = 0.5 mm), $T_{99\%}$ is much shorter than 6 hours regardless of D_T (regions 1 & 2). On the other hand, when the gel is thicker (e.g., h = 1 mm), $T_{99\%}$ is highly dependent on D_T, which is governed by hydrogel crosslinking density. For example, $T_{99\%}$ is under 6 hours if the crosslinking density of a 1mm thick gel is adjusted such that D_T is greater than 2.05×10^{-7} cm^2/sec (region 1). On the other hand, $T_{99\%}$ is longer than 6 hours if the crosslinking density of the 1mm-thick hydrogel is high enough to decrease D_E to below 2.05×10^{-7} cm^2/sec (region 3). The modeling results shown in Figure 1F suggest that the degree of tyrosinase-mediated gel stiffening should be highly effective for thin hydrogels (h < 0.5 mm) and for thick hydrogels (e.g., h = 1 mm) with lower crosslinking density. Furthermore, our estimation of tyrosinase diffusivity in non-stiffened or stiffened hydrogels (i.e., 3×10^{-7} to 4×10^{-7} cm^2/sec. (3.21)Equation 5 and Figure 4.1F) suggested that 6 hour of incubation was sufficient for the hydrogels (actual thickness ~1 mm) to be equilibrated with tyrosinase (region 1). While this model prediction did not take into account enzymatic reaction, the results nonetheless provide general guidance for fabricating the primary hydrogel network.

4.3.2 Tyrosinase-mediated in situ stiffening of step-polymerized PEG-peptide hydrogels

Prior to testing the hypothesis that tyrosinase could be used to stiffen hydrogels crosslinked by bis-tyrosine-bearing peptide (e.g., CYGGGYC), we first examined the formation of DOPA from tyrosinase-mediated oxidation of soluble model peptide CYGGGYC. Scanning of UV/Vis absorbance from 250-500 nm demonstrated the formation of DOPA. As shown in Figure 4.3A, solution containing only the model peptide CYGGGYC exhibited strong absorbance at 280 nm. Immediately upon the addition of 1 kU/ml tyrosinase into the peptide solution (e.g., Peptide +

tyrosinase, 0 hour), the observed peak absorbance redshifted slightly to 285 nm and an absorbance shoulder between 300-500 nm emerged. After 24-hour incubation, the peak absorbance redshifted further to 295 nm, and the absorbance shoulder became even more pronounced. The absorbance redshift could also be easily observed in the peptide/tyrosinase solutions. As the incubation time was increased, the color of the solution turned from light yellow to dark brown (data was not shown). As previously reported, the redshift in absorbance and the emergence of dark brown color are clear indications DOPA formation in the solution [256].

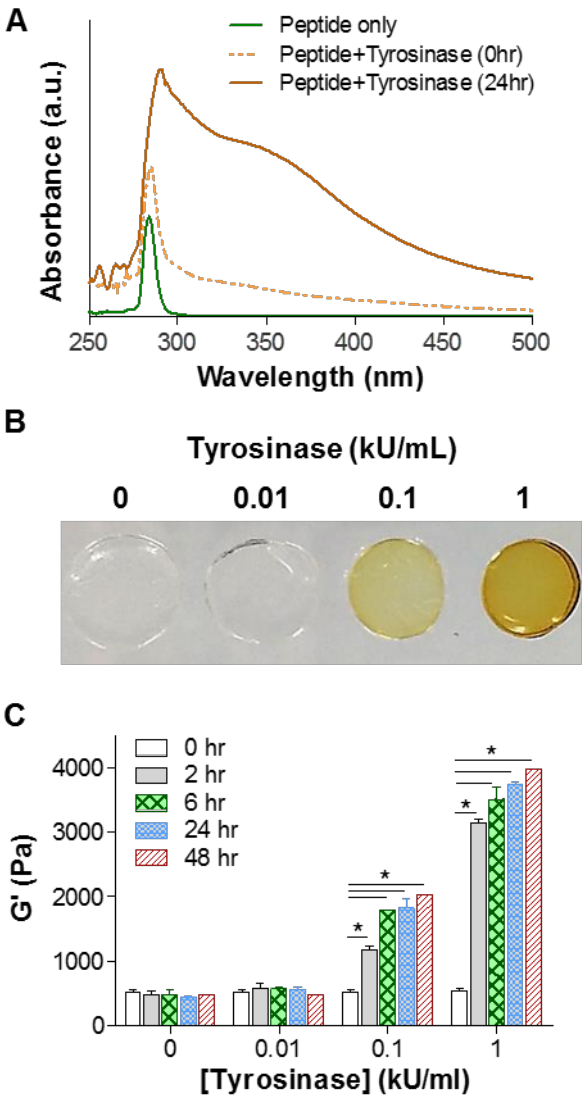

Figure 4.3. Tyrosinase-mediated in situ stiffening of PEG-based hydrogels. (A) UV/Vis absorbance spectrum of 5 mM CYGGGYC peptide, peptide/tyrosinase (1 kU/ml) mixture before (0 hour) and after 24-hour incubation. (B) Photographs of PEG-peptide (i.e., 2.5 wt% PEG8NB, 5mM CYGGGYC) hydrogels treated with different concentrations of tyrosinase. (C) Effect of tyrosinase concentration of shear moduli (G') of the PEG-peptide hydrogels. Crosslinked hydrogels were incubated in PBS for one day prior to 6 hours of tyrosinase treatment. Afterward, the gels were transferred to PBS and gel moduli were monitored periodically using oscillatory rheometer. Data represent Mean ± SEM (N = 3). Asterisks indicate $p<0.05$ (compared with gels at 0 hour, i.e., prior to tyrosinase treatment).

After confirming that tyrosine-containing peptides could be oxidized into DOPA by tyrosinase, we sought to test whether the same phenomenon would occur in bis-tyrosine-containing peptide crosslinked PEG8NB hydrogels, which were polymerized from light initiated thiol-norbornene photo-click reaction using 2.5 wt% $PEG8NB_{20kDa}$ and 5 mM CYGGGYC ($R_{[thiol]/[ene]}$ = 1). After swelling for 24 hours, hydrogels were placed in buffer solution containing different concentrations of tyrosinase (i.e., 0, 0.01, 0.1, and 1 kU/ml) for 6 hours. As shown in Figure 4.3B, the hydrogels incubated in 0 and 0.01 kU/ml tyrosinase remained transparent. On the other hand, the color of gels incubated in 0.1 and 1 kU/ml tyrosinase turned to light yellow and brown, respectively. Since tyrosine residues were immobilized in the hydrogel network, the darker color formed in the initially transparent hydrogels indicated the formation of DOPA. Furthermore, the diameter of the hydrogel incubated in 1 kU/ml tyrosinase reduced about 20%, suggesting shrinkage of the hydrogel upon the formation of DOPA in the hydrogel network. Finally, we evaluated the shear moduli (G') of these hydrogels (Figure 4.3C) and found that gels incubated in 0 and 0.01 kU/ml tyrosinase for 6 hours showed no difference in moduli before and after incubation (i.e., 0, 2, and 6 hour). The moduli remained similar after prolonged incubation in PBS for another 18 hour and 42 hours (i.e., total time 24 and 48 hour). For gels incubated in 0.1 kU/ml tyrosinase, however, moduli increased rapidly from 500 Pa to respectively 1,200 Pa and 1,900 Pa after 2 hour and 6 hours of tyrosinase incubation. After 6 hours of incubation, gels were again moved to PBS for another 18 hour and 42 hour (i.e., total time 24 and 48 hour) and the moduli remained at around 1,900 Pa to 2,000 Pa. The stiffening effect after tyrosinase incubation suggests that DOPA formed in the hydrogel network led to increased crosslinking density. Similar phenomenon occurred in gels incubated in 1 kU/ml tyrosinase, except that the increases in moduli were even higher (to more than 3,100 Pa). Interestingly, the moduli increased for another 200-400 Pa after the gels were transferred to PBS, indicating that tyrosinase retained in the hydrogel continued to crosslink tyrosine residues after the gels were transferred to PBS. In addition, hydrogels pre- and post-stiffening (by 1 kU/ml tyrosinase) did not exhibit noticeable stress relaxation (Figure 4.4) since both the primary and secondary crosslinks (i.e., thioether bonds and DOPA dimers) were all covalent bonds. These results show that tyrosinase indeed could be used to effectively stiffen hydrogels containing pendant tyrosine residues. Through simple peptide sequence design (i.e., adding additional tyrosine residues) and exogenously adding tyrosinase, we have achieved tunable in situ gel stiffening. Although tyrosinase has been used to crosslink DOPA-bearing macromers

into hydrogels [244, 245], we believe the present work represents the first example of using tyrosinase to tune matrix stiffness.

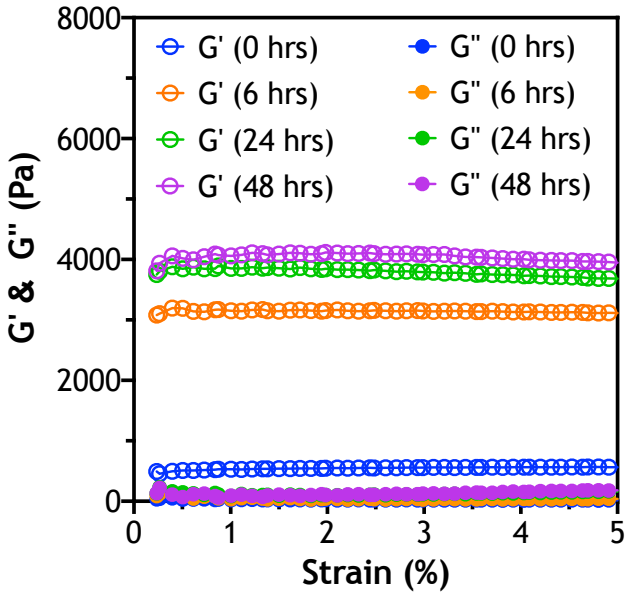

Figure 4.4. Moduli (G' and G") of 2.5 wt% PEG-CYGGGYC hydrogels showing no stress relaxation regardless of tyrosinase treatment conditions. Hydrogels were incubated in PBS for one day prior to 6 hour of 1 kU/ml tyrosinase treatment. Afterward, the gels were transferred to PBS and gel moduli were monitored periodically using oscillatory rheometer. Error bars were omitted for clarity (N = 3).

4.3.3 Controlling the degree of in situ gel stiffening

In addition to adjusting enzyme concentration and incubation time, we also evaluated the effect of initial gel crosslinking density on the degree of *in situ* gel stiffening. Figure 4.5A shows the results of tyrosinase-mediated *in situ* gel stiffening using PEG8NB at three weight percentages during gel crosslinking (2.5 wt%, 3.0 wt%, and 3.5 wt%). As expected, gels crosslinked with higher weight percent of PEG8NB were stiffer following thiol-norbornene photo-crosslinking (~ 800 Pa, 1,800 Pa, and 2,800 Pa for 2.5 wt%, 3.0 wt%, and 3.5 wt%, respectively). After 6 hours of tyrosinase treatment (0.1 kU/ml), hydrogels had various degree of stiffening where stiffer gels exhibited moderate degrees of stiffening (~ 1.8-fold, 1.3-fold, and 1.1-fold increase in G' for 2.5 wt%, 3.0 wt%, and 3.5 wt%, respectively). The decreases in the degree of stiffening at higher weight percent PEG hydrogels could be attributed to the hindered tyrosinase diffusion in highly crosslinked gels. This shortcoming, however, could be circumvented by using a higher concentration of tyrosinase (Figure 4.3C). Figure 4.5B shows that the degree of stiffening could

be tuned by mixing peptides without tyrosine in its sequence. As expected, hydrogels crosslinked with 100% tyrosinase-sensitive peptide (i.e., CYGGGYC) showed the highest degree of stiffening. The degree of gel stiffening in gels crosslinked by 50% CYGGGYC peptide fell in between gels crosslinked by 100% and 0% CYGGGYC peptide. The moduli of gels crosslinked with purely tyrosinase-insensitive CGGGC peptide remained relatively unchanged after tyrosinase treatment. Finally, we examined whether the stiffening process could be temporally controlled. At day-1 post-gelation, PEG8NB-CYGGGYC hydrogels were incubated in 0.1 kU/ml tyrosinase solution for 3 hour and once again at day-3 post-gelation (Figure 4.5C). Although a step-wise increase in gel stiffness was observed, the degree of stiffening was lower after the second tyrosinase treatment. It is also worth noting that between the two tyrosinase treatments, gel moduli gradually increased, which again was a result of residual reactivity from tyrosinase trapped in the hydrogel.

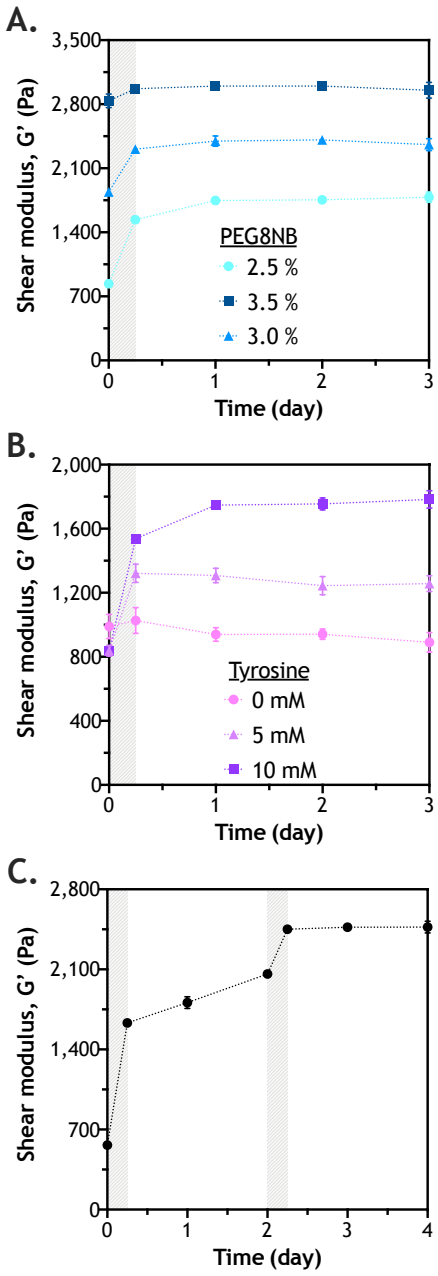

Figure 4.5. Controlling the degree of *in situ* gel stiffening. (A) Effect of PEG8NB weight percent (2.5, 3.0, and 3.5 wt%) on the degree of gel stiffening. The concentration of CYGGGYC was adjusted such that a stoichiometric ratio of thiol-to-ene moieties was maintained (i.e., 5, 6, and 7 mM peptide, respectively). Hydrogels were allowed to swell for one day post-gelation, followed by tyrosinase treatment for 6 hours (shaded area). (B) Effect of tyrosinase-sensitive peptide content on the degree of in situ gel stiffening. PEG8NB content was fixed at 2.5 wt%, whereas tyrosinase-sensitive (i.e., CYGGGYC) and insensitive (i.e., CGGGC) peptide crosslinkers were mixed at different percentages (0, 50, and 100% CYGGGYC). (C) Temporal control in gel stiffening. Swollen hydrogels (2.5 wt% PEG8NB and 5 mM CYGGGYC) were treated with tyrosinase at day 1 for 3 hour and again at day 3 for another 3 hours. Data represent Mean ± SEM (N = 3).

4.3.4 Designing stiffening hydrogels with protease-sensitivity

The design of hydrogels for cell encapsulation often requires incorporating integrin-binding and protease-cleavable motifs that permit cell binding to the matrix and protease-mediated cleavage of the pericellular matrix, respectively [257, 258]. These motifs have proven critical in cell migration, proliferation, and differentiation. For thiol-norbornene hydrogels, integrin-binding motifs are commonly incorporated as pendant peptides (e.g., CRGDS), whereas protease-cleavable motifs are incorporated as hydrogel crosslinkers [251, 252, 259, 260]. Based on this design principle, we used three versions of protease-cleavable peptide crosslinkers, including regular MMP-sensitive peptide without tyrosine residues (designated as 0Y, sequence: KCGPQGIWGQCK), and MMP-sensitive peptide with two or four tyrosine residues (designated as 2Y (Figure 4.6A) and 4Y (Figure 4.6B), respectively). These peptides also contain two cysteine residues that are essential in thiol-norbornene gel crosslinking. Since these peptides will be used for cell encapsulation, we tested whether gels crosslinked by 2Y peptide were susceptible to tyrosinase-mediated *in situ* stiffening in cell culture media (CM). We found that, while PEG-2Y hydrogels were stiffened by 0.1 kU/ml tyrosinase in both PBS and in CM, the degree of stiffening in CM was much less than that in PBS (Figure 4.6C) at the same tyrosinase concentration (i.e., 0.1 kU/ml). This deficit, however, could be easily rectified by using a higher concentration (i.e., 1 kU/ml) of tyrosinase (Figure 4.6C). In this study, we still observed increases in gel moduli after the gels were transferred to PBS. This phenomenon, however, was less apparent when the gels were transferred to tyrosinase-free CM (Figure 4.6C). The decreased responsiveness in tyrosinase-mediated stiffening in CM suggested that the components in serum-containing CM might hinder enzymatic reaction.

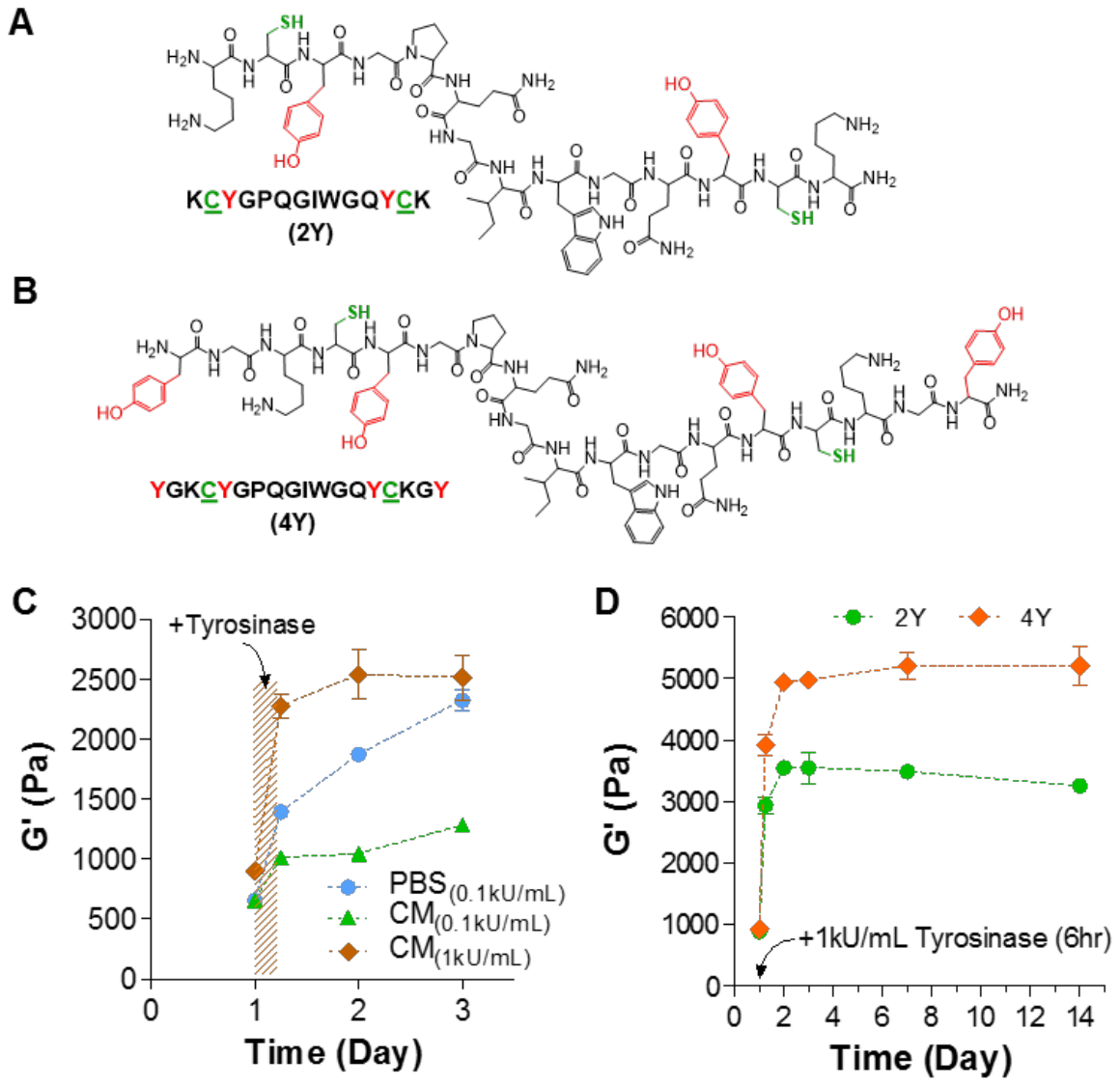

Figure 4.6. In situ stiffening of MMP-sensitive PEG8NB-peptide hydrogels. (A, B) Chemical structures of bis-cysteine MMP-sensitive peptide crosslinker bearing additional two (A) or four (B) tyrosine residues for tyrosinase-mediated gel stiffening. (C) Effect of solution composition on elastic moduli of in situ stiffened PEG-peptide hydrogels. CM: PSC culture media. Gel formulation: 2.5wt% PEG8NB with 2Y peptide. (D) Effect of tyrosine residues (2 or 4 tyrosines) on elastic moduli of in situ stiffened PEG-peptide hydrogels (2.5 wt% PEG8NB). Data represent Mean ± SEM (N = 3).

We also explored *in situ* gel stiffening using different tyrosine-containing peptides. Specifically, 2Y and 4Y peptides were used to crosslinked PEG8NB, and the resulting gels were stiffened using 1 kU/ml tyrosinase in CM for 6 hours. Since the concentration of tyrosine residues in PEG8NB-4Y hydrogels was two-fold higher than that in PEG8NB-2Y hydrogels, it was not a

surprise to obtain almost a two-fold difference in the degree of stiffening when 4Y peptide was used. This study demonstrated that the tyrosinase-mediated gel stiffening could be achieved through the adjustment of multiple parameters, including the content of macromer or tyrosinase-sensitive peptide in the hydrogels, or simply through using peptides with a higher number of tyrosine residues.

4.3.5 Proteolytic degradation of stiffened hydrogels

Proteolytic susceptibility of a biomimetic hydrogel supports various aspects of cell fate processes. Here, we demonstrated that PEG8NB-peptide hydrogels stiffened by tyrosinase were still susceptible to collagenase mediated proteolysis. Figure 4.7A shows the timeline of the stiffening and degradation study using PEG8NB hydrogels crosslinked by either 2Y or 4Y MMP-sensitive peptide (Figure 4.7B). Figure 4.7 showed the profiles of collagenase induced mass loss of PEG-2Y and PEG-4Y hydrogels without (Figure 4.7B) and with (Figure 4.7C) tyrosinase-mediated in situ gel stiffening. Similar to data reported in literature, non-stiffened hydrogels crosslinked by MMP-sensitive peptide started to lose mass as soon as the gels were placed in collagenase solution [252, 261]. Furthermore, the mass loss profiles exhibited good linearity with time owing to the step-polymerized hydrogel network structure [261]. Interestingly, the gels crosslinked by 4Y peptide appears to degrade slower than those crosslinked by 2Y peptide. We reason that the delayed proteolysis in PEG-4Y hydrogels was due to the presence of additional aromatic tyrosine residues that reduced the accessibility of collagenase to the MMP-sensitive peptide sequence, as the swelling ratio (Figure 4.2A), mesh size (Figure 4.2B), and diffusion coefficient (Figure 4.2C) of the two sets of hydrogels appeared to be very similar before tyrosinase-mediated stiffening. The degradation profiles of tyrosinase-stiffened hydrogels (Figure 4.7C), on the other hand, were drastically different than their non-stiffened counterparts. Although collagenase treatment still caused changes in gel mass, the hydrogels actually gained weight (i.e., negative mass loss) during the first two days; after which, the gels started to lose mass (i.e., positive mass loss). We have previously described similar degradation profiles in highly crosslinked gelatin-based thiol-norbornene hydrogels [262]. We reason that the initial mass gain in stiffened hydrogel was due to partial network cleavage that allowed water infiltration. Since the stiffened hydrogels were composed of thiol-norbornene crosslinks and DOPA dimer crosslinks, simply cleaving the peptide linker was not sufficient to cause gel mass loss. Therefore, a longer incubation time (> 2 days) was required to cause positive gel mass loss. Furthermore, PEG-4Y hydrogels

exhibited less responsiveness to collagenase-mediated degradation. This was again attributed to the potential decrease in collagenase accessibility to its peptide substrate due to the presence of additional DOPA crosslinks; because both stiffened PEG-2Y and PEG-4Y hydrogels had similar gel properties (Figure 4.2C). Although the proteolytic degradation profiles were different in non-stiffened and stiffened hydrogels, this study nonetheless demonstrated that tyrosinase-stiffened hydrogels were still susceptible to proteolytic degradation. Furthermore, the delayed degradation behavior in stiffened hydrogels may more closely resemble a stiffened tumor matrix.

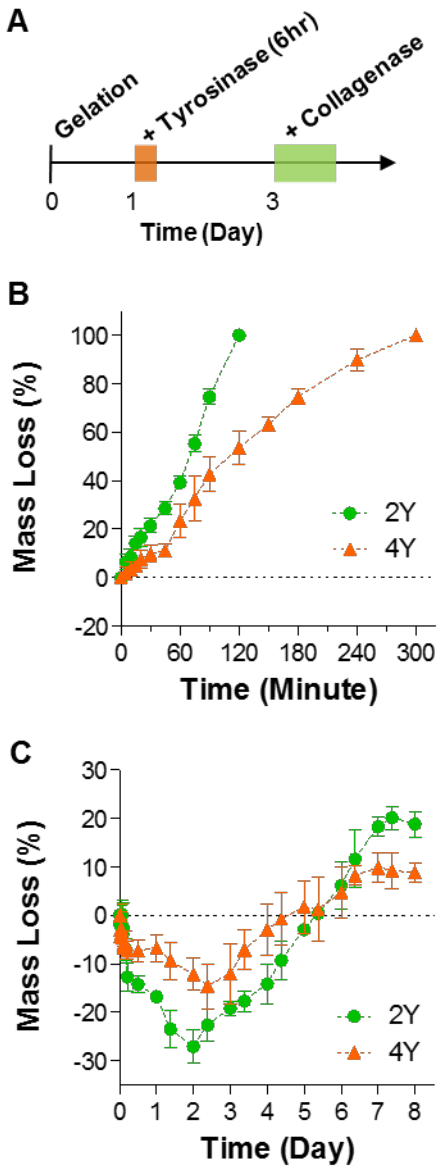

Figure 4.7. Proteolytic degradation of MMP-sensitive PEG8NB-peptide hydrogels. (A) Timeline of the study. (B, C) Collagenase-mediated mass loss of non-stiffened hydrogels (B) and tyrosinase-stiffened hydrogels (C). All gels were formed with 2.5 wt% PEG8NB with 5 mM MMP-sensitive peptide (2Y or 4Y). Data represent Mean ± SEM (N = 3).

4.4 Probing the effect of *in situ* gel stiffening on myofibroblastic activation in human pancreatic stellate cells

We have previously reported the use of biomimetic PEG-peptide hydrogels for studying pancreatic cancer cell growth, morphogenesis, and drug sensitivity [260]. The diagnosis and treatments of pancreatic cancer remain difficult owing to the complicated interactions between

various components in the pancreatic tumor mass, including primary tumor cells, stromal cells (e.g., stellate cells, cancer associated fibroblasts (PSCs)), immune cells, cytokines, proteases (e.g., matrix metalloproteinases (MMPs)), and ECM proteins (e.g., collagen, fibronectin, laminin, etc.) [234]. Experimental evidence suggests that activated PSCs are the major stromal cells that secrete cytokines to enhance proliferation of primary tumor cells and increase their metastasis potential through epithelial-mesenchymal transition (EMT) [263, 264]. Activated PSCs become cancer associated fibroblasts (CAFs) which are responsible for depositing and organizing ECM proteins, such as collagen and laminin, leading to the stiffening of the local desmoplasia. PSCs remain in a quiescent/dormant state until they are 'activated' by various environmental cues whose identities are gradually being identified [263]. For example, PSCs are activated by transforming growth factor β (TGF-β) through Smad2/3 phosphorylation [265]. TGF-β-activated PSCs express a higher content of α smooth muscle actin (α-SMA), which leads to increased intracellular cytoskeletal tension and myofibroblast-like contractile phenotype. In spite of its potential importance, the influence of matrix stiffness on PSCs activation is largely unexplored.

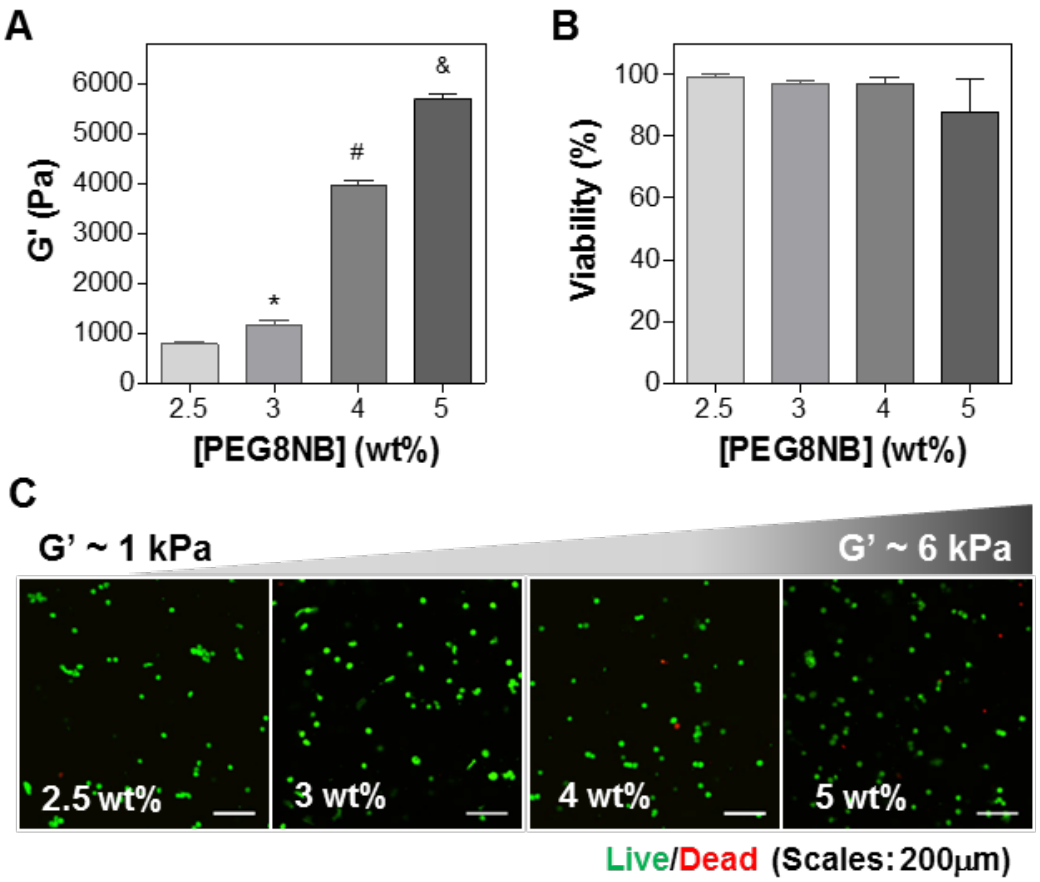

Figure 4.8. (A) Elastic moduli of PEG-peptide hydrogels formed by different concentrations of PEG8NB (MW: 20 kDa) with MMP-sensitive peptide crosslinker (sequence: KCGPQGIWGQCK). All hydrogels also contained 1mM of integrin-binding ligand CRGDS. The stoichiometric ratio of thiol-to-norbornene was maintained at 1. Asterisks represent $p < 0.05$ compared to gels formed with 2.5 wt% PEG8NB. (B) Viability of PSCs encapsulated in thiol-norbornene PEG-peptide hydrogels through quantifying the number of live cells (stained green) to dead cells (stained red) using confocal images as shown in (C). Data represent Mean ± SEM (N = 3).

We utilized human pancreatic stellate cells (PSCs) as a model to evaluate the biological relevance of tyrosinase-mediated gel stiffening strategy. Prior to the stiffening experiments, we demonstrated that regular thiol-norbornene PEG-peptide hydrogels formed with different stiffness (2.5-4 wt% PEG8NB) were cytocompatible for *in situ* encapsulation of PSCs (Figure 4.8D). The cells were able to survive for at least one week in the hydrogels with soft (2.5 wt%) and stiff (4 wt%) hydrogels, as demonstrated by the steady increase in metabolic activity (Figure 4.9F). However, cells grown in stiff hydrogels appeared to have lower metabolic activity (Figure 4.9F).

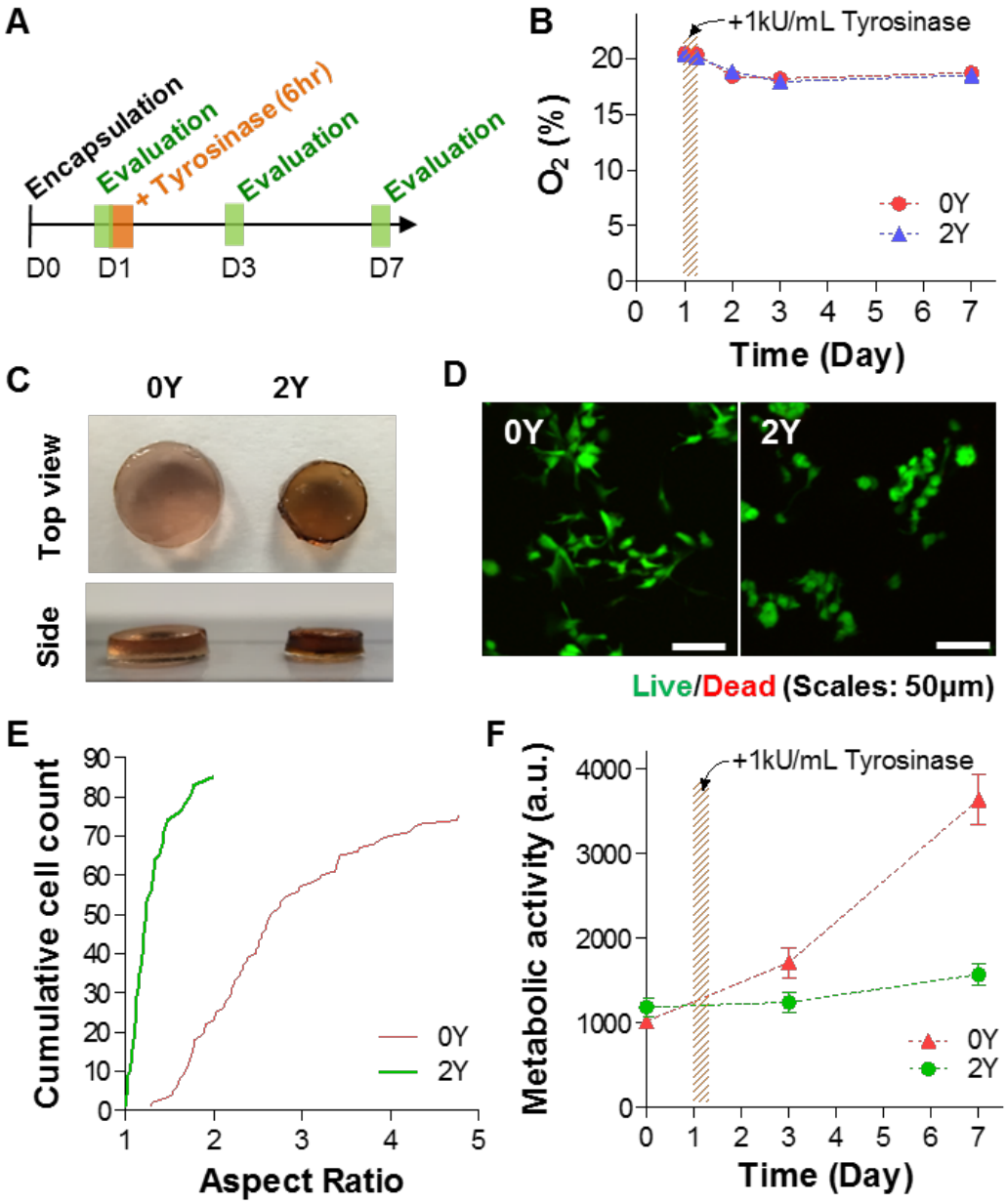

Figure 4.9. Effect of matrix stiffening on pancreatic stellate cell fate in 3D. (A) Timeline of the study. (B) Oxygen contents in PSC culture media with 0Y or 2Y PEG-peptide hydrogels. Tyrosinase-mediated stiffening was conducted on day-1 for 6 hours. (C) Photographs of cell-laden hydrogels crosslinked by 0Y or 2Y MMP-sensitive peptide. (D) Representative confocal z-stack images of live/dead stained PSCs encapsulated in 0Y or 2Y MMP-sensitive PEG-peptide hydrogels. (E) Aspect ratio of encapsulated PSCs at day-7 post-encapsulation. (F) Metabolic activity of encapsulated PSCs. All gels were treated with 1kU/ml tyrosinase at day-1 post-encapsulation. Data represent Mean ± SEM (N = 3).

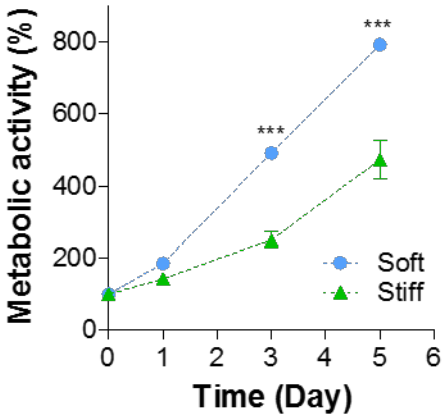

Figure 4.10. Metabolic activity of PSCs encapsulated in soft (2.5 wt%) or stiff (4 wt%) PEG-peptide hydrogels. Data represent Mean ± SEM (N = 3). ****p<0.0001.*

Figure 4.9A outlines the timeline of the *in situ* stiffening experiments, including cell encapsulation, tyrosinase-mediated stiffening, and evaluations. On day-0, PSCs (1×10^6 cells/ml) were encapsulated in 2.5 wt% PEG8NB hydrogels crosslinked by either regular MMP-sensitive peptide (designated as 0Y, sequence: KCGPQGIWGQCK) or tyrosinase-MMP dually-sensitive peptide linker (2Y, Figure 4.11A). Evaluations were conducted at day-1 (prior to stiffening), day-3, and day-7. Because tyrosinase-mediated oxidation consumes dissolved oxygen (Figure 4.9C), we characterized the oxygen content in serum-containing PSC cell culture media where the stiffening occurred. As shown in Figure 4.11B, the oxygen content (O_2) in both the control group (i.e., 0Y) and the experimental group (i.e., 2Y) were essentially identical throughout the course of the study. Although this enzymatic reaction consumes oxygen, no significant decrease in oxygen content was detected. This was most likely due to the fact that the reaction took place in a cell culture incubator where oxygen (21%) was allowed to freely diffuse into the media. The maintenance of oxygen content in the stiffened hydrogels implies that hypoxia would not be an issue affecting cell fate behavior in the stiffened hydrogels.

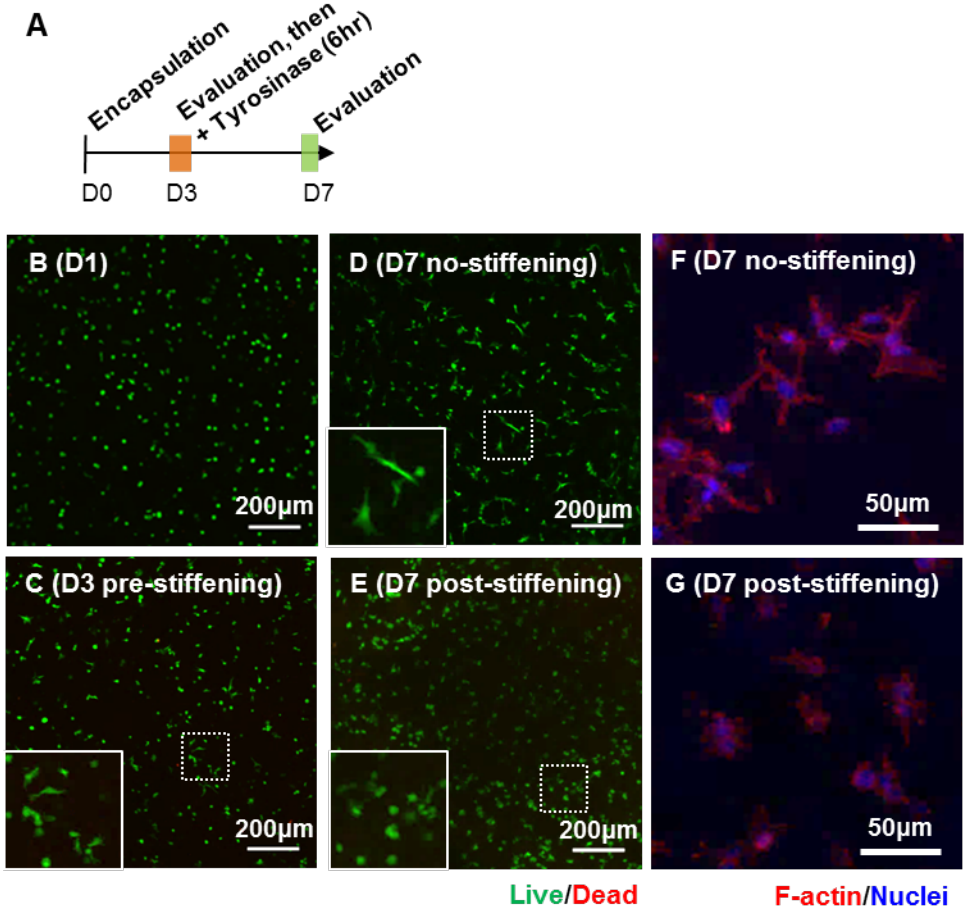

Figure 4.11. (A) Timeline of the study. Representative confocal *z*-stack images of live/dead stained PSCs encapsulated in PEG-peptide hydrogels at day-1 (B), day-3 before stiffening (C), day-7 without stiffening (D), and day-7 with stiffening (E). Representative confocal *z*-stack images of F-actin stained PSCs at day-7 without (F) and with stiffening (G).

Figure 4.9D shows the pictures of the two sets of gels (0Y and 2Y) after treated with 1 kU/ml tyrosinase for 6 hours. From the top view, it can be seen that the size of the gel shrunk significantly in 2Y hydrogels, which were susceptible to tyrosinase-mediated stiffening. From the side view, however, the gel thickness remained roughly the same, suggesting that 2Y gels would be stiffer than the 0Y gels that were tyrosinase-insensitive. Live/dead staining and confocal imaging results revealed that almost all cells were viable in the hydrogels regardless of the stiffening conditions. Furthermore, there was higher degree of spreading in PSCs encapsulated in 0Y hydrogels than in 2Y gels (Figure 4.9D). The spreading of PSCs was quantified by measuring the aspect ratio of the cells encapsulated in 0Y and 2Y hydrogels (Figure 4.10E). Although the peptide crosslinker in both 0Y and 2Y hydrogels contained MMP-sensitive sequence, only 2Y hydrogels were

susceptible to tyrosinase-mediated *in situ* stiffening. As a result, the degree of spreading of cells in stiffened 2Y hydrogels was significantly less than those in 0Y hydrogels. We also quantified the metabolic activity in the encapsulated PSCs using Alamarblue® reagent (Figure 4.11F). While both cell-laden hydrogels were treated with tyrosinase, only cells encapsulated in 2Y hydrogels showed reduced metabolic activity after the gels were stiffened by tyrosinase. It is worth noting that the reduction in metabolic activity was not due to cell death as most of the cells were still viable as revealed by live/dead staining (Figure 4.9D). Together, these results demonstrate that the enzyme-mediated stiffening strategy was effective in affecting cell fate process in 3D. In a separate experiment, we performed *in situ* gel stiffening at day-3 post encapsulation (Figure 4.11A). In this case, cells were allowed to spread for three days prior to stiffening (Figure 4.11B and C). After stiffening with 1kU/ml tyrosinase, the cells were further cultured for 4 days and results showed that while cells in non-stiffened (i.e., 0 kU/ml tyrosinase) hydrogels continued extending their cellular processes in 3D (Figure 4.11D and F), the spreading of cells after *in situ* stiffening was significantly hindered (Figure 4.11E and G). The effect of stiffening on cells was also observed in the metabolic activity (Figure 4.10A) and the aspect ratio (Figure 4.12B) of the cells.

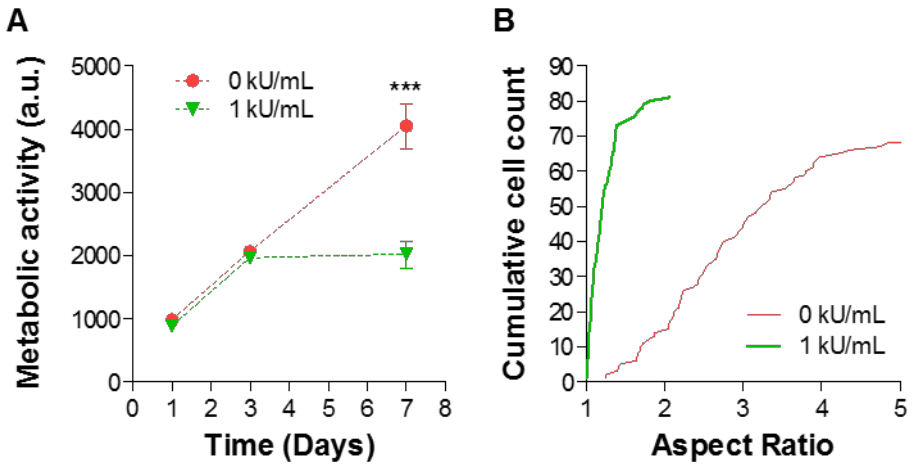

Figure 4.12. (A) Metabolic activity and (B) aspect ratio of PSCs encapsulated in PEG-peptide hydrogels without or with 1 kU/ml tyrosinase-mediated gel stiffening (at day-3). Metabolic activity data represent Mean ± SEM (N = 3). ****p<0.0001*.

In addition to cell morphology changes, we were interested in examining the molecular level changes in cells encapsulated in the stiffened hydrogels. We isolated mRNA from the cells and performed quantitative PCR (qPCR) on select genes that are known to be associated with the activation of PSCs, including α-smooth muscle actin (α-SMA, Figure 4.13A), connective tissue

growth factor (CTGF, Figure 4.13B), and hypoxia-inducible factor 1α (HIF-1α, Figure 4.13C). We found that the expression levels of α-SMA were significantly higher in stiffened 2Y hydrogels than in 0Y hydrogels at day-7 post-encapsulation (i.e., day-6 post-stiffening). On the other hand, a significant difference in HIF1α expression was detected day-3 post-encapsulation (i.e., day-2 post-stiffening). The expression of CTGF in cells encapsulated in 0Y and 2Y hydrogels increased over time, but there was no statistically significant difference between the two groups.

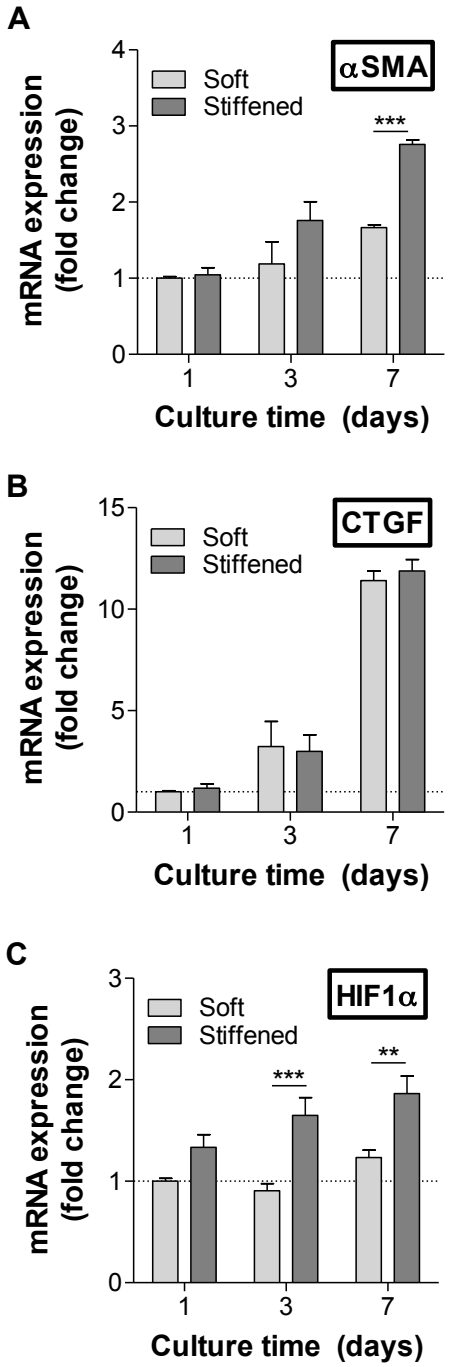

Figure 4.13. Effect of matrix stiffening on gene expression in pancreatic stellate cells. mRNA samples were collected from cell-laden hydrogels before stiffening (day-1), as well as day-2 and day-6 post-stiffening using 1kU/mL tyrosinase (i.e., day-3, day-7 culture time). Soft: Cell-laden hydrogels crosslinked by regular MMP-sensitive peptide (i.e., 0Y peptide). Stiffened: Cell-laden hydrogels crosslinked by 2Y peptide. GAPDH was used as the housekeeping gene and the expression levels of α-SMA (A), CTGF (B), and HIF-1α (C) in different samples were normalized to that in day-1 soft gel (1-fold). Experiments were repeated independently for three times with three samples in each group. (Data represent Mean ± SEM, N = 3). ***p<0.01, ***p<0.001.*

We chose to detect the expression of α-SMA, CTGF, and α-SMA in encapsulated PSCs because these genes have been associated with myofibroblastic activation [265]. The increased expression of α-SMA is a hallmark sign of myofibroblastic activation in many cells, such as hepatic stellate cells (HSCs) and valvular interstitial cells (VICs). Burdick and colleagues showed that αSMA expression was significantly higher when HSCs were cultured on the surface of stiff hydrogels [266, 267]. Accompanied with the increased expression of α-SMA was the extensive spreading and protrusion of the cells. Differing from these earlier works, which were conducted on planar gel surface, we encapsulated PSCs in 3D hydrogels with different stiffness. Although increased α-SMA expression was detected (Figure 4.13A), the cell spreading in 3D was restricted due to a tightened network (Figure 4.11D). On the other hand, no statistically significant difference was found in the expression of CTGF between non-stiffened and stiffened matrices. Kwon et al. recently showed that the expression of CTGF in PSCs was significantly upregulated when the cells were treated with TGF-β [265]. Although both biochemical (e.g., TGF-β) and biophysical (e.g., matrix stiffness) signals are capable of activating stellate cells, the downstream molecular mechanisms involving these two environmental cues are different, and further studies are required. Lastly, we detected elevated HIF1α expression in PSCs encapsulated in stiffened gels (Figure 4.11C) and this result was not due to hypoxia (Figure 4.13B). Recent work has connected the relationship between increased expression of HIF-1α in HSCs and the degree of liver fibrosis due to increased TGF-β signaling and EMT [268]. Other work on PSC showed that cellular stress, including hypoxia, could induce activation of PSCs [269]. Our results suggested that increased matrix stiffness, which can be considered a form of cellular stress, likely increased the expression of HIF-1α independent of oxygen tension in the system. Future mechanistic studies, however, are needed to test this hypothesis.

Table 4.1. Primer sequences used in real time PCR.

Gene	Forward (5'→3')	Reverse (5'→3')	
GAPDH	GAAGGTGAAGGTCGGAGTC	GAAGATGGTGATGGGATTTC	[270]
ACTA2 (α-SMA)	AAAAGACAGCTACGTGGGTGA	GCCATGTTCTATCGGGTACTTC	Harvard Primer Bank, http://pga.mgh.harvard.edu/primerbank/
CTGF	AGGAGTGGGTGTGTGACGA	CCAGGCAGTTGGCTCTAATC	[233]

4.5 Material and Methods

4.5.1 Materials

Hydroxyl-terminated 8-arm PEG (20 kDa) and 5-norbornene-2-carboxylic acid was obtained from JenKem Technology USA and Sigma-Aldrich, respectively. All reagents for chemical synthesis were purchased from Sigma-Aldrich unless otherwise noted. Reagents and Fmoc-amino acids for solid phase peptide synthesis were acquired from Anaspec or ChemPep.

4.5.2 Modeling of tyrosinase diffusion in hydrogels

The time-scale of tyrosinase diffusion into PEG-peptide hydrogel was estimated by Fick's 2nd Law of Diffusion in planar geometry equation (3.21) with appropriate initial (3.22) and boundary conditions (3.23) as listed below:

$$\frac{\partial C_E(x,t)}{\partial t} = -D_E^{gel} \cdot \frac{\partial^2 C_E(x,t)}{\partial x^2} \tag{3.21}$$

$$C_E(x,0) = 0 \tag{3.22}$$

$$\frac{\partial C_E(\frac{h}{2},0)}{\partial x} = 0 \tag{3.23}$$

Here, C_E and D_E are the concentration and diffusion coefficient of tyrosinase in a hydrogel, respectively; z is the coordinate perpendicular to the gel; t is the time of gel incubation in tyrosinase solution; h is thickness of the gel; C_{E0} is the tyrosinase concentration in the buffer solution, which is assumed to be constant. Diffusion in this case was assumed to be symmetrical and only in the z-direction since the gels' diameter (~10 mm) was much greater than its thickness (< 1 mm). Equations (3.21) was solved using Polymath software using a range of diffusion coefficients (~9 × 10^{-8} to 5 × 10^{-7} cm^2/s) and gel thickness (~0.5-1 mm). The time needed for C_E at the center plane of the gel (i.e., $z = 0$) to reach 99% of that in solution was plotted against the diffusion coefficient at a specific gel thickness. The diffusion coefficient of tyrosinase is a function of hydrogel crosslinking density (ρ_x) and can be expressed using the Lustig-Peppas relationship [218]:

$$D_E(x,t) = D_E^{sol} \cdot (1 - \frac{R_E}{\xi}) \cdot e^{-Y/(Q-1)} \tag{3.24}$$

Here, D_E^{sol} is the diffusion coefficient of tyrosinase in aqueous solution. Y is the critical volume (Y = 1 for PEG-based gels) required for a successful translational movement of the substrate relative to the average free volume of a water molecule. ρ_x is the crosslinking density of

the hydrogel dictated by the volumetric swelling ratio (Q) and mesh size (ξ) that are determined experimentally.

4.5.3 Macromer and peptide synthesis

Macromer eight-arm PEGNB (PEG8NB) and photoinitiator lithium phenyl-2,4,6-trimethylbenzoylphosphinate (LAP) were synthesized as described elsewhere [252, 271, 272]. The three MMP-sensitive bis-cysteine peptide crosslinkers, including KCGPQGIWGQCK, KCYGPQGIWGQYCK (designated as 2Y peptide), and YGKCYGPQGIWGQYCKGY (designated as 4Y peptide), were purchased from GenScript (purity > 90%). All other peptides, including CYGGGYC and CRGDS, were synthesized in an automated microwave-assisted peptide synthesizer (Liberty 1, CEM) using standard Fmoc coupling chemistry. Crude peptide was cleaved in a trifluoroacetic acid (TFA) cleavage cocktail, purified using reverse phase HPLC, and characterized by mass spectrometry. The purity of peptides was at least 90%.

4.5.4 Thiol-norbornene hydrogel crosslinking

The crosslinking of thiol-norbornene hydrogels was initiated by 365 nm light exposure and with 1 mM LAP as the photoinitiator. PEG8NB (Figure 4.1A), bis-cysteine peptide crosslinker (e.g., CYGGGYC, Figure 4.1B), and LAP at desired concentrations were mixed in phosphate-buffered saline (PBS) and irradiated under 365nm light (5 mW/cm^2) for 2 minute (Figure 4.1C). For all gel formulations, the stoichiometric ratio of thiol to norbornene was maintained at one to afford the highest degree of gel crosslinking. Gels were maintained in DPBS at 37°C for at least 24 hours prior to characterization or stiffening experiments.

4.5.5 Tyrosinase-mediated *in situ* gel stiffening and characterization

Hydrogels were formed and swollen for 24 hours in PBS at 37˚C, followed by incubation in tyrosinase solution for 6 hours. Afterwards, gels were transferred to PBS. Hydrogel elastic moduli (G' & G") before and after tyrosinase-mediated stiffening were obtained using oscillatory rheometry in strain-sweep mode (8 mm parallel plate geometry with a gap size of 750 μm). Due to volumetric shrinkage after stiffening, the gap size was reduced to 550 μm when measuring moduli of the stiffened hydrogels. The reported gel elastic moduli were averaged from the linear region of the modulus-strain curves.

4.5.6 Proteolytic degradation of stiffened hydrogels

Collagenase was used to evaluate the susceptibility of tyrosinase-stiffened hydrogels to protease-mediated gel degradation. Hydrogels were prepared and stiffened as described in the sections above. The stiffened hydrogels were incubated in PBS for two days, followed by collagenase-1 (40 U/ml) mediated degradation. At pre-determined time intervals, the gels were removed from the protease solution, blotted dry, and weighed to determine the % mass loss, which is defined as the percentage of weight loss at each time interval to the initial weight obtained before protease treatment. The process was repeated until the gels were fully degraded.

4.5.7 Oxygen detection

Solution oxygen contents were recorded with an oxygen microsensor (MicroX4, PreSens) at specific time points during *in situ* stiffening. For this experiment, hydrogels were prepared using sterile-filtered macromers, MMP-sensitive peptides, photoinitiator, and tyrosinase. After the thiol-ene gelation, the hydrogels were incubated in PBS for a day at 37˚C before transferring to complete PSC culture media (ScienCell). Oxygen content (O_2) before and after tyrosinase treatments were recorded periodically for 7 day.

4.5.8 Human pancreatic stellate cell (PSC) culture and encapsulation

Primary human pancreatic stellate cells (PSC or HPSteC) were obtained from ScienCell Research Laboratories and maintained in stellate cell media supplemented with 2% fetal bovine serum (FBS), antibiotics, and growth supplements (ScienCell). The cells were cultured on poly-L-lysine (PLL) coated plates according to the manufacturer's protocol. Cell culture media were refreshed every 2-3 day. Prior to encapsulation, cells were detached from the plate by trypsin-EDTA treatment for 3 minutes. Trypsin was neutralized with equal volume of media and transferred into 5ml of FBS pre-warmed to room temperature. Trypsinized cells were centrifuged at 1,000 rpm for 5 minutes, counted, and mixed with sterile-filtered pre-polymer solutions (PEG8NB, peptide crosslinker (e.g., MMP-sensitive linker: KCGPQGIWGQCK), 1 mM CRGDS, and 1 mM LAP). Twenty-five microliter (25 μl) of the cell-polymer mixtures were transferred to a 1 ml syringe (tip cut open for solution loading and gel removal) and placed under 365 nm light tube in an aseptic laminar flow hood for *in situ* gel crosslinking and cell encapsulation. The encapsulation was achieved within 2 minutes. In all experiments, cells were encapsulated with a cell density of 1 million cells/ml. After encapsulation, cell-laden hydrogels were maintained in

complete stellate cell medium and placed in a CO_2 incubator. Cell culture media was refreshed every 2-3 day.

4.5.9 *In situ* stiffening of cell-laden hydrogels and characterization of cell viability and morphology

To induce *in situ* stiffening, cell-laden hydrogels were transferred to a 48-well plate with wells containing cell media supplemented with 1kU/ml tyrosinase. Gels were incubated for 6 hour at 37^{o}C in 5% CO_2. Following the stiffening process, cell-laden hydrogels were transferred to and maintained in a 24-well plate containing only cell culture media. Encapsulated PSCs were stained with live/dead staining kit (Life Technologies) and imaged via confocal microscopy (Olympus Fluoview FV100 laser scanning microscope). To qualitatively assess the viability of the cells, *z*-stack images (100 μm thick, 10 μm per slice) were obtained from a minimum of three random fields of view for all experiments. Cell viability was also quantitatively assessed using AlamarBlue® reagent. In brief, cell-laden hydrogels were incubated in 500 μl of cell culture media diluted by 1:10 dilution of the reagent for 2.5 hour. Following incubation, 200 μl of diluted media was transferred to a clear 96-well microplate, and the resulting fluorescence from the cells within hydrogels was determined by a microplate reader (SynergyHTX, BioTek; ex 560 nm, em 590 nm). F-actin staining was conducted to visualize cell spreading. Briefly, encapsulated cells were fixed in 4% paraformaldehyde for 1 hour at room temperature on an orbital shaker. Following fixation, hydrogels were washed with DPBS (2 time for 10 minute each) and permeabilized using 100X dilution of saponin (100 mg/ml in DMSO) in DPBS for 1 hour, followed by two successive washes in DPBS for 10 minute each. Cell-laden gels were then incubated overnight at 4^{o}C in DPBS solution containing 100 nM working solution of rhodamine phalloidin (F-actin) and a 1:1000 dilution of DAPI (cell nuclei). On the day of imaging, cell-laden gels were washed three times in DPBST (DPBS with 1 *v/v%* of Tween-20) and imaged with confocal microscopy as described above. Cell spreading was quantified using three different fields for each condition. The perpendicular major (length) and minor (width) axes of individual cells were measured using Nikon imaging software (NIS-Elements) and length to width aspect ratios were determined. For each condition the total number of cells assessed ranged from 75 to 90 cells. GraphPad Prism 6 software was used to determine the cumulative distribution of aspect ratios collected.

4.5.10 mRNA isolation, reverse transcription, and quantitative real time PCR

On predetermined days, hydrogels containing encapsulated PSCs were collected, placed in Dna_{se}/Rna_{se}-free microtubes, and flash frozen using liquid nitrogen. Samples were then stored at -80ºC until use. To extract mRNA, frozen gels were homogenized in 300 µl of lysis buffer (NucleoSpin RNA II kit, Clontech) and were subjected to two additional cycles of freeze-thaw in order to lyse cells. Lysates were purified using NucleoSpin Filters. Following purification, 300 µl of Rnase-free 70% ethanol was added to the lysates and mixed thoroughly. The mixtures were then transferred to NucleoSpin RNA columns for RNA extraction following manufacturer's protocol. Using 30 µl of Dna_{se}/Rna_{se}-free water, the isolated RNAs were eluted and then quantified by UV spectrometry (NanoDrop 2000, Thermo Scientific). Using PrimeScript RT reagent kit (Clontech) the total isolated RNA was converted into single-stranded cDNA. Gene expression level was assessed by quantitative real-time PCR and analyzed following a published protocol. Real-time PCR primer sequences can be found listed in Table 4.1.

4.5.11 Statistics

Statistical analyses were conducted by Two-Way ANOVA followed by Bonferroni's post-hoc test using GraphPad Prism 6 software. The control group was specified in the respective figure caption. All experiments were conducted independently for at least three times and data presented were Mean ± SEM. Single, double, and triple asterisks represent $p < 0.05$, 0.001, and 0.0001, respectively. $p<0.05$ was considered statistically significant.

4.6 Conclusion

In summary, we have developed a dynamic hydrogel platform capable of undergoing on-demand and *in situ* gel stiffening by means of tyrosinase-mediated DOPA formation. Building upon the biomimetic features afforded by the diverse thiol-norbornene hydrogels, we designed simple peptide crosslinkers containing additional tyrosine residues for tyrosinase-mediated gel stiffening. Through exogenously adding tyrosinase, the hydrogels could be stiffened on-demand and with high controllability. The hydrogel system was cytocompatible for *in situ* cell encapsulation and the stiffening process did not induce cell damage. The stiffened hydrogel network restricted cell spreading and enhanced expression of genes relevant to myofibroblastic activation of PSCs, including α-SMA and HIF-1α. This hydrogel system provides an alternative

stiffening strategy for *in situ* hydrogel stiffening without creating additional radicals during the stiffening process. Finally, the stiffening process takes hours to days to complete, and hence more closely mimics the actual tissue stiffening process *in vivo*. Future work will be focused on exploiting this stiffening strategy for molecular mechanisms related to the stiffening microenvironment found in pancreatic desmoplasia.

CHAPTER 5. BIOMIMETIC AND ENZYME-RESPONSIVE DYNAMIC HYDROGELS FOR STUDYING CELL-MATRIX INTERACTIONS IN PANCREATIC DUCTAL ADENOCARCINOMA

(As published in *Biomaterials*, 2018 (160) 24-36)

5.1 Abstract

Tumor microenvironment (TME) governs most aspects of cancer progression and *in vitro* 3D cell culture platforms are increasingly developed to emulate the interactions between components of the stromal tissues and cancer cells. However, conventional cell culture platforms are inadequate in recapitulating the TME which has complex compositions and dynamically changing matrix mechanics. In this study, we developed a dynamic gelatin-hyaluronic acid hybrid hydrogel system through integrating modular thiol-norbornene photopolymerization and enzyme-triggered on-demand matrix stiffening. In particular, gelatin was dually modified with norbornene and 4-hydroxyphenylacetic acid to render this bioactive protein photo-crosslinkable (through thiol-norbornene gelation) and responsive to tyrosinase-triggered on-demand stiffening (through HPA dimerization). In addition to the modified gelatin that provides basic cell adhesive motifs and protease cleavable sequences, hyaluronic acid (HA), an essential tumor matrix, was modularly and covalently incorporated into the cell-laden gel network. We systematically characterized macromer modification, gel crosslinking, as well as enzyme-triggered stiffening and degradation. We also evaluated the influence of matrix composition and dynamic stiffening on pancreatic ductal adenocarcinoma (PDAC) cell fate in 3D. We found that either HA-containing matrix or a dynamically stiffened microenvironment inhibited PDAC cell growth. Interestingly, these two factors synergistically induced cell phenotypic changes that resembled cell migration and/or invasion in 3D. Additional mRNA expression array analyses revealed changes unique to the presence of HA, to a stiffened microenvironment, or to the combination of both. Finally, we presented immunostaining and mRNA expression data to demonstrate that these irregular PDAC cell phenotypes were a result of matrix-induced epithelial-mesenchymal transition (EMT).

5.2 Introduction

Pancreatic cancer is currently the third leading cause of all cancer-related deaths. More than 53,000 new pancreatic cancer cases and 43,000 deaths are projected in 2017 [273]. The exceptionally dense stromal tissue (i.e., desmoplasia) in pancreatic ductal adenocarcinoma (PDAC), the most common form of pancreatic cancer, is considered the major hurdle to effective treatments [274]. Pancreatic desmoplasia is rich in extracellular matrix (ECM) proteins (e.g., collagen, fibronectin), glycosaminoglycans (GAGs, e.g., hyaluronic acid (HA)), cytokines (e.g., epidermal growth factor (EGF), transforming growth factor-β (TGF-β)), as well as immune and stromal cells [47, 83, 275, 276]. The compositions in the stroma tissue act collectively to induce epithelial-mesenchymal transition (EMT) in cancer cells [277]. EMT is a complex process regulated by interactions of cancer-stromal cell, as well as bi-directional signaling between cancer cells and the surrounding tumor matrix [1, 36]. For example, inflammatory cytokines and growth factors, including TGF-β and EGF, are known to promote EMT in PDAC cells [23, 36, 234, 278]. These cytokines are abnormally expressed during tumor progression, leading to downregulation of epithelial markers (e.g., E-cadherin) and upregulation of mesenchymal markers (e.g., N-cadherin, SNAIL, TWIST, SLUG, and ZEB1, etc.) [279, 280]. Under the stimulation of abnormally expressed cytokines, PDAC cells lose cell-cell junctions and transform into cells with a migratory and invasive phenotype. Moreover, these cellular changes render cancer cells chemo-resistant [72, 277, 279, 281].

In addition to soluble cytokines, many ECM components are overexpressed by stromal and cancer cells during tumor progression. The accumulation of ECM proteins and GAGs around cancer cells builds up a dense desmoplasia that not only physically restricts penetration of chemotherapeutics but also causes abnormal mechanotransduction in cancer cells [135, 282]. For example, excessive accumulation of HA was detected in cell culture and in mature PDAC stroma [283]. HA binds to cell surface receptors, including CD44, layilin, and receptor for hyaluronan-mediated motility (RHAMM) [84, 283, 284]. The activation of these receptors has been positively correlated with enhanced cancer cell proliferation, invasion, and drug resistance [285]. In addition, HA accumulation also leads to elevated fluid stress that could induce abnormal mechanosensing in the cancer cells and limit the transport of anti-cancer drugs [43, 79]. Nonetheless, the roles of HA in a stiffening microenvironment on PDAC cell EMT have not been extensively studied owing

to the lack of an appropriate three-dimensional (3D) culture system capable of mimicking the dynamic stroma stiffening process.

To investigate cancer cell responses induced by ECM, most studies utilized two-dimensional (2D) tissue culture plate coated with matrix proteins or 3D hydrogels with static or degrading mechanical property [119]. Unfortunately, these convenient culture platforms do not capture the dynamic landscape of a stiffening tumor microenvironment (TME). Some dynamic hydrogels have been developed to mimic the temporal mechanical changes of tumor matrix. For example, Suggs and colleagues developed an alginate-based hydrogel that could be dynamically stiffened by temperature-induced calcium release [96]. MCF10A mammary epithelial cells, which are non-tumorigenic, were nonetheless found to exhibit an invasive phenotype when cultured in a stiffened matrix, a result consistent with earlier work [10, 286]. In another example, Xu *et al.* developed a double-network dynamic hydrogel via a two-step light-mediated polymerization process [287]. Methacrylate and cysteine dually functionalized HA were crosslinked into hydrogels through ultraviolet (UV) light polymerization, followed by infiltrating the hydrogel with additional macromers, photoinitiators, and secondary UV light-mediated polymerization. The authors concluded that encapsulated cancer cells became invasive in the stiffened gel. Although these strategies presented dynamic matrix stiffening, the components and approaches were either not biologically relevant to the TME due to the inclusion of alginate, or exposed cells to UV light excessively.

Our group has reported several semi-synthetic poly(ethylene glycol) (PEG)-peptide hydrogels for *in vitro* culture of pancreatic cancer cells [260, 278, 288, 289]. For example, we have evaluated PDAC cell EMT in hydrogels immobilized with fibronectin or laminin-derived peptides [288]. We have also studied the influence of matrix-entrapped collagen-1 and soluble cytokines (e.g., TGF-β1 and EGF) on PDAC cell fate, including proliferation, chemo-resistance, and EMT in 3D [260]. In order to mimic the dynamic tumor stromal tissue, we have recently developed a tyrosinase-triggered post-gelation crosslinking platform for on-demand stiffening of cell-laden hydrogels [213]. These hydrogels were prepared by thiol-norbornene photopolymerization using 8-arm PEG-norbornene (PEG8NB) and a simple peptide linker (i.e., KCYGPQGIWGQYCK) sensitive to both matrix metalloproteinase (MMP) induced cleavage and tyrosinase-triggered di-tyrosine crosslinking. Following the thiol-norbornene gelation, the tyrosine residues in the primary network served as substrates for exogenously added tyrosinase, which catalyzes di-tyrosine

crosslinking and increases hydrogel crosslinking density and stiffness. Furthermore, enzyme-triggered on-demand stiffened hydrogels altered morphology of pancreatic stellate cells (PSCs) cultured in 3D and resulted in upregulation of α-smooth muscle actin (α-SMA), a signature marker of myofibroblastic activation.

Although the tyrosinase-stiffened PEG-peptide hydrogels have been useful in studying the effect of dynamic matrix stiffening on cancer stromal cell fate, these gels represented minimal tumor-related matrix components. In a separate study, our group designed biomimetic hydrogels formed by visible light initiated crosslinking of gelatin-norbornene (Gel_{NB}) and thiolated HA (THA) [289]. These gels were established to understand the effect of individual matrix component and static gel stiffness on PDAC cells grown in 3D but did not encompass dynamic stiffening feature. Here, we present a pathophysiologically relevant dynamic biomimetic hydrogel system where the gel network was formed by THA and dually-functionalized gelatin. The later was chemically modified with norbornene (NB) and hydroxyphenylacetic acid (HPA), yielding a multifunctional and cell responsive macromer (i.e., Gel_{NBHPA}). Through orthogonal thiol-norbornene photopolymerization, Gel_{NBHPA} were modularly crosslinked by THA or by inert macromer PEG-tetra-thiol (PEG4SH). The bioactive peptide sequences on gelatin permitted cell adhesion and MMP-mediated local matrix cleavage. The conjugated HPA moieties rendered the cell-laden hydrogels sensitivity to tyrosinase-triggered di-HPA crosslinking, which led to physiologically relevant degree of on-demand stiffening in the presence of PDAC cells. With this new hybrid biomimetic hydrogel system, the effects of matrix biochemical and biophysical cues could be easily decoupled for gaining new insights into the effects of matrix compositions on PDAC cell behavior. We systematically characterized gel crosslinking and enzyme-triggered stiffening and degradation. We also studied the independent and synergistic effects of matrix compositions and dynamic stiffening on PDAC cell fate in 3D by analyzing cell morphological changes, immunostaining, and expression of PDAC-related genes at the mRNA level. Through modularly crosslinking and dynamically stiffening of tumor-mimetic matrices, we discovered the unique role of HA on PDAC cell fate processes and modulation of gene expression.

5.3 Result and Discussion

5.3.1 Principles of dynamic hydrogel design and macromer synthesis

In order to recapitulate the bioactive components and the stiffening tumor microenvironment in PDAC (Figure 5.1A), we prepared gelatin-hyaluronic acid (Gel_{NB}&HA) hydrogels capable of undergoing on-demand stiffening. We synthesized Gel_NB and Gel_{NBHPA} (Figure 5.1B), which could be modularly crosslinked with commercially available THA (Figure 5.1C) through thiol-norbornene photopolymerization. Gel_{NBHPA} was synthesized through sequentially reacting gelatin with carbic anhydride (yielding Gel_{NB}) and 4-HPA (yielding Gel_{NBHPA}). The degrees of gelatin functionalization, as characterized by fluoraldehyde assay, was ~ 37% and ~ 41% respectively for NB and HPA modification (equivalent to 1.6 mM NB and 1.64 mM HPA per wt% gelatin, data was not shown). The presence of NB group on gelation permitted rapid gelation with THA (within 2 minute) through orthogonal thiol-norbornene photopolymerization (Figure 5.1D). When Gel_{NBHPA} was used, the gels could be dynamically stiffened due to tyrosinase-triggered HPA dimerization (Figure 5.1E).

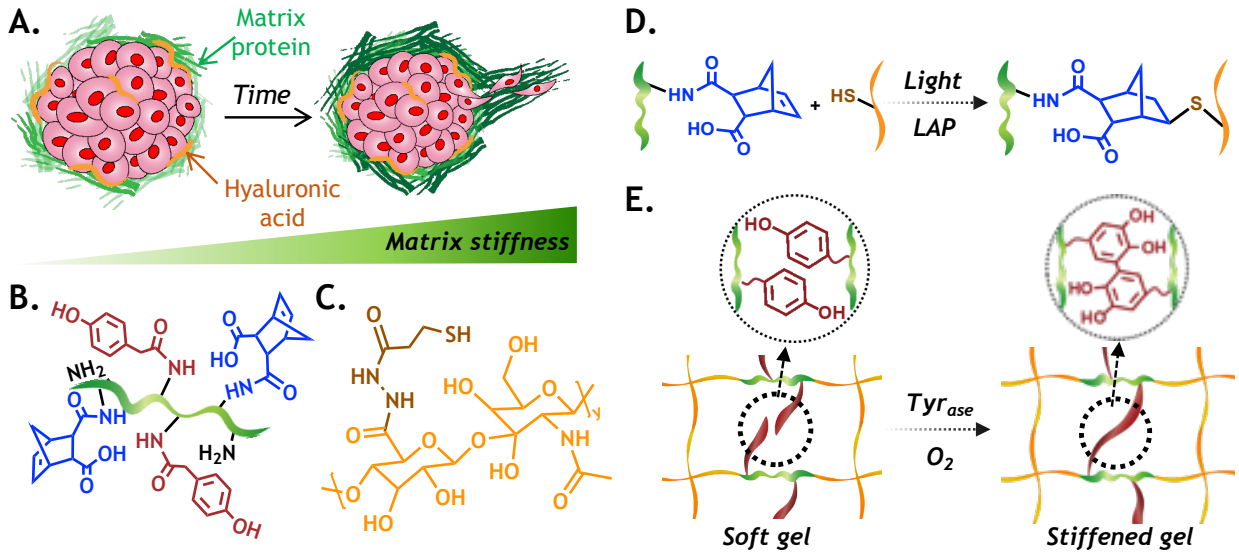

Figure 5.1. Enzyme-triggered on-demand stiffening of biomimetic hydrogels for in vitro cancer cell research. (A) Schematic of a tumor microenvironment with various matrix proteins and glycosaminoglycans (e.g., HA). Accumulation of these ECM leads to matrix stiffening and tumor progression. Chemical structures of (B) Gel_{NBHPA} and (C) THA. (D) Thiol-norbornene photopolymerization. (E) Schematic of tyrosinase-triggered di-HPA crosslinking for on-demand hydrogel stiffening.

Successful conjugation of NB and HPA moieties was characterized by the ^{1}HNMR (Figure 5.2A). Chemical shifts between 6.1-6.3 ppm (blue region) indicated successful NB functionalization on the gelatin backbone (7.2-7.4 ppm, green region). After HPA conjugation, new chemical shifts emerged (6.9-7.2 ppm, red region) in Gel_{NBHPA}, indicating the presence of aromatic HPA [290]. The modification of HPA on Gel_{NB} was further confirmed by UV/Vis absorbance spectrometry (Figure 5.2B) through detecting increased absorbance at 280 nm [291]. UV/Vis spectrometry were also used to monitor tyrosinase-triggered HPA dimerization. Due to the limited amount of tyrosine residue in the unmodified gelatin sequence (< 0.5 %) [292], addition of tyrosinase (tyr_{ase}, 1 kU/ml) did not change the absorbance signature of GelNB significantly (Figure 5.2C). However, when Gel_{NBHPA} was treated with tyr_{ase}, new absorbance shoulder emerged at ~ 320 nm (Figure 5.2D), suggesting that HPA motifs were dimerized by tyrosinase [293].

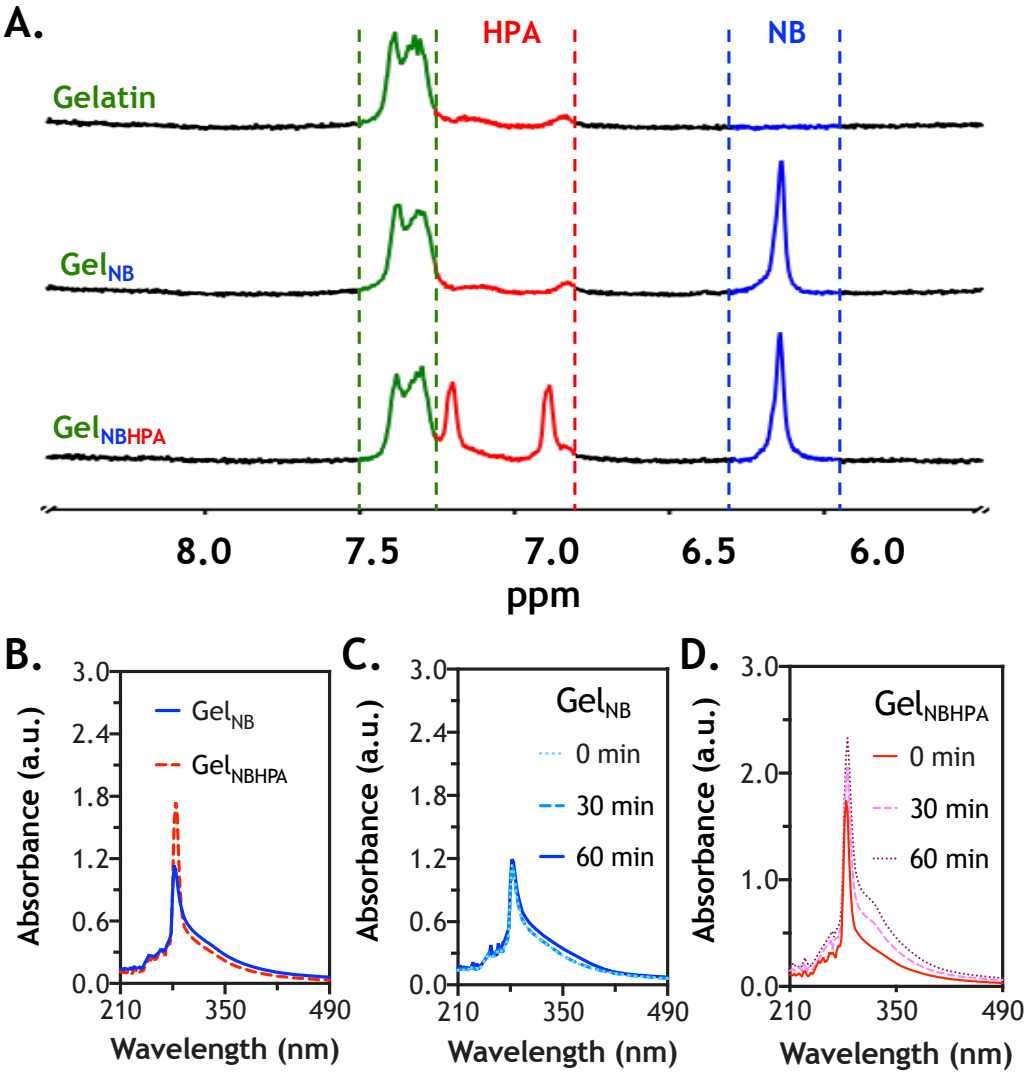

Figure 5.2. Characterization of functionalized gelatin macromers. (A) ^{1}NMR spectra of Gelatin, Gel_{NB}, and Gel_{NBHPA}. UV/Vis absorbance spectra of soluble (B) Gel_{NB} and Gel_{NBHPA}, (C) soluble Gel_{NB}, and (D) soluble Gel_{NBHPA} treated with tyr_{ase}, 1 kU/ml.

5.3.2 Gel crosslinking and tyrosinase-mediated dynamic stiffening

To evaluate if conjugation of HPA on Gel_{NB} altered the efficiency of light-mediated thiol-norbornene photopolymerization, we conducted *in situ* photorheometry using Gel_{NB} or Gel_{NBHPA} (7 wt%) and with PEG4SH (1.4 wt%) as the thiol crosslinker. As shown in Figure 5.3A and Figure 5.3B, gel points (i.e., storage modulus G' surpassed loss modulus G") were ~9 and ~18 seconds for gelation using Gel_{NB} and Gel_{NBHPA}, respectively. However, G' reached plateau within 2 minutes for both gelatin macromers. Furthermore, gels prepared from Gel_{NBHPA} had lower moduli

(~1 kPa) compared with gels crosslinked by Gel_{NB} (~1.7 kPa). Hydrogels crosslinked by Gel_{NBHPA} and PEG4SH were used to evaluate the efficiency of tyrosinase-triggered on-demand stiffening. As shown in Figure 5.3C, gel moduli did not change overtime when the solution contained no tyr_{ase}. Gel moduli only increased slightly when incubating with low tyr_{ase} concentration (0.1 kU/ml) for 4 hours. When tyr_{ase} concentration was increased to above 0.5 kU/ml, hydrogels were significantly stiffened after only two hours of incubation. The color of gels treated with higher tyr_{ase} concentrations was darker (Figure 5.3D), indicative of HPA dimer formation and higher degree of stiffening.

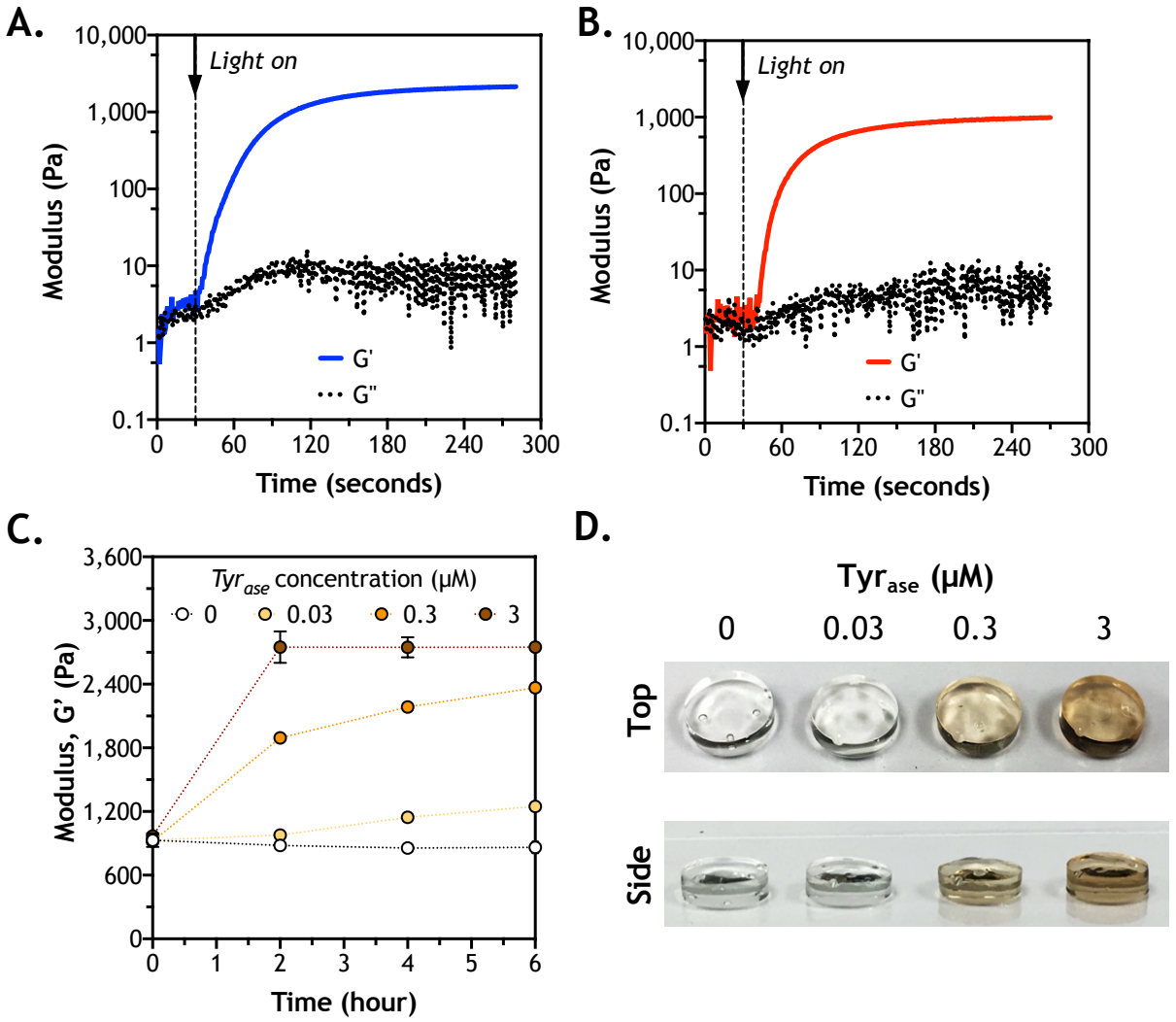

Figure 5.3. Characterization of thiol-norbornene gelation using functionalized gelation macromers. Evaluation of storage (G') and loss (G") moduli of thiol-norbornene gelation using (A) Gel_{NB}&PEG and (B) Gel_{NBHPA}&PEG. Gel_{NB} or Gel_{NBHPA} was added at 7 wt%, whereas PEG4SH was added at 1.4 wt% (R = 0.5). (C) On-demand stiffening of Gel_{NB}&PEG hydrogels via adding tyr_{ase} at different concentrations (N = 3, Mean ± SEM). (D) Photograph of tyr_{ase}-stiffened hydrogels.

In addition to tyr_{ase} concentration, HPA contents in the hydrogel could also be modularly adjusted to control the degree of stiffening. As shown in Figure 5.4A, hydrogels formed with pure Gel_{NB} (i.e., 0% Gel_{NBHPA}) were not susceptible to tyr_{ase} -triggered stiffening. However, when the amount of Gel_{NBHPA} was modularly increased to 50 % (i.e., half Gel_{NB}, half Gel_{NBHPA}) and 100 % (i.e., pure Gel_{NBHPA}), gel was stiffened from ~1 kPa to ~2.2 kPa and ~2.9 kPa, respectively. We further adjusted the weight percentages of Gel_{NBHPA} (e.g., 3, 5, 7 wt%) and PEG4SH (e.g., 0.6, 1, 1.4 wt%) in the macromer precursor solution to obtain gels with varying HPA contents but similar

initial shear moduli (~1 kPa, Figure 5.4B). Following tyrosinase treatment, gels with higher HPA content (i.e., 11.2 mM in 7 wt% Gel_{NBHPA}) were stiffened to a higher degree (~2.7 kPa, Figure 5.4B). We also prepared gels with different thiol/norbornene stoichiometric ratio ($R_{thiol/ene}$) but with the same HPA contents (i.e., 7 wt% Gel_{NBHPA} and PEG4SH at 0.8, 1.4, 2, or 2.8 wt%. Figure 5.4C). There was a positive correlation between $R_{thiol/ene}$, initial gel modulus and these gels could all be dynamically stiffened regardless of the initial moduli (Figure 5.4C). Most importantly, once stiffened by tyr_{ase} (1 kU/ml), all gels remained stiff for the next few days and the degree of stiffening (~1 kPa to ~8 kPa) was relevant to the stiffness change in a stiffening TME [294].

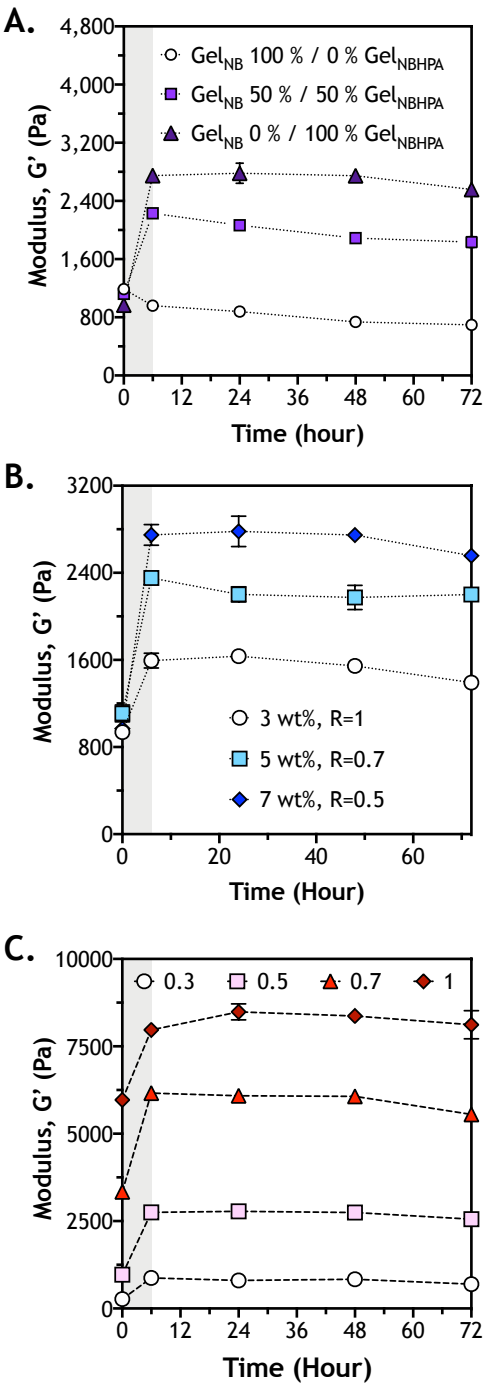

Figure 5.4. Effect of macromer compositions on tyr_{ase}-triggered on-demand gel stiffening. (A) Shear moduli of hydrogels formed by 7 wt% of gelatin macromer (Gel_{NB} and/or Gel_{NBHPA}) and 1.4 wt% PEG4SH. Gels were formed with different fraction of Gel_{NBHPA} and Gel_{NB}. (B) Shear moduli of hydrogels formed by 3, 5, or 7 wt% of Gel_{NBHPA} and with 0.7 wt% of PEG4SH, yielding gels with varied HPA contents but with similar initial modulus. (C) Shear moduli of hydrogels formed by 7 wt% of Gel_{NBHPA} but with varied PEG4SH content to yield thiol/ene ratio of 0.3, 0.5, 0.7, and 1. These gels contained the same HPA content but different initial modulus. All hydrogels were treated with 1 kU/ml tyr_{ase} from 0-6 hour (N = 3, Mean ± SEM).

5.3.3 Enzyme-mediated degradation of soft and stiffened hydrogels

Owing to the use of naturally derived macromers (i.e., gelation and HA), this hydrogel system was susceptible to degradation by cell-secreted collagenase and hyaluronidase. To evaluate the degradability of these hydrogels, we crosslinked gels modularly using Gel_{NB}, Gel_{NBHPA}, PEG4SH, and THA. Prior to enzymatic degradation, we evaluated the stiffness of these gels prior to and after tyr_{ase}-treatment. As expected, hydrogels crosslinked with Gel_{NB} were not sensitive to tyr_{ase}-triggered stiffening, as demonstrated by their relatively constant moduli (~1 kPa. Figure 5.5A). On the other hand, the use of Gel_{NBHPA} rendered the hydrogels sensitive to tyr_{ase} -triggered on-demand stiffening (Figure 5.5A). For example, 1 kU/ml of tyr_{ase} treatment to gels crosslinked by 0.7 wt% THA led to significant increase of gel moduli from ~1 kPa to ~3.5 kPa. Next, soft gels (~1 kPa) or tyr_{ase}-stiffened gels (~3.5 kPa) were treated with collagenase-1 (40 U/mL, Figure 5.5B) or hyaluronidase (300 U/ml, Figure 5.5C). In general, stiffened gels degraded slower due to higher crosslinking density contributed by the additional di-HPA linkages [213]. Different from collagenase-mediated degradation where all gels were degraded regardless of stiffness, limited hyaluronidase-mediated degradation was observed (~25 % mass loss) in tyr_{ase}-stiffened gels.

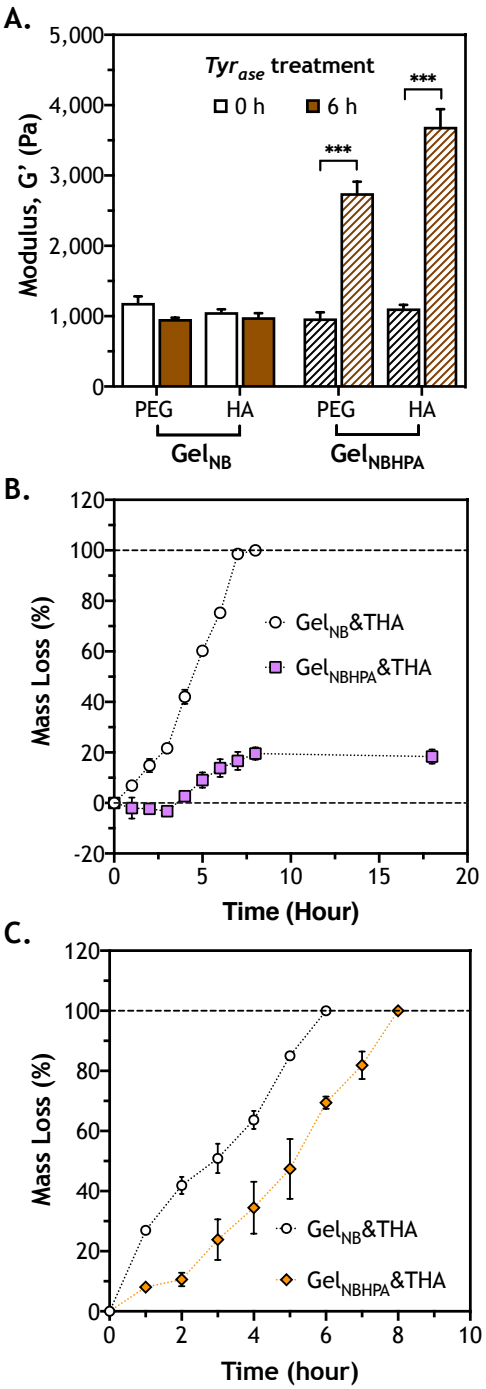

Figure 5.5. Effect of tyrosinase-mediated gel stiffening on enzyme-mediated degradation. (A) Comparison of modulus changes in hydrogels modularly crosslinked by Gel_{NB} or Gel_{NBHPA} with PEG4SH or THA. Gel moduli were characterized prior to and after treating with 1 kU/ml tyr_{ase} for 6 hour ($^{***}p < 0.001$). (B) Mass loss profiles of Gel_{NB}&HA (soft) or Gel_{NBHPA}&HA (tyr_{ase}-stiffened) hydrogels treated with collagenase (40 U/ml). (C) Mass loss profiles of Gel_{NB}&HA (soft) or Gel_{NBHPA}&HA (tyr_{ase}-stiffened) hydrogels treated with hyaluronidase (300 U/ml). Hydrogels were formed by 7 wt% Gel_{NB} or Gel_{NBHPA} with 0.7 wt% THA (N = 3, Mean ± SEM).

5.3.4 Effect of matrix compositions on PDAC morphological changes

To study the influences of matrix compositions on PDAC cells, we evaluated proliferation and morphology of COLO-357 cells, a PDAC cell line with wild-type KRAS, in modularly crosslinked hydrogels, including: (1) Gel_{NB} with PEG4SH (Gel_{NB}&PEG), (2) Gel_{NB} with THA (Gel_{NB}&HA), (3) Gel_{NBHPA} with PEG4SH (Gel_{NBHPA}&PEG), and (4) Gel_{NBHPA} with THA (Gel_{NBHPA}&HA). Note that only gels with Gel_{NBHPA} were susceptible to tyr_{ase}-mediated dynamic stiffening. These gels were formulated such that they had similar initial shear moduli (i.e., 7 wt% Gel_{NB} or Gel_{NBHPA}, 1.4 wt% PEG4SH or 0.7 wt% THA, G'~ 1 kPa). Live/dead staining images showed high cell viability after the initial cell encapsulation process and throughout the 14-day *in vitro* culture (Figure 5.6A). Cells grew into spheroids or clusters in all gels but were visibly larger in Gel/PEG hydrogels (i.e., soft and HA-free). Cell proliferation was significantly inhibited (i.e., smaller spheroids) when the hydrogels were soft and contained HA (i.e., Gel_{NB}&HA) or stiffened but contained no HA (i.e., Gel_{NBHPA}&PEG). Interestingly, the morphology of the spheroids/clusters in Gel_{NBHPA}&HA gels became highly irregular (Figure 5.6A, right column), an indication of increased cell motility. This could be attributed to higher cell proliferation and/or migration. F-actin staining images also revealed extensive spreading of PDAC cells encapsulated in Gel_{NBHPA}&HA gels (Figure 5.6B**)**.

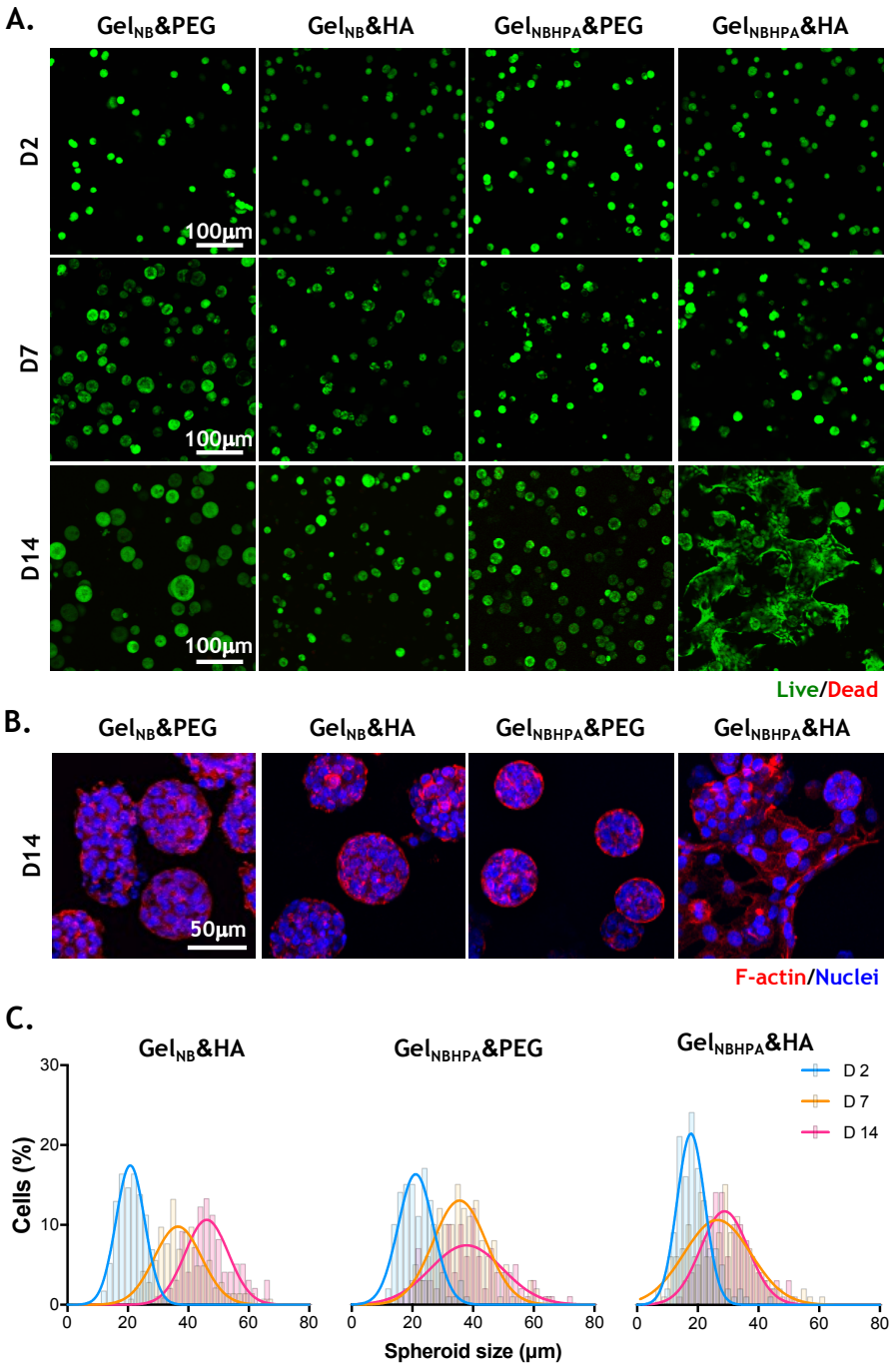

Figure 5.6. Effect of matrix compositions on morphological changes of COLO-357 cells. (A) Representative confocal *z*-stack live/dead stained images of cells in Gel_{NB}&PEG, Gel_{NB}&HA, Gel_{NBHPA}&PEG, and Gel_{NBHPA}&HA gels. Gels were incubated with tyrosinase for 6 hours at day 2 and transferred to fresh media. (B) Confocal *z*-stack images of F-actin staining of encapsulated cells on day 14 post-encapsulation. Cell nuclei were counter-stained with DAPI. (C) Cell spheroid diameters as a function of time and hydrogel formulations. Histograms were fitted with Gaussian distribution.

To quantify changes of spheroid sizes in matrices with different compositions, we analyzed spheroids size from live/dead stained images (Figure 5.6A). The average diameter of spheroids was around 20 μm on day 2 in all gels (Figure 5.7). Cells encapsulated in soft HA-free matrix (i.e., Gel_{NB}&PEG) grew into relative large spheroids (~ 50 μm), whereas the size of cell spheroids in Gel_{NB}&HA and Gel_{NBHPA}&PEG gels maintained at around 20-30 μm on day 14 (Figure 5.8B and C). As for PDAC cells encapsulated in Gel_{NBHPA}&HA gels, the spheroids appeared to have similar sizes as the other groups at early days (~20 μm from day 2 to day 7, Figure 5.8A). However, due to the highly irregular cell morphology on day 14, we did not analyze cluster sizes in this condition (Figure 5.8).

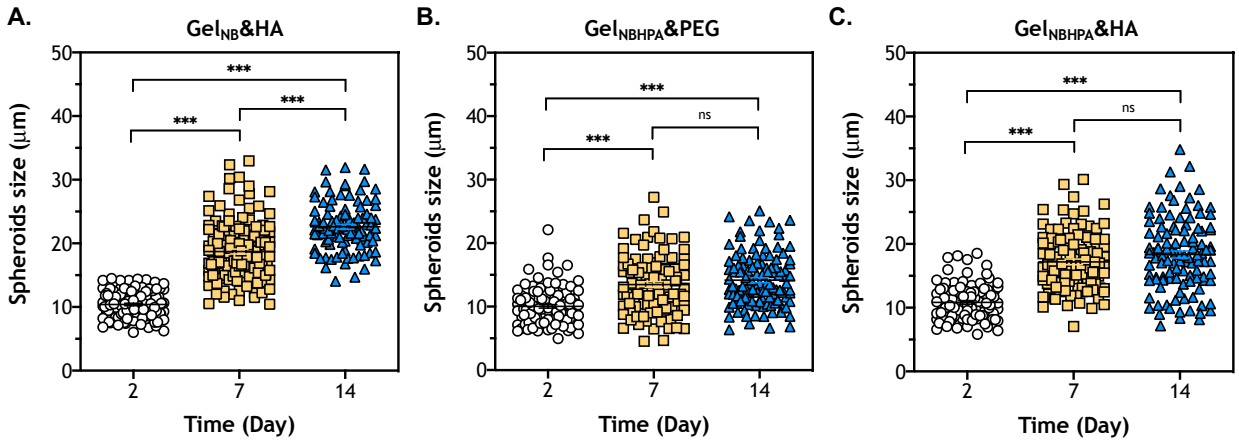

Figure 5.7. Effect of gel formulations on spheroids size. COLO357 cells were grown in soft and HA-free (Gel_{NB}&PEG), soft and HA-containing (Gel_{NB}&HA) or stiffened and HA-free (Gel_{NBHPA}&PEG) hydrogels (****p<0.005*).

To gain insight into the influences of microenvironment changes on PDAC cells, we evaluated mRNA expression profiles using TaqMan® Array - Human Pancreatic Adenocarcinoma, which contained pre-deposited primer sets for 92 PDAC-associated and 4 housekeeping genes. Cells were encapsulated in the four groups of hydrogels as described in Figure 5.6A, following by tyr_{ase} incubation for 6 hour on day 2 and culturing for additional 12 day (14 day in total). As described before, only gels containing HPA groups would be stiffened. mRNA expression levels were detected using quantitative real time-PCR in TaqMan® Array with pre-deposited primers. The expression levels were normalized to GAPDH (housekeeping gene), then to the respective gene in the control group (i.e., Gel_{NB}&PEG gels). The expression levels of all mRNA in this group were set as one-fold). mRNA expression levels in the remaining three groups (each with three

biological repeats) were ranked from the highest to the lowest fold-changes and then plotted into heat maps (Figure 5.8 and Table 5.1). Among the 92 PDAC-related mRNA, 29, 24, and 48 were up-regulated by more than 2-fold for cells encapsulated in Gel_{NB}&HA (i.e., soft and with HA), Gel_{NBHPA}&PEG (i.e., stiffened and HA-free), and Gel_{NBHPA}&HA (i.e., stiffened and HA-containing) gels, respectively. Furthermore, 52, 48 and 32 mRNA were down-regulated by more than 2-fold in respective gels. The much higher number of mRNA (i.e., 48) upregulated in the cells encapsulated in Gel_{NBHPA}&HA gels suggested a potential synergistic effect of HA and a stiffening matrix on PDAC cell progression.

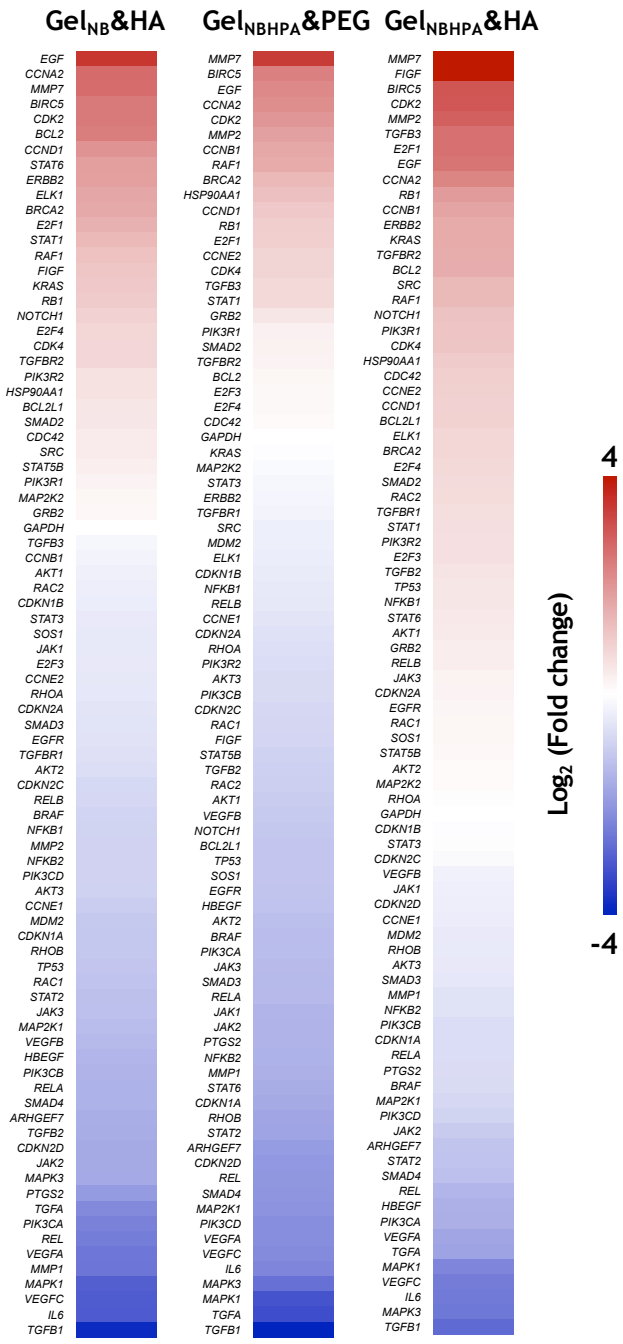

Figure 5.8. Effect of matrix compositions on PDAC-related gene expression in COLO-357 cells. Heat maps of Taqman® array analyses of gene expression in cells encapsulated in Gel$_{NB}$&PEG (control group, data not shown in the figure as expression levels of all genes were set as one-fold), Gel$_{NB}$&HA, Gel$_{NBHPA}$&PEG, and Gel$_{NBHPA}$&HA hydrogels. Gene expression levels (plotted in $\log_2$ scale) were normalized to GAPDH within each group, then normalized to respective gene in Gel$_{NB}$&PEG hydrogels. Each of the four gel formulations contained three biological replicates. Warm (red) colors showed high expression, whereas cold (blue) colors showed low expression.

We further examined the expression of genes that were only upregulated in cells encapsulated in stiffened gels (Figure 5.9A), in HA-containing gels (Figure 5.9B), as well as in stiffened and HA-containing gels (Figure 5.9C). We found that the expression of MMP-2 (encodes matrix metalloproteinase-2), TGF-β3, CCNB1 (encodes Cyclin B1), CCNE2 (encodes Cyclin E2), and E2F3 (encodes E2F transcription factor 3) were significantly upregulated in cells encapsulated in tyr_{ase}-stiffened gels (Figure 5.9A). We also identified mRNAs that were exclusively upregulated by the presence of HA regardless of matrix stiffness, including FIGF (encodes VEGF-D), ERBB2 (encodes ErbB2 Receptor Tyrosine Kinase 2), KRAS (encodes K-Ras), SRC (encodes Src), NOTCH1 (encodes Notch-1), BCL2L1 (encodes Bcl-2-Like Protein 1), ELK1 (encodes ETS Transcription Factor), STAT6 (encodes Signal Transducer and Activator of Transcription 6), MAP2K2 (encodes Mitogen-Activated Protein Kinase 2), and STAT5B (encodes Signal Transducer and Activator of Transcription 5B) (Figure 5.9B). Finally, genes that were upregulated only in a stiffened and HA-containing matrix were RAC2 (encodes Small GTP Binding Protein Rac2), TGFβR1 (encodes TGFβ receptor 1), TGF-β2, TP53 (encodes Tumor suppressor P53), NFKB1 (encodes Nuclear Factor $_{K}$B1), AKT1 (encodes serine-threonine protein kinase), RELB (encodes NF-KB Subunit), JAK3 (encodes Janus Kinase 3), CDKN2A (encodes Cyclin Dependent Kinase Inhibitor 2A), EGFR (encodes EGF receptor), RAC1 (encodes Small GTP Binding Protein Rac1), SOS1 (encodes SOS Ras/Rac Guanine Nucleotide Exchange Factor 1), AKT2 (encodes AKT Serine/Threonine Kinase 2), and RHOA (encodes Ras Homolog Family Member A) (Figure 5.9C).

Table 5.1. Taqman gene array analysis of COLO-357 cells in gels. All experiments here were conducted independently three samples per groups. Each group was compared to cells encapsulated in soft (Gel_{NB}&PEG) gels and pairs of groups were compared with one-way ANOVA on IBM SPSS software, and following by the Bonferroni post-analysis.

		Sum of Squares	df	Mean Square	F	Sig.
AKT1	Between Groups	4.134	2	2.067	8.771	.017
	Within Groups	1.414	6	.236		
	Total	5.548	8			
AKT2	Between Groups	3.498	2	1.749	2.120	.201
	Within Groups	4.950	6	.825		
	Total	8.448	8			
AKT3	Between Groups	.296	2	.148	2.925	.130
	Within Groups	.303	6	.051		
	Total	.599	8			
ARHGEF7	Between Groups	.909	2	.454	1.719	.257
	Within Groups	1.587	6	.264		
	Total	2.495	8			
BCL2	Between Groups	7.670	2	3.835	10.082	.012
	Within Groups	2.282	6	.380		
	Total	9.953	8			
BCL2L1	Between Groups	9.361	2	4.680	7.411	.024
	Within Groups	3.789	6	.632		
	Total	13.150	8			
BIRC5	Between Groups	.789	2	.394	1.038	.410
	Within Groups	2.280	6	.380		
	Total	3.069	8			
BRAF	Between Groups	.470	2	.235	.728	.521
	Within Groups	1.938	6	.323		
	Total	2.408	8			
BRCA2	Between Groups	1.261	2	.631	2.849	.135
	Within Groups	1.328	6	.221		
	Total	2.589	8			
CCNA2	Between Groups	.313	2	.156	.312	.743
	Within Groups	3.008	6	.501		
	Total	3.321	8			
CCNB1	Between Groups	7.404	2	3.702	37.217	.000
	Within Groups	.597	6	.099		
	Total	8.001	8			
CCND1	Between Groups	.581	2	.291	.210	.816
	Within Groups	8.292	6	1.382		
	Total	8.873	8			
CCNE1	Between Groups	.766	2	.383	1.891	.231
	Within Groups	1.215	6	.202		
	Total	1.980	8			

CCNE2	Between Groups	5.034	2	2.517	16.511	.004
	Within Groups	.915	6	.152		
	Total	5.949	8			
CDC42	Between Groups	1.197	2	.599	3.429	.102
	Within Groups	1.047	6	.175		
	Total	2.245	8			
CDK2	Between Groups	1.290	2	.645	2.306	.181
	Within Groups	1.678	6	.280		
	Total	2.968	8			
CDK4	Between Groups	.246	2	.123	1.178	.370
	Within Groups	.627	6	.104		
	Total	.873	8			
CDKN1A	Between Groups	.957	2	.479	.674	.544
	Within Groups	4.259	6	.710		
	Total	5.216	8			
CDKN1B	Between Groups	.335	2	.168	1.187	.368
	Within Groups	.848	6	.141		
	Total	1.183	8			
CDKN2A	Between Groups	1.487	2	.743	3.949	.080
	Within Groups	1.129	6	.188		
	Total	2.616	8			
CDKN2C	Between Groups	.772	2	.386	4.445	.065
	Within Groups	.521	6	.087		
	Total	1.294	8			
CDKN2D	Between Groups	4.454	2	2.227	29.821	.001
	Within Groups	.448	6	.075		
	Total	4.902	8			
E2F1	Between Groups	4.187	2	2.093	6.437	.032
	Within Groups	1.951	6	.325		
	Total	6.138	8			
E2F3	Between Groups	1.643	2	.822	5.258	.048
	Within Groups	.938	6	.156		
	Total	2.581	8			
E2F4	Between Groups	.960	2	.480	1.095	.393
	Within Groups	2.631	6	.439		
	Total	3.592	8			
EGF	Between Groups	2.182	2	1.091	6.871	.028
	Within Groups	.953	6	.159		
	Total	3.134	8			
EGFR	Between Groups	3.292	2	1.646	6.247	.034
	Within Groups	1.581	6	.264		
	Total	4.873	8			
ELK1	Between Groups	5.575	2	2.788	5.955	.038
	Within Groups	2.809	6	.468		
	Total	8.384	8			
ERBB2	Between Groups	7.205	2	3.602	10.085	.012
	Within Groups	2.143	6	.357		
	Total	9.348	8			

FIGF	Between Groups	57.899	2	28.949	28.546	.001
	Within Groups	6.085	6	1.014		
	Total	63.984	8			
GAPDH	Between Groups	.000	2	.000	.	.
	Within Groups	.000	6	.000		
	Total	.000	8			
GRB2	Between Groups	.154	2	.077	.848	.474
	Within Groups	.545	6	.091		
	Total	.699	8			
HBEGF	Between Groups	.035	2	.017	.036	.964
	Within Groups	2.849	6	.475		
	Total	2.883	8			
HSP90AA1	Between Groups	.625	2	.312	2.921	.130
	Within Groups	.642	6	.107		
	Total	1.266	8			
IL6	Between Groups	1.621	2	.810	.459	.653
	Within Groups	10.599	6	1.766		
	Total	12.219	8			
JAK1	Between Groups	2.566	2	1.283	18.467	.003
	Within Groups	.417	6	.069		
	Total	2.983	8			
JAK2	Between Groups	.750	2	.375	.742	.515
	Within Groups	3.031	6	.505		
	Total	3.781	8			
JAK3	Between Groups	8.075	2	4.037	9.465	.014
	Within Groups	2.559	6	.427		
	Total	10.634	8			
KRAS	Between Groups	3.857	2	1.928	12.249	.008
	Within Groups	.945	6	.157		
	Total	4.801	8			
MAP2K1	Between Groups	2.317	2	1.158	1.914	.227
	Within Groups	3.630	6	.605		
	Total	5.947	8			
MAP2K2	Between Groups	.306	2	.153	.291	.757
	Within Groups	3.150	6	.525		
	Total	3.456	8			
MAPK1	Between Groups	2.200	2	1.100	1.369	.324
	Within Groups	4.821	6	.804		
	Total	7.022	8			
MAPK3	Between Groups	2.993	2	1.497	1.732	.255
	Within Groups	5.184	6	.864		
	Total	8.177	8			
MDM2	Between Groups	1.114	2	.557	1.816	.242
	Within Groups	1.840	6	.307		
	Total	2.954	8			
MMP1	Between Groups	9.851	2	4.925	5.571	.043
	Within Groups	5.304	6	.884		
	Total	15.155	8			

MMP2	Between Groups	21.740	2	10.870	126.866	.000
	Within Groups	.514	6	.086		
	Total	22.254	8			
MMP7	Between Groups	9.717	2	4.859	6.501	.031
	Within Groups	4.484	6	.747		
	Total	14.201	8			
NFKB1	Between Groups	3.180	2	1.590	11.045	.010
	Within Groups	.864	6	.144		
	Total	4.043	8			
NFKB2	Between Groups	1.562	2	.781	4.964	.053
	Within Groups	.944	6	.157		
	Total	2.507	8			
NOTCH1	Between Groups	8.580	2	4.290	11.618	.009
	Within Groups	2.216	6	.369		
	Total	10.796	8			
PIK3CA	Between Groups	2.075	2	1.038	.318	.739
	Within Groups	19.577	6	3.263		
	Total	21.652	8			
PIK3CB	Between Groups	1.512	2	.756	1.565	.284
	Within Groups	2.898	6	.483		
	Total	4.411	8			
PIK3CD	Between Groups	2.590	2	1.295	1.867	.234
	Within Groups	4.163	6	.694		
	Total	6.753	8			
PIK3R1	Between Groups	1.986	2	.993	2.306	.181
	Within Groups	2.584	6	.431		
	Total	4.570	8			
PIK3R2	Between Groups	3.697	2	1.849	5.845	.039
	Within Groups	1.898	6	.316		
	Total	5.595	8			
PTGS2	Between Groups	2.009	2	1.005	6.597	.031
	Within Groups	.914	6	.152		
	Total	2.923	8			
RAC1	Between Groups	2.903	2	1.451	6.954	.027
	Within Groups	1.252	6	.209		
	Total	4.155	8			
RAC2	Between Groups	5.365	2	2.682	5.263	.048
	Within Groups	3.058	6	.510		
	Total	8.422	8			
RAF1	Between Groups	.364	2	.182	.419	.676
	Within Groups	2.610	6	.435		
	Total	2.974	8			
RB1	Between Groups	1.610	2	.805	1.751	.252
	Within Groups	2.759	6	.460		
	Total	4.369	8			
REL	Between Groups	1.176	2	.588	1.368	.324
	Within Groups	2.579	6	.430		
	Total	3.755	8			

RELA	Between Groups	2.599	2	1.300	1.076	.399
	Within Groups	7.243	6	1.207		
	Total	9.842	8			
RELB	Between Groups	2.391	2	1.195	5.562	.043
	Within Groups	1.290	6	.215		
	Total	3.681	8			
RHOA	Between Groups	.854	2	.427	1.161	.375
	Within Groups	2.208	6	.368		
	Total	3.062	8			
RHOB	Between Groups	4.716	2	2.358	2.446	.167
	Within Groups	5.784	6	.964		
	Total	10.500	8			
SMAD2	Between Groups	.291	2	.145	.853	.472
	Within Groups	1.023	6	.170		
	Total	1.314	8			
SMAD3	Between Groups	4.285	2	2.142	8.947	.016
	Within Groups	1.437	6	.239		
	Total	5.721	8			
SMAD4	Between Groups	2.136	2	1.068	9.833	.013
	Within Groups	.652	6	.109		
	Total	2.787	8			
SOS1	Between Groups	2.451	2	1.226	11.434	.009
	Within Groups	.643	6	.107		
	Total	3.094	8			
SRC	Between Groups	3.242	2	1.621	4.947	.054
	Within Groups	1.966	6	.328		
	Total	5.208	8			
STAT1	Between Groups	.998	2	.499	2.700	.146
	Within Groups	1.108	6	.185		
	Total	2.106	8			
STAT2	Between Groups	.526	2	.263	1.611	.275
	Within Groups	.979	6	.163		
	Total	1.505	8			
STAT3	Between Groups	.193	2	.097	.225	.805
	Within Groups	2.575	6	.429		
	Total	2.769	8			
STAT5B	Between Groups	2.801	2	1.400	2.908	.131
	Within Groups	2.889	6	.481		
	Total	5.690	8			
STAT6	Between Groups	15.133	2	7.566	12.083	.008
	Within Groups	3.757	6	.626		
	Total	18.890	8			
TGFA	Between Groups	4.411	2	2.205	7.215	.025
	Within Groups	1.834	6	.306		
	Total	6.245	8			
TGFB1	Between Groups	4.690	2	2.345	6.306	.034
	Within Groups	2.231	6	.372		
	Total	6.922	8			

TGFB2	Between Groups	8.351	2	4.176	6.947	.027
	Within Groups	3.606	6	.601		
	Total	11.957	8			
TGFB3	Between Groups	9.799	2	4.900	5.228	.048
	Within Groups	5.623	6	.937		
	Total	15.422	8			
TGFBR1	Between Groups	3.546	2	1.773	2.493	.163
	Within Groups	4.266	6	.711		
	Total	7.812	8			
TGFBR2	Between Groups	2.749	2	1.374	5.308	.047
	Within Groups	1.554	6	.259		
	Total	4.302	8			
TP53	Between Groups	7.508	2	3.754	4.345	.068
	Within Groups	5.184	6	.864		
	Total	12.693	8			
VEGFA	Between Groups	.992	2	.496	1.827	.240
	Within Groups	1.629	6	.271		
	Total	2.621	8			
VEGFB	Between Groups	2.075	2	1.038	7.348	.024
	Within Groups	.847	6	.141		
	Total	2.922	8			
VEGFC	Between Groups	1.108	2	.554	1.601	.277
	Within Groups	2.076	6	.346		
	Total	3.184	8			

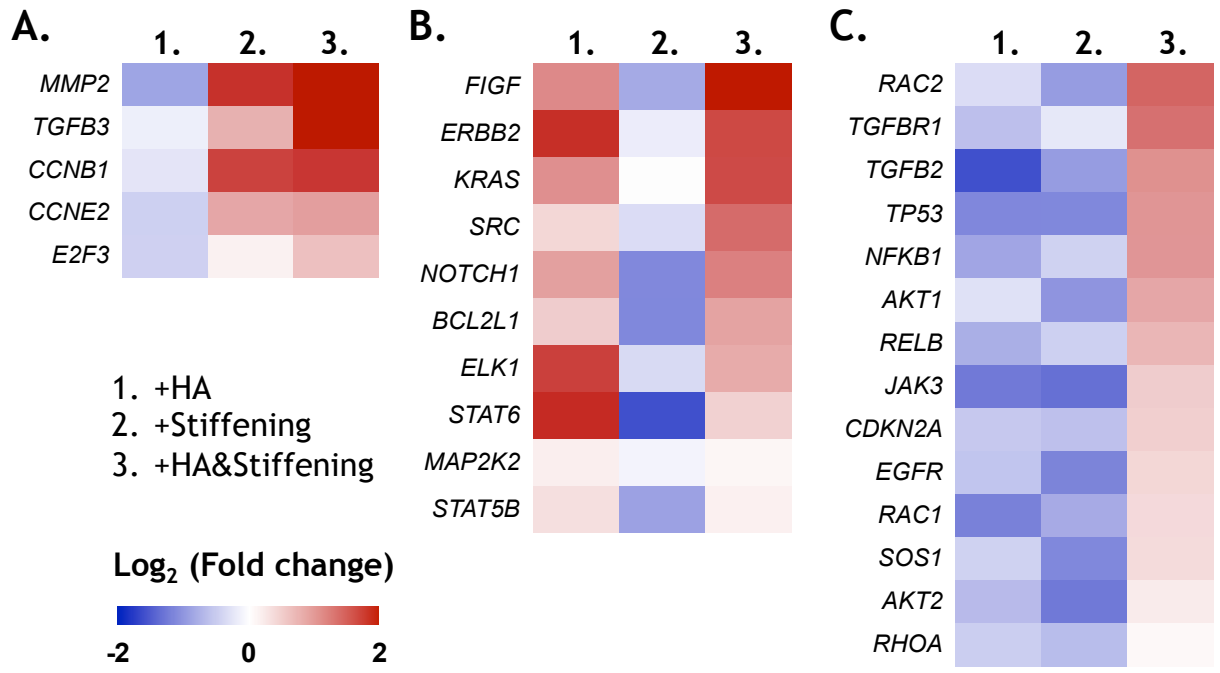

Figure 5.9. Identification of genes that were upregulated in COLO-357 cells encapsulated in specific gel formulations. (A) Stiffening gel regardless of HA presence, (B) HA-containing gel regardless of gel stiffening, and (C) HA-containing and stiffened gel. Gene expression levels (plotted in $\log_2$ scale) were normalized to GAPDH within each group, then normalized to respective gene in Gel_{NB}&PEG hydrogels. Each of the four gel formulations contained three biological replicates. Warm (red) colors showed high expression, whereas cold (blue) colors showed low expression.

5.3.5 Evaluation of relationship between matrices properties and EMT induction

To understand if cell phenotypes observed in Gel_{NBHPA}&HA gels were a result of matrix-induced EMT (Figure 5.6A), we characterized the expression of epithelial and mesenchymal markers using immunostaining (Figure 5.10A) and real-time PCR (Figure 5.10B). Immunostaining results showed that when the HA-containing hydrogels were dynamically stiffened (i.e., Gel_{NBHPA}&HA), the expression of epithelial marker E-cadherin (E-cad) decreased drastically (Figure 5.10A), whereas the expression of N-cadherin (N-cad, a mesenchymal marker) was visibly noticeable. On the other hand, qPCR results (Figure 5.10B) revealed significantly lower level of E-Cad mRNA expression (CDH1, ~0.5-fold), as well as higher expression levels of mesenchymal markers, including N-cad (CDH2, ~2-fold), SNAIL1 (~ 1.7-fold), vimentin (VIM, ~2.6-fold), and Sonic hedgehog (SHH, ~2.3-fold). Importantly, tyrosinase alone did not cause the observed changes in EMT-related mRNA expressions (Figure 5.10B). Spreading cell phenotype and

upregulation of mesenchymal cell markers in HA-containing/stiffened gels were also obtained using a second PDAC cell line, PANC-1 (Figure 5.12A). These results demonstrated that EMT was likely the cause of on cell spreading/invasion in the HA-containing gels that had been dynamically stiffened.

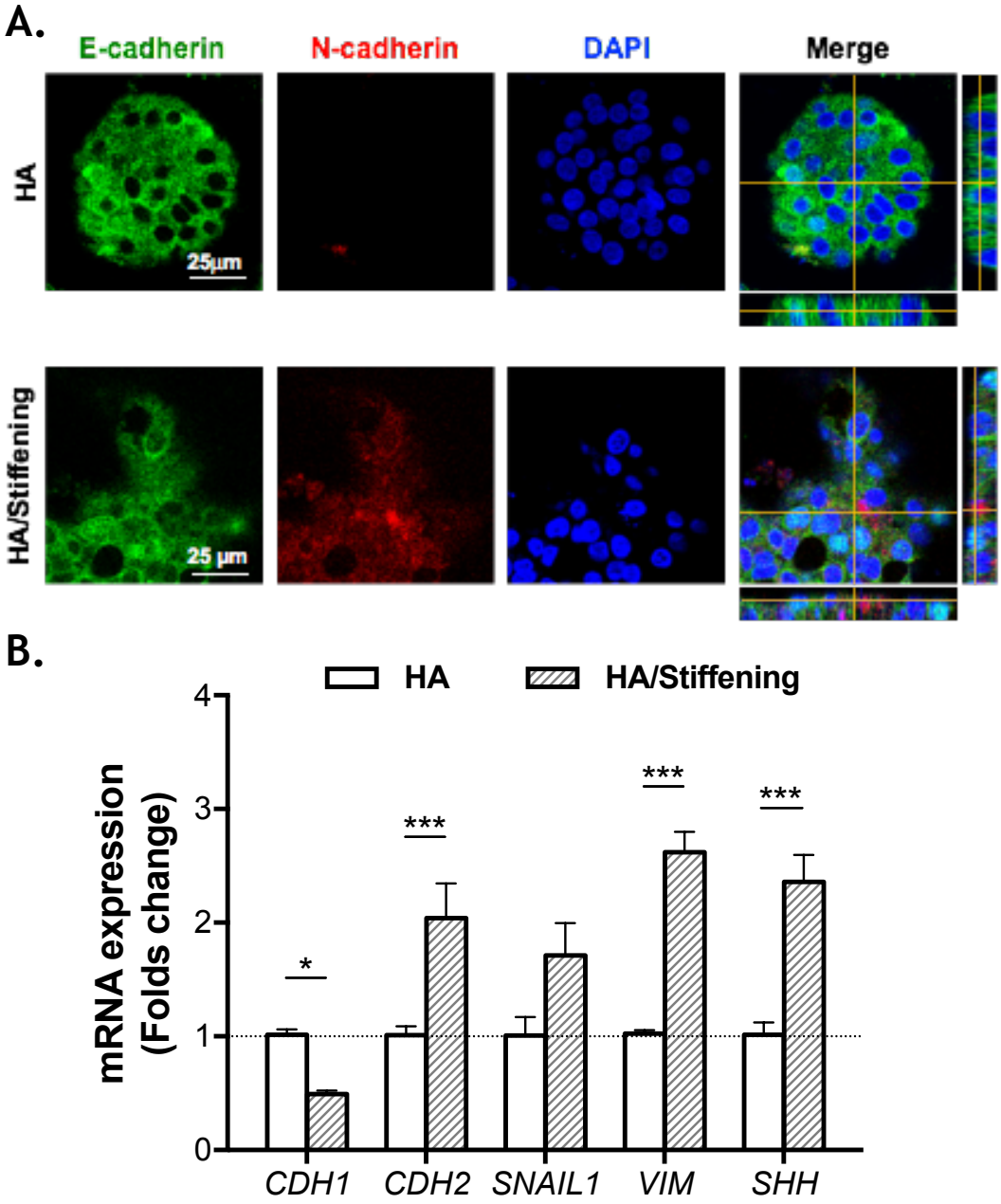

Figure 5.10. Evaluation of selected epithelial and mesenchymal markers in COLO-357 cells grown in HA-containing and soft (i.e., Gel_{NB}&HA) or in HA-containing and tyr_{ase}-stiffened gels (i.e., Gel_{NBHPA}&HA). (A) Immunofluorescence staining of E-cadherin and N-cadherin. Cells were counterstained with DAPI. (B) mRNA expression levels of *CDH1* (E-cadherin), *CDH2* (N-cadherin), SNAIL1, VIM (vimentin), and SHH (sonic hedgehog). All assays were conducted with samples collected at day-14. (Housekeeping gene: GAPDH. N = 3, Mean ± SEM. *$p<0.05$, ***$p<0.001$).

Table 5.2. The relative gene expression levels were analyzed by the $2^{-\Delta\Delta CT}$ method with GAPDH as the internal control (i.e., housekeeping gene) and the expression level of respective gene in the control group (i.e., Gel_{NB}&PEG gel with no HA and no stiffening) as the external control.

Gene	Forward (5'→3')	Reverse (5'→3')	
GAPDH	GAAGGTGAAGGTCGGAGTC	GAAGATGGTGATGGGATTTC	[270]
SNAI1	GAGGCGGTGGCAGACTAG	GACACATCGGTCAGACCAG	[295]
VIM	GAACGCCAGATGCGTGAAATG	CCAGAGGGAGTGAATCCAGATTA	[296]
CDH1	GAAAGCGGCTGATACTGACC	CGTACATGTCAGCCAGCTTC	[297]
CDH2	TGTTTGACTATGAAGGCAGTGG	TCAGTCATCACCTCCACCAT	[297]
MMP14	GCAGAAGTTTTACGGCTTGCA	TCGAACATTGGCCTTGATCTC	[298]
SHH	GGAAGCAGCCTCCCGATT	CGAGTCCAAGGCACATATCCA	[299]

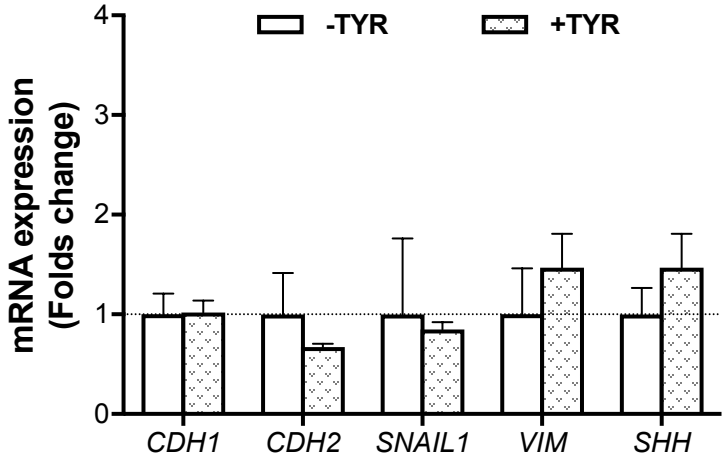

Figure 5.11. Effect of tyrosinase on expression of EMT-related genes. COLO-357 cells were plated in 24 well plate (1.25×10^5 cells/well) and cultured for 2 day. Cells were treated with or without tyr_{ase} (1 kU/ml) for 6 hours, collected for mRNA isolation and RT-PCR analysis of mRNA expression (Mean ± SEM. N = 6).

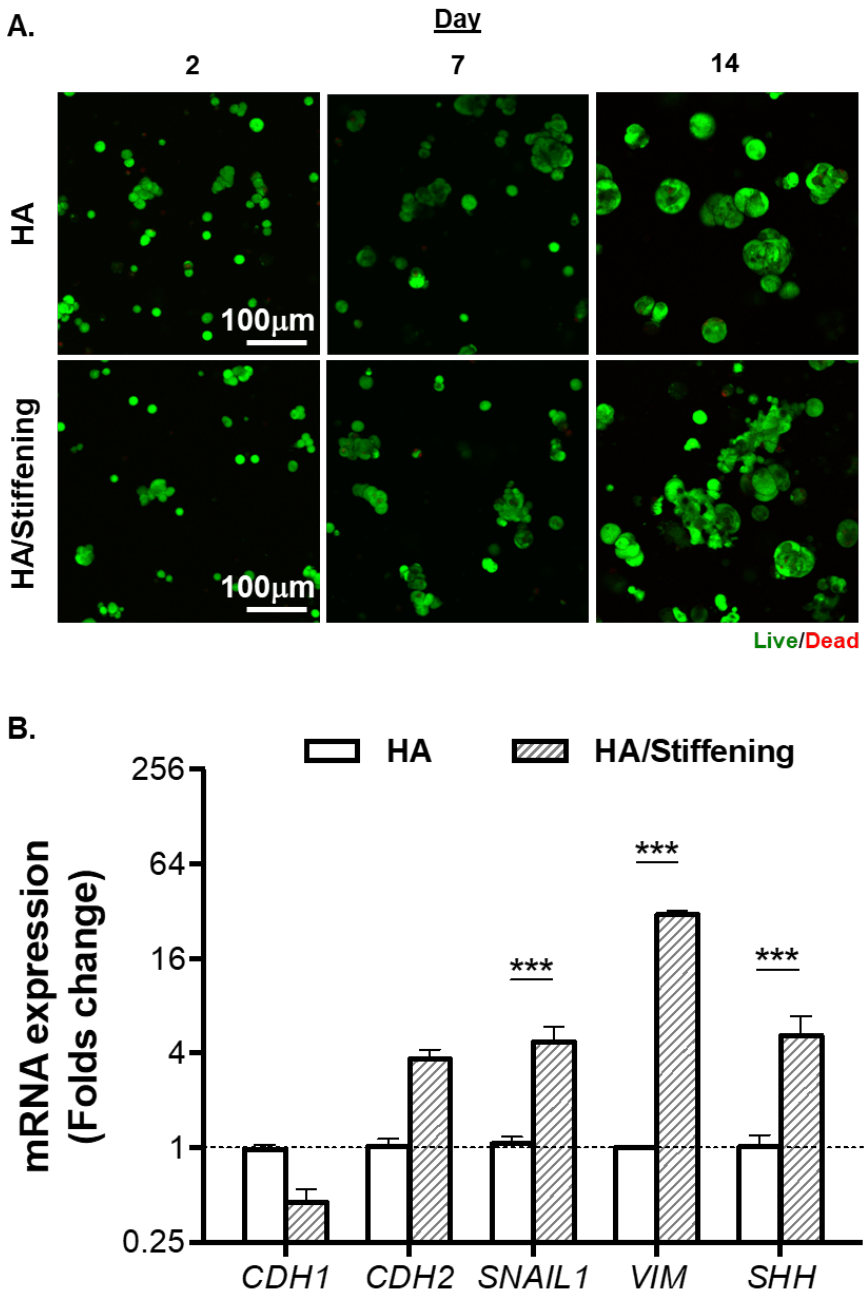

Figure 5.12. Evaluation of selected epithelial and mesenchymal markers in PANC-1 cells grown in HA-containing and soft (i.e., Gel_{NB}&HA) or in HA-containing and tyr_{ase}-stiffened gels (i.e., Gel_{NBHPA}&HA). (A) Representative confocal *z*-stack live/dead stained images of cells in Gel_{NB}&PEG, Gel_{NB}&HA, Gel_{NBHPA}&PEG, and Gel_{NBHPA}&HA gels. Gels were incubated with tyrosinase for 6 hours on day 2 and transferred to fresh media. (B) mRNA expression levels of CDH1 (E-cadherin), CDH2 (N-cadherin), SNAIL1, VIM (vimentin), and SHH (sonic hedgehog). All assays were conducted with samples collected at day 14. (Housekeeping gene: GAPDH. N = 3, Mean ± SEM. ****p<0.001*).

PDAC microenvironment is a complex network of cells, growth factors, and extracellular matrices whose compositions and properties change significantly as the tumor progresses (Figure 5.1). The dynamic changes in the TME pose significant challenges for *in vitro* cancer research and for testing the efficacy of anti-stromal therapeutics. Therefore ideal *in vitro* 3D cell culture platforms for cancer research should have modular and adaptable matrix compositions, as well as dynamically tunable matrix stiffness. Commercial matrices like Matrigel® can provide a convenient 3D culture model but do not have defined compositions and dynamically tunable properties, making it difficult to study the impact of ECM on cancer cell behavior and fate. Alternatively, hydrogels crosslinked by gelatin (Gel) and hyaluronic acid (HA) are increasingly developed as 3D cell culture matrices owing to their protease degradability and bioactive sequences that are critical in promoting cell proliferation and migration. Besides complex features of ECM composition, accumulating evidence suggest that matrix mechanics is an indispensable parameter regulating cancer cell biology [29, 210, 300]. Numerous studies have utilized synthetic hydrogels with tunable stiffness to investigate cancer mechanotransduction. For example, our group has reported Gel_{NB}&HA hydrogels formed by visible light initiated thiol-norbornene photopolymerization to study the influence of hydrogel crosslinking and compositions on PDAC cell fate [289]. Our earlier efforts have demonstrated that matrix compositions influence the expression of some critical genes related to tumor progression, such as MMP-14, SHH [289], and vascular endothelial growth factors (VEGF) [260]. Moreover, PDAC cells grown in stiffer hydrogels were less susceptible to anti-tumor drugs [288], hence reinforcing the importance of developing an adaptable tumor-mimetic matrix for in vitro cancer research.

The hydrogels developed in the current study integrated modular thiol-norbornene crosslinking (Figure 5.1D) [251, 258, 289] with the enzyme-triggered dynamic stiffening strategy (Figure 5.1E) that we reported previously [213]. The basic macromer used in this study was gelatin – denatured collagen with enhanced solubility. Native gelatin and modified gelatin macromers are widely used in tissue engineering and regenerative medicine applications owing to its bioactive peptide sequences that permit integrin-binding and protease-triggered degradation [301]. Our lab has also exploited modularly crosslinked gelatin-based hydrogels as 3D cell culture platforms [262, 289, 302, 303]. For example, we utilized Gel_{NB} as the main functional macromer to construct modular hydrogels for encapsulation and *in vitro* culture of hepatocellular carcinoma (HCC) [262] and PDAC cells [289]. We have also exploited tyrosinase-triggered di-tyrosine crosslinking for

dynamically stiffening cell-laden hydrogels and for evaluating its effect on activation of pancreatic stellate cells (PSCs), the major stroma cells in PDAC [213]. Built upon these work, we report here the use of modified gelatin (Figure 5.1B), THA (Figure 5.1C), and bioinert macromer (e.g., PEG-tetra-thiol, PEG4SH) for constructing gels that were: (1) HA-free and soft (i.e., Gel_{NB}&PEG gel), (2) HA-free and dynamically stiffened (i.e., Gel_{NBHPA}&PEG gel), (3) HA-containing and soft (i.e., Gel_{NB}&HA gel), and (4) HA-containing and dynamically stiffened (i.e., Gel_{NBHPA}&HA gel). Note that gelatin was used in all gel formulations to provide basic cell adhesion and protease-mediated degradation, whereas only gels composed of Gel_{NBHPA} (i.e., Gel_{NBHPA}&PEG and Gel_{NBHPA}&HA) were susceptible to tyrosinase-triggered dynamic stiffening.

We fabricated cell-laden hydrogels with lower thiol-ene ratio but with higher content of Gel_{NBHPA} to obtain gels that were initially soft (G'<1 kPa) but could be stiffened to physiologically-relevant modulus (G' ~3 kPa. Figure 5.3C), akin to what is observed in human PDAC samples and sufficient to induce cell phenotypic and mRNA expression changes [58, 217, 304, 305]. As expected, tyrosinase-triggered HPA dimerization increased gel crosslinking and stiffness (Figure 5.3C, D**,** Figure 5.4A). The degree of gel stiffening was highly tunable owing to the modular crosslinking nature of thiol-norbornene photopolymerization (Figure 5.4A). While soft hydrogels could be rapidly and completely degraded by collagenase (Figure 5.4B) and hyaluronidase (Figure 5.4C) within hours, tyrosinase-stiffened hydrogels were less sensitive to these enzymes. When treated with collagenase, degradation followed a surface erosion mechanism regardless of gel stiffness, as indicated by the almost linear mass loss profiles (Figure 5.4B). This also applied to hyaluronidase-mediated degradation in soft gels (Figure 5.5C). Exogenously added hyaluronidase, however, did not result in complete degradation of the stiffened gels (only ~ 25% mass loss (Figure 5.5C). It was possible that the THA used in this study (from ESI·BIO) had high degree of thiolation, making it difficult for hyaluronidase to cleave HA backbone in a stiffened network. The susceptibility of HA-containing gels to hyaluronidase could be improved by using THA with lower degree of substitution. Nonetheless, all matrices were susceptible to degradation induced by cell-secreted enzymes, a feature critical and necessary in cell-mediated matrix remodeling. It should be noted that these degradation studies were designed to inform the influence of tyrosinase-triggered gel stiffening on subsequent matrix degradation by relevant enzymes (i.e., collagenase and hyaluronidase). The fact that the stiffened gels were susceptible to exogenously added

enzymes (especially collagenase) suggests that the encapsulated PDAC cells would still be able to degrade stiffened matrix locally, hence facilitating their proliferation, invasion, and migration.

The changes in cell morphology among different gel formulations and stiffening conditions indicated that 3D matrix composition exerts a profound impact on PDAC cell fate. Through modular control of gel compositions and dynamic stiffening, we show that the presence of HA in a soft gel (i.e., Gel_{NB}&HA) *or* an HA-free but stiffened gel (i.e., Gel_{NBHPA}&PEG) hindered the growth of PDAC cells in 3D (Figure 5.6A), underscoring the complex relationship between cell proliferation, HA levels, and TME stiffness. On the other hand, smaller spheroids observed in the stiffened and HA-free gel could be a result of stress-induced signaling and physical restriction imposed by tighter network crosslinking after stiffening. We have observed a similar phenomenon in PDAC cells using hydrogels with higher but static stiffness [289]. However, the negative impact of network-immobilized HA on spheroid sizes was surprising since HA has been shown to induce PDAC cell proliferation in 2D culture [306]. The suppression of spheroid growth compared with that in soft and HA-free gel (i.e., Gel_{NB}&PEG) could be due to the dependence of HA-mediated mitogenic signaling on matrix stiffness. Interestingly, when cells were grown in HA-containing *and* stiffened gels (i.e., Gel_{NBHPA}&HA), significant cell spreading was observed (Figure 5.6A and B). This could be attributed to the upregulation of mRNAs implicated in the Ras/MAPK pathway, including RAC1, RAC2, RHOA, and RAF1 (Figure 5.9B), and EMT-induced alterations. The upregulation of these mRNAs could lead to enhanced proliferation and to increased cell migration/invasion as observed in the stiffened and HA-containing hydrogel.

We also identified mRNAs that were upregulated only when the cells were encapsulated in stiffened gels (Figure 5.9A), in HA-containing gels (Figure 5.9B), or in HA-containing *and* stiffened gel (Figure 5.9C). We found that FIGF, ELK1, KRAS, SRC, and NOTCH1 were upregulated in cells grown in HA-containing gels, and that their expression was further upregulated when combined with gel stiffening. These findings are of crucial importance for several reasons. First, increased expression of KRAS and SRC is known to enhance tumorigenesis and metastasis [217, 307], and here we show for the first time that their expression is upregulated by key features found in the PDAC TME. Second, the upregulation of FIGF likely leads to increased levels of VEGF-D, which is known to promote lymph node metastasis in PDAC [24, 308]. Third, NOTCH1 encodes Notch 1, whose activation correlates with increased drug resistance in PDAC [309-311].

Another interesting phenomenon is the elevated expression of MMPs, which are involved in ECM degradation and cancer cell invasion [312, 313]. We noted high levels of MMP-7, the smallest member of the MMP family yet endowed with high proteolytic activity [314], in all experimental groups (compared to that in Gel_{NB}&PEG hydrogel). On the other hand, MMP-2 was only highly expressed in gels that were stiffened dynamically regardless of HA presence (Figure 5.9A). These findings suggest that our modular and dynamic hydrogels are ideal for future studies regarding the influence of matrix components on the expression and activity of MMPs or as an adaptable platform to test the efficacy of anti-MMP therapeutics. Furthermore, in a stiffened tumor-mimetic hydrogel, HA was found to upregulate mRNAs responsible for enhancing cancer cell survival and drug resistance (i.e., AKT1, AKT2, PIK2R1, PIK3R2, NFKNB1, and RELB. Figure 5.8 and Figure 5.9C).

Additional genes in the EGF and TGF-β pathways were significantly upregulated only in the setting of a stiffened and HA-containing microenvironment. These genes included TGF-βR1, TGF-β2, and EGFR (Figure 5.9C). Moreover, TGF-β3 was upregulated in the setting of a stiffened gel and further upregulated when combined with HA (Figure 5.9A). These signaling events may collaboratively lead to enhanced EMT in PDAC cells (Figure 5.10A). In addition, these observations underscore the fact that EGFR and TGF-β pathways are known to cross-talk in the context of upregulated KRAS activity, thereby lead to autocrine dysregulation that promotes invasion and metastasis, as well as to aberrant paracrine actions that contribute to the desmoplasia in the TME and that impair cancer-directed immune mechanisms [315, 316]. While previous efforts have led to current understanding of soluble factors (e.g., growth factors, cytokines, soluble HA) on PDAC cell growth and EMT, the influence of 3D matrix compositions and time-dependent mechanics on PDAC cell fate remains elusive owing to the lack of a modular and adaptable biomimetic culture platform. Although the Gel_{NBHPA}&HA gel system developed here only recapitulated aspects of the complex PDAC stroma, it nonetheless provides a highly relevant dynamic biomaterial platform for studying tumor cell-materials interactions in a reductionistic manner. In this contribution, we reported the unique synergistic roles of HA and a stiffening matrix on PDAC cell behaviors, which has not been reported before. Built upon the current system, other stroma-relevant components (e.g., fibronectin, laminin) may be added in future studies to understand the crosstalk between these stroma components and matrix mechanics on PDAC cell fate processes. Furthermore, the enzyme-responsive matrix stiffening approach is highly

cytocompatible, controllable, and adaptable for creating cell-laden gels with spatial-temporally regulated stiffness. For example, our on-going work is focused on generating biomimetic gels with stiffness gradient to evaluate durotatic cell migration and invasion in 3D. The system can be further exploited in the future for studying molecular signaling induced by specific tumor matrix compositions, as well as for testing the efficacy of anti-stromal therapeutics.

5.4 Material and Methods

Gelatin type B, THA (MW: ~300 kDa), and PEG4SH (MW: 10 kDa) were obtained from Electron Microscopy Sciences, ESI Bio, and JenKem Technology USA, respectively. Collagenase-1 (300 U/mg) and hyaluronidase (770 U/mg) were purchased from Worthington Biochemical. All the other chemicals were obtained from Thermo Fisher unless noted otherwise.

5.4.1 Synthesis of functionalized gelatin macromers

The synthesis of Gel_{NBHPA} was achieved in two steps. First, gelatin-norbornene (Gel_{NB}) was synthesized by reacting gelatin with carbic anhydride as described previously [302]. The second functional group, HPA, was conjugated on the remaining amine groups on Gel_{NB} through standard carbodiimide chemistry with 1-ethyl-3-(3-dimethylaminopropyl)-carbodiimide (EDC) and N-hydroxysuccinimide (NHS) as the coupling reagents [317]. The reaction was carried out for 24 hours and the degree of substitution was determined using fluoraldehyde assay with unmodified gelatin as the standards. The functionalization was also characterized by UV/Vis spectrophotometry (Synergy HTX microplate reader, BioTek Instruments) and ^{1}H NMR (Avance III 500, Brüker).

5.4.2 Hydrogel fabrication and characterization

Hydrogels were prepared by reacting norbornene moieties of functionalized gelatin with thiol motifs on PEG4SH or THA via thiol-norbornene photopolymerization [229, 251]. Briefly, precursor solutions (45 µl/gel) composed of macromers and photoinitiator lithium acylphosphinate (LAP, 1 mM) were injected between two glass slides separated by 1-mm thick spacers. Gelation was achieved in 2 minutes under 365 nm light exposure (5 mW/cm^2). Hydrogels were swollen in DPBS at 37ºC for 2 hours prior to characterization or stiffening experiments. Gelation kinetics and mechanical properties of hydrogels were characterized with a digital rheometer (Bohlin CVO100, Malvern Instruments). *In situ* gelation was performed in time-sweep mode using 10% strain, 1 Hz

frequency, and a gap size of 90 μm. Hydrogel bulk moduli were obtained from averaging the linear region of the modulus-strain curves in strain-sweep mode (8 mm parallel plate geometry with a gap size of 700 μm).

5.4.3 Tyrosinase-initiated reaction for on-demand gel stiffening

Tyrosinase-mediated hydrogel stiffening was performed by incubating the pre-formed hydrogels in tyrosinase solution as described previously [213]. Afterwards, gels were transferred to DPBS (for cell-free gels) or fresh media (for cell-laden gels) in order to remove the residual tyrosinase trapped in the hydrogels.

5.4.4 Enzymatic degradation of soft and stiffened hydrogels

Collagenase-1 and hyaluronidase were used to evaluate the susceptibility of the hydrogels to on-demand enzymatic degradation. Briefly, hydrogels were prepared with or without tyr_{ase} -triggered stiffening as described in the section above. The gels were incubated in DPBS for one day prior to gravimetrically weighing to determine the initial gel mass (M_0). Next, gels were incubated in respective enzyme solution for predefined periods of time and weighed to obtain current mass (M_t) and to determine percentage of mass loss (i.e., $100\%\times(M_0–M_t)/M_0$). The degradation process was continued until the gels were completely degraded or no substantial changes in mass loss were observed.

5.4.5 PDAC cell culture, encapsulation, and characterization

COLO-357, a PDAC cell line with wild-type KRAS, was maintained in high glucose DMEM supplemented with 10% of fetal bovine serum (FBS, Gibco) and penicillin-streptomycin (Gibco, 50 U/ml for both antibiotics). Cells were maintained in a standard cell culture incubator (37°C, 5% CO_2). Prior to encapsulation, cells were trypsinized and suspended in precursor solutions (to 2×10^6 cells/mL) composed of photoinitiator LAP and required macromers (i.e., PEG4SH, THA, Gel_{NB}, or Gel_{NBHPA} at desired concentrations as denoted in each Figure). Cell-precursor solution (25 μl) was loaded to a 1 mL disposable syringe with cut-open tip and exposed to 365 nm light (5 mW/cm^2) for 2 minutes. Cell-laden hydrogels were cultured in a 24-well plate. To evaluate cells viability, cell-laden gels were stained with live/dead staining kit (Life Technologies; Calcein-AM stained live cells green, Ethidium homodimer-1 stained dead cells red) and imaged via confocal microscopy (Olympus Fluoview FV100 laser scanning microscope). *Z*-stack images (100 μm thick, 10 μm per slice) were obtained from a minimum of three random

areas within hydrogels. In addition, cells metabolic activity was obtained by using AlamarBlue assay (AbD Serotec; 10% in culture media, 2.5 hour of incubation time) and quantified via a microplate reader (Synergy HTX, BioTek). Additional cell encapsulation studies were conducted using another human PDAC cell line, PANC-1, which harbors mutated KRAS.

5.4.6 RNA Isolation, reverse transcription PCR, and real-time PCR

Samples of cell-laden hydrogels were collected in DNase/RNase-free microtubes, flash-frozen in liquid nitrogen and stored in -80°C. Total RNA was isolated from the encapsulated cells with NucleoSpin RNA II kit (Clontech). The concentration and purity of RNA were obtained by NanoDrop 2000 Spectrophotometer (Thermo Scientific). Next, purified mRNA samples were converted into complementary DNA (cDNA) with PrimeScript RT Reagent Kit (Clontech, TaKaRa). For Taqman® array experiments, only samples with concentration greater than 100 ng/mL, 260/280 > 2.0, 260/230 > 1.8 were used. cDNA samples were diluted to 100 ng/mL and mixed with same volume of Taqman® fast universal master mix. For 96 well TaqMan® Array Gene Signature Sets, 10 µl mixture was deposited in each well and detected by Applied Biosystems 7500 Fast Real-Time PCR machine. Three biological replicas were used for each experimental condition. Additional qPCR on EMT-related genes was performed using cDNA and SYBR Premix Ex TaqII kit (Clontech) with appropriate primers as listed in Immunofluorescence staining and imaging

F-actin staining was used to visualize cytoskeletal structure of cells encapsulated in 3D environment with different matrix properties. Briefly, encapsulated cells were fixed in 4% paraformaldehyde for an hour at room temperature on an orbital shaker. Following fixation, samples were rinsed with DPBS and permeabilized with 1 mg/mL saponin at room temperature for 45 min. The samples were then washed with DPBS and blocked with 1% BSA and 10% FBS overnight at 4°C with shaking. The gels were then incubated overnight at 4°C in phalloidin solution (100 nM) and then washed with DPBS. Cell nuclei were counter-stained with DAPI (1:1000) for an hour at room temperature and rinsed three times with DPBS. *Z*-stack images (15 µm thick, 1 µm per slice) were obtained with a confocal microscope. To examine potential EMT effect on the encapsulated cells, E-cadherin (E-cad) and N-cadherin (N-cad) were stained by immunofluorescence. In brief, cell-laden gels were fixed, permeabilized, and blocked as described previously [318], followed by incubation with Rabbit anti-E-cad (1:100) and Mouse anti-N-cad (1:100) at 4˚C for two days. After washing with DPBS extensively, samples were incubated with

goat anti-Rabbit IgG (H+L)-Texas red or Alexa Fluor® 488-labeled goat anti-mouse IgG F(ab')^2 for two days at 4˚C with gently shaking. Following by rinsing with DPBS and counter-staining with DAPI (1:1000), the samples were imaged by *z*-stack images (25 μm thick, 1 μm per slice) confocal microscopy with appropriate filters.

5.4.7 Statistical Analysis

All experiments were conducted independently three times with a minimum of three samples per condition. Numerical data were analyzed with two-way ANOVA on GraphPad Prism 7 software and reported as Mean ± SEM. Single, double, and triple asterisks represent $p<0.05$, 0.001, and 0.0001, respectively. $p<0.05$ was considered statistically significant. For analyzing of Taqman® mRNA expression array, pairs of groups were compared with one-way ANOVA using Gel/PEG gels as the control (IBM SPSS software), following by Bonferroni post-analysis (Table 5.1).

5.5 Conclusion

In conclusion, we have designed a biomimetic hydrogel capable of mimicking the diverse biochemical compositions and dynamic biophysical environment of pancreatic desmoplasia. The modular thiol-norbornene crosslinking of gelatin, HA, and PEG-based macromers decoupled the influence of HA and matrix stiffness on PDAC cell fate. Furthermore, the inclusion of HPA motif rendered the gels responsive to tyrosinase-triggered HPA dimerization and additional gel crosslinking. Through modular design, the hydrogels could be stiffened with high controllability. PDAC cells responded to the stiffening or HA-containing gel with limited cell proliferation. On the other hand, we confirmed that HA and matrix stiffening synergistically promoted invasive phenotype in PDAC cells, most likely a result of matrix-induced EMT. The desmoplasia-mimetic hydrogel developed here provides a diverse material platform for studying PDAC cell fate. Future work will focus on utilizing this versatile system for investigating cellular response to therapeutics under various matrix composition and mechanical properties.

CHAPTER 6. DYNAMIC PEG-PEPTIDE HYDROGELS VIA VISIBLE LIGHT AND FMN-INDUCED TYROSINE DIMERIZATION

(As published in *Advanced Healthcare Materials*, 2018 (7) 1800954)

6.1 Abstract

Photo-responsive hydrogels have become invaluable three-dimensional (3D) culture matrices for mimicking aspects of extracellular matrix (ECM). Recent efforts have focused on using ultraviolet (UV) light exposure and multifunctional macromers to induce secondary hydrogel crosslinking and dynamic matrix stiffening in the presence of cells. This contribution reports the design of a novel yet simple dynamic poly(ethylene glycol)-peptide hydrogel system through flavin mononucleotide (FMN) induced di-tyrosine crosslinking. These di-tyrosine linkages effectively increase hydrogel crosslinking density and elastic modulus. In addition, the degree of stiffening in hydrogels at a fixed PEG macromer content can be readily tuned by controlling FMN concentration or the number of tyrosine residues built-in to the peptide linker. Furthermore, tyrosine-bearing pendant biochemical motifs could be spatial-temporally patterned in the hydrogel network via controlling light exposure through a photomask. The visible light and FMN induced tyrosine dimerization process produces cytocompatible and physiologically relevant degree of stiffening, as shown by changes of cell morphology and gene expression in pancreatic cancer and stromal cells. This new dynamic hydrogel scheme should be highly desirable for researchers seeking a photo-responsive hydrogel system without complicated chemical synthesis and secondary UV light irradiation.

6.2 Introduction

Hydrogels with tunable physicochemical properties have been extensively utilized as three-dimension (3D) cell culture platforms [258]. To mimic a cellular microenvironment, hydrogels are commonly immobilized with biochemical motifs, including cell adhesive peptides (e.g., fibronectin-derived peptide sequence, RGD) or proteoglycans derived from extracellular matrix

(ECM) (e.g., heparin sulfate proteoglycan, hyaluronan, *etc.*) [319]. These signaling motifs are crucial for guiding complex cell-matrix interactions, as well as for promoting tissue morphogenesis within the otherwise inert matrix. On the other hand, mechanical properties of native tissue play an indispensable role in stem cell differentiation and cancer progression [213, 241, 267, 320-322]. In order to investigate the effect of matrix mechanics on cell fate processes in 3D, cells are typically encapsulated in gels with varying but static or degrading mechanical property. However, recent studies have revealed the critical influence of spatial-temporal (i.e., dynamic) changes in tissue mechanics on cell behaviors [321]. Unfortunately, conventional cell culture devices cannot be readily adapted to study the influence of dynamic matrix properties on cell fate processes.

Photo-responsive materials are ideal candidates for designing dynamic cell-laden hydrogels. The most common approach is to perform cell encapsulation using photo-responsive materials that are compatible with secondary crosslinking. For example, Burdick and colleagues prepared photo-responsive hydrogel from acrylated hyaluronic acid (AHA) and bis-cysteine-bearing matrix metalloprotease (MMP) sensitive peptides [323, 324]. The hydrogel was partially crosslinked through Michael-type addition between acrylate and thiol motifs, leaving additional acrylates available for photoinitiator (I-2959) and UV-light mediated *in situ* gel stiffening. In another example, Mabry *et al.* and Fiedler *et al.* designed dynamic hydrogels through repeated photopolymerization of cell-laden hydrogels [101, 325]. Photopolymerized hydrogels were submerged in buffer solution containing additional PEG macromers and photoinitiator (lithium phenyl-2,4,6-trimethylbenzoylphosphinate, LAP). The macromer/initiator imbibing gels were polymerized again under UV light exposure to create ‘double network’, which exhibited higher degree of crosslinking and gel stiffness. These gels could also be regionally patterned with bioactive peptides through utilizing a photomask [325]. While the use of I-2959 or LAP enables gel crosslinking and stiffening, these cleavage-type photoinitiators generate highly reactive radicals upon absorbing light at the UV spectrum (e.g., 365 nm) [272]. LAP does absorb light at the visible light wavelength (405 nm) [303]. However, high concentration (e.g., ~6 mM) is generally required to achieve significant degree of additional crosslinking owing to its low molar absorbability at the visible light wavelengths [326].

Non-cleavage type (type II) photoinitiators or photosensitizers, such as eosin-Y (EY) [327, 328], rose bengal (RB) [329], and riboflavin (RF) [330] can also be used to initiate photopolymerization under visible light (400-700 nm) exposure. These types of photoinitiators

have been noticed capable of oxidatively coupling phenolic residues, such as tyrosine and tryptophan [331]. A particularly attractive type II photoinitiator is RF (i.e., *vitamin B_2*) and its natural derivatives, including flavin adenine dinucleotide (FAD) and flavin mononucleotide (FMN). Flavins are natural photo-sensitizers that are commonly used as food additives and have high molar absorbability at the UVA (370 nm) and visible light spectra (440 and 480 nm) [332]. Therefore, flavins have been harnessed as photoinitiators for UV or visible light-initiated hydrogel crosslinking [333-335]. Finally, compared to RF, FMN has much high solubility in water (92 mg/ml for FMN *v.s.* 0.045 mg/ml for RF), making it an ideal choice for preparing photo-responsive hydrogels [336].

Current photo-responsive dynamic hydrogels have been successfully used to answer important biological questions, such as the effect of changing matrix mechanics on activation of human mesenchymal stem cells [239, 337], hepatic stellate cells [267, 326], and valvular interstitial cells [101]. However, the preparation of these dynamic hydrogels usually requires multiple steps of chemical synthesis and purification that may not be friendly to many biomedical laboratories. Here, we introduced a simple photo-responsive dynamic PEG-peptide hydrogel system via visible light and FMN-induced tyrosine dimerization within a step-growth gel network. Following the initial thiol-norbornene gel crosslinking, soluble FMN was added in the hydrogel via diffusion to permit visible light induced tyrosine dimerization, which led to on-demand hydrogel stiffening. The degree of stiffening could be readily tuned through adjusting dosage of visible light exposure and FMN concentration, as well as the amount of tyrosine residues built-in in the sequence of the peptide crosslinkers. In addition to investigating the conditions and parameters for dynamic gel crosslinking, we also demonstrate spatiotemporally tunable stiffening scenarios and post-gelation conjugation/patterning of biochemical motifs. Finally, we evaluated *in vitro* cytocompatibility of the visible light-mediated stiffening process and utilized this platform to study the impact of matrix stiffening on responses of pancreatic cancer cells (PCCs) and cancer-associated fibroblasts (CAFs). Since all components used in this study (i.e., PEG macromers, peptides, LAP, FMN) as well as the visible light source (a cold halogen microscope light) can be acquired commercially, this dynamic hydrogel system should be beneficial to many biomedical laboratories interested in studying cell biology in a dynamically tunable microenvironment.

6.3 Result and Discussion

6.3.1 Dynamic hydrogel stiffening via visible light and FMN-initiated tyrosine dimerization

FMN has been recently used as a visible light photoinitiator in thiol-ene polymerization of PEG-based hydrogels [336]. In the current contribution, we discovered that visible light and FMN initiated photochemistry could be used as a cytocompatible mechanism for tuning crosslinking density of PEG-peptide hydrogels if the peptide crosslinkers contained at least one tyrosine residue. We fabricated the primary hydrogel using PEG8NB (Figure 6.1A) and bis-cysteine peptide linkers (e.g., CYGGGYC, Figure 6.1B) via LAP initiated thiol-norbornene photopolymerization (Figure 6.1C) [33]. In principle, tyrosine residues on the peptide crosslinker were susceptible to visible light and FMN-mediated dimerization, leading to increased crosslinking density of the PEG-peptide hydrogel (Figure 6.1D).

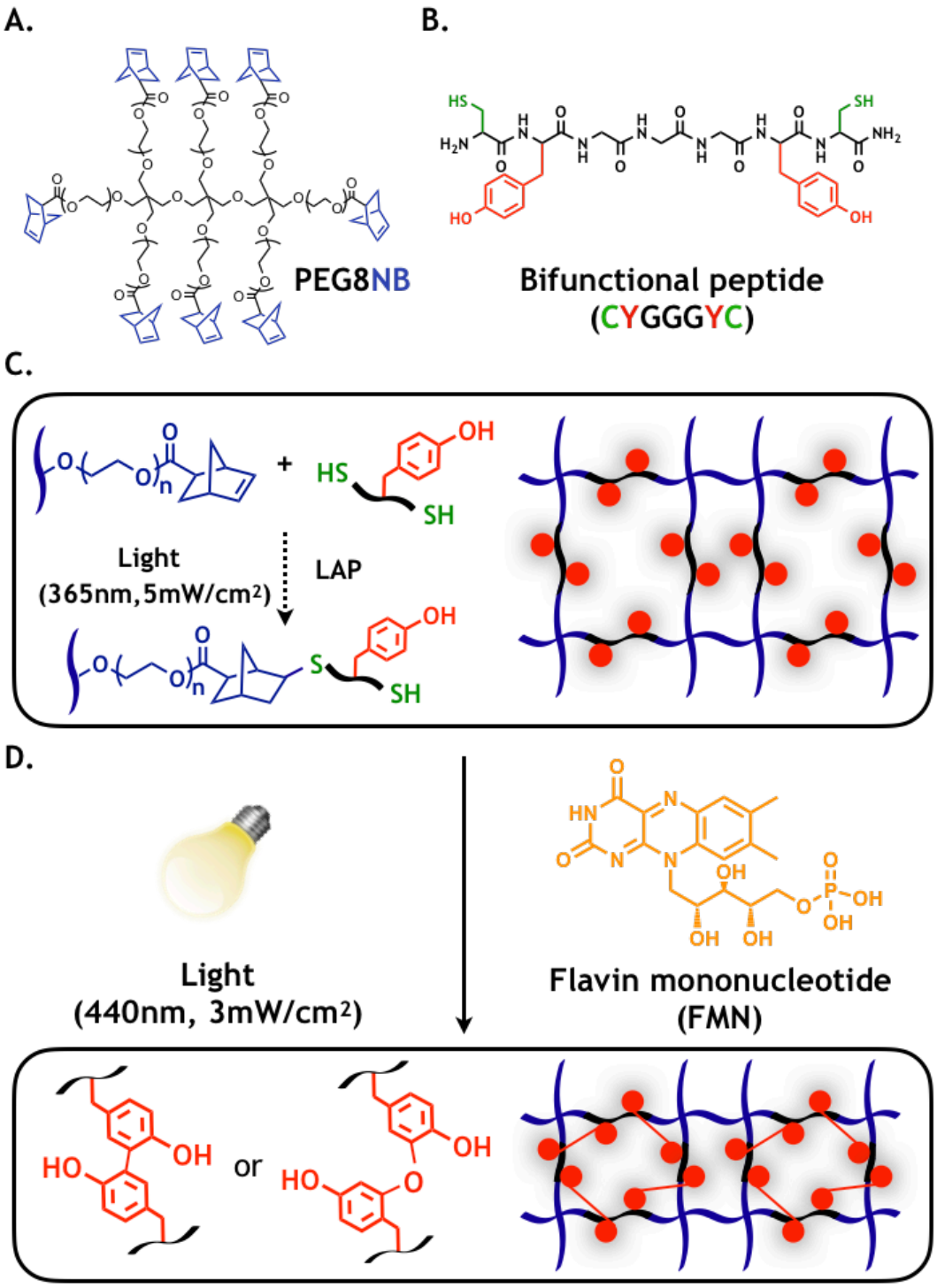

Figure 6.1. Schematics of flavin mononucleotide (FMN) & visible light-mediated dynamic hydrogel fabrication. (A) Chemical structure of PEG8NB. (B) Bis-cysteine-bis-tyrosine containing peptide crosslinker (i.e., CYGGGYC). (C) Crosslinking of primary gel network via thiol-norbornene photopolymerization. (D) FMN and visible light induced di-tyrosine crosslinking and hydrogel stiffening.

Following thiol-norbornene photopolymerization, soft hydrogels (G'~ 1-1.2 kPa) were incubated in buffer solution containing 1 mM FMN for 30 min to allow its equilibration in the gel. We determined that 30 min incubation was sufficient for FMN (MW: 456.3 g/mol; $D_0 = 4.8 \times 10^{-10}$ m^2/s) [338] to reach equilibrium in the hydrogel based on a model developed previously [213]. First, we fabricated hydrogels with different crosslinking densities and measured their respective swelling ratios (Q, Figure 6.2A), which were used to calculate mesh sizes (ξ, Figure 6.2B) [122]. The later were used to derive FMN diffusivity in hydrogels using the Lustig-Peppas relationship [218]. For example, it was determined that for stiff hydrogels with shear moduli of 5 kPa, FMN diffusivity was reduced to 4.54×10^{-10} m^2/s, or 95% of D_0. The small reduction of FMN diffusivity in stiff hydrogel was reasonable due to its small molecular size. We utilized this diffusivity to estimate the time needed for FMN to reach 99% of that in the solution. As shown in Figure 6.2C, 30 minutes of incubation was sufficient for the center of the gel to reach $C_{FMN}/C_0 = 0.99$. Experimentally, hydrogel color changed from transparent to bright yellow (color of FMN) after 30 min incubation in 1 mM FMN solution (Figure 6.4A). After visible-light exposure for 2 minutes, the gels were transferred to PBS for 30 min to allow for the removal of residual soluble FMN. At which time, the gel returned to transparent, suggesting that FMN was not retained in the post-stiffened hydrogels. The initially soft (G' ~1 kPa) hydrogels were effectively stiffened to ~2.3 kPa after the visible light and FMN-initiated stiffening process (Figure 6.1B)and the stiffened hydrogels remained elastic as demonstrated by the strain-independent moduli. It is worth noting that all components used in this study were commercially available, including the linear peptides crosslinkers that can be designed to exhibit other functionality (e.g., protease sensitive sequence). Furthermore, while thiol-norbornene photopolymerization was used here to prepare the primary PEG-peptide hydrogel network, this stiffening strategy can be applied to other step-growth hydrogels, such as those prepared by multi-arm PEG-vinyl sulfone/PEG-maleimide via Michael-type addition, or by other commercially available click-based macromers.

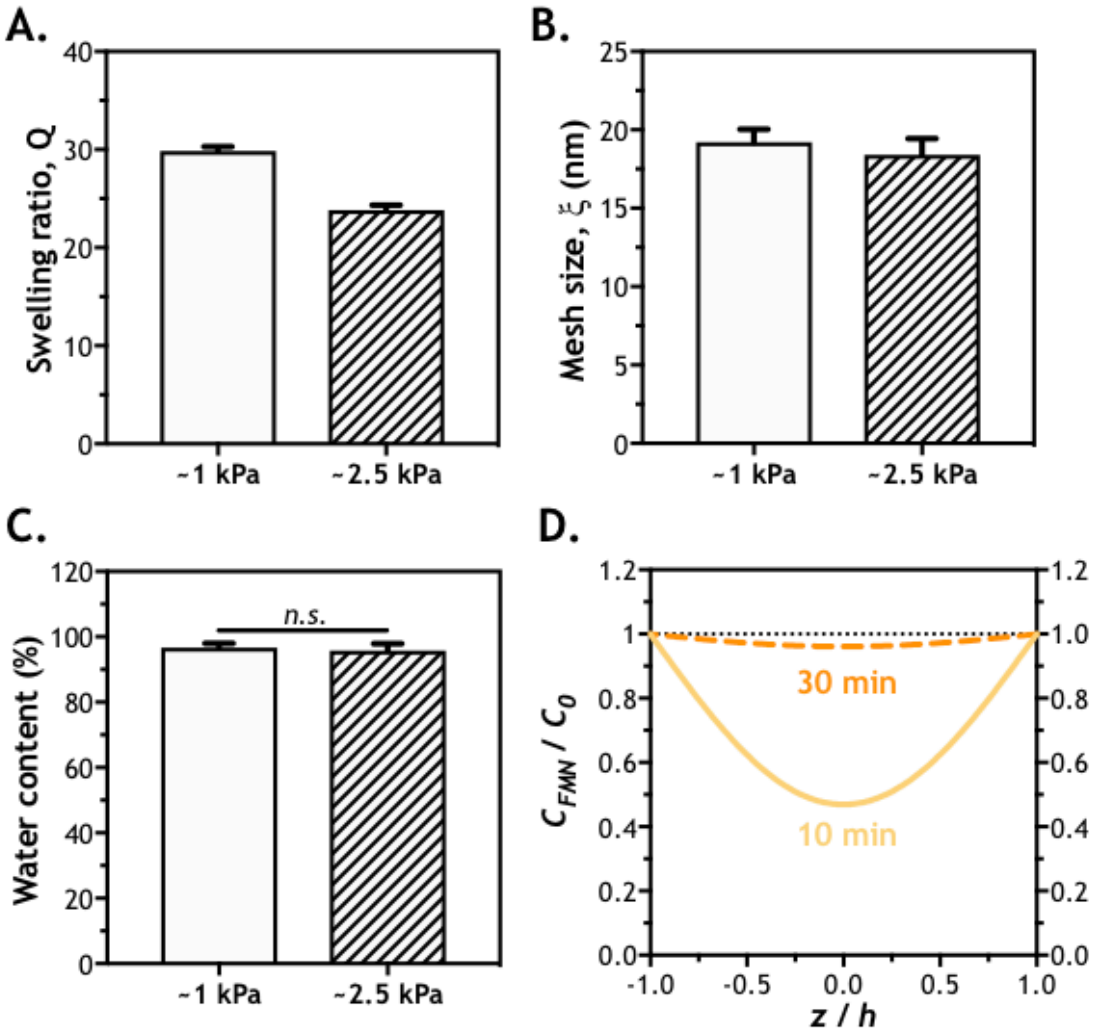

Figure 6.2. (A) Swelling ratio, (B) mesh size, and (C) water content of PEG-peptide hydrogels with G' of 1 or 2.5 kPa. Gels were prepared by PEG8NB (2.5 wt% and 3.0 wt%) and CYGGGYC peptide (5 mM and 6 mM) via light exposure (365 nm, 5 mw/cm^2) for 2 minutes. 1 mM LAP was used as photoinitiator for the initial gelation. (D) Concentration profiles of FMN in PEG-peptide hydrogel as predicted by the Fick's 2nd law of diffusion. D_{FMN} = 4.54×10^{-10} m^2 /s. Gel thickness = 1 mm. Data presented as mean ± SEM, N = 3.

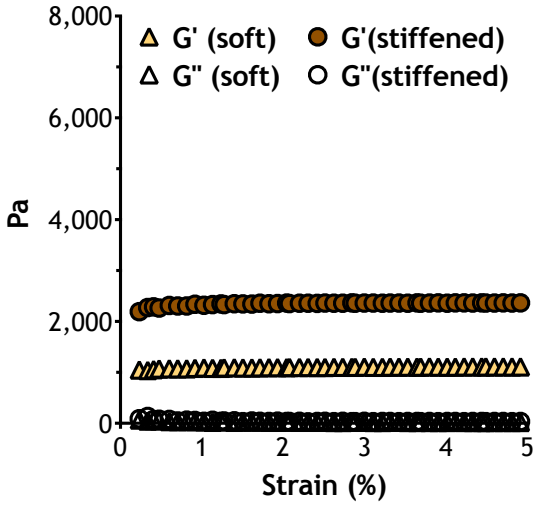

Figure 6.3. Rheological property of gels prepared by macromers PEG8NB (2.5 wt%) with peptide crosslinkers CYGGGYC (5 mM). Gels were crosslinked by thiol-norbornene photopolymerization using 1 mM LAP as the photoinitiator (365 nm, 5 mw/cm^2 for 2 minute). After initial gelation, hydrogels were incubated in 1 mM FMN and stiffened by visible light (440 nm, 3 mW/cm^2, 2 minute). Strain-sweep shear moduli of stiffened gels were measured 24 hours after incubation in PBS.

After establishing the feasibility of FMN-induced photo-stiffening, we adjusted several parameters to identify a range of conditions suitable for inducing stiffening to a pathophysiologically relevant degree (G'~ 4 to 6 kPa).[260, 305] When the gels were incubated in buffer containing 0.1 mM FMN, no significant stiffening was observed (Figure 6.4B) under 3 mW/cm^2 of visible light (440 nm) exposure for 2 minute. When FMN concentrated was increased to 0.5 mM, the same light exposure led to almost 2-fold of stiffening (i.e., G' from ~1.2 to ~ 2.3 kPa. Figure 6.4B). Further increasing FMN concentration to 1 mM did not improve the degree of stiffening. Next, we prepared gels by PEG8NB and peptide crosslinker with 0, 1, 2, or 3 tyrosine residues (i.e., CGGGC, CGGYGGC, CYGGGYC, and KCYGGYGGYCK). Under a stoichiometric ratio of thiol to norbornene, the use of these peptides led to different amount of tyrosine residues immobilized in the hydrogels (i.e., 0, 5, 10, 15 mM, respectively). As expected, gels crosslinked by peptide without tyrosine (i.e., CGGGC) were not susceptible to FMN and visible light-induced stiffening (0 mM group in Figure 6.4C). On the other hand, gels crosslinked with increasing tyrosine residues (i.e., 5 mM CGGYGGC, 10 mM CYGGGYC, or 15 mM KCYGGYGGYCK) exhibited increased gel moduli (from 1 kPa to 1.9, 2.2, and 2.5 kPa, respectively. Figure 6.4C).

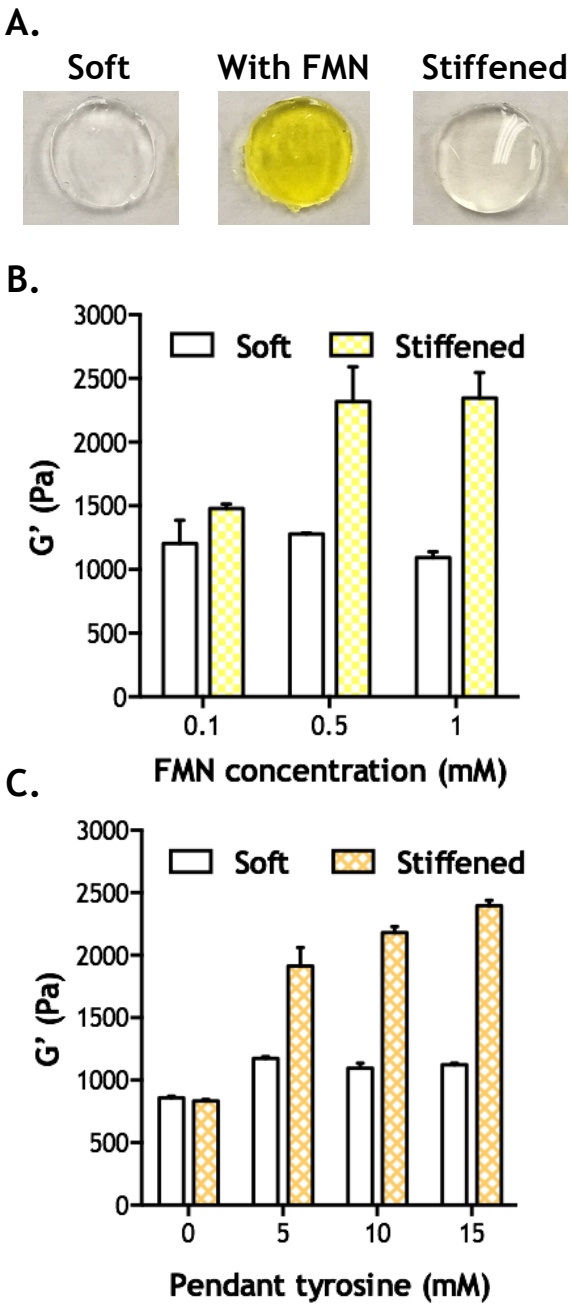

Figure 6.4. Effect of FMN and tyrosine residues on hydrogel stiffening. (A) Images of soft hydrogel (2.5 wt% PEG8NB, 5 mM CYGGGYC) formed by thiol-norbornene photopolymerization (left), gel after incubation with 1 mM FMN for 30 min (middle), and gel after stiffening and additional incubation in PBS for 30 min to remove soluble FMN (right). (B) Shear moduli of hydrogels before and after FMN & visible light-mediated stiffening at different FMN concentrations. (C) Shear moduli of hydrogels formed with different contents of tyrosine residues in the peptide crosslinker (i.e., 0Y, 1Y, 2Y, and 3Y peptides). Data were presented as mean ± SEM (N = 3). P-values were calculated using one-way ANOVA with Bonferroni correction, (*$p<0.05$, **$p<0.01$, and ***$p<0.001$). In collaboration with Han D. Nguyen.

6.3.2 Investigating mechanism of FMN and visible-light mediated di-tyrosine crosslinking

Different from cleavage-type photoinitiators that generate radicals via photolysis, polymerization initiated by non-cleavage type photoinitiators was based on electron transfer (Figure 6.5A)[35]. In the case of FMN, its ground state is excited to short half-life singlet state (^{1}FMN*, $t^{1/2}$ = 5 ns) upon visible light exposure, and then to triplet state (^{3}FMN*, $t^{1/2}$ = 15 μs) with longer half-life through intersystem crossing (ITC).[339, 340] Triplet state FMN (^{3}FMN*) is a strong oxidant capable of generating tyrosyl radical from tyrosine in type 1 reaction (Figure 6.4A).[340] The redox state of ^{3}FMN*, flavin-hydroquinone ($FMNH_2$) could further react with dissolved O_2, regenerating FMN and producing hydrogen peroxide (H_2O_2). On the other hand, in Type 2 reaction, ^{3}FMN* generates tyrosyl radical by means of singlet oxygen ($^1O_2$) excitation without producing hydrogen peroxide (Figure 6.5B). We reasoned that gel stiffening observed in Figure 6.3A was a result of FMN-initiated tyrosyl radicals' combination, leading to di-tyrosine crosslinking. We monitored contents of dissolved O_2 and reactive by-product H_2O_2 during the photoreaction. After 2 minutes of visible light exposure in the presence of 15 mM soluble tyrosine, dissolved O_2 decreased from 20% to 18% (Figure 6.5B). No oxygen reduction was detected in the absence of tyrosine. Under the same light irradiation conditions, H_2O_2 concentration increased from 0 to 0.16 mM in the presence of 15 mM soluble tyrosine (Figure 6.5C). Note that even in the absence of tyrosine, FMN and visible light mediated photooxidation still produced H_2O_2, albeit in lower amounts. The O_2 consumption and H_2O_2 production profiles were indicative of type 1 reaction mechanism. Additional experiments revealed that, in the presence of soluble tyrosine, FMN and visible light exposure led to significant increase of sample absorbance at 314 nm, which was indicative of di-tyrosine formation (Figure 6.5D). These results were consistent with literature regarding the effect of visible light and FMN on tyrosine.[341]

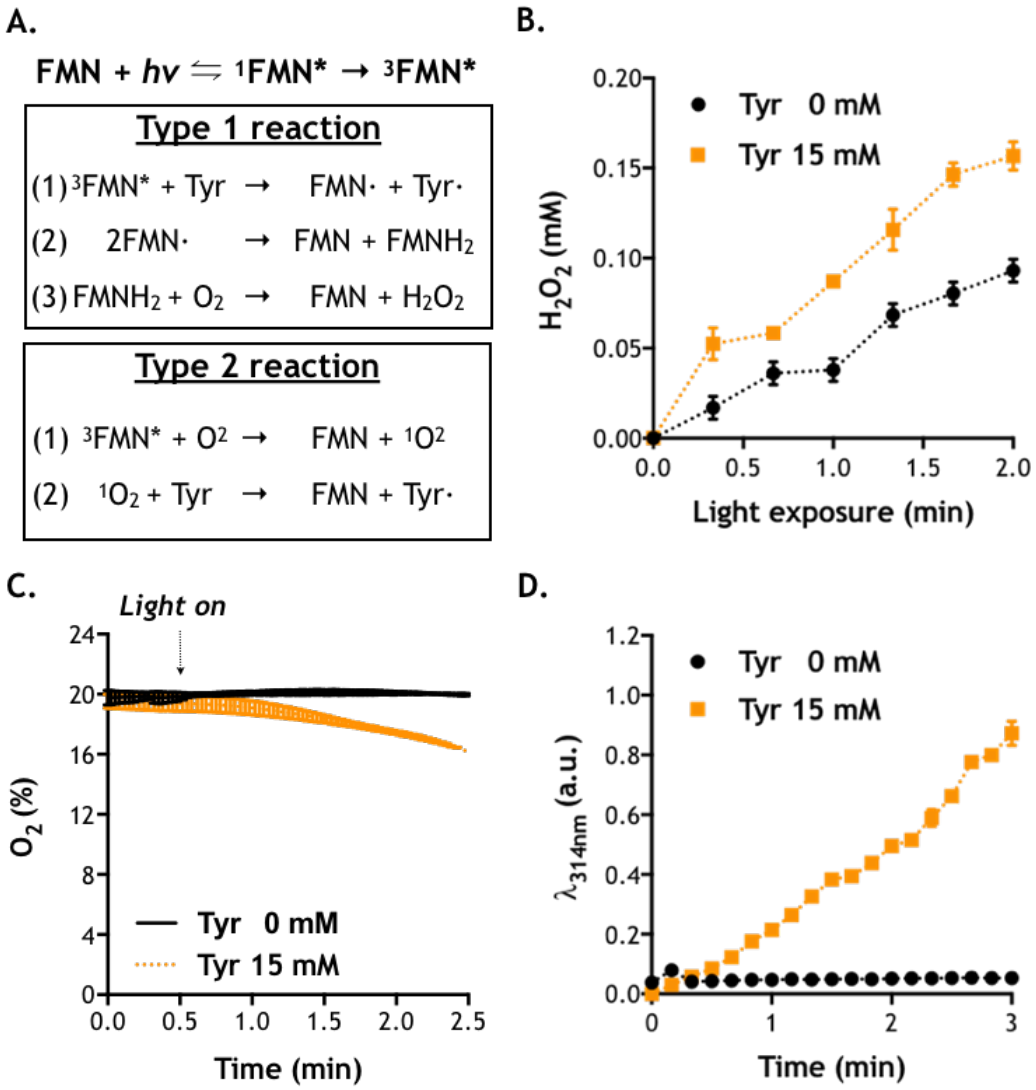

Figure 6.5. Investigation of FMN & visible light-induced photochemistry. (A) Potential mechanisms of FMN-induced tyrosyl radical formation. (B) Oxygen consumption in the absence or presence of 15 mM tyrosine (L-*tyr*). (C) Hydrogen peroxide (H_2O_2) production in the absence or presence of 15 mM L-*tyr*. (D) Solution absorbance at 314 nm as a function of light exposure time. All photo-reactions were conducted in the presence of 1 mM FMN with visible light exposure (440 nm, 3 mW/cm^2). Data were presented as Mean ± SEM (N = 3). In collaboration with Han D. Nguyen.

6.3.3 Cytotoxicity of FMN and visible-light mediated di-tyrosine crosslinking

Prior to applying the FMN-mediated reaction to stiffening cell-laden hydrogels, we evaluated cytotoxicity of this photochemistry using MTT assay. Specifically, COLO-357 cells, a PCC line, were incubated with soluble tyrosine (i.e., 15 mM) in 2D well plate to test effect of the additional tyrosines on cell viability (Figure 6.6A). Additionally, cytotoxicity of FMN & visible

light-mediated reaction were also evaluated by incubating cells with 15 mM tyrosine and 1 mM FMN, followed by exposure of visible light with different duration (i.e., 1 to 5 minute) at 3 mW/cm^2 (Figure 6.6B) or with various intensities (i.e., 1.5, 3, 6 mW/cm^2) for 2 minute (Figure 6.6C). Results indicated that cell viability were above ninety percent for all conditions, suggesting that the parameters used in this study did not cause noticeable cell death. This is not surprising as under these conditions, we only expect a slight elevation of H_2O_2 production (e.g., ~0.15 mM after 2-minute light exposure. Figure 6.5C) and a mild reduction in dissolve oxygen (e.g., ~2 % reduction after 2-minute light exposure (Figure 6.6). Combining the results of dynamic hydrogel stiffening (Figure 6.3) and cytotoxicity of FMN photochemistry (Figure 6.5), we have identified a range of reaction conditions suitable for future cell studies (see section 6.4.5 and 6.4.6).

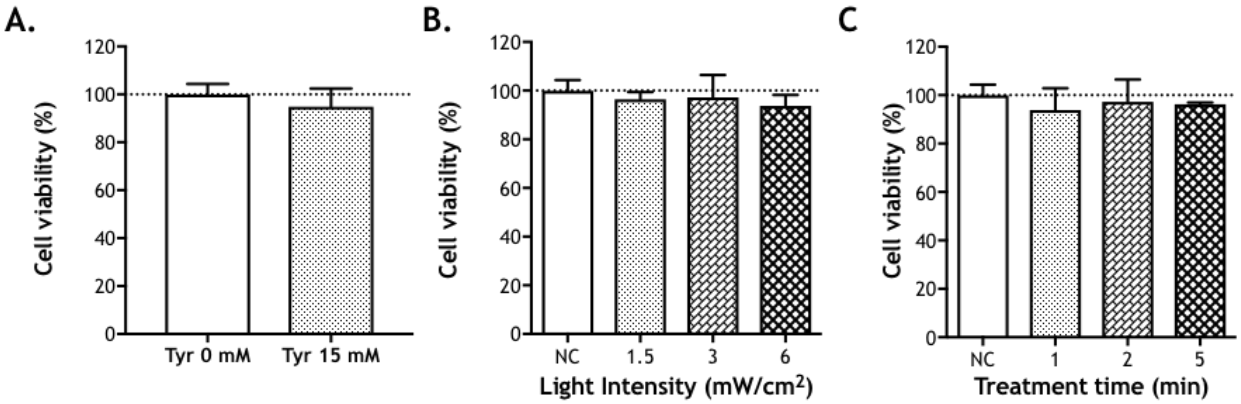

Figure 6.6. Cytotoxicity of visible light and FMN-based photochemistry. COLO-357 cells were cultured in a 24-well plate with seeding density of 5×10^4 cells/well. Cells were cultured for 2 days prior to the visible light treatment and viability was evaluated via MTT assay. (A) Effect of soluble tyrosine. (B) Effect of visible light exposure (3 mW/cm^2) in the presence of 15 mM L-*tyr*. (C) Effect of light intensity (3 minute) in the presence of 15 mM L-*tyr*. All the conditions were normalized to the well without treatment. Data presented as Mean ± SEM, N = 3.

6.3.4 Physicochemical patterning of hydrogel network

We next demonstrated that the degree of dynamic stiffening could be modulated by controlling the duration and intensity of light exposure without changing formulation of gel precursors or concentration of FMN. Specifically, PEG8NB-peptdie hydrogels initially crosslinked with shear moduli of 1 kPa were incubated with 1 mM FMN for 30 minutes, followed by visible light (3 mW/cm^2) irradiation for 0.5-7 minute or with intensity from 0.6-3 mW/cm^2 (for 3 min). Bulk gel moduli were characterized before and after the secondary visible light treatment. As shown in Figure 6.7A, longer duration of light exposure led to higher magnitude of gel

stiffening (~1.7 to ~2.5-fold). Similar degrees of stiffening were achieved via adjusting light intensity (Figure 6.7B). In addition to changes in matrix mechanics, spatially distributed biochemical cues in ECM also regulate cell behavior. To exploit the potential of FMN-mediated photochemistry on presenting biochemical cues spatiotemporally, we designed a proof-of-concept experiment where controlled amounts of 5(6)-Carboxy-X-rhodamine-tyramide (5(6)-ROX-tyramide) were patterned as strips in hydrogels via tuning the duration of light exposure through a photomask (Figure 6.7C). The patterned hydrogels were imaged by confocal microscopy. As shown in Figure 6.7D, higher 5(6)-ROX fluorescence were detected in strips with longer visible light exposure. By analyzing fluorescent intensity semi-quantitatively with Image J (Figure 6.7E), we showed that the 5(6)-ROX patterned gels exhibited regions of higher intensities correlated proportionally to visible light dosage (i.e., 3 and 5 minute). Similar to the patterning of 5(6)-ROX-tyramide, future work may focus on visible light and FMN-based immobilization or patterning of tyrosine-containing peptides/proteins for providing desired biochemical signaling to the cells.

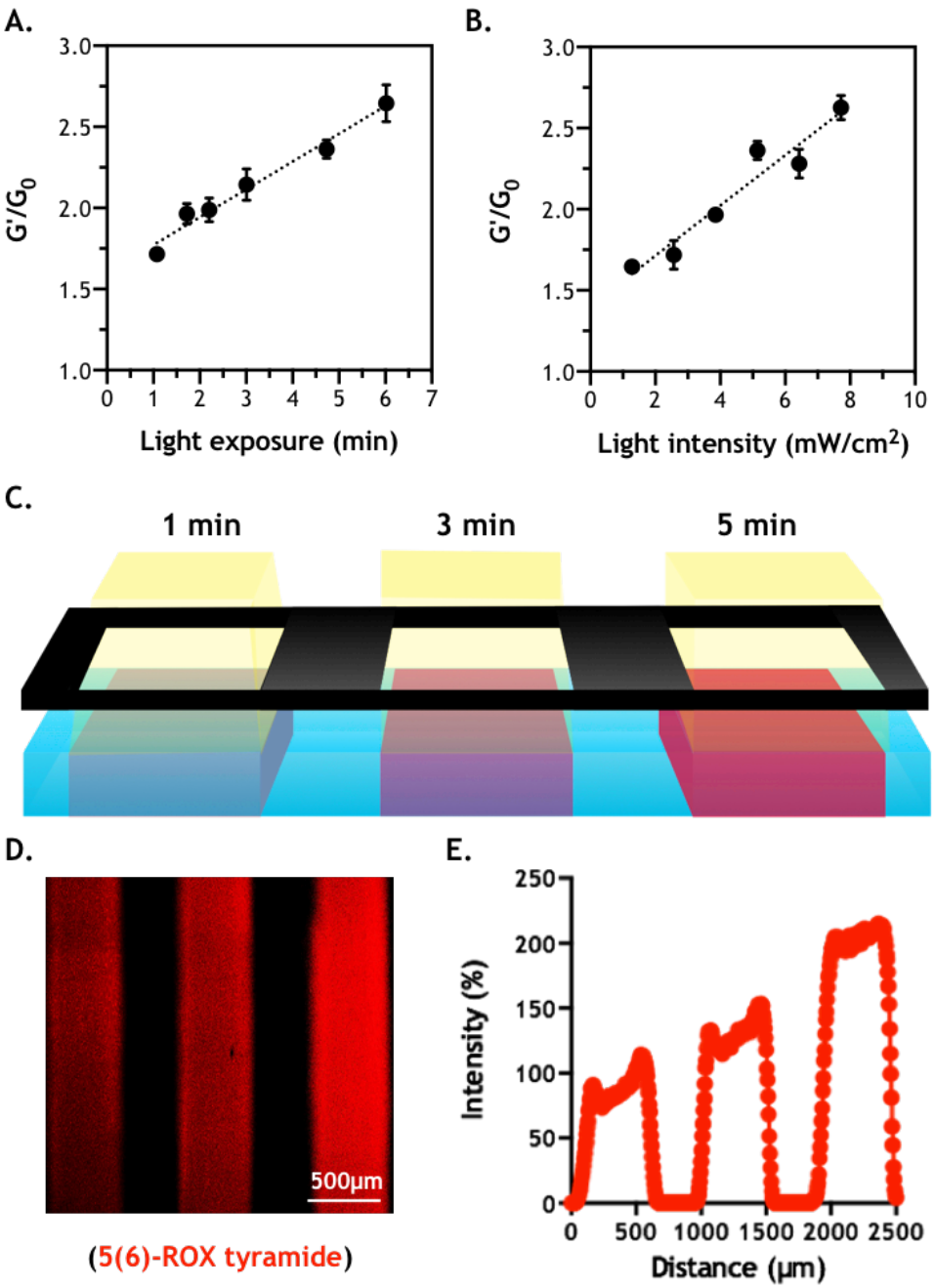

Figure 6.7. Spatial-temporal control of hydrogel stiffening and biochemical patterning. (A) Effect of visible light exposure time on stiffening (at 3 mW/cm^2). (B) Effect of visible light intensity on stiffening (exposure for 2 minute). Data were presented as Mean ± SEM (N = 3). (C) Schematic of photopatterning of biochemical motifs. (D) Photopatterning of hydrogels with 5(6)-ROX-tyramide. Hydrogel was crosslinked by PEG8NB and CYGGGYC peptide. Light intensity was 30 mW/cm^2. (E) Fluorescence intensity profile of the hydrogel photopatterned with 5(6)-ROX-tyramide. Intensity of 5(6)-ROX throughout the gel was normalized to that on region treated with 1 minute of light exposure. Numerical data were presented as Mean ± SEM (N = 3). In collaboration with Han D. Nguyen.

6.3.5 Effect of dynamic matrix stiffening on PCC behavior

To study the influence of the temporal matrix stiffening on cell fate processes, we evaluated formation of multicell spheroids and expression of selected genes at the mRNA level in COLO-357 cells grown in modularly crosslinked and dynamically stiffened hydrogels. We first prepared two groups of cell-laden gels (i.e., PEG8NB crosslinked by CGGGC or KCYGGYGGYCK peptide) with similar initial stiffness (G'~ 1 kPa). All cell-laden gels were treated with soluble FMN (1 mM) and visible light (3 mW/cm^2) for 3 minute one-day post-encapsulation. Only gel crosslinked by tyrosine-containing peptide could be dynamically stiffened. Note that although the stiffened gels would exhibit decreased swelling compared to the non-stiffened and soft gel (Figure 6.2A), they still had high water content (~95.8%) as shown in Figure 6.2B. After 2-week of culture, the encapsulated single cells grew into PCC spheroids in both soft and stiffened gels. However, spheroids formed in gels susceptible to FMN-mediated stiffening were smaller than those formed in the statically soft hydrogels (Figure 6.9A). We quantified spheroid size from the live/dead stained images and found that average diameter of PCC spheroids on day 2 was around 18 μm in both conditions (Figure 6.9B). The differences in spheroid size were statistically significant on day 7 and 14. After two weeks of culture, the average spheroid size in soft gels was ~39 μm and that in the stiffened gels was only ~28 μm. Additionally, cell metabolic activity was consistently and significantly lower in dynamically stiffened matrices (i.e., day 7 and 14, Figure 6.9C). These phenomena could be attributed to slower cell growth imposed by the strain of a tighter hydrogel network, a result similar to our previous findings [289].

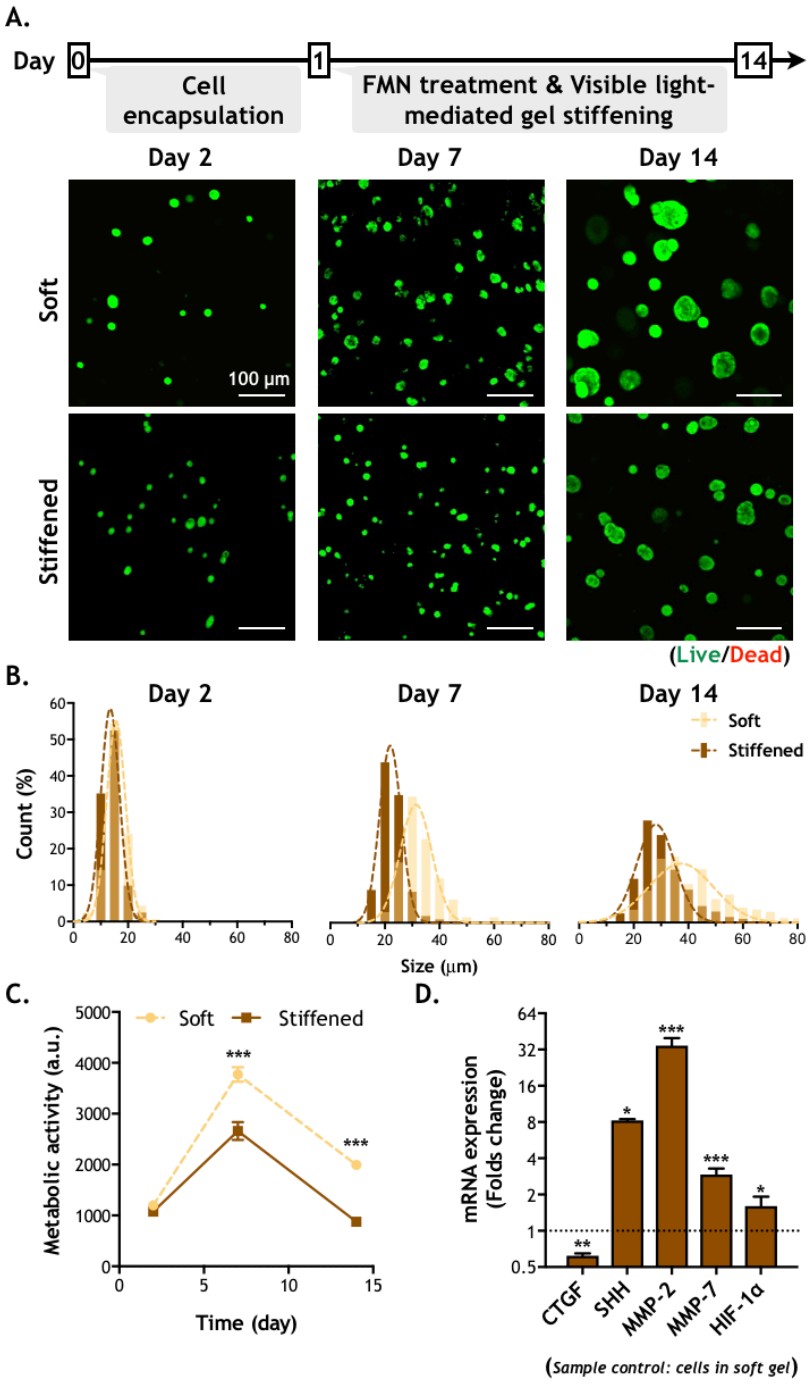

Figure 6.8. Effect of hydrogel stiffening on in vitro culture of COLO-357 cells. (A) Cell spheroid formation in soft (non-stiffened) and stiffened hydrogels. Cell-laden hydrogels were stained with live/dead staining kit and imaged with confocal microscopy. (B) Diameters and (C) metabolic activity of cell spheroids formed in the dynamically stiffened hydrogels (N = 100). (D) mRNA expression on day 14. Housekeeping gene: GAPDH ($2^{-\Delta\Delta Ct}$ method). Data were presented as Mean ± SEM (N = 3) P-values were calculated using one-way ANOVA with Bonferroni correction, (*$p<0.05$, **$p<0.01$, and ***$p<0.001$).

In addition to cell morphology, we also examined the effect of matrix stiffening on mRNA expression of matrix metalloproteinases-2 (MMP-2), MMP-7, and sonic hedgehog (SHH). These genes were selected as they were found to be significantly upregulated in cells underwent enzyme-mediated dynamic matrix stiffening [165]. In the current study, we show similar trends of upregulation at the mRNA levels (Figure 6.8D). Furthermore, we noticed the expression of hypoxia inducible factor 1-alpha (HIF-1α) was also significantly increased in cells experiencing dynamic gel stiffening. HIF-1α was stabilized in cells maintained under hypoxia and has been suggested as a target for cancer therapy [342, 343]. Since the oxygen reduction during hydrogel stiffening was mild (Figure 6.5B), the upregulation of HIF-1α was not likely due to hypoxia in the stiffened gels. Instead, HIF-1α upregulation could be due to increased cellular stress in a stiffened matrix. The up-regulation of MMP-2 and MMP-7 suggested that cancer cells were potentially primed to migration/invasion in a stiffened matrix due to enhanced matrix remodeling by these proteases. While future studies are necessary to test these hypotheses, the experimental results presented here collectively highlight the significant impact of a dynamic stiffening microenvironment on cancer cell fate.

6.3.6 Effect of dynamic stiffening/patterning on cancer-associated fibroblasts

CAFs are a group of activated stromal cells supporting the growth and metastasis of PCCs. While the importance of CAFs in PDAC progression has been recognized, the effects of biophysical cues on their activation have not been fully defined. Utilizing FMN/visible light dynamic hydrogel system, we further examined the effect of matrix stiffening on activation of CAFs. We seeded pancreatic CAFs on top of the initially soft hydrogel (i.e., G'~ 1 kPa) and regionally stiffening half of the gel through a photomask one day after cell seeding. Based on the degree of cell spreading, there appeared to be a distinguishable soft/stiff boundary. On the stiffened region (i.e., right side of the gel), CAFs adopted spreading morphology, likely due to an increased intracellular tension resulted from the higher matrix stiffness. On the other hand, cells grew into smaller clusters in the non-stiffened gel (i.e., left side of the gel) (Figure 6.9A).

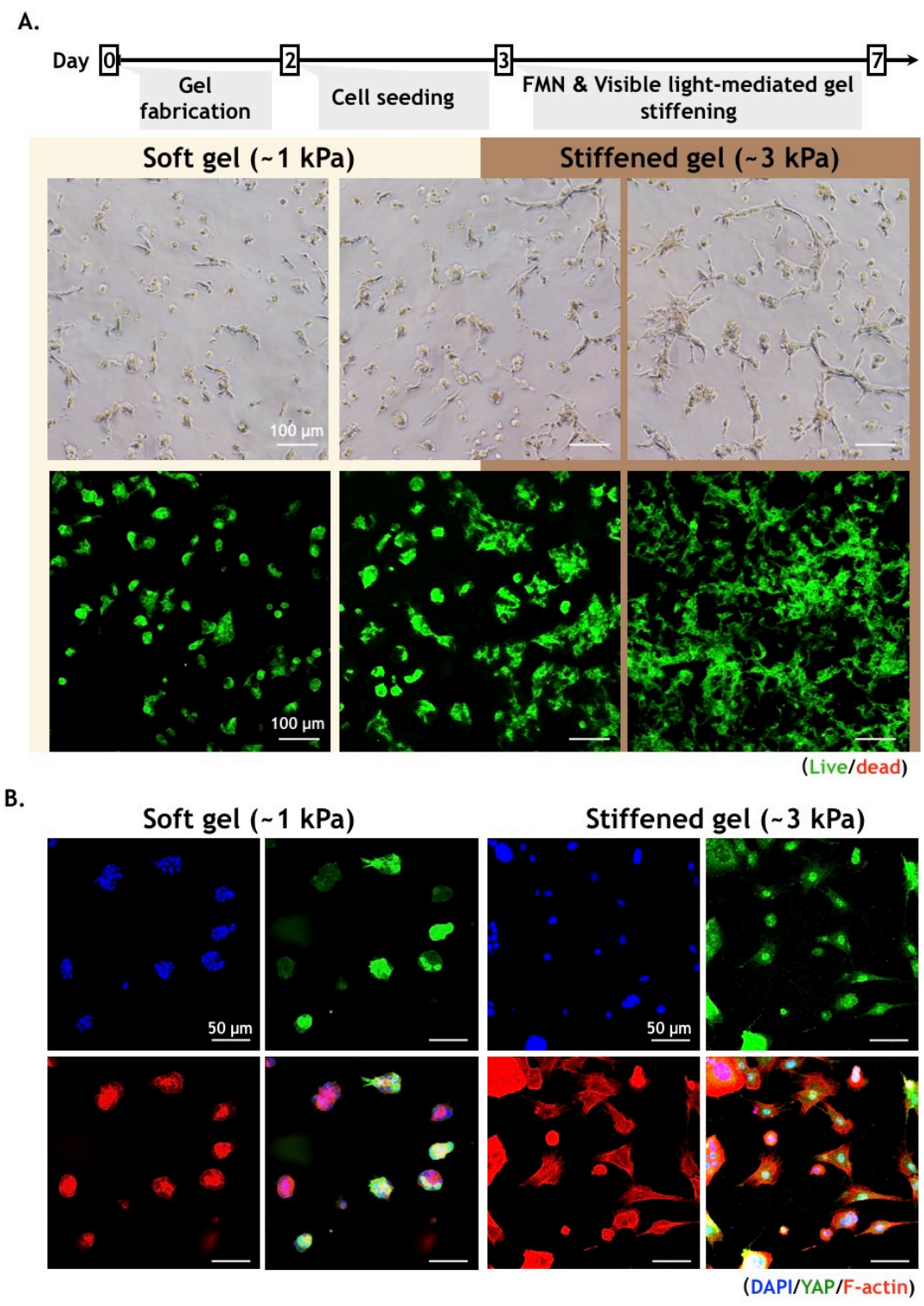

Figure 6.9. Effect of dynamic stiffening on pancreatic stromal cells (KPC/CAFs). (A) Morphology and viability of CAFs cultured on a regionally stiffened (1×10^{-3} M FMN, 2 minutes of visible light at 3 mW/cm^2) PEG-peptide gel (2.5 wt% PEG8NB, 5×10^{-3} M 3Y peptide). (B) Immunostaining of F-actin, YAP, and cell nuclei (counterstained with DAPI).

Increased tissue stiffness during pathophysiological processes can lead to nuclear translocation of yes-associated protein (YAP) in stromal cells [233, 337, 344, 345]. Activation of YAP-related signaling pathways triggers EMT in various cancer cell types, including colorectal, breast, hepatic, and pancreatic origins [71, 305, 346-349]. To gain insight into stiffness-regulated YAP localization in pancreatic CAFs, we performed immunostaining of F-actin, YAP, and nuclei in cells cultured on top of partially stiffened hydrogel. We found that cells adhered on the visible light and FMN-stiffened area of the gel exhibited more nuclear translocation of YAP, as compared to cells attached on the non-stiffened and soft gel (Figure 6.9B). Collectively, these results established a causation link between matrix stiffness and activation of pancreatic CAFs. This contribution presents a visible-light driven dynamic hydrogel system that is highly beneficial for studying tumor-ECM interaction in a more physiological culture condition.

Table 6.1. Primer sequences for real-time PCR

Gene	Forward (5'→3')	Reverse (5'→3')	
GAPDH	GAAGGTGAAGGTCGGAGTC	GAAGATGGTGATGGGATTTC	[270]
MMP2	CTCAGATCCGTGGTGAGATCT	CTTTGGTTCTCCAGCTTCAGG	[350]
MMP9	ATCCAGTTTGGTGTCGCGGAGC	GAAGGGGAAGACGCACAGCT	Harvard Primer Bank
SHH	GGAAGCAGCCTCCCGATT	CGAGTCCAAGGCACATATCCA	[297]
CTGF	AGGAGTGGGTGTGTGACGA	CCAGGCAGTTGGCTCTAATC	[297]
HIF1α	GAACGTCGAAAAGAAAAGTCTCG	CCTTATCAAGATGCGAACTCACA	Harvard Primer Bank

6.4 Material and Methods

6.4.1 Materials

Hydroxyl-terminated 8-arm PEG (20 kDa) and 5-norbornene-2-carboxylic acid were obtained from JenKem Technology USA and Sigma-Aldrich, respectively. Reagents and Fmoc-capping amino acids for solid phase peptide synthesis were acquired from Anaspec or ChemPep. All other reagents for chemical synthesis were purchased from Sigma-Aldrich or Thermo Fisher unless noted otherwise.

6.4.2 Macromers and peptide synthesis

While all macromers, peptides, and LAP photoinitiator can be purchased from commercial vendors, we synthesized these materials using established protocols. PEG8NB and LAP were synthesized as described elsewhere.[252, 272] Bis-cysteine bearing peptides with varied amounts of tyrosines, including CGGGC (0Y), CGGYGGC (1Y), CYGGGYC (2Y), and KCYGGYGGYCK (3Y) were synthesized via standard Fmoc coupling chemistry with an automated microwave-assisted peptide synthesizer (Liberty 1, CEM). Crude products were cleaved in trifluoroacetic acid (TFA) cleavage cocktail and purified by reverse phase High-Performance Liquid Chromatography (HPLC) to obtain final products with over 90% purity. All peptides were characterized by mass spectrometry (MS). 5(6)-Carboxy-X-rhodamine-tyramide was synthesized from 5(6)-Carboxy-X-rhodamine (5(6)-ROX) and L-tyramine using carbodiimide chemistry. Briefly 0.01 mole of 5(6)-ROX was activated by 5-molar excess of 1-ethyl-3-(-3-

dimethylaminopropyl) carbodiimide hydrochloride (EDC) and N-hydroxysuccinimide (NHS) in 1.5 ml solvent composed of 3 parts DMF and 2 parts ddH_2O. After 30 minutes of activation, 5-fold excess (0.05 mole) of L-tyramine was added and the reaction was allowed to proceed 24 h. The final product was purified by column chromatography using silica gel as stationary phase and mobile phase composed of 1-part ethyl acetate and 9 parts hexane.

6.4.3 Hydrogel fabrication and characterization

Gels were prepared by conjugating norbornene moieties of PEG8NB and terminal cysteine moieties of the peptide crosslinker through thiol-norbornene photopolymerization. Briefly, gel precursors (45 µl per sample, 1 mM LAP) were deposited between two glass slides separated by spacers (1 mm). The samples were exposed to 365 nm light (5 mW/cm^2) for 2 minute. Following gelation, hydrogels were incubated in PBS at 37ºC for 24 hours prior to characterization or the stiffening process. Stoichiometric ratio of thiol to norbornene was maintained at one to afford the highest degree of crosslinking within the initial gel network. Shear moduli of the hydrogels were characterized in strain-sweep mode using a digital rheometer (Bohlin CVO 100) fitted with an 8-mm diameter parallel plate geometry. Gap sizes were adjusted to 650 µm and 580 µm for pre- and post-stiffened gels, respectively. Shear modulus measurements were performed in strain-sweep mode (0.1-5% strain) and oscillation frequency was maintained at 1 Hz. Note that most of the gels were prepared with the shear moduli around 1,000 Pa prior to the stiffening process.

6.4.4 Prediction of time needed for FMN diffusion into hydrogel

The time-scale of FMN diffusion into a disc-shaped hydrogel was estimated by Fick's Second Law of Diffusion using mesh size-dependent diffusivity (i.e., Lustig-Peppas estimation of solute diffusivity in a highly swollen hydrogel) [218]. Hydrogel mesh size was calculated from experimentally obtained mass swelling ratio [122]. Correlations between hydrogel shear modulus and mesh size were established and this information was used to determine diffusivity of FMN in hydrogel.

6.4.5 Detection of dissolved oxygen and hydrogen peroxide produced during photo-reaction

The contents of dissolved oxygen and hydrogen peroxide produced during visible light exposure (3 mW/cm^2, 5 minute) were measured in the presence of L-tyrosine (15 mM) and FMN (1 mM) in PBS. Mixtures were deposited in a 24 well plate. Oxygen contents in solution were detected with a dipping-type oxygen microsensor (MicroX4, PreSens) which was extended to ~2

mm above the bottom of well plate. To quantify H_2O_2 production during FMN-mediated photo-reaction, 10 µl of the mixture solutions were collected periodically and quantified with a Quantichrom Peroxide Assay Kit (BioAssay Systems).

6.4.6 FMN and visible light-mediated in situ gel stiffening and molecular patterning

Process of hydrogels stiffening were initiated from incubating the hydrogels in FMN solution for 30 minutes at 37°C. Next, gels were transferred to the top of glass slide and exposure to visible light (480 nm, 3 mW/cm^2) for 2 minutes. The stiffened hydrogels were returned to PBS and incubated for a day prior to second measurement of the shear moduli. For proof-of-concept spatial molecular patterning, hydrogels were fabricated in a rectangular silicon mold (5 (L) × 2 (W) × 1 (H) mm) using 2.5 wt% PEG8NB, 5 mM peptide crosslinkers (KCYGGYGGYCK), and 1 mM LAP. After overnight swelling in DPBS, gels were submerged in buffer solution containing 1 mM FMN and 0.03 mM 5(6)-ROX tyramide for an hour. Next, gel was exposed to strips of visible light (440 nm, 30 mW/cm^2) for 1, 3, and 5 min through a photomask. The patterned gels were washed and imaged by confocal microscopy at 10x objective. Images were analyzed via Image J.

6.4.7 Cells in 3D encapsulation and characterization

COLO-357 cells, a PCC line, were cultured in high glucose DMEM supplemented with 10% fetal bovine serum (FBS, Gibco) and penicillin-streptomycin (Gibco, 50 U/mL for both antibiotics). Cells were maintained in a standard cell culture incubator (37 °C, 5% CO_2). Prior to encapsulation in hydrogels, cells were trypsinized and suspended (to a final cell density of 2×10^6 cells/ml) in buffer solution consisting of LAP and macromer precursors (i.e., PEG8NB and peptide crosslinker) at desired concentrations. Cell-precursor solution (25 µl) was loaded to a 1 mL disposable syringe with cut-open tip and exposed to 365 nm light (5 mW/cm^2) for 2 minutes. These cell-laden gels were cultured in a 24-well plate for two weeks. To evaluate cell viability, cell-laden gels were stained with live/dead staining kit (Biotium; Calcein-AM stained live cells green, Ethidium homodimer-1 stained dead cells red) on day 2, 7, 14, and imaged by confocal microscopy (Olympus Fluoview FV100 laser scanning microscope). *Z*-stack images (10 µm per slice, 100 µm total) were obtained from minimum of three random areas within the cell-laden gels. In addition, cell metabolic activity was evaluated by AlamarBlue assay (AbD Serotec; 10% in culture media, 2.5-hour incubation time).

6.4.8 RNA Isolation, reverse-transcription PCR, and real-time PCR

Cell-laden gels were harvested on day 14 in RNase-free microtubes, followed by flash-freezing in liquid nitrogen and storage at -80°C. Total RNA was isolated from the encapsulated cells with NucleoSpin RNA II kit (Clontech). The concentration and purity of RNA were obtained by NanoDrop 2000 Spectrophotometer (Thermo Scientific). Next, purified RNA samples were converted into complementary DNA (cDNA) with PrimeScript RT Reagent Kit (Clontech, TaKaRa). mRNA expression of selected genes were evaluated by qPCR using SYBR Premix Ex TaqII kit (Clontech) with primers listed in Table 6.1. GAPDH was used as the housekeeping gene. The expression level of genes in the control hydrogel group (i.e., gels prepared by PEG8NB/CGGGC) were used as negative controls, from which to calculate the relative fold changes of each mRNA expression in the experimental hydrogel groups ($2^{-\Delta\Delta CT}$ method).

6.4.9 Effect of spatially-patterned gel mechanics on cancer-associated fibroblasts (CAFs)

Initial PEG-peptide gelation (i.e., 2.5 wt% PEG8NB, 5 mM peptide crosslinker (KCYGGYGGYCK), 1mM CRGDS, and 1 mM LAP) were achieved using 2 min of visible-light exposure (5 mW/cm^2). Precursor solutions were loaded in a rectangular silicon mold (5 L × 2 W × 1 H mm). After swelling the gels in DPBS overnight, 10^6 cells/mL of pancreatic CAFs, which were derived from KRAS/mutp53-induced pancreatic cancer mouse (i.e., KPC/CAFs, a gift from Prof. Murray Korc of IU School of Medicine), were seeded on top of the rectangular gel and cultured for 2 days. Next, the gels were incubated with soluble FMN (1 mM) for 30 min, washed with DPBS to remove excess FMN, and exposed to visible light (3 mW/cm^2) for 2 minute through a photomask covering half of the gel (2.5 × 2 mm). After the visible light/FMN-induced stiffening process, gels were returned to culture media for another 5 day. On day 8, cells were imaged by bright-field microscopy and confocal microscopy for evaluating cell morphology and YAP localization.

6.4.10 Immunostaining of CAFs on top of soft and stiffened gel

After CAFs were cultured on top of partially stiffened gel for 8 days, cells were fixed with 4% paraformaldehyde, permeabilized with saponin (1:1000), and blocked with 1% BSA and 10% FBS at 4°C for overnight. Sample was stained with the primary antibody, Rabbit anti-YAP (1:200) at 4°C for overnight, and washed with PBS thrice for 10 min each, and treated with donkey anti-rabbit 488 (1:200) at 4°C for overnight. Sample were washed again with PBS and stained with F-

actin using Rhodamine Phalloidin (1:200) at 4°C for overnight and washed. Finally, cell nuclei were counterstained with DAPI (1:1000) for one hour, washed stored in ibidi mounting medium to prevent photobleaching. Finally, images were obtained from confocal microscopy at 10X and 20X objectives.

6.4.11 Statistical Analysis

All experiments were repeated three times independently with minimum of four samples per condition. Numerical data were analyzed by two-way ANOVA, and reported as mean ± SEM. Single, double, and triple asterisks represent $p < 0.05$, 0.001, and 0.0001, respectively. $p < 0.05$ was considered statistically significant. For gene expression analysis, pairs of groups were compared by one-way ANOVA with GraphPad Prism 8 software.

6.5 Conclusion

In summary, we have developed a visible light-initiated photo-responsive hydrogel system using synthetically simple macromers and FMN, a vitamin-B_2 derivative, as the photoinitiator. The simple design of tyrosine-bearing peptide crosslinkers permit tunable degree of photo-responsive stiffening and ligand immobilization without complicated macromer modification. We identified parameters critical for tuning gel stiffening and showed that the stiffening/patterning process was highly cytocompatible. Additionally, we evaluated the effect of dynamic matrix stiffening on inhibition of PCCs growth in 3D and on potential activation of cancer-associated fibroblasts. Future work will focus on using this dynamic hydrogel platform for studying cell-cell interactions and durotaxis of PCCs under dynamically tunable matrix properties.

CHAPTER 7. CONCLUSION AND FUTURE RECOMMENDATION

7.1 Summary of Findings

The work presented in this dissertation has demonstrated the capability of a dynamic hydrogel system can be designed to not only recapitulate tumor tissue compositions, but also mimic the dynamical changes of tissue mechanics. The key concept in this design was to utilize dually functionalized peptide crosslinker (i.e., cysteine and tyrosine containing peptides, e.g., CYGGGYC, CHAPTER 3) and norbornene and phenolic group modified gelatin (GelNBHPA, CHAPTER 6). The gelation techniques (i.e., thiol-norbornene photopolymerization), and external stimuli (i.e., enzyme and visible light exposure) were utilized to induce the additional gel property changes. These systems and techniques should offer researchers useful platforms to effortlessly study tumor-stroma interaction in cancer progression. Enzyme-mediated dynamic gel systems have shown their capability in temporally modulating the gel mechanical property. These systems may have potential to fabricate gels with gradient stiffness.

For the first technique using the incubation of soluble enzyme to stiffen gel system, the peptide crosslinkers (i.e., CYGGGYC) was designed, allowing for both thiol-norbornene photopolymerization with macromers PEG8NB and tyrosinase-catalytic reaction. Next, we built the computational model to predict enzyme diffusion and reaction profile within hydrogel to identify the key parameters in process of gel stiffening. We validated model prediction by the experimental data that included enzyme diffusion in gel, enzymatic reaction kinetics, and characterization of gel property (CHAPTER 3). After optimizing the gel stiffening process, we studied impact of matrix stiffening on pancreatic stellate cells (PSCs) using a PEG-based dynamic stiffening gel system (CHAPTER 4). In this chapter, we suggested that the matrix stiffening might lead to PSCs activation which secreted extra α-actin. To further incorporate the primary native ECM of PDAC in the gel system such as HA, we introduced a biomimetic and dynamic gel system with the bifunctional gelatin (Ge_{NBHPA}) and THA (CHAPTER 5). We verified the system proteolytic degradability (i.e., collagenase-1 and hyaluronidase) and the capability of enzyme-mediated dynamical gel stiffening. The gel systems were then used to encapsulate two pancreatic cancer cell line (COLO-357 and PANC-1) for evaluating impact of matrix stiffening and HA on cancer cell fate. In CHAPTER 5, we found that the pancreatic cancer cells exhibited the spreading

morphology, different gene expression profile, and EMT characteristics when culturing in a stiffening and HA-contained gel. In this study, we only explore the synergistic effect of matrix stiffening and HA. The potential future study can be focus on other important ECM in PDAC tissue, such as fibronectin and collagen. In addition to using enzymatic reaction for tuning matrix stiffness, of the same macromers were also explored for their susceptibility to visible light and flavin mononucleotide (FMN)-mediated photocrosslinking (CHAPTER 6). The use of photo-responsive dynamic hydrogel permitted tunable degree of gel stiffening and ligand immobilization without complex macromer synthesis. This system was exploited for investigating the influence of matrix stiffening on cancer cells growth in 4D. Furthermore, cancer-associated fibroblasts (CAFs) were used to demonstrate the power of local gel stiffening on inducing EMT.

Gel with gradient stiffness has been beneficial for investigating cellular durotaxis, which is a unique biological event picturing cell migration toward tissue with higher stiffness. In the cancer study, cancer stromal cells (i.e., PSCs and CAFs) have been shown highly responsive to their surrounding tissue mechanics. Additionally, invasion path of these stromal cells has been reported to associate with the gradient stiffness of tissue. To evaluate effect of matrix stiffness gradient on migration of stromal cells (i.e., durotaxis), live cell imaging may be utilized to evaluate cell migration in gels with various degree of stiffness gradients. In brief, stromal cells such as PSCs or CAFs may be seeded on top of the gel fabricated in a microchannel with two reservoirs on both ends. One reservoir can be filled with soluble tyr_{ase} to generate a gradient of enzyme concentration, which would result in a gradient of reaction, and hence a hydrogel with a stiffness gradient. Finally, durotaxis of PCCs, PSCs, CAFs can be evaluated via real-time live cell imaging. In addition to live cell imaging, evaluating critical mechanotransduction-associated gene expression should provide insights into the mechanisms by which the cells sense their local environment.

LIST OF REFERENCES

[1] K. Polireddy, Q. Chen, Cancer of the Pancreas: Molecular Pathways and Current Advancement in Treatment, J Cancer 7(11) **2016** 1497-514.

[2] A. Arcucci, M.R. Ruocco, G. Granato, A.M. Sacco, S. Montagnani, Cancer: An Oxidative Crosstalk between Solid Tumor Cells and Cancer Associated Fibroblasts, Biomed Res Int 2016**2016** 4502846.

[3] L. Wan, K. Pantel, Y. Kang, Tumor metastasis: moving new biological insights into the clinic, Nat Med 19(11) **2013** 1450-64.

[4] D. von Ahrens, T.D. Bhagat, D. Nagrath, A. Maitra, A. Verma, The role of stromal cancer-associated fibroblasts in pancreatic cancer, J Hematol Oncol 10(1) **2017** 76.

[5] E. De Vlieghere, F. Gremonprez, L. Verset, L. Marien, C.J. Jones, B. De Craene, G. Berx, B. Descamps, C. Vanhove, J.P. Remon, W. Ceelen, P. Demetter, M. Bracke, B.G. De Geest, O. De Wever, Tumor-environment biomimetics delay peritoneal metastasis formation by deceiving and redirecting disseminated cancer cells, Biomaterials 54**2015** 148-57.

[6] R.L. Siegel, K.D. Miller, A. Jemal, Cancer statistics, 2019, CA Cancer J Clin 69(1) **2019** 7-34.

[7] L. Rahib, B.D. Smith, R. Aizenberg, A.B. Rosenzweig, J.M. Fleshman, L.M. Matrisian, Projecting cancer incidence and deaths to 2030: the unexpected burden of thyroid, liver, and pancreas cancers in the United States, Cancer Res 74(11) **2014** 2913-21.

[8] R.L. Siegel, K.D. Miller, A. Jemal, Cancer statistics, 2018, CA Cancer J Clin 68(1) **2018** 7-30.

[9] D. Avery, P. Govindaraju, M. Jacob, L. Todd, J. Monslow, E. Pure, Extracellular matrix directs phenotypic heterogeneity of activated fibroblasts, Matrix Biol 67**2018** 90-106.

[10] O. Chaudhuri, S.T. Koshy, C. Branco da Cunha, J.W. Shin, C.S. Verbeke, K.H. Allison, D.J. Mooney, Extracellular matrix stiffness and composition jointly regulate the induction of malignant phenotypes in mammary epithelium, Nat Mater 13(10) **2014** 970-8.

[11] S. Allazetta, L. Kolb, S. Zerbib, J. Bardy, M.P. Lutolf, Cell-Instructive Microgels with Tailor-Made Physicochemical Properties, Small 11(42) **2015** 5647-56.

[12] L. Huang, A. Holtzinger, I. Jagan, M. BeGora, I. Lohse, N. Ngai, C. Nostro, R. Wang, L.B. Muthuswamy, H.C. Crawford, C. Arrowsmith, S.E. Kalloger, D.J. Renouf, A.A. Connor, S. Cleary, D.F. Schaeffer, M. Roehrl, M.S. Tsao, S. Gallinger, G. Keller, S.K. Muthuswamy, Ductal pancreatic cancer modeling and drug screening using human pluripotent stem cell- and patient-derived tumor organoids, Nat Med 21(11) **2015** 1364-71.

[13] C.D. Hartman, B.C. Isenberg, S.G. Chua, J.Y. Wong, Vascular smooth muscle cell durotaxis depends on extracellular matrix composition, Proc Natl Acad Sci U S A 113(40) **2016** 11190-11195.

[14] C.A. Acevedo, E. Sánchez, P. Díaz-Calderón, J.J. Blaker, J. Enrione, F. Quero, Synergistic effects of crosslinking and chitosan molecular weight on the microstructure, molecular mobility, thermal and sorption properties of porous chitosan/gelatin/hyaluronic acid scaffolds, Journal of Applied Polymer Science 134(18) **2017**.

[15] R.S. Stowers, S.C. Allen, K. Sanchez, C.L. Davis, N.D. Ebelt, C. Van Den Berg, L.J. Suggs, Extracellular Matrix Stiffening Induces a Malignant Phenotypic Transition in Breast Epithelial Cells, Cellular and Molecular Bioengineering 10(1) **2016** 114-123.

[16] D. Rodenhizer, T. Dean, E. D'Arcangelo, A.P. McGuigan, The Current Landscape of 3D In Vitro Tumor Models: What Cancer Hallmarks Are Accessible for Drug Discovery?, Adv Healthc Mater 7(8) **2018** e1701174.

[17] B.A. Krantz, K.H. Yu, E.M. O'Reilly, Pancreas adenocarcinoma: novel therapeutics, Chin Clin Oncol 6(3) **2017** 30.

[18] D. He, R.X. Wang, J.P. Mao, B. Xiao, D.F. Chen, W. Tian, Three-dimensional spheroid culture promotes the stemness maintenance of cranial stem cells by activating PI3K/AKT and suppressing NF-kappaB pathways, Biochem Biophys Res Commun 488(3) **2017** 528-533.

[19] Y.A. Yoo, M.H. Kang, H.J. Lee, B.H. Kim, J.K. Park, H.K. Kim, J.S. Kim, S.C. Oh, Sonic hedgehog pathway promotes metastasis and lymphangiogenesis via activation of Akt, EMT, and MMP-9 pathway in gastric cancer, Cancer Res 71(22) **2011** 7061-70.

[20] S. Yang, L. Zhang, V. Purohit, S.K. Shukla, X. Chen, F. Yu, K. Fu, Y. Chen, J. Solheim, P.K. Singh, W. Song, J. Dong, Active YAP promotes pancreatic cancer cell motility, invasion and tumorigenesis in a mitotic phosphorylation-dependent manner through LPAR3, Oncotarget 6(34) **2015** 36019-31.

[21] S. Morvaridi, D. Dhall, M.I. Greene, S.J. Pandol, Q. Wang, Role of YAP and TAZ in pancreatic ductal adenocarcinoma and in stellate cells associated with cancer and chronic pancreatitis, Sci Rep 5**2015** 16759.

[22] P. Bailey, D.K. Chang, K. Nones, A.L. Johns, A.M. Patch, M.C. Gingras, D.K. Miller, A.N. Christ, T.J. Bruxner, M.C. Quinn, C. Nourse, L.C. Murtaugh, I. Harliwong, S. Idrisoglu, S. Manning, E. Nourbakhsh, S. Wani, L. Fink, O. Holmes, V. Chin, M.J. Anderson, S. Kazakoff, C. Leonard, F. Newell, N. Waddell, S. Wood, Q. Xu, P.J. Wilson, N. Cloonan, K.S. Kassahn, D. Taylor, K. Quek, A. Robertson, L. Pantano, L. Mincarelli, L.N. Sanchez, L. Evers, J. Wu, M. Pinese, M.J. Cowley, M.D. Jones, E.K. Colvin, A.M. Nagrial, E.S. Humphrey, L.A. Chantrill, A. Mawson, J. Humphris, A. Chou, M. Pajic, C.J. Scarlett, A.V. Pinho, M. Giry-Laterriere, I. Rooman, J.S. Samra, J.G. Kench, J.A. Lovell, N.D. Merrett, C.W. Toon, K. Epari, N.Q. Nguyen, A. Barbour, N. Zeps, K. Moran-Jones, N.B. Jamieson, J.S. Graham, F. Duthie, K. Oien, J. Hair, R. Grutzmann, A. Maitra, C.A. Iacobuzio-Donahue, C.L. Wolfgang, R.A. Morgan, R.T. Lawlor, V. Corbo, C. Bassi, B. Rusev, P. Capelli, R. Salvia, G. Tortora, D. Mukhopadhyay, G.M. Petersen, I. Australian Pancreatic Cancer Genome, D.M. Munzy, W.E. Fisher, S.A. Karim, J.R. Eshleman, R.H. Hruban, C. Pilarsky, J.P. Morton, O.J. Sansom, A. Scarpa, E.A. Musgrove, U.M. Bailey, O. Hofmann, R.L. Sutherland, D.A. Wheeler, A.J. Gill, R.A. Gibbs, J.V. Pearson, N. Waddell, A.V. Biankin, S.M. Grimmond, Genomic analyses identify molecular subtypes of pancreatic cancer, Nature 531(7592) **2016** 47-52.

[23] L.F. Sempere, J.R. Gunn, M. Korc, A novel 3-dimensional culture system uncovers growth stimulatory actions by TGFbeta in pancreatic cancer cells, Cancer biology & therapy 12(3) **2011** 198-207.

[24] J. Gore, I.E. Imasuen-Williams, A.M. Conteh, K.E. Craven, M. Cheng, M. Korc, Combined targeting of TGF-beta, EGFR and HER2 suppresses lymphangiogenesis and metastasis in a pancreatic cancer model, Cancer Lett 379(1) **2016** 143-53.

[25] Z. Qin, J. Feng, Y. Liu, L.L. Deng, C. Lu, PDGF-D promotes dermal fibroblast invasion in 3-dimensional extracellular matrix via Snail-mediated MT1-MMP upregulation, Tumour Biol 37(1) **2016** 591-9.

[26] K. Santhana Kumar, D. Tripolitsioti, M. Ma, J. Grahlert, K.B. Egli, G. Fiaschetti, T. Shalaby, M.A. Grotzer, M. Baumgartner, The Ser/Thr kinase MAP4K4 drives c-Met-induced motility and invasiveness in a cell-based model of SHH medulloblastoma, Springerplus 4**2015** 19.

[27] F.C. Kelleher, Hedgehog signaling and therapeutics in pancreatic cancer, Carcinogenesis 32(4) **2011** 445-51.

[28] J.M. Bailey, A.M. Mohr, M.A. Hollingsworth, Sonic hedgehog paracrine signaling regulates metastasis and lymphangiogenesis in pancreatic cancer, Oncogene 28(40) **2009** 3513-25.

[29] V. Brancato, V. Comunanza, G. Imparato, D. Cora, F. Urciuolo, A. Noghero, F. Bussolino, P.A. Netti, Bioengineered tumoral microtissues recapitulate desmoplastic reaction of pancreatic cancer, Acta Biomater 49**2017** 152-166.

[30] C.J. Whatcott, C.H. Diep, P. Jiang, A. Watanabe, J. LoBello, C. Sima, G. Hostetter, H.M. Shepard, D.D. Von Hoff, H. Han, Desmoplasia in Primary Tumors and Metastatic Lesions of Pancreatic Cancer, Clin Cancer Res 21(15) **2015** 3561-8.

[31] D. Kudo, A. Suto, K. Hakamada, The Development of a Novel Therapeutic Strategy to Target Hyaluronan in the Extracellular Matrix of Pancreatic Ductal Adenocarcinoma, Int J Mol Sci 18(3) **2017**.

[32] Z. Wang, J. Li, X. Chen, W. Duan, Q. Ma, X. Li, Disrupting the balance between tumor epithelia and stroma is a possible therapeutic approach for pancreatic cancer, Med Sci Monit 20**2014** 2002-6.

[33] A. Nyga, U. Cheema, M. Loizidou, 3D tumour models: novel in vitro approaches to cancer studies, J Cell Commun Signal 5(3) **2011** 239-48.

[34] D. Ansari, M. Carvajo, M. Bauden, R. Andersson, Pancreatic cancer stroma: controversies and current insights, Scand J Gastroenterol 52(6-7) **2017** 641-646.

[35] J.G. Moffat, J. Rudolph, D. Bailey, Phenotypic screening in cancer drug discovery - past, present and future, Nat Rev Drug Discov 13(8) **2014** 588-602.

[36] H.Y. Jung, L. Fattet, J. Yang, Molecular pathways: linking tumor microenvironment to epithelial-mesenchymal transition in metastasis, Clin Cancer Res 21(5) **2015** 962-968.

[37] Y.A. DeClerck, Desmoplasia: a response or a niche?, Cancer Discov 2(9) **2012** 772-4.

[38] H. Saini, K. Rahmani Eliato, C. Silva, M. Allam, G. Mouneimne, R. Ros, M. Nikkhah, The Role of Desmoplasia and Stromal Fibroblasts on Anti-cancer Drug Resistance in a Microengineered Tumor Model, Cellular and Molecular Bioengineering 11(5) **2018** 419-433.

[39] H. Yang, K. Yu, X. Mu, X. Shi, Y. Wei, Y. Guo, H.J. Qi, A molecular dynamics study of bond exchange reactions in covalent adaptable networks, Soft Matter 11(31) **2015** 6305-17.

[40] R. Malik, P.I. Lelkes, E. Cukierman, Biomechanical and biochemical remodeling of stromal extracellular matrix in cancer, Trends Biotechnol 33(4) **2015** 230-6.

[41] L.K. Chim, A.G. Mikos, Biomechanical forces in tissue engineered tumor models, Curr Opin Biomed Eng 6**2018** 42-50.

[42] A. Santi, F.G. Kugeratski, S. Zanivan, Cancer Associated Fibroblasts: The Architects of Stroma Remodeling, Proteomics 18(5-6) **2018** e1700167.

[43] M. Javle, T. Golan, A. Maitra, Changing the course of pancreatic cancer--Focus on recent translational advances, Cancer Treat Rev 44**2016** 17-25.

[44] A. Malandrino, M. Mak, R.D. Kamm, E. Moeendarbary, Complex mechanics of the heterogeneous extracellular matrix in cancer, Extreme Mech Lett 21**2018** 25-34.

[45] F. Kai, A.P. Drain, V.M. Weaver, The Extracellular Matrix Modulates the Metastatic Journey, Dev Cell 49(3) **2019** 332-346.

[46] R.R. Bynigeri, A. Jakkampudi, R. Jangala, C. Subramanyam, M. Sasikala, G.V. Rao, D.N. Reddy, R. Talukdar, Pancreatic stellate cell: Pandora's box for pancreatic disease biology, World J Gastroenterol 23(3) **2017** 382-405.

[47] J. Haqq, L.M. Howells, G. Garcea, M.S. Metcalfe, W.P. Steward, A.R. Dennison, Pancreatic stellate cells and pancreas cancer: current perspectives and future strategies, Eur J Cancer 50(15) **2014** 2570-82.

[48] S. Hamada, A. Masamune, T. Takikawa, N. Suzuki, K. Kikuta, M. Hirota, H. Hamada, M. Kobune, K. Satoh, T. Shimosegawa, Pancreatic stellate cells enhance stem cell-like phenotypes in pancreatic cancer cells, Biochem Biophys Res Commun 421(2) **2012** 349-54.

[49] T.C.Y. Pang, J.S. Wilson, M.V. Apte, Pancreatic stellate cells: what's new?, Curr Opin Gastroenterol 33(5) **2017** 366-373.

[50] N. Gagliano, G. Celesti, L. Tacchini, S. Pluchino, C. Sforza, M. Rasile, V. Valerio, L. Laghi, V. Conte, P. Procacci, Epithelial-to-mesenchymal transition in pancreatic ductal adenocarcinoma: Characterization in a 3D-cell culture model, World J Gastroenterol 22(18) **2016** 4466-83.

[51] I. Roy, K.A. Boyle, E.P. Vonderhaar, N.P. Zimmerman, E. Gorse, A.C. Mackinnon, R.F. Hwang, J. Franco-Barraza, E. Cukierman, S. Tsai, D.B. Evans, M.B. Dwinell, Cancer cell chemokines direct chemotaxis of activated stellate cells in pancreatic ductal adenocarcinoma, Lab Invest 97(3) **2017** 302-317.

[52] M. Erkan, C. Reiser-Erkan, C.W. Michalski, S. Deucker, D. Sauliunaite, S. Streit, I. Esposito, H. Friess, J. Kleeff, Cancer-stellate cell interactions perpetuate the hypoxia-fibrosis cycle in pancreatic ductal adenocarcinoma, Neoplasia 11(5) **2009** 497-508.

[53] Y. Fu, S. Liu, S. Zeng, H. Shen, The critical roles of activated stellate cells-mediated paracrine signaling, metabolism and onco-immunology in pancreatic ductal adenocarcinoma, Mol Cancer 17(1) **2018** 62.

[54] M. Sada, K. Ohuchida, K. Horioka, T. Okumura, T. Moriyama, Y. Miyasaka, T. Ohtsuka, K. Mizumoto, Y. Oda, M. Nakamura, Hypoxic stellate cells of pancreatic cancer stroma regulate extracellular matrix fiber organization and cancer cell motility, Cancer Lett 372(2) **2016** 210-8.

[55] H. Habisch, S. Zhou, M. Siech, M.G. Bachem, Interaction of stellate cells with pancreatic carcinoma cells, Cancers (Basel) 2(3) **2010** 1661-82.

[56] S.P. Pothula, Z. Xu, D. Goldstein, R.C. Pirola, J.S. Wilson, M.V. Apte, Key role of pancreatic stellate cells in pancreatic cancer, Cancer Lett 381(1) **2016** 194-200.

[57] B.K. Robinson, E. Cortes, A.J. Rice, M. Sarper, A. Del Rio Hernandez, Quantitative analysis of 3D extracellular matrix remodelling by pancreatic stellate cells, Biol Open 5(6) **2016** 875-82.

[58] D. Lachowski, E. Cortes, D. Pink, A. Chronopoulos, S.A. Karim, P.M. J, A.E. Del Rio Hernandez, Substrate Rigidity Controls Activation and Durotaxis in Pancreatic Stellate Cells, Sci Rep 7(1) **2017** 2506.

[59] M. Weniger, K.C. Honselmann, A.S. Liss, The Extracellular Matrix and Pancreatic Cancer: A Complex Relationship, Cancers (Basel) 10(9) **2018**.

[60] A. Begum, T. Ewachiw, C. Jung, A. Huang, K.J. Norberg, L. Marchionni, R. McMillan, V. Penchev, N.V. Rajeshkumar, A. Maitra, L. Wood, C. Wang, C. Wolfgang, A. DeJesus-Acosta, D. Laheru, I.M. Shapiro, M. Padval, J.A. Pachter, D.T. Weaver, Z.A. Rasheed, W. Matsui, The extracellular matrix and focal adhesion kinase signaling regulate cancer stem cell function in pancreatic ductal adenocarcinoma, PLoS One 12(7) **2017** e0180181.

[61] N. Sato, X.B. Cheng, S. Kohi, A. Koga, K. Hirata, Targeting hyaluronan for the treatment of pancreatic ductal adenocarcinoma, Acta Pharm Sin B 6(2) **2016** 101-5.

[62] A.D. Doyle, N. Carvajal, A. Jin, K. Matsumoto, K.M. Yamada, Local 3D matrix microenvironment regulates cell migration through spatiotemporal dynamics of contractility-dependent adhesions, Nat Commun 6**2015** 8720.

[63] S.P. Carey, Z.E. Goldblatt, K.E. Martin, B. Romero, R.M. Williams, C.A. Reinhart-King, Local extracellular matrix alignment directs cellular protrusion dynamics and migration through Rac1 and FAK, Integr Biol (Camb) 8(8) **2016** 821-35.

[64] P. Yeung, H.S. Sin, S. Chan, G.C. Chan, B.P. Chan, Microencapsulation of Neuroblastoma Cells and Mesenchymal Stromal Cells in Collagen Microspheres: A 3D Model for Cancer Cell Niche Study, PLoS One 10(12) **2015** e0144139.

[65] L. Schaefer, D.P. Reinhardt, Special issue: Extracellular matrix: Therapeutic tools and targets in cancer treatment, Adv Drug Deliv Rev 97**2016** 1-3.

[66] A. Dongre, R.A. Weinberg, New insights into the mechanisms of epithelial-mesenchymal transition and implications for cancer, Nat Rev Mol Cell Biol 20(2) **2019** 69-84.

[67] A.C. Brown, V.F. Fiore, T.A. Sulchek, T.H. Barker, Physical and chemical microenvironmental cues orthogonally control the degree and duration of fibrosis-associated epithelial-to-mesenchymal transitions, J Pathol 229(1) **2013** 25-35.

[68] E. Giannoni, F. Bianchini, L. Masieri, S. Serni, E. Torre, L. Calorini, P. Chiarugi, Reciprocal activation of prostate cancer cells and cancer-associated fibroblasts stimulates epithelial-mesenchymal transition and cancer stemness, Cancer Res 70(17) **2010** 6945-56.

[69] B.N. Smith, N.A. Bhowmick, Role of EMT in Metastasis and Therapy Resistance, J Clin Med 5(2) **2016**.

[70] S.S. Sikandar, A.H. Kuo, T. Kalisky, S. Cai, M. Zabala, R.W. Hsieh, N.A. Lobo, F.A. Scheeren, S. Sim, D. Qian, F.M. Dirbas, G. Somlo, S.R. Quake, M.F. Clarke, Role of epithelial to mesenchymal transition associated genes in mammary gland regeneration and breast tumorigenesis, Nat Commun 8(1) **2017** 1669.

[71] J.H. Park, J.E. Shin, H.W. Park, The Role of Hippo Pathway in Cancer Stem Cell Biology, Mol Cells 41(2) **2018** 83-92.

[72] J.A. Castellanos, N.B. Merchant, N.S. Nagathihalli, Emerging targets in pancreatic cancer: epithelial-mesenchymal transition and cancer stem cells, Onco Targets Ther 6**2013** 1261-7.

[73] N. Gaianigo, D. Melisi, C. Carbone, EMT and Treatment Resistance in Pancreatic Cancer, Cancers (Basel) 9(9) **2017**.

[74] T. Brabletz, R. Kalluri, M.A. Nieto, R.A. Weinberg, EMT in cancer, Nat Rev Cancer 18(2) **2018** 128-134.

[75] J.Y. Shih, P.C. Yang, The EMT regulator slug and lung carcinogenesis, Carcinogenesis 32(9) **2011** 1299-304.

[76] I. Pastushenko, C. Blanpain, EMT Transition States during Tumor Progression and Metastasis, Trends Cell Biol 29(3) **2019** 212-226.

[77] P.P. Provenzano, S.R. Hingorani, Hyaluronan, fluid pressure, and stromal resistance in pancreas cancer, Br J Cancer 108(1) **2013** 1-8.

[78] K.S. Rankin, D. Frankel, Hyaluronan in cancer - from the naked mole rat to nanoparticle therapy, Soft Matter 12(17) **2016** 3841-8.

[79] R.K. Sironen, M. Tammi, R. Tammi, P.K. Auvinen, M. Anttila, V.M. Kosma, Hyaluronan in human malignancies, Exp Cell Res 317(4) **2011** 383-91.

[80] B.P. Toole, Hyaluronan-CD44 Interactions in Cancer: Paradoxes and Possibilities, Clin Cancer Res 15(24) **2009** 7462-7468.

[81] K.L. Schwertfeger, M.K. Cowman, P.G. Telmer, E.A. Turley, J.B. McCarthy, Hyaluronan, Inflammation, and Breast Cancer Progression, Front Immunol 6**2015** 236.

[82] B.P. Toole, M.G. Slomiany, Hyaluronan: a constitutive regulator of chemoresistance and malignancy in cancer cells, Semin Cancer Biol 18(4) **2008** 244-50.

[83] T. Chanmee, P. Ontong, N. Itano, Hyaluronan: A modulator of the tumor microenvironment, Cancer Lett 375(1) **2016** 20-30.

[84] B.P. Toole, Hyaluronan: from extracellular glue to pericellular cue, Nat Rev Cancer 4(7) **2004** 528-39.

[85] Y.I. Shen, H.E. Abaci, Y. Krupsi, L.C. Weng, J.A. Burdick, S. Gerecht, Hyaluronic acid hydrogel stiffness and oxygen tension affect cancer cell fate and endothelial sprouting, Biomater Sci 2(5) **2014** 655-665.

[86] F. Rehfeldt, A.E. Brown, M. Raab, S. Cai, A.L. Zajac, A. Zemel, D.E. Discher, Hyaluronic acid matrices show matrix stiffness in 2D and 3D dictates cytoskeletal order and myosin-II phosphorylation within stem cells, Integr Biol (Camb) 4(4) **2012** 422-30.

[87] G.D. Prestwich, Hyaluronic acid-based clinical biomaterials derived for cell and molecule delivery in regenerative medicine, J Control Release 155(2) **2011** 193-9.

[88] A. Chopra, M.E. Murray, F.J. Byfield, M.G. Mendez, R. Halleluyan, D.J. Restle, D. Raz-Ben Aroush, P.A. Galie, K. Pogoda, R. Bucki, C. Marcinkiewicz, G.D. Prestwich, T.I. Zarembinski, C.S. Chen, E. Pure, J.Y. Kresh, P.A. Janmey, Augmentation of integrin-mediated mechanotransduction by hyaluronic acid, Biomaterials 35(1) **2014** 71-82.

[89] Y. Ma, R.F. Hwang, C.D. Logsdon, S.E. Ullrich, Dynamic mast cell-stromal cell interactions promote growth of pancreatic cancer, Cancer Res 73(13) **2013** 3927-37.

[90] V.L. Veenstra, A. Garcia-Garijo, H.W. van Laarhoven, M.F. Bijlsma, Extracellular Influences: Molecular Subclasses and the Microenvironment in Pancreatic Cancer, Cancers (Basel) 10(2) **2018**.

[91] X. Gong, C. Lin, J. Cheng, J. Su, H. Zhao, T. Liu, X. Wen, P. Zhao, Generation of Multicellular Tumor Spheroids with Microwell-Based Agarose Scaffolds for Drug Testing, PLoS One 10(6) **2015** e0130348.

[92] C. Voutouri, C. Polydorou, P. Papageorgis, V. Gkretsi, T. Stylianopoulos, Hyaluronan-Derived Swelling of Solid Tumors, the Contribution of Collagen and Cancer Cells, and Implications for Cancer Therapy, Neoplasia 18(12) **2016** 732-741.

[93] C.C. Lin, M. Korc, Designer hydrogels: Shedding light on the physical chemistry of the pancreatic cancer microenvironment, Cancer Lett 436**2018** 22-27.

[94] J. Cha, S.G. Kang, P. Kim, Strategies of Mesenchymal Invasion of Patient-derived Brain Tumors: Microenvironmental Adaptation, Sci Rep 6(1) **2016** 24912.

[95] H. Mohammadi, E. Sahai, Mechanisms and impact of altered tumour mechanics, Nat Cell Biol 20(7) **2018** 766-774.

[96] R.S. Stowers, S.C. Allen, L.J. Suggs, Dynamic phototuning of 3D hydrogel stiffness, Proc Natl Acad Sci U S A 112(7) **2015** 1953-8.

[97] L. Fu, A. Haage, N. Kong, G. Tanentzapf, H. Li, Dynamic protein hydrogels with reversibly tunable stiffness regulate human lung fibroblast spreading reversibly, Chem Commun (Camb) 55(36) **2019** 5235-5238.

[98] L. Przybyla, J.M. Muncie, V.M. Weaver, Mechanical Control of Epithelial-to-Mesenchymal Transitions in Development and Cancer, Annu Rev Cell Dev Biol 32**2016** 527-554.

[99] J.D. Humphrey, E.R. Dufresne, M.A. Schwartz, Mechanotransduction and extracellular matrix homeostasis, Nat Rev Mol Cell Biol 15(12) **2014** 802-12.

[100] S.E. Chung, Y. Jung, S. Kwon, Three-dimensional fluidic self-assembly by axis translation of two-dimensionally fabricated microcomponents in railed microfluidics, Small 7(6) **2011** 796-803.

[101] K.M. Mabry, R.L. Lawrence, K.S. Anseth, Dynamic stiffening of poly(ethylene glycol)-based hydrogels to direct valvular interstitial cell phenotype in a three-dimensional environment, Biomaterials 49**2015** 47-56.

[102] K. Stock, M.F. Estrada, S. Vidic, K. Gjerde, A. Rudisch, V.E. Santo, M. Barbier, S. Blom, S.C. Arundkar, I. Selvam, A. Osswald, Y. Stein, S. Gruenewald, C. Brito, W. van Weerden, V. Rotter, E. Boghaert, M. Oren, W. Sommergruber, Y. Chong, R. de Hoogt, R. Graeser, Capturing tumor complexity in vitro: Comparative analysis of 2D and 3D tumor models for drug discovery, Sci Rep 6**2016** 28951.

[103] J. Iovanna, M.C. Mallmann, A. Goncalves, O. Turrini, J.C. Dagorn, Current knowledge on pancreatic cancer, Front Oncol 2**2012** 6.

[104] S. Suklabaidya, P. Dash, B. Das, V. Suresh, P.K. Sasmal, S. Senapati, Experimental models of pancreatic cancer desmoplasia, Lab Invest 98(1) **2018** 27-40.

[105] T. Voskoglou-Nomikos, J.L. Pater, L. Seymour, Clinical predictive value of the in vitro cell line, human xenograft, and mouse allograft preclinical cancer models, Clin Cancer Res 9(11) **2003** 4227-39.

[106] D. Mahadevan, D.D. Von Hoff, Tumor-stroma interactions in pancreatic ductal adenocarcinoma, Mol Cancer Ther 6(4) **2007** 1186-97.

[107] E.L. Fong, X. Wan, J. Yang, M. Morgado, A.G. Mikos, D.A. Harrington, N.M. Navone, M.C. Farach-Carson, A 3D in vitro model of patient-derived prostate cancer xenograft for controlled interrogation of in vivo tumor-stromal interactions, Biomaterials 77**2016** 164-72.

[108] D.M. van Marion, U.M. Domanska, H. Timmer-Bosscha, A.M. Walenkamp, Studying cancer metastasis: Existing models, challenges and future perspectives, Crit Rev Oncol Hematol 97**2016** 107-17.

[109] S.J. Bidarra, P. Oliveira, S. Rocha, D.P. Saraiva, C. Oliveira, C.C. Barrias, A 3D in vitro model to explore the inter-conversion between epithelial and mesenchymal states during EMT and its reversion, Sci Rep 6**2016** 27072.

[110] V. Brancato, A. Garziano, F. Gioiella, F. Urciuolo, G. Imparato, V. Panzetta, S. Fusco, P.A. Netti, 3D is not enough: Building up a cell instructive microenvironment for tumoral stroma microtissues, Acta Biomater 47**2017** 1-13.

[111] P.S. Thakuri, C. Liu, G.D. Luker, H. Tavana, Biomaterials-Based Approaches to Tumor Spheroid and Organoid Modeling, Adv Healthc Mater 7(6) **2018** e1700980.

[112] T. Rodrigues, B. Kundu, J. Silva-Correia, S.C. Kundu, J.M. Oliveira, R.L. Reis, V.M. Correlo, Emerging tumor spheroids technologies for 3D in vitro cancer modeling, Pharmacol Ther 184**2018** 201-211.

[113] S.L. Ham, R. Joshi, G.D. Luker, H. Tavana, Engineered Breast Cancer Cell Spheroids Reproduce Biologic Properties of Solid Tumors, Adv Healthc Mater 5(21) **2016** 2788-2798.

[114] X. Xu, L.A. Gurski, C. Zhang, D.A. Harrington, M.C. Farach-Carson, X. Jia, Recreating the tumor microenvironment in a bilayer, hyaluronic acid hydrogel construct for the growth of prostate cancer spheroids, Biomaterials 33(35) **2012** 9049-60.

[115] X. Yue, T.D. Nguyen, V. Zellmer, S. Zhang, P. Zorlutuna, Stromal cell-laden 3D hydrogel microwell arrays as tumor microenvironment model for studying stiffness dependent stromal cell-cancer interactions, Biomaterials 170**2018** 37-48.

[116] T.R. Hoare, D.S. Kohane, Hydrogels in drug delivery: Progress and challenges, Polymer 49(8) **2008** 1993-2007.

[117] T. Hoare, R. Pelton, Impact of microgel morphology on functionalized microgel-drug interactions, Langmuir 24(3) **2008** 1005-12.

[118] M. Guvendiren, J.A. Burdick, Stiffening hydrogels to probe short- and long-term cellular responses to dynamic mechanics, Nat Commun 3**2012** 792.

[119] C.M. Kirschner, K.S. Anseth, Hydrogels in Healthcare: From Static to Dynamic Material Microenvironments, Acta Mater 61(3) **2013** 931-944.

[120] J.H. Bae, J.M. Lee, B.G. Chung, Hydrogel-encapsulated 3D microwell array for neuronal differentiation, Biomed Mater 11(1) **2016** 015019.

[121] C.L. McGann, R.E. Dumm, A.K. Jurusik, I. Sidhu, K.L. Kiick, Thiol-ene Photocrosslinking of Cytocompatible Resilin-Like Polypeptide-PEG Hydrogels, Macromol Biosci 16(1) **2016** 129-38.

[122] C.C. Lin, A.T. Metters, Hydrogels in controlled release formulations: network design and mathematical modeling, Adv Drug Deliv Rev 58(12-13) **2006** 1379-408.

[123] G. Cirillo, O. Vittorio, S. Hampel, U.G. Spizzirri, N. Picci, F. Iemma, Incorporation of carbon nanotubes into a gelatin-catechin conjugate: innovative approach for the preparation of anticancer materials, Int J Pharm 446(1-2) **2013** 176-82.

[124] M.F. Estrada, S.P. Rebelo, E.J. Davies, M.T. Pinto, H. Pereira, V.E. Santo, M.J. Smalley, S.T. Barry, E.J. Gualda, P.M. Alves, E. Anderson, C. Brito, Modelling the tumour microenvironment in long-term microencapsulated 3D co-cultures recapitulates phenotypic features of disease progression, Biomaterials 78**2016** 50-61.

[125] K.A. Kyburz, K.S. Anseth, Three-dimensional hMSC motility within peptide-functionalized PEG-based hydrogels of varying adhesivity and crosslinking density, Acta Biomater 9(5) **2013** 6381-92.

[126] S.A. Fisher, P.N. Anandakumaran, S.C. Owen, M.S. Shoichet, Tuning the Microenvironment: Click-Crosslinked Hyaluronic Acid-Based Hydrogels Provide a Platform for Studying Breast Cancer Cell Invasion, Advanced Functional Materials 25(46) **2015** 7163-7172.

[127] R.G. Mannino, A.N. Santiago-Miranda, P. Pradhan, Y. Qiu, J.C. Mejias, S.S. Neelapu, K. Roy, W.A. Lam, 3D microvascular model recapitulates the diffuse large B-cell lymphoma tumor microenvironment in vitro, Lab Chip 17(3) **2017** 407-414.

[128] M.N. Mason, A.T. Metters, C.N. Bowman, K.S. Anseth, Predicting Controlled-Release Behavior of Degradable PLA-b-PEG-b-PLA Hydrogels, Macromolecules 34(13) **2001** 4630-4635.

[129] A.A. Aimetti, A.J. Machen, K.S. Anseth, Poly(ethylene glycol) hydrogels formed by thiol-ene photopolymerization for enzyme-responsive protein delivery, Biomaterials 30(30) **2009** 6048-54.

[130] A. Borrmann, O. Fatunsin, J. Dommerholt, A.M. Jonker, D.W. Lowik, J.C. van Hest, F.L. van Delft, Strain-promoted oxidation-controlled cyclooctyne-1,2-quinone cycloaddition (SPOCQ) for fast and activatable protein conjugation, Bioconjug Chem 26(2) **2015** 257-61.

[131] M. Singh, S. Mukundan, M. Jaramillo, S. Oesterreich, S. Sant, Three-Dimensional Breast Cancer Models Mimic Hallmarks of Size-Induced Tumor Progression, Cancer Res 76(13) **2016** 3732-43.

[132] S.M. Hodgson, S.A. McNelles, L. Abdullahu, I.A. Marozas, K.S. Anseth, A. Adronov, Reproducible Dendronized PEG Hydrogels via SPAAC Cross-Linking, Biomacromolecules 18(12) **2017** 4054-4059.

[133] J. Carthew, J.E. Frith, J.S. Forsythe, V.X. Truong, Polyethylene glycol–gelatin hydrogels with tuneable stiffness prepared by horseradish peroxidase-activated tetrazine–norbornene ligation, Journal of Materials Chemistry B 6(9) **2018** 1394-1401.

[134] R.G. Wells, The role of matrix stiffness in regulating cell behavior, Hepatology 47(4) **2008** 1394-400.

[135] S.C. Wei, L. Fattet, J.H. Tsai, Y. Guo, V.H. Pai, H.E. Majeski, A.C. Chen, R.L. Sah, S.S. Taylor, A.J. Engler, J. Yang, Matrix stiffness drives epithelial-mesenchymal transition and tumour metastasis through a TWIST1-G3BP2 mechanotransduction pathway, Nat Cell Biol 17(5) **2015** 678-88.

[136] J.S. McLane, L.A. Ligon, Stiffened Extracellular Matrix and Signaling from Stromal Fibroblasts via Osteoprotegerin Regulate Tumor Cell Invasion in a 3-D Tumor in Situ Model, Cancer Microenviron 9(2-3) **2016** 127-139.

[137] J.M. Barnes, L. Przybyla, V.M. Weaver, Tissue mechanics regulate brain development, homeostasis and disease, J Cell Sci 130(1) **2017** 71-82.

[138] J.L. Young, A.J. Engler, Hydrogels with time-dependent material properties enhance cardiomyocyte differentiation in vitro, Biomaterials 32(4) **2011** 1002-9.

[139] T. Chen, H.D. Embree, L.Q. Wu, G.F. Payne, In vitro protein-polysaccharide conjugation: tyrosinase-catalyzed conjugation of gelatin and chitosan, Biopolymers 64(6) **2002** 292-302.

[140] N. Dadoo, W.M. Gramlich, Spatiotemporal Modification of Stimuli-Responsive Hyaluronic Acid/Poly(N-isopropylacrylamide) Hydrogels, ACS Biomaterials Science & Engineering 2(8) **2016** 1341-1350.

[141] K.M. Rao, K. Rao, C.S. Ha, Stimuli Responsive Poly(Vinyl Caprolactam) Gels for Biomedical Applications, Gels 2(1) **2016**.

[142] G.R. Deen, X.J. Loh, Stimuli-Responsive Cationic Hydrogels in Drug Delivery Applications, Gels 4(1) **2018**.

[143] N. Falcone, H.B. Kraatz, Supramolecular Assembly of Peptide and Metallopeptide Gelators and Their Stimuli-Responsive Properties in Biomedical Applications, Chemistry 24(54) **2018** 14316-14328.

[144] J.F. Mano, Stimuli-Responsive Polymeric Systems for Biomedical Applications, Advanced Engineering Materials 10(6) **2008** 515-527.

[145] J. Hoque, N. Sangaj, S. Varghese, Stimuli-Responsive Supramolecular Hydrogels and Their Applications in Regenerative Medicine, Macromol Biosci 19(1) **2019** e1800259.

[146] K. Vats, D.S.W. Benoit, Dynamic Manipulation of Hydrogels to Control Cell Behavior: A Review, Tissue Engineering Part B: Reviews 19(6) **2013** 455-469.

[147] L.C. Bahlmann, A. Fokina, M.S. Shoichet, Dynamic bioengineered hydrogels as scaffolds for advanced stem cell and organoid culture, MRS Communications 7**2017**.

[148] M. Romero-Lopez, A.L. Trinh, A. Sobrino, M.M. Hatch, M.T. Keating, C. Fimbres, D.E. Lewis, P.D. Gershon, E.L. Botvinick, M. Digman, J.S. Lowengrub, C.C. Hughes, Recapitulating the human tumor microenvironment: Colon tumor-derived extracellular matrix promotes angiogenesis and tumor cell growth, Biomaterials 116**2017** 118-129.

[149] X. Wu, W. Huang, W.-H. Wu, B. Xue, D. Xiang, Y. Li, M. Qin, F. Sun, W. Wang, W.-B. Zhang, Y. Cao, Reversible hydrogels with tunable mechanical properties for optically controlling cell migration, Nano Research 11(10) **2018** 5556-5565.

[150] Y.C. Yeh, E.A. Corbin, S.R. Caliari, L. Ouyang, S.L. Vega, R. Truitt, L. Han, K.B. Margulies, J.A. Burdick, Mechanically dynamic PDMS substrates to investigate changing cell environments, Biomaterials 145**2017** 23-32.

[151] T. Yuan, J. Fei, Y. Xu, X. Yang, J. Li, Stimuli-Responsive Dipeptide-Protein Hydrogels through Schiff Base Coassembly, Macromol Rapid Commun 38(20) **2017** 1700408.

[152] Z. Zheng, J. Hu, H. Wang, J. Huang, Y. Yu, Q. Zhang, Y. Cheng, Dynamic Softening or Stiffening a Supramolecular Hydrogel by Ultraviolet or Near-Infrared Light, ACS Appl Mater Interfaces 9(29) **2017** 24511-24517.

[153] R. Yang, H. Liang, Dynamic electro-regulation of the stiffness gradient hydrogels, RSC Advances 8(12) **2018** 6675-6679.

[154] Z.Q. Cao, G.J. Wang, Multi-Stimuli-Responsive Polymer Materials: Particles, Films, and Bulk Gels, Chem Rec 16(3) **2016** 1398-435.

[155] M.H. Joyce, S. Allen, L. Suggs, A. Brock, Novel Nanomaterials Enable Biomimetic Models of the Tumor Microenvironment, Journal of Nanotechnology 2017**2017** 1-8.

[156] O.Y. Wouters, D.T. Ploeger, S.M. van Putten, R.A. Bank, 3,4-Dihydroxy-L-Phenylalanine as a Novel Covalent Linker of Extracellular Matrix Proteins to Polyacrylamide Hydrogels with a Tunable Stiffness, Tissue Eng Part C Methods 22(2) **2016** 91-101.

[157] R. Bodvik, L. Karlson, K. Edwards, J. Eriksson, E. Thormann, P.M. Claesson, Aggregation of modified celluloses in aqueous solution: transition from methylcellulose to hydroxypropylmethylcellulose solution properties induced by a low-molecular-weight oxyethylene additive, Langmuir 28(38) **2012** 13562-9.

[158] K. Uto, T. Aoyagi, C.A. DeForest, M. Ebara, Dynamic alterations of hepatocellular function by on-demand elasticity and roughness modulation, Biomater Sci 6(5) **2018** 1002-1006.

[159] J.D. Tang, S.R. Caliari, K.J. Lampe, Temperature-Dependent Complex Coacervation of Engineered Elastin-like Polypeptide and Hyaluronic Acid Polyelectrolytes, Biomacromolecules 19(10) **2018** 3925-3935.

[160] K. Uto, M. Ebara, T. Aoyagi, Temperature-responsive poly(epsilon-caprolactone) cell culture platform with dynamically tunable nano-roughness and elasticity for control of myoblast morphology, Int J Mol Sci 15(1) **2014** 1511-24.

[161] L. Wu, A. Magaz, A. Darbyshire, A. Howkins, A. Reynolds, I.W. Boyd, H. Song, J.H. Song, M. Loizidou, M. Emberton, M. Birchall, W. Song, Thermoresponsive Stiffness Softening of Hierarchically Porous Nanohybrid Membranes Promotes Niches for Mesenchymal Stem Cell Differentiation, Adv Healthc Mater 8(10) **2019** e1801556.

[162] A.A. Abdeen, J. Lee, N.A. Bharadwaj, R.H. Ewoldt, K.A. Kilian, Temporal Modulation of Stem Cell Activity Using Magnetoactive Hydrogels, Adv Healthc Mater 5(19) **2016** 2536-2544.

[163] D.E. Apostolides, T. Sakai, C.S. Patrickios, Dynamic Covalent Star Poly(ethylene glycol) Model Hydrogels: A New Platform for Mechanically Robust, Multifunctional Materials, Macromolecules 50(5) **2017** 2155-2164.

[164] M.W. Tibbitt, K.S. Anseth, Dynamic microenvironments: the fourth dimension, Sci Transl Med 4(160) **2012** 160ps24.

[165] H.Y. Liu, H.D. Nguyen, C.C. Lin, Dynamic PEG-Peptide Hydrogels via Visible Light and FMN-Induced Tyrosine Dimerization, Adv Healthc Mater 7(22) **2018** e1800954.

[166] H.Y. Liu, M. Korc, C.C. Lin, Biomimetic and enzyme-responsive dynamic hydrogels for studying cell-matrix interactions in pancreatic ductal adenocarcinoma, Biomaterials 160**2018** 24-36.

[167] K. Vats, D.S. Benoit, Dynamic manipulation of hydrogels to control cell behavior: a review, Tissue Eng Part B Rev 19(6) **2013** 455-69.

[168] K.S. Straley, S.C. Heilshorn, Dynamic, 3D-Pattern Formation Within Enzyme-Responsive Hydrogels, Advanced Materials 21(41) **2009** 4148-4152.

[169] L.S. Teixeira, J. Feijen, C.A. van Blitterswijk, P.J. Dijkstra, M. Karperien, Enzyme-catalyzed crosslinkable hydrogels: emerging strategies for tissue engineering, Biomaterials 33(5) **2012** 1281-90.

[170] P.A. Parmar, S.C. Skaalure, L.W. Chow, J.P. St-Pierre, V. Stoichevska, Y.Y. Peng, J.A. Werkmeister, J.A. Ramshaw, M.M. Stevens, Temporally degradable collagen-mimetic hydrogels tuned to chondrogenesis of human mesenchymal stem cells, Biomaterials 99**2016** 56-71.

[171] M. Reihmann, H. Ritter, Enzyme-Catalyzed Synthesis of Polymers, Enzyme-Catalyzed Synthesis of Polymers 194**2006** 1-49.

[172] O.B. Ayyub, P. Kofinas, Enzyme Induced Stiffening of Nanoparticle-Hydrogel Composites with Structural Color, ACS Nano 9(8) **2015** 8004-11.

[173] G.M. Guebitz, G.S. Nyanhongo, Enzymes as Green Catalysts and Interactive Biomolecules in Wound Dressing Hydrogels, Trends Biotechnol 36(10) **2018** 1040-1053.

[174] S. Shoda, H. Uyama, J. Kadokawa, S. Kimura, S. Kobayashi, Enzymes as Green Catalysts for Precision Macromolecular Synthesis, Chem Rev 116(4) **2016** 2307-413.

[175] X. Wang, S. Chen, D. Wu, Q. Wu, Q. Wei, B. He, Q. Lu, Q. Wang, Oxidoreductase-Initiated Radical Polymerizations to Design Hydrogels and Micro/Nanogels: Mechanism, Molding, and Applications, Adv Mater 30(17) **2018** e1705668.

[176] F. Lee, J.E. Chung, M. Kurisawa, An injectable enzymatically crosslinked hyaluronic acid–tyramine hydrogel system with independent tuning of mechanical strength and gelation rate, Soft Matter 4(4) **2008** 880-887.

[177] B.Y. Kim, Y. Lee, J.Y. Son, K.M. Park, K.D. Park, Dual Enzyme-Triggered In Situ Crosslinkable Gelatin Hydrogels for Artificial Cellular Microenvironments, Macromol Biosci 16(11) **2016** 1570-1576.

[178] P. Le Thi, Y. Lee, D.H. Nguyen, K.D. Park, In situ forming gelatin hydrogels by dual-enzymatic cross-linking for enhanced tissue adhesiveness, Journal of Materials Chemistry B 5(4) **2017** 757-764.

[179] S. Sakai, T. Ashida, S. Ogino, M. Taya, Horseradish peroxidase-mediated encapsulation of mammalian cells in hydrogel particles by dropping, J Microencapsul 31(1) **2014** 100-4.

[180] K. Xu, K. Narayanan, F. Lee, K.H. Bae, S. Gao, M. Kurisawa, Enzyme-mediated hyaluronic acid-tyramine hydrogels for the propagation of human embryonic stem cells in 3D, Acta Biomater 24**2015** 159-71.

[181] J.J. Roberts, P. Naudiyal, K.S. Lim, L.A. Poole-Warren, P.J. Martens, A comparative study of enzyme initiators for crosslinking phenol-functionalized hydrogels for cell encapsulation, Biomater Res 20**2016** 30.

[182] M. Khanmohammadi, S. Sakai, M. Taya, Impact of immobilizing of low molecular weight hyaluronic acid within gelatin-based hydrogel through enzymatic reaction on behavior of enclosed endothelial cells, Int J Biol Macromol 97**2017** 308-316.

[183] M. Khanmohammadi, M.B. Dastjerdi, A. Ai, A. Ahmadi, A. Godarzi, A. Rahimi, J. Ai, Horseradish peroxidase-catalyzed hydrogelation for biomedical applications, Biomater Sci 6(6) **2018** 1286-1298.

[184] S. Jus, I. Stachel, W. Schloegl, M. Pretzler, W. Friess, M. Meyer, R. Birner-Gruenberger, G.M. Guebitz, Cross-linking of collagen with laccases and tyrosinases, Materials Science and Engineering: C 31(5) **2011** 1068-1077.

[185] Y. Lee, K.M. Park, J.W. Bae, K.D. Park, Facile surface PEGylation via tyrosinase-catalyzed oxidative reaction for the preparation of non-fouling surfaces, Colloids Surf B Biointerfaces 102**2013** 585-9.

[186] S.H. Kim, Y.H. An, H.D. Kim, K. Kim, S.H. Lee, H.G. Yim, B.G. Kim, N.S. Hwang, Enzyme-mediated tissue adhesive hydrogels for meniscus repair, Int J Biol Macromol 110**2018** 479-487.

[187] V.J. Hearing, Jr., T.M. Ekel, P.M. Montague, J.M. Nicholson, Mammalin tyrosinase. Stoichiometry and measurement of reaction products, Biochim Biophys Acta 611(2) **1980** 251-68.

[188] J.C. Espin, R. Varon, L.G. Fenoll, M.A. Gilabert, P.A. Garcia-Ruiz, J. Tudela, F. Garcia-Canovas, Kinetic characterization of the substrate specificity and mechanism of mushroom tyrosinase, Eur J Biochem 267(5) **2000** 1270-9.

[189] K. Marumo, J.H. Waite, Optimization of hydroxylation of tyrosine and tyrosine-containing peptides by mushroom tyrosinase, Biochim Biophys Acta 872(1-2) **1986** 98-103.

[190] M.-C. Figueroa-Espinoza, M.-H. Morel, X. Rouau, Effect of Lysine, Tyrosine, Cysteine, and Glutathione on the Oxidative Cross-Linking of Feruloylated Arabinoxylans by a Fungal Laccase, Journal of Agricultural and Food Chemistry 46(7) **1998** 2583-2589.

[191] N. Tanaka, S. Murao, Difference between Various Copper-containing Enzymes (PolyporusLaccase, Mushroom Tyrosinase and Cucumber Ascorbate Oxidase) and Bilirubin Oxidase, Agricultural and Biological Chemistry 47(7) **2014** 1627-1628.

[192] S. Ba, V. Vinoth Kumar, Recent developments in the use of tyrosinase and laccase in environmental applications, Crit Rev Biotechnol 37(7) **2017** 819-832.

[193] K.J. Lewis, K.S. Anseth, Hydrogel scaffolds to study cell biology in four dimensions, MRS Bull 38(3) **2013** 260-268.

[194] Y. Li, E. Kumacheva, Hydrogel microenvironments for cancer spheroid growth and drug screening, Sci Adv 4(4) **2018** eaas8998.

[195] G. Choe, J. Park, H. Park, J.Y. Lee, Hydrogel Biomaterials for Stem Cell Microencapsulation, Polymers (Basel) 10(9) **2018** 997.

[196] M.C. Cushing, K.S. Anseth, Materials science. Hydrogel cell cultures, Science 316(5828) **2007** 1133-4.

[197] B. Trappmann, B.M. Baker, W.J. Polacheck, C.K. Choi, J.A. Burdick, C.S. Chen, Matrix degradability controls multicellularity of 3D cell migration, Nat Commun 8(1) **2017** 371.

[198] K. Wang, W. Wang, X. Wu, J. Xiao, Y. Liu, A. Liu, Effect of photochemical UV/riboflavin-mediated cross-links on different properties of fish gelatin films, Journal of Food Process Engineering 40(5) **2017**.

[199] T.E. Brown, J.S. Silver, B.T. Worrell, I.A. Marozas, F.M. Yavitt, K.A. Gunay, C.N. Bowman, K.S. Anseth, Secondary Photocrosslinking of Click Hydrogels To Probe Myoblast Mechanotransduction in Three Dimensions, J Am Chem Soc 140(37) **2018** 11585-11588.

[200] A. Cipitria, M. Salmeron-Sanchez, Mechanotransduction and Growth Factor Signalling to Engineer Cellular Microenvironments, Adv Healthc Mater 6(15) **2017**.

[201] K.S. Anseth, C.N. Bowman, L. Brannon-Peppas, Mechanical properties of hydrogels and their experimental determination, Biomaterials 17(17) **1996** 1647-1657.

[202] K.S. Anseth, C.N. Bowman, Kinetic Gelation model predictions of crosslinked polymer network microstructure, Chemical Engineering Science 49(14) **1994** 2207-2217.

[203] O. Chaudhuri, Viscoelastic hydrogels for 3D cell culture, Biomater Sci 5(8) **2017** 1480-1490.

[204] D. Caccavo, S. Cascone, G. Lamberti, A.A. Barba, Hydrogels: experimental characterization and mathematical modelling of their mechanical and diffusive behaviour, Chem Soc Rev 47(7) **2018** 2357-2373.

[205] A.M. Kloxin, C.J. Kloxin, C.N. Bowman, K.S. Anseth, Mechanical properties of cellularly responsive hydrogels and their experimental determination, Adv Mater 22(31) **2010** 3484-94.

[206] O. Chaudhuri, L. Gu, D. Klumpers, M. Darnell, S.A. Bencherif, J.C. Weaver, N. Huebsch, H.P. Lee, E. Lippens, G.N. Duda, D.J. Mooney, Hydrogels with tunable stress relaxation regulate stem cell fate and activity, Nat Mater 15(3) **2016** 326-34.

[207] H. Shih, C.C. Lin, Cross-linking and degradation of step-growth hydrogels formed by thiol-ene photoclick chemistry, Biomacromolecules 13(7) **2012** 2003-12.

[208] A.M. Kloxin, M.W. Tibbitt, A.M. Kasko, J.A. Fairbairn, K.S. Anseth, Tunable hydrogels for external manipulation of cellular microenvironments through controlled photodegradation, Adv Mater 22(1) **2010** 61-6.

[209] R.M. Schweller, J.L. West, Encoding Hydrogel Mechanics via Network Cross-Linking Structure, ACS Biomater Sci Eng 1(5) **2015** 335-344.

[210] H. Laklai, Y.A. Miroshnikova, M.W. Pickup, E.A. Collisson, G.E. Kim, A.S. Barrett, R.C. Hill, J.N. Lakins, D.D. Schlaepfer, J.K. Mouw, V.S. LeBleu, N. Roy, S.V. Novitskiy, J.S. Johansen, V. Poli, R. Kalluri, C.A. Iacobuzio-Donahue, L.D. Wood, M. Hebrok, K. Hansen, H.L. Moses, V.M. Weaver, Genotype tunes pancreatic ductal adenocarcinoma tissue tension to induce matricellular fibrosis and tumor progression, Nat Med 22(5) **2016** 497-505.

[211] F. Calvo, N. Ege, A. Grande-Garcia, S. Hooper, R.P. Jenkins, S.I. Chaudhry, K. Harrington, P. Williamson, E. Moeendarbary, G. Charras, E. Sahai, Mechanotransduction and YAP-dependent matrix remodelling is required for the generation and maintenance of cancer-associated fibroblasts, Nat Cell Biol 15(6) **2013** 637-46.

[212] J.A. Burdick, W.L. Murphy, Moving from static to dynamic complexity in hydrogel design, Nat Commun 3**2012** 1269.

[213] H.Y. Liu, T. Greene, T.Y. Lin, C.S. Dawes, M. Korc, C.C. Lin, Enzyme-mediated stiffening hydrogels for probing activation of pancreatic stellate cells, Acta Biomater 48**2017** 258-269.

[214] Y.M. Kim, J. Yun, C.K. Lee, H. Lee, K.R. Min, Y. Kim, Oxyresveratrol and hydroxystilbene compounds. Inhibitory effect on tyrosinase and mechanism of action, J Biol Chem 277(18) **2002** 16340-4.

[215] P. Kord Forooshani, B.P. Lee, Recent approaches in designing bioadhesive materials inspired by mussel adhesive protein, J Polym Sci A Polym Chem 55(1) **2017** 9-33.

[216] M.S. Rehmann, K.M. Skeens, P.M. Kharkar, E.M. Ford, E. Maverakis, K.H. Lee, A.M. Kloxin, Tuning and Predicting Mesh Size and Protein Release from Step Growth Hydrogels, Biomacromolecules 18(10) **2017** 3131-3142.

[217] A. Rubiano, D. Delitto, S. Han, M. Gerber, C. Galitz, J. Trevino, R.M. Thomas, S.J. Hughes, C.S. Simmons, Viscoelastic properties of human pancreatic tumors and in vitro constructs to mimic mechanical properties, Acta Biomater 67**2018** 331-340.

[218] S.R. Lustig, N.A. Peppas, Solute diffusion in swollen membranes. IX. Scaling laws for solute diffusion in gels, Journal of Applied Polymer Science 36(4) **1988** 735-747.

[219] A.A. Aimetti, M.W. Tibbitt, K.S. Anseth, Human neutrophil elastase responsive delivery from poly(ethylene glycol) hydrogels, Biomacromolecules 10(6) **2009** 1484-9.

[220] L.G. Fenoll, J.N. Rodriguez-Lopez, F. Garcia-Molina, F. Garcia-Canovas, J. Tudela, Michaelis constants of mushroom tyrosinase with respect to oxygen in the presence of monophenols and diphenols, Int J Biochem Cell Biol 34(4) **2002** 332-6.

[221] A.J. Winder, A stopped spectrophotometric assay for the dopa oxidase activity of tyrosinase, J Biochem Biophys Methods 28(3) **1994** 173-83.

[222] R.P. Ferrari, E. Laurenti, E.M. Ghibaudi, L. Casella, Tyrosinase-catecholic substrates in Vitro model: kinetic studies on the o-quinone/o-semiquinone radical formation, Journal of Inorganic Biochemistry 68(1) **1997** 61-69.

[223] M.C. Reed, A. Lieb, H.F. Nijhout, The biological significance of substrate inhibition: a mechanism with diverse functions, Bioessays 32(5) **2010** 422-9.

[224] D.A. Barry, J.Y. Parlange, L. Li, H. Prommer, C.J. Cunningham, F. Stagnitti, Analytical approximations for real values of the Lambert W-function, Mathematics and Computers in Simulation 53(1-2) **2000** 95-103.

[225] M. Schleeger, J. Heberle, S. Kakorin, Simplifying the Analysis of Enzyme Kinetics of Cytochrome <i>c</i> Oxidase by the Lambert-W Function, Open Journal of Biophysics 02(04) **2012** 117-129.

[226] K.S. Anseth, A.T. Metters, S.J. Bryant, P.J. Martens, J.H. Elisseeff, C.N. Bowman, In situ forming degradable networks and their application in tissue engineering and drug delivery, J Control Release 78(1-3) **2002** 199-209.

[227] P.J. Flory, Principles of polymer chemistry, Cornell University Press, Ithaca, NY **1953**.

[228] I. Yazici, O. Okay, Spatial inhomogeneity in poly(acrylic acid) hydrogels, Polymer 46(8) **2005** 2595-2602.

[229] C.C. Lin, K.S. Anseth, Cell-cell communication mimicry with poly(ethylene glycol) hydrogels for enhancing beta-cell function, Proc Natl Acad Sci U S A 108(16) **2011** 6380-5.

[230] R.C. Sharma, R. Ali, Hydrodynamic properties of mushroom tyrosinase, Phytochemistry 20(3) **1981** 399-401-401.

[231] R.G. Duggleby, J.F. Morrison, The analysis of progress curves for enzyme-catalysed reactions by non-linear regression, Biochim Biophys Acta 481(2) **1977** 297-312.

[232] W.W. Cleland, The kinetics of enzyme-catalyzed reactions with two or more substrates or products. I. Nomenclature and rate equations, Biochim Biophys Acta 67**1963** 104-37.

[233] S. Dupont, L. Morsut, M. Aragona, E. Enzo, S. Giulitti, M. Cordenonsi, F. Zanconato, J. Le Digabel, M. Forcato, S. Bicciato, N. Elvassore, S. Piccolo, Role of YAP/TAZ in mechanotransduction, Nature 474(7350) **2011** 179-83.

[234] J. Gore, M. Korc, Pancreatic cancer stroma: friend or foe?, Cancer Cell 25(6) **2014** 711-2.

[235] A.J. Engler, S. Sen, H.L. Sweeney, D.E. Discher, Matrix elasticity directs stem cell lineage specification, Cell 126(4) **2006** 677-89.

[236] M.W. Tibbitt, K.S. Anseth, Hydrogels as extracellular matrix mimics for 3D cell culture, Biotechnol Bioeng 103(4) **2009** 655-63.

[237] C.C. Lin, K.S. Anseth, PEG hydrogels for the controlled release of biomolecules in regenerative medicine, Pharm Res 26(3) **2009** 631-43.

[238] C.C. Lin, K.S. Anseth, Controlling Affinity Binding with Peptide-Functionalized Poly(ethylene glycol) Hydrogels, Adv Funct Mater 19(14) **2009** 2325.

[239] C. Yang, M.W. Tibbitt, L. Basta, K.S. Anseth, Mechanical memory and dosing influence stem cell fate, Nat Mater 13(6) **2014** 645-52.

[240] A.M. Kloxin, A.M. Kasko, C.N. Salinas, K.S. Anseth, Photodegradable hydrogels for dynamic tuning of physical and chemical properties, Science 324(5923) **2009** 59-63.

[241] S. Khetan, M. Guvendiren, W.R. Legant, D.M. Cohen, C.S. Chen, J.A. Burdick, Degradation-mediated cellular traction directs stem cell fate in covalently crosslinked three-dimensional hydrogels, Nat Mater 12(5) **2013** 458-65.

[242] A.M. Rosales, K.M. Mabry, E.M. Nehls, K.S. Anseth, Photoresponsive elastic properties of azobenzene-containing poly(ethylene-glycol)-based hydrogels, Biomacromolecules 16(3) **2015** 798-806.

[243] H. Shih, C.-C. Lin, Tuning stiffness of cell-laden hydrogel via host–guest interactions, Journal of Materials Chemistry B 4(29) **2016** 4969-4974.

[244] A.M. Jonker, A. Borrmann, E.R. van Eck, F.L. van Delft, D.W. Lowik, J.C. van Hest, A fast and activatable cross-linking strategy for hydrogel formation, Adv Mater 27(7) **2015** 1235-40.

[245] S. Das, F. Pati, Y.J. Choi, G. Rijal, J.H. Shim, S.W. Kim, A.R. Ray, D.W. Cho, S. Ghosh, Bioprintable, cell-laden silk fibroin-gelatin hydrogel supporting multilineage differentiation of stem cells for fabrication of three-dimensional tissue constructs, Acta Biomater 11**2015** 233-46.

[246] K.A. Mosiewicz, L. Kolb, A.J. van der Vlies, M.M. Martino, P.S. Lienemann, J.A. Hubbell, M. Ehrbar, M.P. Lutolf, In situ cell manipulation through enzymatic hydrogel photopatterning, Nat Mater 12(11) **2013** 1072-8.

[247] F. Anjum, P.S. Lienemann, S. Metzger, J. Biernaskie, M.S. Kallos, M. Ehrbar, Enzyme responsive GAG-based natural-synthetic hybrid hydrogel for tunable growth factor delivery and stem cell differentiation, Biomaterials 87**2016** 104-117.

[248] L.S. Wang, C. Du, J.E. Chung, M. Kurisawa, Enzymatically cross-linked gelatin-phenol hydrogels with a broader stiffness range for osteogenic differentiation of human mesenchymal stem cells, Acta Biomater 8(5) **2012** 1826-37.

[249] E.J. Land, C.A. Ramsden, P.A. Riley, Tyrosinase autoactivation and the chemistry of ortho-quinone amines, Accounts of chemical research 36(5) **2003** 300-8.

[250] K.S. Lim, M.H. Alves, L.A. Poole-Warren, P.J. Martens, Covalent incorporation of non-chemically modified gelatin into degradable PVA-tyramine hydrogels, Biomaterials 34(29) **2013** 7097-105.

[251] C.C. Lin, C.S. Ki, H. Shih, Thiol-norbornene photo-click hydrogels for tissue engineering applications, J Appl Polym Sci 132(8) **2015** 41563.

[252] B.D. Fairbanks, M.P. Schwartz, A.E. Halevi, C.R. Nuttelman, C.N. Bowman, K.S. Anseth, A Versatile Synthetic Extracellular Matrix Mimic via Thiol-Norbornene Photopolymerization, Adv Mater 21(48) **2009** 5005-5010.

[253] M.W. Tibbitt, A.M. Kloxin, L. Sawicki, K.S. Anseth, Mechanical Properties and Degradation of Chain and Step Polymerized Photodegradable Hydrogels, Macromolecules 46(7) **2013** 2785-2792.

[254] C.L. Bell, N.A. Peppas, Water, solute and protein diffusion in physiologically responsive hydrogels of poly (methacrylic acid-g-ethylene glycol), Biomaterials 17(12) **1996** 1203-18.

[255] M.B. Mellott, K. Searcy, M.V. Pishko, Release of protein from highly cross-linked hydrogels of poly(ethylene glycol) diacrylate fabricated by UV polymerization, Biomaterials 22(9) **2001** 929-41.

[256] I. Behbahani, S.A. Miller, D.H. Okeeffe, A Comparison of Mushroom Tyrosinase Dopaquinone and Dopachrome Assays Using Diode-Array Spectrophotometry: Dopachrome Formation vs Ascorbate-Linked Dopaquinone Reduction, Microchemical Journal 47(1-2) **1993** 251-260.

[257] M.P. Lutolf, J.A. Hubbell, Synthetic biomaterials as instructive extracellular microenvironments for morphogenesis in tissue engineering, Nat Biotechnol 23(1) **2005** 47-55.

[258] C.C. Lin, Recent advances in crosslinking chemistry of biomimetic poly(ethylene glycol) hydrogels, RSC Adv 5(50) **2015** 39844-398583.

[259] T.Y. Lin, C.S. Ki, C.C. Lin, Manipulating hepatocellular carcinoma cell fate in orthogonally cross-linked hydrogels, Biomaterials 35(25) **2014** 6898-906.

[260] C.S. Ki, T.Y. Lin, M. Korc, C.C. Lin, Thiol-ene hydrogels as desmoplasia-mimetic matrices for modeling pancreatic cancer cell growth, invasion, and drug resistance, Biomaterials 35(36) **2014** 9668-77.

[261] C.C. Lin, A. Raza, H. Shih, PEG hydrogels formed by thiol-ene photo-click chemistry and their effect on the formation and recovery of insulin-secreting cell spheroids, Biomaterials 32(36) **2011** 9685-95.

[262] T. Greene, C.-C. Lin, Modular Cross-Linking of Gelatin-Based Thiol–Norbornene Hydrogels for in Vitro 3D Culture of Hepatocellular Carcinoma Cells, ACS Biomaterials Science & Engineering 1(12) **2015** 1314-1323.

[263] K. Kikuta, A. Masamune, T. Watanabe, H. Ariga, H. Itoh, S. Hamada, K. Satoh, S. Egawa, M. Unno, T. Shimosegawa, Pancreatic stellate cells promote epithelial-mesenchymal transition in pancreatic cancer cells, Biochem Biophys Res Commun 403(3-4) **2010** 380-4.

[264] G. Luo, J. Long, B. Zhang, C. Liu, J. Xu, Q. Ni, X. Yu, Stroma and pancreatic ductal adenocarcinoma: an interaction loop, Biochim Biophys Acta 1826(1) **2012** 170-8.

[265] J.J. Kwon, S.C. Nabinger, Z. Vega, S.S. Sahu, R.K. Alluri, Z. Abdul-Sater, Z. Yu, J. Gore, G. Nalepa, R. Saxena, M. Korc, J. Kota, Pathophysiological role of microRNA-29 in pancreatic cancer stroma, Sci Rep 5**2015** 11450.

[266] M. Guvendiren, M. Perepelyuk, R.G. Wells, J.A. Burdick, Hydrogels with differential and patterned mechanics to study stiffness-mediated myofibroblastic differentiation of hepatic stellate cells, J Mech Behav Biomed Mater 38**2014** 198-208.

[267] S.R. Caliari, M. Perepelyuk, E.M. Soulas, G.Y. Lee, R.G. Wells, J.A. Burdick, Gradually softening hydrogels for modeling hepatic stellate cell behavior during fibrosis regression, Integr Biol (Camb) 8(6) **2016** 720-8.

[268] M.J. Kim, S.A. Park, C.H. Kim, S.Y. Park, J.S. Kim, D.K. Kim, J.S. Nam, Y.Y. Sheen, TGF-beta Type I Receptor Kinase Inhibitor EW-7197 Suppresses Cholestatic Liver Fibrosis by Inhibiting HIF1alpha-Induced Epithelial Mesenchymal Transition, Cellular physiology and biochemistry 38(2) **2016** 571-88.

[269] V. Rebours, M. Albuquerque, A. Sauvanet, P. Ruszniewski, P. Levy, V. Paradis, P. Bedossa, A. Couvelard, Hypoxia pathways and cellular stress activate pancreatic stellate cells: development of an organotypic culture model of thick slices of normal human pancreas, PLoS One 8(9) **2013** e76229.

[270] H. Ling, J.R. Sylvestre, P. Jolicoeur, Notch1-induced mammary tumor development is cyclin D1-dependent and correlates with expansion of pre-malignant multipotent duct-limited progenitors, Oncogene 29(32) **2010** 4543-54.

[271] A. Raza, C.C. Lin, The influence of matrix degradation and functionality on cell survival and morphogenesis in PEG-based hydrogels, Macromol Biosci 13(8) **2013** 1048-58.

[272] B.D. Fairbanks, M.P. Schwartz, C.N. Bowman, K.S. Anseth, Photoinitiated polymerization of PEG-diacrylate with lithium phenyl-2,4,6-trimethylbenzoylphosphinate: polymerization rate and cytocompatibility, Biomaterials 30(35) **2009** 6702-7.

[273] R.L. Siegel, K.D. Miller, A. Jemal, Cancer Statistics, 2017, CA Cancer J Clin 67(1) **2017** 7-30.

[274] J. Kleeff, M. Korc, M. Apte, C. La Vecchia, C.D. Johnson, A.V. Biankin, R.E. Neale, M. Tempero, D.A. Tuveson, R.H. Hruban, J.P. Neoptolemos, Pancreatic cancer, Nature reviews. Disease primers 2**2016** 16022.

[275] J. Kota, J. Hancock, J. Kwon, M. Korc, Pancreatic cancer: Stroma and its current and emerging targeted therapies, Cancer Lett 391**2017** 38-49.

[276] M. Korc, Pancreatic cancer-associated stroma production, Am J Surg 194(4 Suppl) **2007** S84-6.

[277] X. Zheng, J.L. Carstens, J. Kim, M. Scheible, J. Kaye, H. Sugimoto, C.C. Wu, V.S. LeBleu, R. Kalluri, Epithelial-to-mesenchymal transition is dispensable for metastasis but induces chemoresistance in pancreatic cancer, Nature 527(7579) **2015** 525-530.

[278] C.S. Ki, H. Shih, C.C. Lin, Effect of 3D matrix compositions on the efficacy of EGFR inhibition in pancreatic ductal adenocarcinoma cells, Biomacromolecules 14(9) **2013** 3017-26.

[279] S. Lamouille, J. Xu, R. Derynck, Molecular mechanisms of epithelial-mesenchymal transition, Nat Rev Mol Cell Biol 15(3) **2014** 178-96.

[280] M. Zeisberg, E.G. Neilson, Biomarkers for epithelial-mesenchymal transitions, J Clin Invest 119(6) **2009** 1429-37.

[281] Z. Wang, Y. Li, A. Ahmad, S. Banerjee, A.S. Azmi, D. Kong, F.H. Sarkar, Pancreatic cancer: understanding and overcoming chemoresistance, Nat Rev Gastroenterol Hepatol 8(1) **2011** 27-33.

[282] M. Egeblad, M.G. Rasch, V.M. Weaver, Dynamic interplay between the collagen scaffold and tumor evolution, Curr Opin Cell Biol 22(5) **2010** 697-706.

[283] L.A. Gurski, X. Xu, L.N. Labrada, N.T. Nguyen, L. Xiao, K.L. van Golen, X. Jia, M.C. Farach-Carson, Hyaluronan (HA) interacting proteins RHAMM and hyaluronidase impact prostate cancer cell behavior and invadopodia formation in 3D HA-based hydrogels, PLoS One 7(11) **2012** e50075.

[284] M.L. Borowsky, R.O. Hynes, Layilin, a novel talin-binding transmembrane protein homologous with C-type lectins, is localized in membrane ruffles, J Cell Biol 143(2) **1998** 429-42.

[285] M. Gotte, G.W. Yip, Heparanase, hyaluronan, and CD44 in cancers: a breast carcinoma perspective, Cancer Res 66(21) **2006** 10233-7.

[286] M.J. Paszek, N. Zahir, K.R. Johnson, J.N. Lakins, G.I. Rozenberg, A. Gefen, C.A. Reinhart-King, S.S. Margulies, M. Dembo, D. Boettiger, D.A. Hammer, V.M. Weaver, Tensional homeostasis and the malignant phenotype, Cancer Cell 8(3) **2005** 241-54.

[287] W. Xu, J. Qian, Y. Zhang, A. Suo, N. Cui, J. Wang, Y. Yao, H. Wang, A double-network poly(Nvarepsilon-acryloyl L-lysine)/hyaluronic acid hydrogel as a mimic of the breast tumor microenvironment, Acta Biomater 33**2016** 131-41.

[288] A. Raza, C.S. Ki, C.C. Lin, The influence of matrix properties on growth and morphogenesis of human pancreatic ductal epithelial cells in 3D, Biomaterials 34(21) **2013** 5117-27.

[289] H. Shih, T. Greene, M. Korc, C.C. Lin, Modular and Adaptable Tumor Niche Prepared from Visible Light Initiated Thiol-Norbornene Photopolymerization, Biomacromolecules 17(12) **2016** 3872-3882.

[290] L.S. Wang, J.E. Chung, P.P. Chan, M. Kurisawa, Injectable biodegradable hydrogels with tunable mechanical properties for the stimulation of neurogenesic differentiation of human mesenchymal stem cells in 3D culture, Biomaterials 31(6) **2010** 1148-57.

[291] M. Hu, M. Kurisawa, R. Deng, C.M. Teo, A. Schumacher, Y.X. Thong, L. Wang, K.M. Schumacher, J.Y. Ying, Cell immobilization in gelatin-hydroxyphenylpropionic acid hydrogel fibers, Biomaterials 30(21) **2009** 3523-31.

[292] J.E. Eastoe, The amino acid composition of mammalian collagen and gelatin, Biochem J 61(4) **1955** 589-600.

[293] L.G. Fenoll, J.N. Rodriguez-Lopez, F. Garcia-Sevilla, P.A. Garcia-Ruiz, R. Varon, F. Garcia-Canovas, J. Tudela, Analysis and interpretation of the action mechanism of mushroom tyrosinase on monophenols and diphenols generating highly unstable o-quinones, Biochim Biophys Acta 1548(1) **2001** 1-22.

[294] A.V. Nguyen, K.D. Nyberg, M.B. Scott, A.M. Welsh, A.H. Nguyen, N. Wu, S.V. Hohlbauch, N.A. Geisse, E.A. Gibb, A.G. Robertson, T.R. Donahue, A.C. Rowat, Stiffness of pancreatic cancer cells is associated with increased invasive potential, Integr Biol (Camb) 8(12) **2016** 1232-1245.

[295] Y. Messai, M.Z. Noman, A. Derouiche, N. Kourda, I. Akalay, M. Hasmim, I. Stasik, S. Ben Jilani, M. Chebil, A. Caignard, B. Azzarone, A. Gati, A. Ben Ammar Elgaaied, S. Chouaib, Cytokeratin 18 expression pattern correlates with renal cell carcinoma progression: relationship with Snail, Int J Oncol 36(5) **2010** 1145-54.

[296] C. Lou, F. Zhang, M. Yang, J. Zhao, W. Zeng, X. Fang, Y. Zhang, C. Zhang, W. Liang, Naringenin Decreases Invasiveness and Metastasis by Inhibiting TGF-β-Induced Epithelial to Mesenchymal Transition in Pancreatic Cancer Cells, PLoS One2012.

[297] N.R. Alexander, N.L. Tran, H. Rekapally, C.E. Summers, C. Glackin, R.L. Heimark, N-cadherin gene expression in prostate carcinoma is modulated by integrin-dependent nuclear translocation of Twist1, Cancer Res 66(7) **2006** 3365-9.

[298] T.C. Silveira Correa, R.R. Massaro, C.A. Brohem, S.R. Taboga, M.L. Lamers, M.F. Santos, S.S. Maria-Engler, RECK-mediated inhibition of glioma migration and invasion, Journal of cellular biochemistry 110(1) **2010** 52-61.

[299] S. Jabari, M. Meissnitzer, K. Quint, S. Gahr, T. Wissniowski, E.G. Hahn, D. Neureiter, M. Ocker, Cellular plasticity of trans- and dedifferentiation markers in human hepatoma cells in vitro and in vivo, Int J Oncol 35(1) **2009** 69-80.

[300] N. Rath, M.F. Olson, Regulation of pancreatic cancer aggressiveness by stromal stiffening, Nat Med 22(5) **2016** 462-3.

[301] K. Yue, G. Trujillo-de Santiago, M.M. Alvarez, A. Tamayol, N. Annabi, A. Khademhosseini, Synthesis, properties, and biomedical applications of gelatin methacryloyl (GelMA) hydrogels, Biomaterials 73**2015** 254-71.

[302] Z. Mũnoz, H. Shih, C.-C. Lin, Gelatin hydrogels formed by orthogonal thiol–norbornene photochemistry for cell encapsulation, Biomater. Sci. 2(8) **2014** 1063-1072.

[303] T. Greene, T.-Y. Lin, O.M. Andrisani, C.-C. Lin, Comparative study of visible light polymerized gelatin hydrogels for 3D culture of hepatic progenitor cells, Journal of Applied Polymer Science 134(11) **2017**.

[304] K. Arda, N. Ciledag, E. Aktas, B.K. Aribas, K. Kose, Quantitative assessment of normal soft-tissue elasticity using shear-wave ultrasound elastography, AJR Am J Roentgenol 197(3) **2011** 532-6.

[305] A.J. Rice, E. Cortes, D. Lachowski, B.C.H. Cheung, S.A. Karim, J.P. Morton, A. Del Rio Hernandez, Matrix stiffness induces epithelial-mesenchymal transition and promotes chemoresistance in pancreatic cancer cells, Oncogenesis 6(7) **2017** e352.

[306] N. Sato, S. Kohi, K. Hirata, M. Goggins, Role of hyaluronan in pancreatic cancer biology and therapy: Once again in the spotlight, Cancer Sci 107(5) **2016** 569-75.

[307] M.P. di Magliano, C.D. Logsdon, Roles for KRAS in pancreatic tumor development and progression, Gastroenterology 144(6) **2013** 1220-9.

[308] H. Kurahara, S. Takao, K. Maemura, H. Shinchi, S. Natsugoe, T. Aikou, Impact of vascular endothelial growth factor-C and -D expression in human pancreatic cancer: its relationship to lymph node metastasis, Clin Cancer Res 10(24) **2004** 8413-20.

[309] Z. Wang, Y. Li, D. Kong, S. Banerjee, A. Ahmad, A.S. Azmi, S. Ali, J.L. Abbruzzese, G.E. Gallick, F.H. Sarkar, Acquisition of epithelial-mesenchymal transition phenotype of gemcitabine-resistant pancreatic cancer cells is linked with activation of the notch signaling pathway, Cancer Res 69(6) **2009** 2400-7.

[310] E. Ristorcelli, D. Lombardo, Targeting Notch signaling in pancreatic cancer, Expert Opin Ther Targets 14(5) **2010** 541-52.

[311] C. Gungor, H. Zander, K.E. Effenberger, Y.K. Vashist, T. Kalinina, J.R. Izbicki, E. Yekebas, M. Bockhorn, Notch signaling activated by replication stress-induced expression of midkine drives epithelial-mesenchymal transition and chemoresistance in pancreatic cancer, Cancer Res 71(14) **2011** 5009-19.

[312] M.A. Shields, S. Dangi-Garimella, A.J. Redig, H.G. Munshi, Biochemical role of the collagen-rich tumour microenvironment in pancreatic cancer progression, Biochem J 441(2) **2012** 541-52.

[313] S. Lunardi, R.J. Muschel, T.B. Brunner, The stromal compartments in pancreatic cancer: are there any therapeutic targets?, Cancer Lett 343(2) **2014** 147-55.

[314] K. Jakubowska, A. Pryczynicz, J. Januszewska, I. Sidorkiewicz, A. Kemona, A. Niewinski, L. Lewczuk, B. Kedra, K. Guzinska-Ustymowicz, Expressions of Matrix Metalloproteinases 2, 7, and 9 in Carcinogenesis of Pancreatic Ductal Adenocarcinoma, Dis Markers 2016**2016** 9895721.

[315] M. Grusch, M. Petz, T. Metzner, D. Ozturk, D. Schneller, W. Mikulits, The crosstalk of RAS with the TGF-beta family during carcinoma progression and its implications for targeted cancer therapy, Curr Cancer Drug Targets 10(8) **2010** 849-57.

[316] M. Kang, S. Choi, S.J. Jeong, S.A. Lee, T.K. Kwak, H. Kim, O. Jung, M.S. Lee, Y. Ko, J. Ryu, Y.J. Choi, D. Jeong, H.J. Lee, S.K. Ye, S.H. Kim, J.W. Lee, Cross-talk between TGFbeta1 and EGFR signalling pathways induces TM4SF5 expression and epithelial-mesenchymal transition, Biochem J 443(3) **2012** 691-700.

[317] Y. Wang, J. Wang, Mixed hydrogel bead-based tumor spheroid formation and anticancer drug testing, Analyst 139(10) **2014** 2449-58.

[318] T.Y. Lin, J.C. Bragg, C.C. Lin, Designing Visible Light-Cured Thiol-Acrylate Hydrogels for Studying the HIPPO Pathway Activation in Hepatocellular Carcinoma Cells, Macromol Biosci 16(4) **2016** 496-507.

[319] C.A. DeForest, K.S. Anseth, Advances in bioactive hydrogels to probe and direct cell fate, Annu Rev Chem Biomol Eng 3**2012** 421-44.

[320] L. Kass, J.T. Erler, M. Dembo, V.M. Weaver, Mammary epithelial cell: influence of extracellular matrix composition and organization during development and tumorigenesis, Int J Biochem Cell Biol 39(11) **2007** 1987-94.

[321] M.C. Lampi, C.A. Reinhart-King, Targeting extracellular matrix stiffness to attenuate disease: From molecular mechanisms to clinical trials, Sci Transl Med 10(422) **2018**.

[322] S. van Helvert, C. Storm, P. Friedl, Mechanoreciprocity in cell migration, Nat Cell Biol 20(1) **2018** 8-20.

[323] S. Khetan, J.A. Burdick, Patterning network structure to spatially control cellular remodeling and stem cell fate within 3-dimensional hydrogels, Biomaterials 31(32) **2010** 8228-34.

[324] S. Khetan, J.S. Katz, J.A. Burdick, Sequential crosslinking to control cellular spreading in 3-dimensional hydrogels, Soft Matter 5(8) **2009** 1601-1606.

[325] C. Fiedler, E. Aisenbrey, J. Wahlquist, C. Heveran, V. Ferguson, S. Bryant, R. McLeod, Enhanced mechanical properties of photo-clickable thiol–ene PEG hydrogels through repeated photopolymerization of in-swollen macromer, Soft matter 12(44) **2016** 9095-9104.

[326] S.R. Caliari, M. Perepelyuk, B.D. Cosgrove, S.J. Tsai, G.Y. Lee, R.L. Mauck, R.G. Wells, J.A. Burdick, Stiffening hydrogels for investigating the dynamics of hepatic stellate cell mechanotransduction during myofibroblast activation, Sci Rep 6**2016** 21387.

[327] H. Shih, A.K. Fraser, C.C. Lin, Interfacial thiol-ene photoclick reactions for forming multilayer hydrogels, ACS Appl Mater Interfaces 5(5) **2013** 1673-80.

[328] H. Shih, C.C. Lin, Visible-light-mediated thiol-ene hydrogelation using eosin-Y as the only photoinitiator, Macromol Rapid Commun 34(3) **2013** 269-73.

[329] T. Mazaki, Y. Shiozaki, K. Yamane, A. Yoshida, M. Nakamura, Y. Yoshida, D. Zhou, T. Kitajima, M. Tanaka, Y. Ito, T. Ozaki, A. Matsukawa, A novel, visible light-induced, rapidly cross-linkable gelatin scaffold for osteochondral tissue engineering, Sci Rep 4**2014** 4457.

[330] A.G. Savelyev, K.N. Bardakova, E.V. Khaydukov, A.N. Generalova, V.K. Popov, B.N. Chichkov, V.A. Semchishen, Flavin mononucleotide photoinitiated cross-linking of hydrogels: Polymer concentration threshold of strengthening, Journal of Photochemistry and Photobiology A: Chemistry 341**2017** 108-114.

[331] B.P. Partlow, M.B. Applegate, F.G. Omenetto, D.L. Kaplan, Dityrosine Cross-Linking in Designing Biomaterials, ACS Biomaterials Science & Engineering 2(12) **2016** 2108-2121.

[332] A.M. Edwards, Structure and general properties of flavins, Methods in molecular biology (Clifton, N.J.) 1146**2014** 3-13.

[333] S.H. Kim, C.C. Chu, Fabrication of a biodegradable polysaccharide hydrogel with riboflavin, vitamin B2, as a photo-initiator and L-arginine as coinitiator upon UV irradiation, J Biomed Mater Res B Appl Biomater 91(1) **2009** 390-400.

[334] B. Choi, S. Kim, B. Lin, K. Li, O. Bezouglaia, J. Kim, D. Evseenko, T. Aghaloo, M. Lee, Visible-light-initiated hydrogels preserving cartilage extracellular signaling for inducing chondrogenesis of mesenchymal stem cells, Acta Biomater 12**2015** 30-41.

[335] J. Heo, R.H. Koh, W. Shim, H.D. Kim, H.G. Yim, N.S. Hwang, Riboflavin-induced photo-crosslinking of collagen hydrogel and its application in meniscus tissue engineering, Drug Deliv Transl Res 6(2) **2016** 148-58.

[336] R. Batchelor, G. Kwandou, P. Spicer, M. Stenzel, (−)-Riboflavin (vitamin B2) and flavin mononucleotide as visible light photo initiators in the thiol–ene polymerisation of PEG-based hydrogels, Polymer Chemistry 8(6) **2017** 980-984.

[337] C. Yang, F.W. DelRio, H. Ma, A.R. Killaars, L.P. Basta, K.A. Kyburz, K.S. Anseth, Spatially patterned matrix elasticity directs stem cell fate, Proc Natl Acad Sci U S A 113(31) **2016** E4439-45.

[338] K. Belousov, I. Denisov, K. Lukyanenko, A. Yakimov, A. Bukatin, I. Kukhtevich, V. Sorokin, E. Esimbekova, P. Belobrov, A. Evstrapov, Dissolution and mixing of flavin mononucleotide in microfluidic chips for bioassay, Journal of Physics: Conference Series, IOP Publishing, 2016, p. 012058.

[339] H. Gorner, Oxygen uptake after electron transfer from amines, amino acids and ascorbic acid to triplet flavins in air-saturated aqueous solution, J Photochem Photobiol B 87(2) **2007** 73-80.

[340] A.M. Edwards, Structure and general properties of flavins, Flavins and Flavoproteins, Springer2014, pp. 3-13.

[341] A.M. Edwards, E. Silva, Effect of visible light on selected enzymes, vitamins and amino acids, J Photochem Photobiol B 63(1-3) **2001** 126-31.

[342] T.A. Mace, A.L. Collins, S.E. Wojcik, C.M. Croce, G.B. Lesinski, M. Bloomston, Hypoxia induces the overexpression of microRNA-21 in pancreatic cancer cells, J Surg Res 184(2) **2013** 855-60.

[343] E. Monti, M.B. Gariboldi, HIF-1 as a target for cancer chemotherapy, chemosensitization and chemoprevention, Current molecular pharmacology 4(1) **2011** 62-77.

[344] S.R. Caliari, S.L. Vega, M. Kwon, E.M. Soulas, J.A. Burdick, Dimensionality and spreading influence MSC YAP/TAZ signaling in hydrogel environments, Biomaterials 103**2016** 314-323.

[345] B.D. Cosgrove, K.L. Mui, T.P. Driscoll, S.R. Caliari, K.D. Mehta, R.K. Assoian, J.A. Burdick, R.L. Mauck, N-cadherin adhesive interactions modulate matrix mechanosensing and fate commitment of mesenchymal stem cells, Nat Mater 15(12) **2016** 1297-1306.

[346] D.D. Shao, W. Xue, E.B. Krall, A. Bhutkar, F. Piccioni, X. Wang, A.C. Schinzel, S. Sood, J. Rosenbluh, J.W. Kim, Y. Zwang, T.M. Roberts, D.E. Root, T. Jacks, W.C. Hahn, KRAS and YAP1 converge to regulate EMT and tumor survival, Cell 158(1) **2014** 171-84.

[347] H.H. Ling, C.C. Kuo, B.X. Lin, Y.H. Huang, C.W. Lin, Elevation of YAP promotes the epithelial-mesenchymal transition and tumor aggressiveness in colorectal cancer, Exp Cell Res 350(1) **2017** 218-225.

[348] Y. Liu, K. He, Y. Hu, X. Guo, D. Wang, W. Shi, J. Li, J. Song, YAP modulates TGF-beta1-induced simultaneous apoptosis and EMT through upregulation of the EGF receptor, Sci Rep 7**2017** 45523.

[349] M. Debaugnies, A. Sanchez-Danes, S. Rorive, M. Raphael, M. Liagre, M.A. Parent, A. Brisebarre, I. Salmon, C. Blanpain, YAP and TAZ are essential for basal and squamous cell carcinoma initiation, EMBO reports 19(7) **2018**.

[350] H.K. Yang, K.C. Jeong, Y.K. Kim, S.T. Jung, Role of matrix metalloproteinase (MMP) 2 and MMP-9 in soft tissue sarcoma, Clin Orthop Surg 6(4) **2014** 443-54.

VITA

Education

Purdue University, West Lafayette, IN **01/2016-08/2019**

Ph.D. in Biomedical Engineering

National Tsing Hua University, Hsinchu, Taiwan **09/2012-06/2014**

M.S. in Chemical Engineering

National Tsing Hua University, Hsinchu, Taiwan **09/2008-06/2012**

B.S. in Interdisciplinary Program of Engineering

(Major: Chemical Engineering and Quantitative Financial)

Research Experiences

Research Assistant, Purdue University, West Lafayette **01/2016-Present**

Topic: *Development of a Dynamic Hydrogel System for Investigating Cell-Matrix Interactions in Pancreatic Cancer*

- Designed functional polymers or peptides utilizing bioconjugation techniques for fabrication of cell-cultured hydrogel
- Conducted *in vitro* cell studies to validate biocompatibility and feasibility of the system through engineering and biological approaches
- Utilized design of experiment (DOE) methodologies and statistical analysis methods for data analysis

Research Assistant, NTHU, Taiwan **07/2012-06/2014**

Topic: *A pH-Responsive Carrier System that Generates NO Bubbles to Trigger Drug Release and Reverse P-Glycoprotein-Mediated Multidrug Resistance (MDR)*

- Designed microfluidic devices for particles preparation
- Performed the corresponding *in vitro* and *in vivo* study to evaluate system efficacy

Teaching Assistant, National Tsing Hua University, Taiwan **09/2013-01/2014**

Course: *Artificial Organs and Tissue Engineering and Material and Energy Balance*

R&D Engineer Intern, Foxconn, Shenzhen, China **06/2012-08/2012**

Topic: *Formulation of the cutting fluid in Computer Numerical Control (CNC) and testing for iPhone production*

- Optimized mechanical property and formulation of the cutting fluids for iPhone manufacture

Teaching Assistant, Chemical Engineering, NTHU, Taiwan

- Course: *Artificial Organs and Tissue Engineering, Material and Energy Balance*

Production and R&D Intern, Foxconn, Hua Nan Test and Measurement Center, China

- Project: *Formulating Cutting Fluid and associated testing for making iPhone product*
- Optimized formulation of the cutting fluids and analyze physical and chemical property of which from different manufactures

Skills

Engineering	Hydrogel and drug delivery systems design, Solid phase peptide synthesis (SPPS), Microfludics, Computational modeling
Analytical techniques	UV-VIS, MS, NMR, FTIR, HPLC, SEM, Rheology, RNA/DNA/Protein extraction and quantification, Western blotting, Flow cytometry, Real-time PCR
Biological approaches	*In vitro* 2D and 3D cell culture, Live cell imaging, Fluorescence and Confocal microscopy, *In vivo* imaging system (IVIS), ELISA, Immunostaining
Software	MestReNova, Chemdraw, Pymol, ImageJ, AutoCAD, Minitab, SPSS, Stata SE, GraphPad Prism, Illustrator, MS Office

Honor and Award

1. Purdue Graduate Student Government Travel Grant, Purdue University, 2018
2. Dr. I-Chi Mei Memorial Medal, NTHU, 2012
3. Achievement Award of graduated student, College of Engineering, NTHU, 2012
4. Academic Achievement Award, NTHU, 2012
5. Global Industrial Leadership Scholarship, College of Engineering, NTHU, 2011
6. Interdisciplinary Program of Engineering, NTHU Summer Intern Abroad Scholarship, College of Engineering, NTHU, 2010
7. Dean's list, NTHU, 2010, 2011, and 2012

Conference Attendance

- **Liu, H.-Y.**; Lin, C.-C., "Tuning enzyme diffusion and reaction on temporal hydrogel stiffening," American Chemical Society. Orlando, Fl, US **2019** and Cancer Research Day. Indianapolis, IN, US **2019**
- **Liu, H.-Y.**; Nguyen, H.D.; Lin, C.-C., "Dynamic PEG–peptide hydrogels via visible light and FMN-induced tyrosine dimerization," American Chemical Society. Orlando, Fl, US **2019**
- **Liu, H.-Y.**; Korc, M.; Lin, C.-C. "Biomimetic and enzyme-responsive dynamic hydrogels for studying cell-matrix interactions in pancreatic ductal adenocarcinoma," Society for Biomaterials. Atlanta, GA, US **2018** and American Association for Cancer Research (AACR). Chicago, IL, US **2018**
- **Liu, H.-Y.**; Lin, C.-C., "Enzyme-mediated hydrogel for studying pancreatic cancer malignancy," Society for Biomaterials. Minneapolis, MN, US **2017**
- Shih, H.; **Liu, H.-Y.**; Lin, C.-C., "Improving gelation efficiency and cytocompatibility of visible light polymerized thiol-norbornene hydrogels via addition of soluble tyrosine," Society for Biomaterials. Minneapolis, MN, US **2017**

PUBLICATION

[1] B.N. Hudson, C.S. Dawes, H.Y. Liu, N. Dimmitt, F. Chen, H. Konig, C.-C. Lin, Stabilization of enzyme-immobilized hydrogels for extended hypoxic cell culture, Emergent Materials 2019.

[2] H.D. Nguyen, H.Y. Liu, B.N. Hudson, C.-C. Lin, Enzymatic Cross-Linking of Dynamic Thiol-Norbornene Click Hydrogels, ACS Biomaterials Science & Engineering 5(3) 2019 1247-1256.

[3] H.Y. Liu, C.C. Lin, A Diffusion-Reaction Model for Predicting Enzyme-Mediated Dynamic Hydrogel Stiffening, Gels 5(1) 2019.

[4] H.Y. Liu, H.D. Nguyen, C.C. Lin, Dynamic PEG-Peptide Hydrogels via Visible Light and FMN-Induced Tyrosine Dimerization, Adv Healthc Mater 7(22) 2018 e1800954.

[5] H.Y. Liu, M. Korc, C.C. Lin, Biomimetic and enzyme-responsive dynamic hydrogels for studying cell-matrix interactions in pancreatic ductal adenocarcinoma, Biomaterials 1602018 24-36.

[6] H. Shih, H.Y. Liu, C.C. Lin, Improving gelation efficiency and cytocompatibility of visible light polymerized thiol-norbornene hydrogels via addition of soluble tyrosine, Biomater Sci 5(3) 2017 589-599.

[7] H.Y. Liu, T. Greene, T.Y. Lin, C.S. Dawes, M. Korc, C.C. Lin, Enzyme-mediated stiffening hydrogels for probing activation of pancreatic stellate cells, Acta Biomater 482017 258-269.

[8] M.F. Chung*, H.Y. Liu*, K.J. Lin, W.T. Chia, H.W. Sung, A pH-Responsive Carrier System that Generates NO Bubbles to Trigger Drug Release and Reverse P-Glycoprotein-Mediated Multidrug Resistance, Angew Chem Int Ed Engl 54(34) 2015 9890-3.

[9] W.L. Chiang, T.T. Lin, R. Sureshbabu, W.T. Chia, H.C. Hsiao, H.Y. Liu, C.M. Yang, H.W. Sung, A rapid drug release system with a NIR light-activated molecular switch for dual-modality photothermal/antibiotic treatments of subcutaneous abscesses, J Control Release 1992015 53-62.

[10] Z.X. Liao, S.F. Peng, Y.L. Chiu, C.W. Hsiao, H.Y. Liu, W.H. Lim, H.M. Lu, H.W. Sung, Enhancement of efficiency of chitosan-based complexes for gene transfection with poly(gamma-glutamic acid) by augmenting their cellular uptake and intracellular unpackage, J Control Release 1932014 304-15.

[11] M.F. Chung, W.T. Chia, H.Y. Liu, C.W. Hsiao, H.C. Hsiao, C.M. Yang, H.W. Sung, Inflammation-induced drug release by using a pH-responsive gas-generating hollow-microsphere system for the treatment of osteomyelitis, Adv Healthc Mater 3(11) 2014 1854-61.

[12] W.L. Chiang, Y.C. Hu, H.Y. Liu, C.W. Hsiao, R. Sureshbabu, C.M. Yang, M.F. Chung, W.T. Chia, H.W. Sung, Injectable microbeads with a thermo-responsive shell and a pH-responsive core as a dual-switch-controlled release system, Small 10(20) 2014 4100-5.